UNIVERSITY OF ADELAIDE LIBRARY
25-7-97

REMOVAL OF EM COUPLING FROM FREQUENCY-DOMAIN IP DATA USING A HOMOGENEOUS ANISOTROPIC HALFSPACE WITH COMPLEX RESISTIVITIES IN A CONTROLLED RANDOM SEARCH PROCEDURE.

by

Gerard M. M^{C} Neill B.Sc.(Hons)

A Thesis Submitted to the Faculty of science

Department of GEOLOGY and GEOPHYSICS

Ih fulfillment of the requirements

for the Degree of

MASTER OF SCIENCE

at the

UNIVERSITY OF ADELAIDE

Revised Febuary 1997

NAME: GERARD McNEILL COURSE: MSc

This work contains no material which has been accepted for the award of any other degree or diploma in any university or other tertiary institution and, to the best of my knowledge and belief, contains no material previously published or written by another person, except where due reference has been made in the text.

I give consent to this copy of my thesis, when deposited in the University Libraries, being available for photocopying and loan.

SIGNATURE: ..... DATE: 08/07/97

TABLE OF CONTENTS:

Page.

List of Figures 7
List of Plates 13
Abstract 14
Statement by Author 16
Acknowledgements 17

(1.0) Introduction 18

SECTION I: A SUMMARY OF IMPORTANT ASPECTS OF EM COUPLING THEORY AND REVIEW OF FORWARD MODELING

(2.0) The IP effect and EM coupling problem 23
(2.1) Frequency Dependent Complex Resistivities 23
(2.2) Anisotropy 24
(2.3) EM Coupling Response for an anisotropic half-space 28

(3.0) Forward Modeling 32
(3.1) Real Resistivity Models 34
(3.2) Complex Resistivity Models 38
(3.2.1) Simplified Constant IP phase model 39
(3.2.2) Cole-Cole Dispersion 43
(3.3) Summary of Forward Modeling 52

TABLE OF CONTENTS:

Page.

SECTION II: UNIQUENESS OF THE INVERSE SOLUTION AND RESOLUTION OF MODEL PARAMETERS

(4.0) Prediction Error Surfaces and the Inverse Solution 54

(4.1) Effect of the General Survey characteristics 57

(4.1.1) Varying the Separation 58

(4.1.2) Survey Frequency Range 59

(4.1.3) Varying the dc Resistivity 60

(4.2) Effect of Varying Anisotropy - K 63

(4.3) Effect of Varying the Cole-Cole Parameters 67

(4.3.1) Chargeability - m 72

(4.3.2) Time Constant - τ_o 75

(4.3.3) Frequency Dependence - c 79

(4.3.4) Interdependence of Parameters 82

(4.4) Summary 87

SECTION III: INVERSION OF THEORETICAL AND FIELD CR-IP DATA

(5.0) The Controlled Random Search Algorithm 89

(6.0) Inverting Theoretical Data 93

(6.1) Theoretical data with varying amounts of noise 94

(6.2) Inverting model data with an annealing condition applied 100

..(6.3) Summary 107

TABLE OF CONTENTS:

	Page.
(7.0) Decoupling Field CR-IP Survey Data	108
(7.1) Test Line 1	110
(7.1.1) Decoupled using Program CRS_CIP	111
(7.1.2) Decoupled using Program CRS_CC	114
(7.2) Test Line 2	119
(7.2.1) Decoupled using Program CRS_CIP	119
(7.2.2) Decoupled using Program CRS_CC	122
(7.3) Discussion of Problem Points and Algorithm Failure	125
(7.3.1) Ambiguities in the Cole-Cole Dispersion Parameters	126
(7.3.2) Problems with the Anisotropic Half-Space Model	128
(7.4) The GDPHM Decoupling Routine	134
(7.4.1) Line 1: Comparison of the Decoupling Results Returned from the CRS Algorithms and GDPHM	136
(7.4.2) Line 2: Comparison of the Decoupling Results Returned from the CRS Algorithms and GDPHM	138
(8.0) Conclusions	141
References	145

TABLE OF CONTENTS:

Page.

Appendix I : Raw Data TEST LINE 1 - Pseudosections of Apparent Resistivity, 0.125Hz Raw Phase, 3-pt Decoupled Phase and Spectral plots 149

Appendix II : CRS Decoupled Data TEST LINE 1 - Pseudosections of Constant IP Phase parameters, Cole-Cole response and Cole-Cole dispersion parameters with L_1 Norm Error 150

Appendix III: Raw Data TEST LINE 2 - Pseudosections of Apparent Resistivity, 0.125Hz Raw Phase, 3-pt Decoupled Phase and Spectral plots 152

Appendix IV : CRS Decoupled Data TEST LINE 2 - Pseudosections of Constant IP Phase parameters, Cole-Cole response and Cole-Cole dispersion parameters with L_1 Norm Error 153

Appendix V : Pseudosections of GDPHM Decoupled Data TEST LINE 1 and TEST LINE 2 154

Appendix VI : Brief description of decoupling programs CRS_CC and CRS_CIP 155

LIST OF FIGURES:

Page.

(2.0) Physical examples of Anisotropic constants less than and greater than one. 27

(2.1) Geometry for the mutual impedance of straight grounded wires on the surface of the earth 29

(3.0) Geometry of the dipole-dipole array with pseudosection plot points 33

(3.1) EM coupling curve as well as magnitude and phase response for an isotropic model (K=1.0) 36

(3.2) EM coupling curves for anisotropic models with anisotropic constant K = 0.2, 0.5, 3.0 and 5.0 37

(3.3) EM coupling curves for an anisotropic model with K = 5.0 and phases (ϕ_{ip}) of 25, 50, 75 and 100 mrad 41

(3.4) EM coupling curves for an anisotropic model with K = 0.5 and phases (ϕ_{ip}) of 25, 50, 75 and 100 mrad 42

(3.5) EM coupling curve as well as magnitude and phase response for an isotropic model (K=1.0) having a Cole-Cole complex resistivity; R_o = 100 ohm-m, m = .3, τ_o = 1 and c = .5 45

(3.6) EM coupling curves for varying anisotropic constant values K = 0.2, 0.5, 3.0 and 5.0 having a Cole-Cole complex resistivity; R_o = 100 ohm-m, m = .3, τ_o = 1 and c = .5 48

LIST OF FIGURES:

Page.

(3.7) EM coupling curves for an isotropic model (K=1.0) with Cole-Cole complex resistivities of varying chargeability; m = 0.1, 0.5, 0.7 and 1.0 — 49

(3.8) EM coupling curves for an isotropic model (K=1.0) with Cole-Cole complex resistivities of varying time constant; $\tau_o = 10^{-2}$, 10^{-1}, 10^{1}, and 10^{2} sec — 50

(3.9) EM coupling curves for an isotropic model (K=1.0) with Cole-Cole complex resistivities of varying frequency dependence; c = 0.1, 0.25, 0.4 and 0.65 — 51

(4.1) L1 NORM inversion error - Grid search over isotropic half-spaces with R_o of 100 ohm-m and IP phase of 25 mrad; at n = 2, 4, 6 (15 frequencies) and n = 6 (5 frequencies) — 61

(4.2) L1 NORM inversion error - Grid search over isotropic half-spaces with an IP phase of 25 mrad at n= 6; with R_o = 10 ohm-m over 5, 15 and 35 frequencies as well as R_o = 1000 ohm-m over 15 frequencies — 62

(4.3) L1 NORM inversion error - Grid search over anisotropic half-spaces with a constant IP phase shift of 25 mrad, at n = 6 with K = 0.2, 0.5, 3.0 and 5.0 — 65

(4.4) L1 NORM inversion error - Grid search over an isotropic half-space having a Cole-Cole complex resistivity with R_o = 100 ohm-m, m = 0.3, τ_o = 1.0 sec and c = 0.5. Error for m v K, τ_o v K, c v K and R_o v K — 68

LIST OF FIGURES:

Page.

(4.5) L1 NORM inversion error - Grid search over an isotropic half-space having a Cole-Cole complex resistivity with R_o = 100 ohm-m, m = 0.3, τ_o = 1.0 sec and c = 0.5. Error for m v τ_o, c v τ_o and R_o v τ_o 70

(4.6) L1 NORM inversion error - Grid search over an isotropic half-space having a Cole-Cole complex resistivity with R_o = 100 ohm-m, m = 0.3, τ_o = 1.0 sec and c = 0.5. Error for m v R_o, c v R_o and c v m 71

(4.7) L1 NORM inversion error - Grid search over an isotropic half-space having a Cole-Cole complex resistivity with R_o = 100 ohm-m, m = 0.1, τ_o = 1.0 sec and c = 0.5. Error for m v K, m v τ_o, c v m and m v R_o 73

(4.8) L1 NORM inversion error - Grid search over an isotropic half-space having a Cole-Cole complex resistivity with R_o = 100 ohm-m, m = 0.7, τ_o = 1.0 sec and c = 0.5. Error for m v K, m v τ_o, c v m and m v R_o 74

(4.9) L1 NORM inversion error - Grid search over an isotropic half-space having a Cole-Cole complex resistivity with R_o = 100 ohm-m, m = 0.3, τ_o = 0.01 sec and c = 0.5. Error for τ_o v K, m v τ_o, c v τ_o and R_o v τ_o 76

LIST OF FIGURES:

Page.

(4.10) L1 NORM inversion error - Grid search over an isotropic half-space having a Cole-Cole complex resistivity with R_o = 100 ohm-m, m = 0.3, τ_o = 100 sec and c = 0.5. Error for τ_o v K, m v τ_o, c v τ_o and R_o v τ_o 77

(4.11) L1 NORM inversion error - Grid search over an isotropic half-space having a Cole-Cole complex resistivity with R_o = 100 ohm-m, m = 0.3, τ_o = 1.0 sec and c = 0.1. Error for c v K, c v τ_o, c v m and c v R_o 80

(4.12) L1 NORM inversion error - Grid search over an isotropic half-space having a Cole-Cole complex resistivity with R_o = 100 ohm-m, m = 0.3, τ_o = 1.0 sec and c = 0.7. Error for c v K, c v τ_o, c v m and c v R_o 81

(4.13) L1 NORM inversion error - Grid search over an isotropic half-space having a Cole-Cole complex resistivity with R_o = 10 ohm-m, m = 0.3, τ_o = 1.0 sec and c = 0.5. Error for m v K, τ_o v K, c v K and R_o v K 83

(4.14) L1 NORM inversion error - Grid search over an isotropic half-space having a Cole-Cole complex resistivity with R_o = 10 ohm-m, m = 0.3, τ_o = 1.0 sec and c = 0.5. Error for m v τ_o, c v τ_o and m v c 85

LIST OF FIGURES:

Page.

(4.15) L1 NORM inversion error - Grid search over an isotropic half-space having a Cole-Cole complex resistivity with R_o = 100 ohm-m and m = 0.3 Error for parameters; c v m (with τ_o = 0.01 and 100) m v τ_o (with c = 0.1 and 0.7) 86

(5.0) Flow Diagram for the CRS Procedure. 90

(5.1) An illustration of trial point selection. 92

(6.1) L1 NORM inversion error surfaces with initial parameter cloud generated when decoupling theoretical model data generated from a constant IP phase shift model with R_o = 10 ohm-m, ϕ_{ip} = 25 mrad and;
a) K = 1.0 b) K = 0.5 with 5% noise
c) K = 1.0 d) K = 0.5 with 10% noise 95

(6.2) L1 NORM inversion error surfaces with the final parameter cloud after inverting theoretical model data generated from a constant IP phase shift model with R_o = 10 ohm-m, ϕ_{ip} = 25 mrad and;
a) K = 1.0 b) K = 0.5 with 5% noise
c) K = 1.0 d) K = 0.5 with 10% noise 97

(6.3) L1 NORM inversion error surfaces with initial parameter cloud generated when decoupling theoretical model data generated from a constant IP phase shift model with ϕ_{ip} = 25 mrad contaminated by 10% noise with;
a) K = 1, R_o = 1.0 ohm-m b) K = 4, R_o = 10 ohm-m
c) K = 1, R_o = 100 ohm-m d) K = 4, R_o = 100 ohm-m 103

LIST OF FIGURES:

Page.

(6.4) L1 NORM inversion error surfaces with the final parameter cloud after inverting theoretical model data generated from a constant IP phase shift model with ϕ_{ip} = 25 mrad contaminated by 10% noise with; a) K = 1, R_o = 1.0 ohm-m b) K = 4, R_o = 10 ohm-m c) K = 1, R_o = 100 ohm-m d) K = 4, R_o = 100 ohm-m — 105

(7.1) L1 NORM inversion error surfaces generated from a grid search of Anisotropy (K) and Constant IP phase (ϕ_{ip}) over reciprocal points at 27300N, n = 4 and 27250N, n = 3 in TEST LINE 2 — 130

(7.2) L1 NORM inversion error surfaces generated from a grid search of Anisotropy (K) and Constant IP phase (ϕ_{ip}) over reciprocal points at 27600N, n = 4 and 27500N, n = 4 in TEST LINE 2 — 132

(7.3) L1 NORM inversion error surfaces generated from a grid search of Anisotropy (K) and Chargeability (m) over reciprocal points at 27600N, n = 4 and 27500N, n = 4 in TEST LINE 2 — 133

LIST OF PLATES:

Plate

(1.0) Raw CR-IP data for Test Line 1

(2.0) Constant IP phase parameters returned for Test Line 1

(3.0) Cole-Cole dc Resistivity and IP phase response
at 0.125, 1.0 and 8.0 Hz for Test Line 1

(4.0) Cole-Cole Dispersion parameters returned for Test Line 1

(5.0) Raw CR-IP data for Test Line 2

(6.0) Constant IP phase parameters returned for Test Line 2

(7.0) Cole-Cole dc Resistivity and IP phase response
at 0.125, 1.0 and 8.0 Hz for Test Line 2

(8.0) Cole-Cole Dispersion parameters returned for Test Line 2

(9.0) GDPHM dc Resistivity and IP phase response
at 0.125, 1.0 and 8.0 Hz for Test Line 1

(10.0) GDPHM dc Resistivity and IP phase response
at 0.125, 1.0 and 8.0 Hz for Test Line 2

ABSTRACT

Electromagnetic coupling is an intrinsic component of IP data, manifesting itself as a distortion of the received waveform, which can mask or distort the true IP response. The recognition and removal of first order EM coupling is relatively straight forward, if simplistic. However, simple removal techniques can be insufficient when the data is noisy or the coupling extreme.

An anisotropic half-space has been used to model the EM coupling response of grounded wires over the earth. An advantage of this model over more complex layered earth models is that it allows for resistivity variations between layers as well as those within layers. Forward modeling of the total EM-IP response for an anisotropic half-space with real, as well as complex resistivities, has been carried out.

Error surfaces in parameter space have been produced in order to investigate the uniqueness and resolution of the inverse parameter solutions for an anisotropic half-space with complex resistivities. The presence of multiple minima in the error surfaces indicates the inverse solution is non-unique. Poorly defined minima indicate the inverse parameter solutions can be difficult to resolve in certain situations.

A robust EM decoupling technique, which iteratively inverts the total EM-IP response to a homogeneous anisotropic half-space combined with a Cole-Cole dispersion IP model, has been developed and tested. The algorithm assigns vertical and horizontal components of resistivity at each point of a pseudosection independently of neighboring points. The controlled random search

procedure is used as it attacks the multi-minima problem by returning a range of possible parameter solutions. The relative reliability of the model response at each point as well as the resolution of given model parameters can then be determined. The centroid of the returned solution set is considered to be the best estimate of the response at this point.

The decoupling technique was applied to theoretical data with noise present, returning acceptable estimates of the model parameters. The CRS algorithm was used to decouple two lines of field CR-IP data and the results compared to the three point decoupled phase. The algorithm is successful in locating the global solution for the majority of points in the pseudosections. However, it has failed on specific examples where excess noise or complex geological conditions are not adequately accounted for by an anisotropic half-space model.

Decoupled data returned from an anisotropic half-space with a Cole-Cole dispersion was compared to the results obtained using Zonge Engineering and Research Organization's (ZERO) inhouse decoupling routine (GDPHM). The IP phase response returned when using the Cole-Cole dispersion is consistently more frequency dependent, over the polarizable areas, than that returned from the GDPHM routine. This indicates either the failure of the GDPHM routine to account for frequency dependence in the IP phase response or alternatively the failure of the anisotropic half-space to adequately account for the EM coupling response of the earth.

STATEMENT BY AUTHOR:

To the best of my knowledge and belief, this thesis contains no material which has been accepted for the award of any other degree in any other university or contains material previously published or written by another person, except where due reference has been made in the text.

This thesis has been submitted in fulfillment of the requirements of a Masters degree at the University of Adelaide and is deposited in the University Library to be made available to borrowers under the rules of the Library.

Quotations from this thesis are permitted provided that accurate acknowledgement of the source is made. Requests for permission for extended quotations or reproduction of this thesis in whole or part may be made to the Author.

Signed: .....

Gerard M. McNeill

ACKNOWLEDGEMENTS:

I wish to thank Zonge engineering and research organization for their financial and technical support throughout the entirety of my graduate studies. Of particular help has been the assistance of Scott MacInnes whose software contributions were of a great assistance in producing my decoupling programs.

Thanks are also extended to Bob Smith, of CRA Exploration and the A.S.E.G. Research Foundation who have provided financial assistance for my project.

Finally I would like to thank my supervisor Peter Brooker for his guidance and patience over the years.

(1.0) INTRODUCTION:

The induced polarization (IP) method consists of various electrical techniques which attempt to describe and measure the resistivity of the earth as a complex frequency dependent quantity. IP methods were first developed in the 1950s after strong IP effects were found to be associated with rocks containing economical mineralization (Marshall and Madden, 1959; Wait, 1959). Mineral exploration has been the primary focus of the method although, it has had a limited application in oil exploration (Carlson et al, 1981; Hughs, 1983) as well as being a useful tool in ground water research (Vacquier et al, 1957; Bodmer et al, 1968).

Frequency dependent electrical resistivity measurements are usually made by driving a current through two active grounded electrodes and measuring the resulting voltage across two passive grounded electrodes. The major difference from a dc resistivity measurement is in the use of a time dependent signal or transmitted waveform. Measurements can be made in the time or frequency domain depending on the objectives of a given survey. In frequency domain IP methods the phase shift between the transmitted and received waveforms is attributed to IP effects.

Two major problems have plagued the frequency domain IP method since it was first developed. The first is the distortion of the received waveform due to inductive coupling which can obscure the IP response. The other is the discrimination of IP anomalies due to economic sources from those due to uneconomic sources. Inductive coupling between the transmitter and receiver arrays is a complicated function of the geometry of field array

setups, structure of the ground and the transmitted waveform. The removal of electromagnetic (EM) coupling is essential for the accurate determination of the source of a given IP anomaly.

Infield techniques for removing EM coupling have existed for several years, with the most frequently used methods being the linear and quadratic phase fitting techniques (Hallof, 1974), which assume that the IP response is independent of frequency. These techniques produce results strongly influenced by noise and fail to totally remove the effects of EM coupling in certain situations. Also the assumption that the IP response is independent of frequency is not true for certain types of mineralization, especially for sulfides and alluvial clays (Song, 1984). These problems have not prevented phase fitting techniques from being a valuable field tool for the initial recognition and estimation of EM coupling contamination.

The complex resistivity (CR) method was developed (Zonge, 1972) to aid in the discrimination of IP responses resulting from different types of mineralization as well as to allow for better decoupling of the data. CR methods differ from more conventional frequency domain IP methods in that measurements are made over a wide range of frequencies, 0.001 to 1000 hertz, rather than a single base frequency and its harmonics. Two differing modes of thought have developed on the interpretation of CR data. One centres on the assertion that the quantity and texture of mineralization is solely responsible for the spectral response of rocks (Pelton et al., 1978). The other is based on the idea that the structure and electrical properties of the host rock will also determine the form of the spectral IP response (Wynn, 1974; Zonge and Wynn, 1975; Wynn and Zonge, 1975).

Pelton et al. (1978) suggest the use of one or more Cole-Cole dispersions to perform mineral discrimination and remove EM coupling from CR data. It was shown that certain IP spectra could be approximated by a Cole-Cole dispersion where the time constant and chargeability parameters could be used to discriminate between uneconomical and economical mineralization. The removal of inductive coupling using two or more Cole-Cole dispersions to approximate the total EM response has been successful in certain situations (Major and Silic, 1981; Wong and Strangeway, 1981). Ideally, this decoupling technique requires the two responses to be well separated in the frequency spectra. However, problems arise in conductive areas where the IP and EM coupling components of the total EM response are overprinting each other. Also, the lack of a physical justification for using a Cole-Cole dispersion to decouple CR data (explanations are based purely on empirical results) means valuable information on the source of EM coupling is lost.

Zonge and Wynn (1975) make use of the differing characteristics apparent in the complex plane plot, namely the slope of the curve at three well separated frequencies, to classify responses due to different mineralization types and environment. This classification of mineralization and the geological environment in which it occurs can be used to determine the starting parameters for further modeling of the total EM response (Wynn and Zonge, 1975). Zonge Engineering and Research Organization have developed the program GDPHM to iteratively invert the complete EM response for CR data to a layered earth model. Problems can arise when the mineralization environment cannot be adequately approximated by a layered earth model.

The program EMCUPL (Kauahikauna and Anderson, 1979; Kauahikauna, 1984) computes the EM coupling response of a layered half-space containing complex resistivities. This program is flexible, allowing for a varying number of layers and forms of complex conductivity to be employed. O'Conner (1990) has modified the program to include an anisotropic component in the complex conductivities which he uses to produce the EM response for a series of anisotropic half-space and two layer anisotropic earth models. An anisotropic component in a given complex conductivity, or complex resistivity, greatly simplifies the representation of the directional bias in resistivity due to geological structure. O'Conner demonstrates that a layered earth model can be represented by an anisotropic half-space and compares the EM responses for both. The suggestion is made that the simpler anisotropic half-space model would be more efficient in an iterative inversion procedure to decouple CR data, as it requires fewer parameters and less computational time.

The main purpose of this thesis is the investigation of a decoupling technique based on an anisotropic half-space with complex resistivities. The benefits of using this model in an iterative inversion are its lack of reliance on any prior knowledge of mineralization environment and its ability to efficiently provide an approximation of even the most complex geological situation. It has the potential to approximate the EM coupling response from a simple isotropic layered earth model or a complex set of intersecting vertical fractures containing electrolytes of varying conductivities.

In section one of this thesis a summary of the relevant aspects of IP and EM coupling theory for an anisotropic half-space is given. This is followed by an outline of work done on forward modeling using an algorithm supplied by Scott MacInnes of Zonge Engineering and Research Organization. O'Conner's work using real resistivities is repeated and the results compared to verify the accuracy of Zonge's algorithm. The results of using a simplified constant IP phase and Cole-Cole complex resistivities with various degrees of anisotropy are presented.

Section Two outlines the use of inversion error surfaces in parameter space to determine the linearity and uniqueness of the inversion problem. This is achieved by examining the effect of varying parameters of a given complex resistivity model on the inversion error surface to determine if multiple minima exist in the inversion error. A global search procedure is used to overcome non-uniqueness in the inverse parameter solution and to determine how well resolved the model parameters are.

The final section outlines the controlled random search procedure and details the results of inverting theoretical data with noise present. This is followed by the inversion of two examples of field CR data using a controlled random search procedure with an annealing condition applied. In the first case the pseudosection is of relatively noise free data affected by moderate EM coupling. The second case is for extreme coupling in a high over low resistivity environment in which the data is badly affected by noise. Results are compared with those obtained from Zonge's in house decoupling program (GDPHM). A discussion on the relative success of the technique as well as problems encountered is given.

SECTION I: A SUMMARY OF IMPORTANT ASPECTS OF EM COUPLING THEORY AND A REVIEW OF FORWARD MODELING

(2.0) THE IP EFFECT AND EM COUPLING PROBLEM:

The following is a summary of important aspects of theory derived through previous work on the IP effect and EM coupling problem. This covers work done by Wait (1959) on the frequency dependence of resistivity as well as the directional dependence of resistivity (Frischknecht, 1966). A brief summary of work done on the EM response for an anisotropic half-space (O'Conner, 1990) is also given.

(2.1) Frequency Dependent Complex Resistivities

In the past, laboratory experimentation on rock samples and field measurements have indicated that rock resistivity, or conductivity, is frequency dependent. Early studies using rock samples allowed the resistivity to be conveniently described in terms of a complex function of frequency (Wait, 1959). The current density J for a rock is related to the electric field E, for a time harmonic field, by

$$J_j = \sigma_j(\omega)E_j \qquad (2.0)$$

$\sigma_j(\omega) = \sigma_j + i\omega\epsilon_j$ is complex conductivity
σ_j = real conductivity
$\omega = 2\pi f$ is angular frequency
f = frequency
ϵ_j = permittivity
$i = \sqrt{-1}$

Complex resistivity is the inverse of complex conductivity

$$\rho_j(w) = (\sigma_j(\omega))^{-1} \qquad (2.1)$$

The current can be separated into conduction and quadrature components. The conduction current is in phase with the E field and is directly proportional to the conductivity. Conduction currents are related to the ordered motion of free charges, such as the motion of ions in the pore fluids of rocks. The quadrature current is out of phase with the E field and is proportional to the angular frequency and permittivity. Quadrature currents are related to time dependent changes in the distribution of bound charges.

Polarization effects in rock media tend to be prominent in the quadrature component of current and hence are represented by phase effects in frequency domain IP methods. Electromagnetic coupling contributes to the quadrature as well as conduction current components.

(2.2) Anisotropy

The directional dependence of any effective physical property is termed anisotropy. Directional dependence of resistivity due to variations of the electrical properties within a media is termed electrical anisotropy. Anisotropy of a media will be defined in terms of the electrical properties of the media for the purposes of this thesis.

Anisotropic media have the current density distorted in the direction of the lowest resistivity and it is this which sets it apart from isotropic media. The anisotropy of a media with complex resistivities will be a complex function of frequency. The anisotropic effect can be divided into micro- and macro-, anisotropic components (Keller and Frischknecht, 1966) with micro-anisotropic effects being due to preferential orientation of particles in the rock media while macro-anisotropic effects are due to large scale electrical features in the rock. Micro-anisotropy is observable in rock samples and is a property of rock type. Macro-anisotropy is related to large scale geological features such as structure, brecciation or interbedded sedimentary units.

An anisotropic half-space forward model is used as it takes into account not only macro- but also micro-anisotropic effects occurring for a given point under the ground. Anisotropy is represented at each point by assigning vertical and horizontal components of resistivity. These components of resistivity are assigned independently of those at neighboring points. This allows for a simplistic as well as realistic representation, as the anisotropic half-space model will allow for anisotropic effects within stratigraphic units as well as those occurring between units.

The constant of anisotropy for a half-space with different horizontal and vertical resistivities is taken as the square root of the ratio of vertical and horizontal components of resistivity.

$$K(w) = \left[\frac{\rho_v(\omega)}{\rho_h(\omega)} \right]^{\frac{1}{2}} \qquad (2.3)$$

$$\rho_x = \rho_y = \rho_h(\omega) \quad \text{horizontal component}$$
$$\rho_z = \rho_v(\omega) \quad \text{vertical component}$$

The constant of anisotropy (K) differs from the coefficient of anisotropy defined for layered rocks. The coefficient of anisotropy for layered rocks is the ratio of components of resistivity which are perpendicular and parallel to the orientation of layering in the rock. It will always be greater than or equal to one. The constant of anisotropy (K), for an anisotropic half-space, is calculated using the ratio of the vertical and horizontal components of resistivity. It can be greater than or less than one. These two measures of anisotropy are only equivalent for horizontally layered rocks, where the horizontal component of resistivity is parallel to the layering in the rock.

O'Conner (1990) describes the classification of simple geological structures using the anisotropic constant. Essentially, values of anisotropy (K) greater than one indicate flat lying laminated structures and layering with a low over high resistivity contrast (Fig 2a). Values of K less than one are expected for vertical pipe-like structures and high over low resistivity contrast (Fig 2b). A resistive flat lying layer over a conductive unit will produce a vertical distortion in the directional dependence of the resistivity. This would produce an anisotropic constant less than one.

It should be pointed out that current can be channeled horizontally along a fault or vertical structure because the resistivity will be predominantly lower in a horizontal direction. This would produce an anisotropic constant greater than one. More complicated orientations could be used by changing the anisotropic constant such that the x and z or y and z directions are equal.

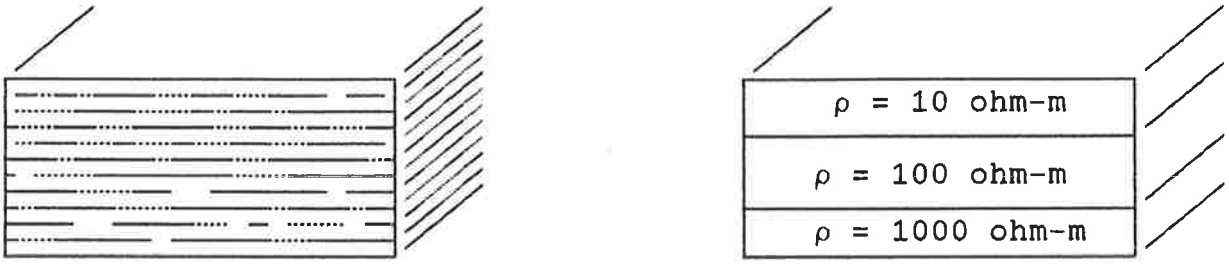

$K(\omega) > 1.0$

$\rho_h(\omega) < \rho_v(\omega)$

(a) FLAT LYING LAMINATED STRUCTURES
AND LAYERED STRUCTURES (LOW OVER HIGH RESISTIVITY)

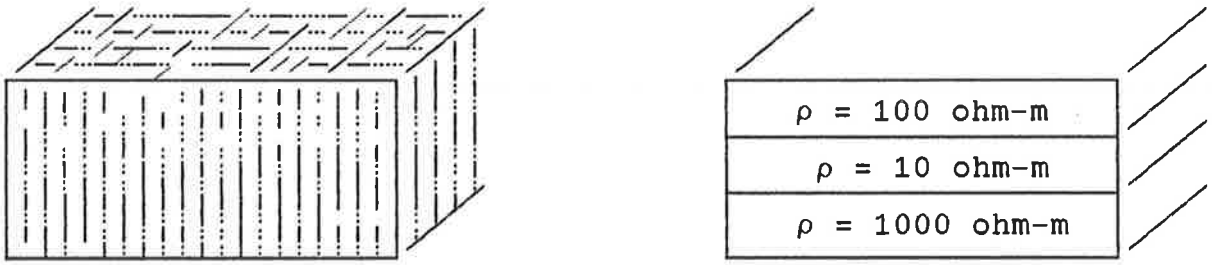

$K(\omega) < 1.0$

$\rho_h(\omega) > \rho_v(\omega)$

(b) VERTICAL VEINLETS, FRACTURES
AND LAYERED STRUCTURES (HIGH OVER LOW RESISTIVITY)

Figure 2.0: Physical examples for an (a) Anisotropic constant (K) greater than one and (b) Anisotropic constant (K) less than one

(2.3) EM Coupling Response for an Anisotropic half-space

Sunde (1949) presents a basic approach to solving the mutual impedance of grounded wires on a homogeneous half-space and gives approximations that allow a numerical approach to the problem. Numerical methods have been used to solve the mutual impedance of grounded wires over a host of earth models from a simple homogeneous isotropic earth (Millet, 1967) to the more complicated layered earth with complex conductivities (Dey and Morrison, 1973).

The following is a summary of the important aspects of earlier work on EM coupling as it applies to the mutual impedance of grounded wires over a homogeneous anisotropic half-space.

Mutual impedance or EM coupling occurs between the receiver and transmitter arrays of most field setups and can be divided into three contributing types; capacitive, resistive and inductive components. The capacitive component is due to electrostatic effects between the receiver and transmitter wires and the earth. Resistive effects are due to current being driven into the ground at the transmitter electrodes. An inductive effect occurs due to mutual induction directly between the transmitter and receiver arrays as well as indirectly via structures in the earth. The contribution of the capacitive component to the total EM coupling response is negligible.

Mutual impedance between two grounded wires on the surface of the earth (Fig 2.1) can be represented in terms of two functions P and Q.

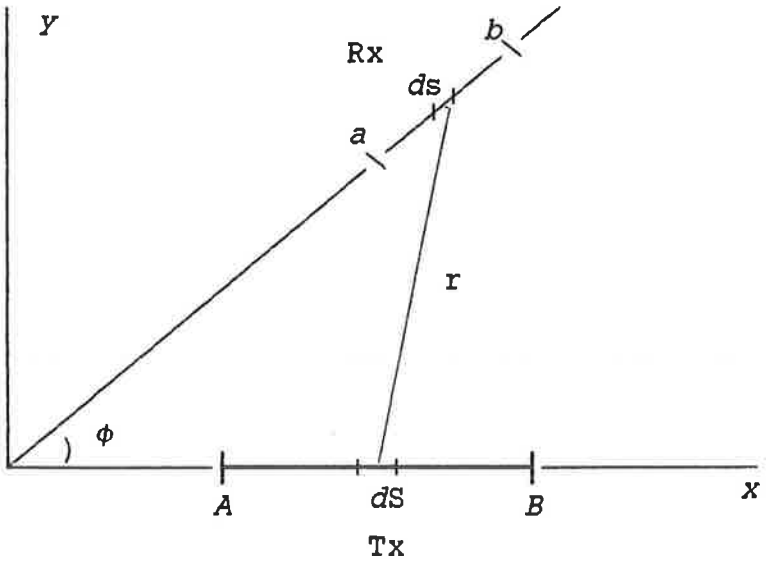

Figure 2.1: Geometry of straight grounded wires (A,B) and (a,b) on the surface of the earth for the calculation of the complex impedance. When measurements are made for a dipole-dipole array the angle ϕ is zero.

The complex impedance due to coupling is given by Wynn and Zonge (1975),

$$Z_{Ss} = P + Q \qquad \text{Complex Impedance} \quad (2.4)$$

where,

$$P = \int_{A}^{B}\int_{a}^{b} P(r)\cos\phi \; dSds \qquad \text{Inductive term} \quad (2.5)$$

$$Q = \int_{A}^{B}\int_{a}^{b} \frac{d^2}{dSds} Q(r) \; dSds \qquad \text{Resistive term} \quad (2.6)$$

$$= Q(r_{Aa}) - Q(r_{Ba}) - Q(r_{Ab}) + Q(r_{Bb})$$

P is vectorial in nature and is a function of frequency as well as separation between the transmitter and receiver wires. The vectorial nature of P means that during integration a cosine of the angle ϕ between the two line elements dS and ds is implicitly included. It is for this reason that P is called the purely inductive term as its calculation is of the mutual impedance along the entire length of the wires. Inductive coupling will be at a minimum when the dipole size is small, frequency is low, resistivity is high and the wires are perpendicular. The maximum inductive coupling will occur when the dipole is large, frequency is high, resistivity is low and wires are parallel.

Q is scalar in nature, varying only with the distances between the grounded electrodes of each dipole. Q is called the grounding function or resistive term as it represents the mutual impedance between the grounded ends of the dipoles. In the case of an isotropic half-space, the resistive coupling is determined only by frequency and separation between transmitter and receiver wires. For the case of a layered earth, resistive coupling also becomes dependent on the resistivity profile of the ground.

In an anisotropic half-space the inductive component, P(r), depends only on the horizontal resistivities. The expression for P(r) can be shown to be the same as that for an isotropic half-space (O'Conner, 1990). However, there are some differences between the expressions for Q(r) for isotropic and anisotropic cases. O'Conner (1990) demonstrated the major difference between the two cases by deriving the expression for Q(r), in the anisotropic case, at a frequency of zero;

$$Q(r) = \frac{1}{2\pi r(\sigma_h \cdot \sigma_v)^{\frac{1}{2}}} \quad \text{for an anisotropic half-space at a frequency of zero} \qquad (2.7)$$

where r is the separation between grounded points
$\sigma_h = \rho_h^{-1}$ is the horizontal conductivity
$\sigma_v = \rho_v^{-1}$ is the vertical conductivity

Q(r) then depends on frequency, separation of grounded points and also the anisotropy of the ground. The anisotropy of the ground can be shown to be an approximation of the resistivity profile of a layered earth model. The contribution of the Q(r) function to the mutual impedance approaches zero as the separation between grounded points gets very large. To prevent any contribution from resistive coupling, an ungrounded loop can be used for either the transmitter or receiver as the Q(r) function will be zero. In this case, the mutual impedance will have no grounded component and would be independent of vertical resistivities and as such anisotropy.

(3.0) FORWARD MODELING:

Calculating the EM coupling and IP responses for given earth models allows an insight into how coupling manifests itself in CR data. Previous work has concentrated on the use of both isotropic and anisotropic layered earth models (Hohmann, 1973; Dey and Morrison, 1973; Wynn and Zonge, 1975). Tripp et al. (1990) inverts diagonals (Fig 3.0) of spectral IP data to a layered earth model using an iterative procedure.

A simpler model to employ in an iterative procedure would be an anisotropic half-space with complex resistivities, which requires fewer parameters to generate a wide variety of EM responses. O'Conner (1990) uses an anisotropic half-space with real resistivities to produce EM coupling responses for a series of situations. This work is repeated in chapter 3.1 to verify the accuracy and effectiveness of the modeling algorithm supplied by MacInnes of Zonge Engineering and Research Organization. His algorithm uses the closed form of the integral for the inductive coupling component (2.5) derived by Wait (1959), where as the program EMCUPL (Kauahikauna,1984) modified by O'Conner (1990) uses a numerical approximation.

The effects of parameter changes on the total EM response for an anisotropic half-space with a given complex resistivity model are investigated. Results of using constant IP phase shift complex resistivities as well as the Cole-Cole dispersion IP model are presented. Data presentation is in the form of a complex plane plot of real and imaginary components of the CR-IP response, normalized by the real component at the lowest

The normalized CR-IP response is calculated at five frequencies per decade, logarithmically spaced, ranging from 0.001 to 10000 Hz. Separate plots of magnitude and phase versus frequency are also supplied for the isotropic cases.

The dipole-dipole survey array configuration (Fig 3.0), a common method used to collect IP data, is employed when calculating the EM coupling response. This array consists of equal length transmitter and receiver dipoles separated by a multiple of the dipole length. A separation of two dipole lengths corresponds to an n-spacing of one with each consecutive increase in separation resulting in an increase in n-spacing as well as the depth of investigation.

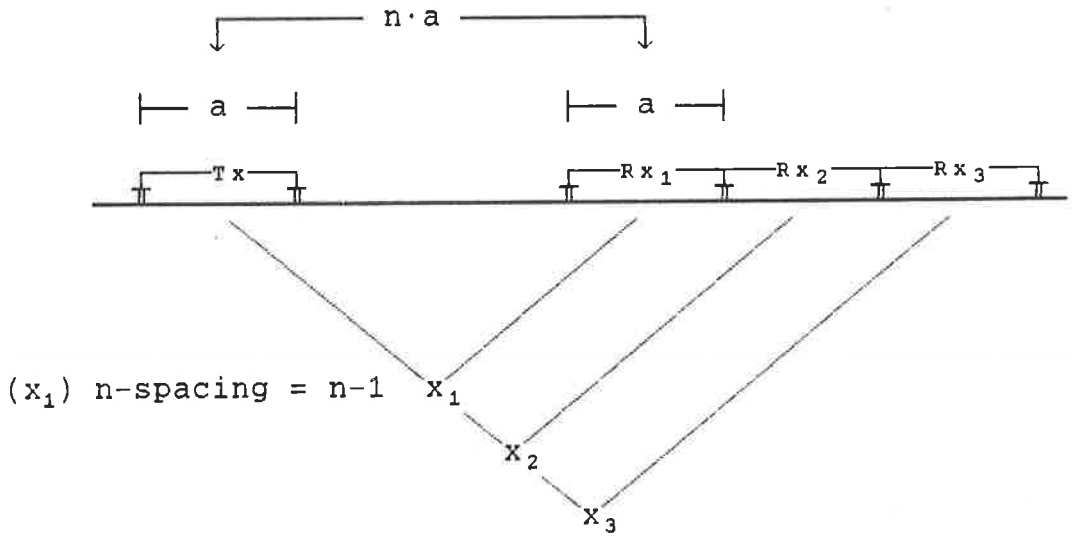

Figure 3.0: The Dipole-Dipole field survey array showing the relationship between n-spacing and the length of transmitter and receiver dipoles (ie: a-spacing). The pseudo depth points (x_1,x_2,x_3) form a diagonal of CR-IP data.

(3.1) Real Resistivity Models

EM responses for an anisotropic half-space with real resistivities were calculated using both MacInnes' algorithm and the modified version of EMCUPL, used by O'Conner (1990), and the results are compared. The two algorithms produced identical results; however, comparisons of computational times indicated MacInnes' algorithm was consistently quicker than the modified EMCUPL.

Data has been calculated for a 100 m dipole-dipole array, at an n-spacing of 6, over a half-space with a mean resistivity of 100 ohm-m. Figure 3.1 is the isotropic case where the ratio of vertical to horizontal resistivity (K^2) is one. Models were run varying values of the constant of anisotropy from one fifth to five (Fig 3.2) to illustrate the effect of anisotropy on the EM response.

This modeling indicates that coupling effects become more apparent in the imaginary component of the complex EM coupling curve at lower frequencies than they do in the real component. That is, EM coupling will be evident in the phase measurements of the CR data before any effects are seen in the magnitude. A significant difference in the shape and form of the coupling curve occurs for cases where the anisotropic constant (K) is less than one and cases where it is greater than one.

Complex EM coupling curves for K greater than one (Figs. 3.2c and 3.2d) tend to plot in the first quadrant of the complex plane and are of the same basic form as the isotropic case. At lower frequencies, below 30 Hz, the curves are indistinguishable from the isotropic half-space response. It is

interesting to note that conventional IP methods make a measurement at around 0.125 Hz. This would mean a conventional IP technique would not be able to distinguish an isotropic from anisotropic half-space and so offer minimal information on the underlying structure. At frequencies above 30 Hz the real component decreases and the imaginary component increases relative to the isotropic case. In CR data this is seen as a relative increase in magnitude and decrease in phase. The high frequency intercept of the real axis, which appears as a phase reversal in CR data, is shifted towards the origin relative to the isotropic case.

Complex EM coupling curves for K less than one (Figs. 3.2a and 3.2b) begin in the first quadrant but plot almost entirely in the fourth quadrant of the complex plane. There are now two intercepts of the real axis at high and low frequencies, causing the majority of the phase spectra to be negative. Also, the real component goes through a minimum before increasing to a value greater than one. As the anisotropy increases in the vertical direction, the high frequency intercept shifts away from the origin, causing an increase in magnitude past the dc or starting value in CR data.

EM coupling curves associated with an increase in the vertical resistance, with an anisotropic constant greater than one, are termed positive coupling (Hallof and Pelton, 1980). Those associated with an increase in horizontal resistivity, with an anisotropic constant less than one, are termed negative coupling (Hallof and Pelton, 1980).

Anisotropy produces results which are comparable to those obtained using a layered earth model. A conductive over resistive type of layering in a layered earth model tends to channel

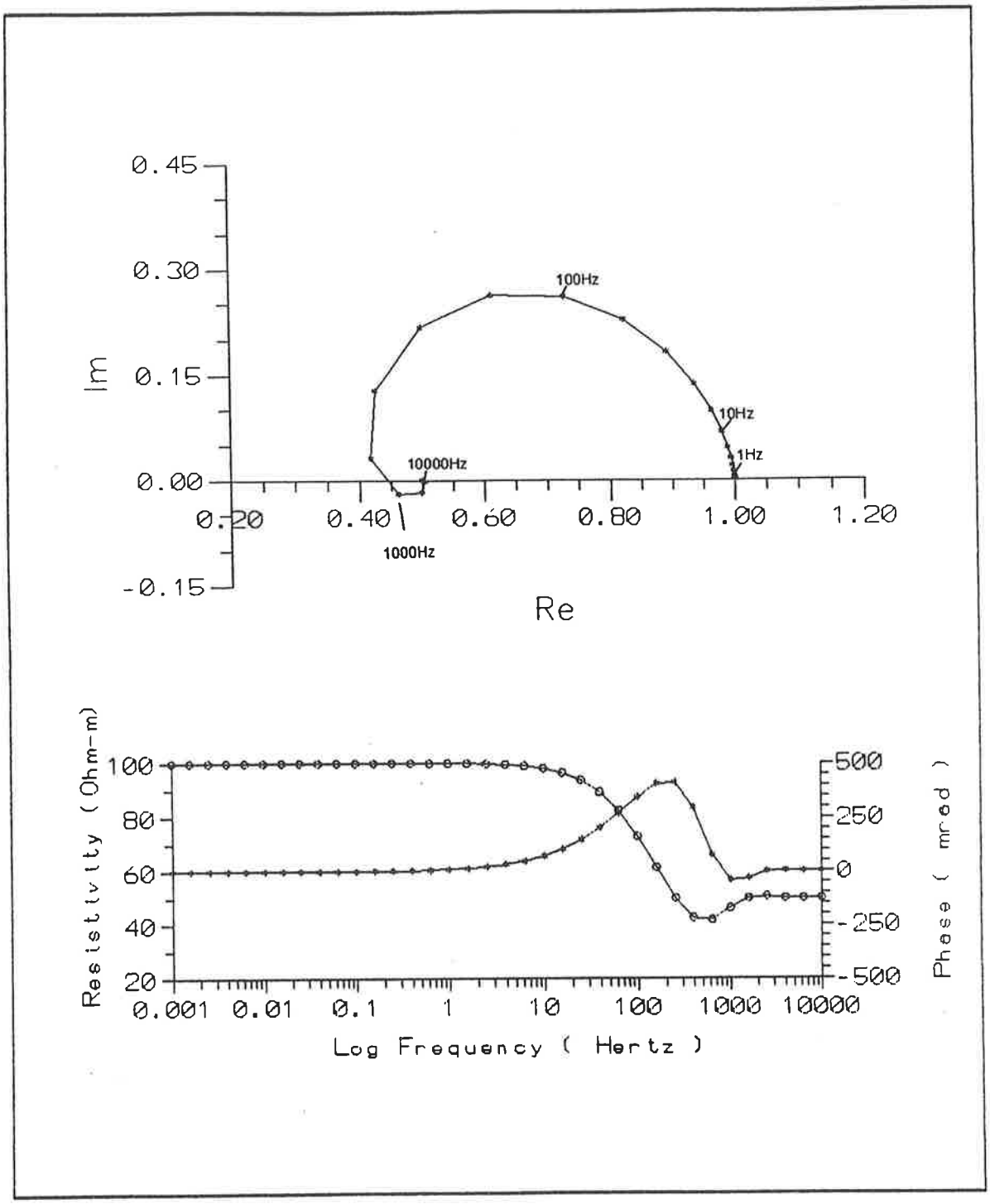

Fig. 3.1: The Complex Impedance curve and corresponding resistivity and phase angle data for an isotropic (K=1) half-space with a real mean dc resistivity of 100 Ohm-m. Calculated for a 100 m dipole-dipole array at an n-spacing of 6 over frequencies from 0.001 to 10 000 Hz.

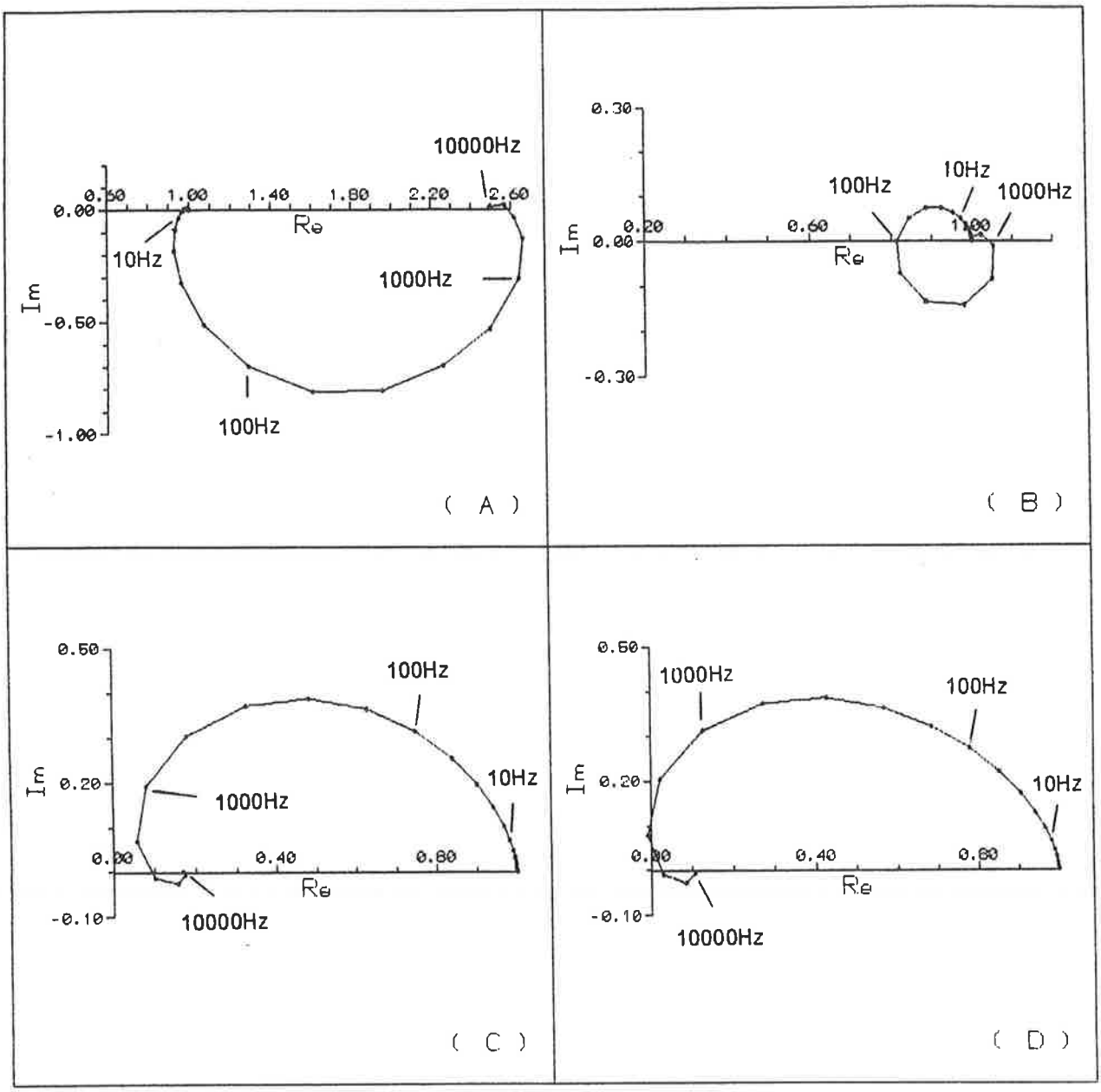

Fig. 3.2: Complex Impedance curves calculated for a 100 m dipole-dipole array over anisotropic half-spaces with a real resistivity of 100 Ohm-m and anisotropic constants of (a) K = 0.2 (b) K = 0.5 (c) K = 3.0 (d) K = 5.0

current horizontally and produce a positive coupling curve. The vertical component of resistivity is greater than the horizontal component, which is similar to having an anisotropic constant greater than one. For some cases of resistive over conductive types of layering the current can be channeled down into the conductive layer to produce a negative coupling curve. This type of negative coupling is relatively moderate in most cases and requires a relatively large contrast between the layers. An advantage of the anisotropic half-space is its ability to produce an extreme negative coupling response associated with steeply dipping low resistivity structures.

(3.2) Complex Resistivity Models

The apparent resistivity measurement taken in a CR-IP survey is essentially the average response returned from a large block of earth. The anisotropic half-space model with complex resistivities uses the geometric average of resistivity (3.0), which is assumed to be equivalent to the apparent resistivity.

$$\rho_{ave} = (\rho_v \cdot \rho_h)^{\frac{1}{2}} \qquad (3.0)$$

ρ_v is the vertical component of complex resistivity
ρ_h is the horizontal component of complex resistivity

When the vertical and horizontal complex resistivities have differing IP contributions, the constant of anisotropy will be complex. The vertical and horizontal IP contributions have been assumed to be equal so as to keep the constant of anisotropy a real quantity.

The modeling algorithm uses the constant of anisotropy, a real quantity, and the geometric average of the complex resistivity containing the IP parameters. When modeling the total EM response, the horizontal and vertical components of resistivity are calculated using

$$\rho_v = \rho_{ave} \cdot K_o$$

$$\rho_h = \frac{\rho_{ave}}{K_o}$$

where K_o is the anisotropic constant

K_o is a real quantity

(3.2.1) Simplified Constant IP phase model

The total EM response was calculated using a constant phase shift applied to the complex resistivity to produce a simplified IP phase effect. This simplified model is based on the three point decoupled phase and has no physical meaning. A constant IP phase shift is used to determine whether a simple shift in phase can account for the IP effect while amplitude variations and the late frequency phase response can be accounted for by EM coupling. In an anisotropic half-space this IP effect is represented by a constant imaginary component of the complex resistivity, which is

$$\begin{aligned} \rho(\omega) &= R_o(\cos(\phi_{ip}) + i\sin(\phi_{ip})) \\ &= R_o \exp(\phi_{ip}) \end{aligned} \qquad (3.1)$$

R_o is dc resistivity, ϕ_{ip} is the constant IP phase

The parameters entered for modeling are the constant of anisotropy, the geometric average of the zero frequency (dc) resistivity and the constant IP phase. The geometric average of the dc resistivity will be referred to as the mean dc resistivity. Vertical and horizontal constant IP phases were assumed to be equivalent to keep the constant of anisotropy a real quantity.

Again, data was calculated for a 100 m dipole-dipole array, at an n-spacing of 6, over an anisotropic half-space with a mean dc resistivity of 100 Ohm-m. The EM responses for complex resistivities with constant IP phases of 25, 50, 75 and 100 mrad over anisotropic half-spaces with constants K of 3.0 and 0.2 were calculated (Figs 3.3 and 3.4).

When coupling is positive, an increase in constant IP phase shift leads the complex coupling curve to be rotated about the origin (Fig 3.3). An increase in the imaginary component is apparent at low frequencies and becomes less evident as the frequency increases. In CR data a noticeable shift in the phase values at low frequencies occurs and is close to the constant IP phase shift value. The magnitude is relatively free of any IP effect.

The negative coupling case has a more complicated relationship to variations in the constant IP phase shift (Fig 3.4). As the constant IP phase shift is increased, the curve appears to rotate about the origin as well as uncurl, with the high frequency intercept occurring at a lower frequency. In this case the imaginary component is characterized by an increase in value at low frequencies. At high frequencies the difference in imaginary component, due to the increased IP phase, is greater. A slight difference in the real component related to variations in the constant IP phase shift is evident at higher frequencies. In CR-IP data this is seen as a shift in phase values at low frequencies, equal to the constant IP phase, with the shift becoming slightly greater as the frequency increases.

In all cases, the EM coupling and IP responses are easy to separate, with the low frequencies being mostly coupling free. However, it is interesting that a complex relationship between the two responses is apparent for the negative coupling case. The

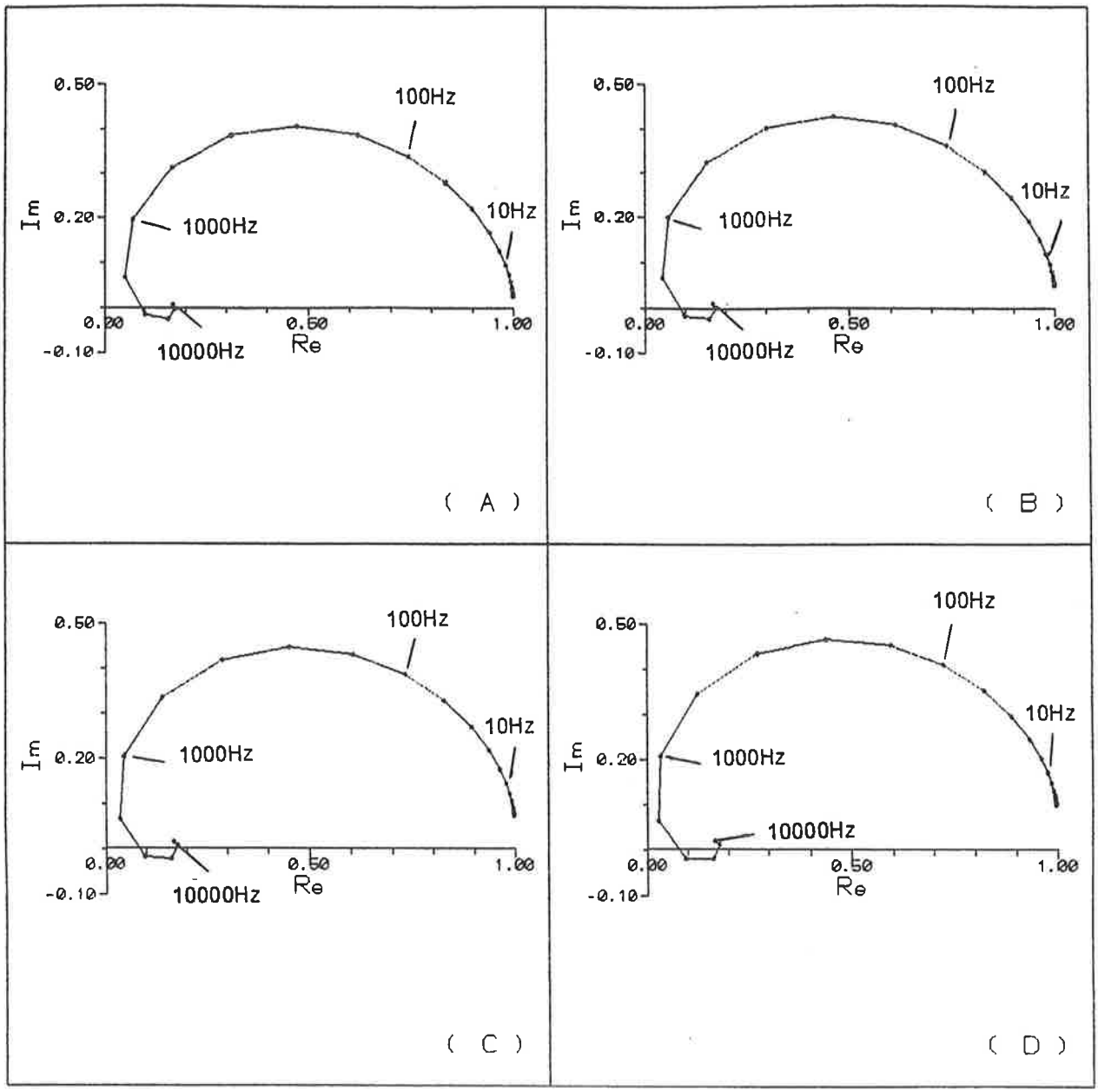

Fig. 3.3: Complex Impedance curves calculated for a 100 m dipole-dipole array over an anisotropic half-space with K=3.0 and constant IP phase shift complex resistivities with a dc resistivity at 100 Ohm-m and constant IP phases of (a) ϕ_{ip} = 25 mrad (b) ϕ_{ip} = 50 mrad (c) ϕ_{ip} = 75 mrad (d) ϕ_{ip} = 100 mrad

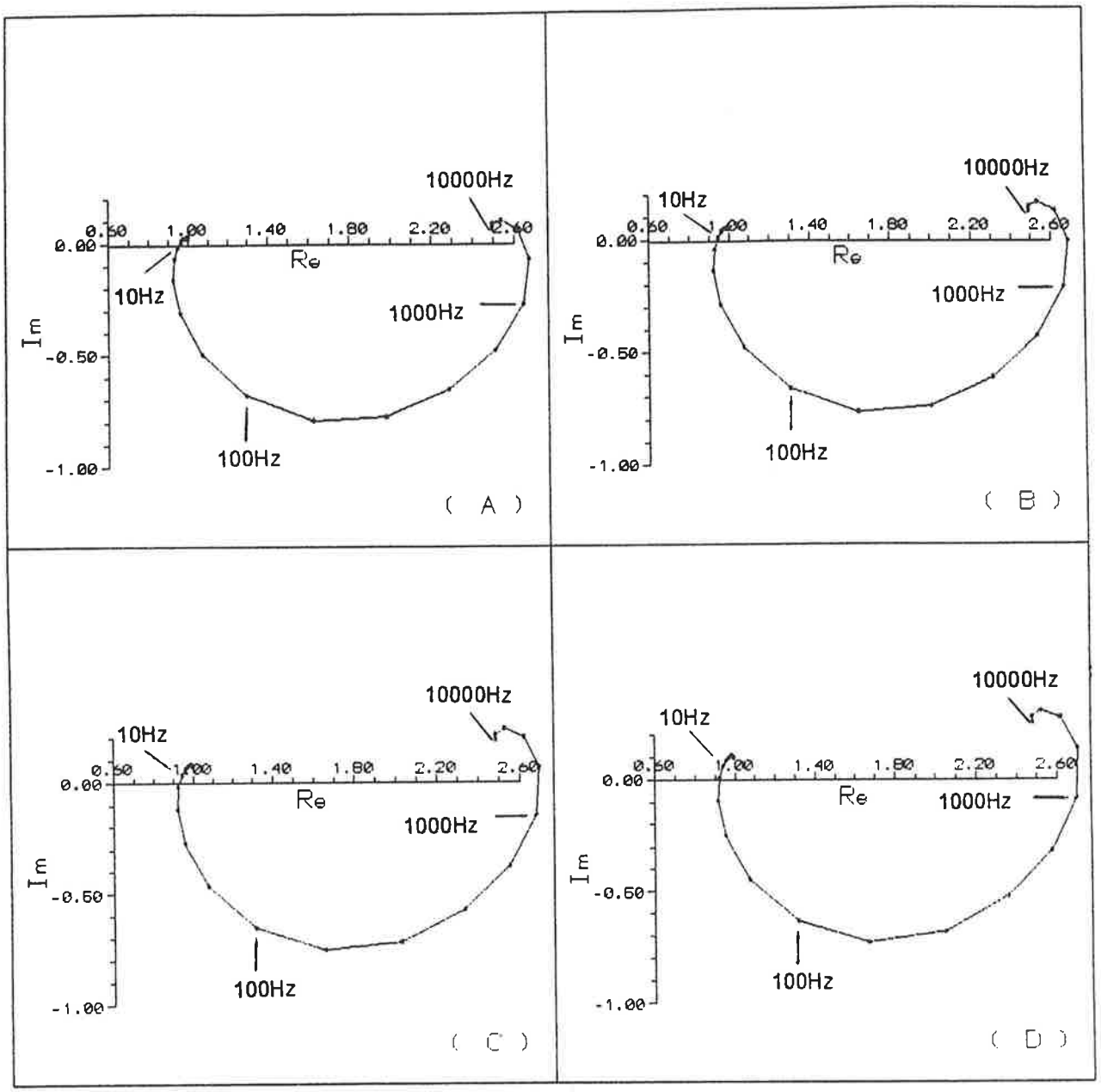

Fig. 3.4: Complex Impedance curves calculated for a 100 m dipole-dipole array over an anisotropic half-space with K=0.2 and constant IP phase shift complex resistivities with a dc resistivity at 100 Ohm-m and constant IP phases of (a) ϕ_{ip} = 25 mrad (b) ϕ_{ip} = 50 mrad (c) ϕ_{ip} = 75 mrad (d) ϕ_{ip} = 100 mrad

IP model used is simple, and this would suggest that the changes evident in the higher frequencies contain not only the contributions of each response but also information on how the two interact with each other. In general, the low frequency end of the total EM spectra, below one hertz, tends to be dominated by the IP response, while the late frequency response is dominated by an EM coupling component.

(3.2.1) Cole-Cole dispersion

A Cole-Cole dispersion (Pelton et al., 1978) describes the complex impedance of a mineralized rock in terms of an analog electrical circuit, giving the essential elements of the response. A Cole-Cole complex impedance model was used to calculate the IP component of the total EM response from an anisotropic half-space. The Cole-Cole complex resistivity is a function of frequency, where resistivity is given by

$$\rho(\omega) = R_o \cdot (1 - m(1 - 1/(1 + (i\omega\tau_o)^c)) \qquad (3.2)$$

$\rho(\omega)$ is the complex resistivity
$\omega = 2\pi f$ is angular frequency
R_o is dc resistivity, resistance of unblocked pores in a mineralized rock sample.
m is chargeability
τ_o is the time constant
c is frequency dependence

$$m = \left(1 + R_1/R_o \right)^{-1} \qquad (3.2.1)$$

R_1 is the resistance of blocked pores

$$\tau_o = X \left(R_o/m \right)^{\frac{1}{c}} \qquad (3.2.2)$$

X is the reactive interfacial component of complex impedance

From equation 3.2 it is apparent that at low frequencies the IP component of amplitude of the complex resistivity asymptotes to R_o. Jagger and Fell. (1988) have found through forward modeling that at high frequencies it approximates $R_o(1-m)$. The following outlines the results of forward modeling carried out to achieve a better understanding of how the various Cole-Cole parameters and the anisotropic parameter interact to affect the total EM response from an anisotropic earth model.

Data was calculated for a 100 m dipole-dipole array, at an n-spacing of 6, over an anisotropic half-space with a mean dc resistivity (R_o) of 100 Ohm-m. Initially, the Cole-Cole parameters were chosen to model a porphyry-copper type mineralization (O'Conner 1990). Chargeability (m) is set to 0.3, time constant (τ_o) to 1.0 , and frequency dependence (c) at 0.5. This Cole-Cole dispersion is for an average sulfide content of 7.5 volume percent with an average grain size of 7.5 mm. The response for an isotropic half-space (Fig 3.5) is characterized by a steady increase in phase and decrease in magnitude up to a frequency of 10 Hz, where the EM coupling begins to dominate the response. The form of the complex plane curve differs markedly

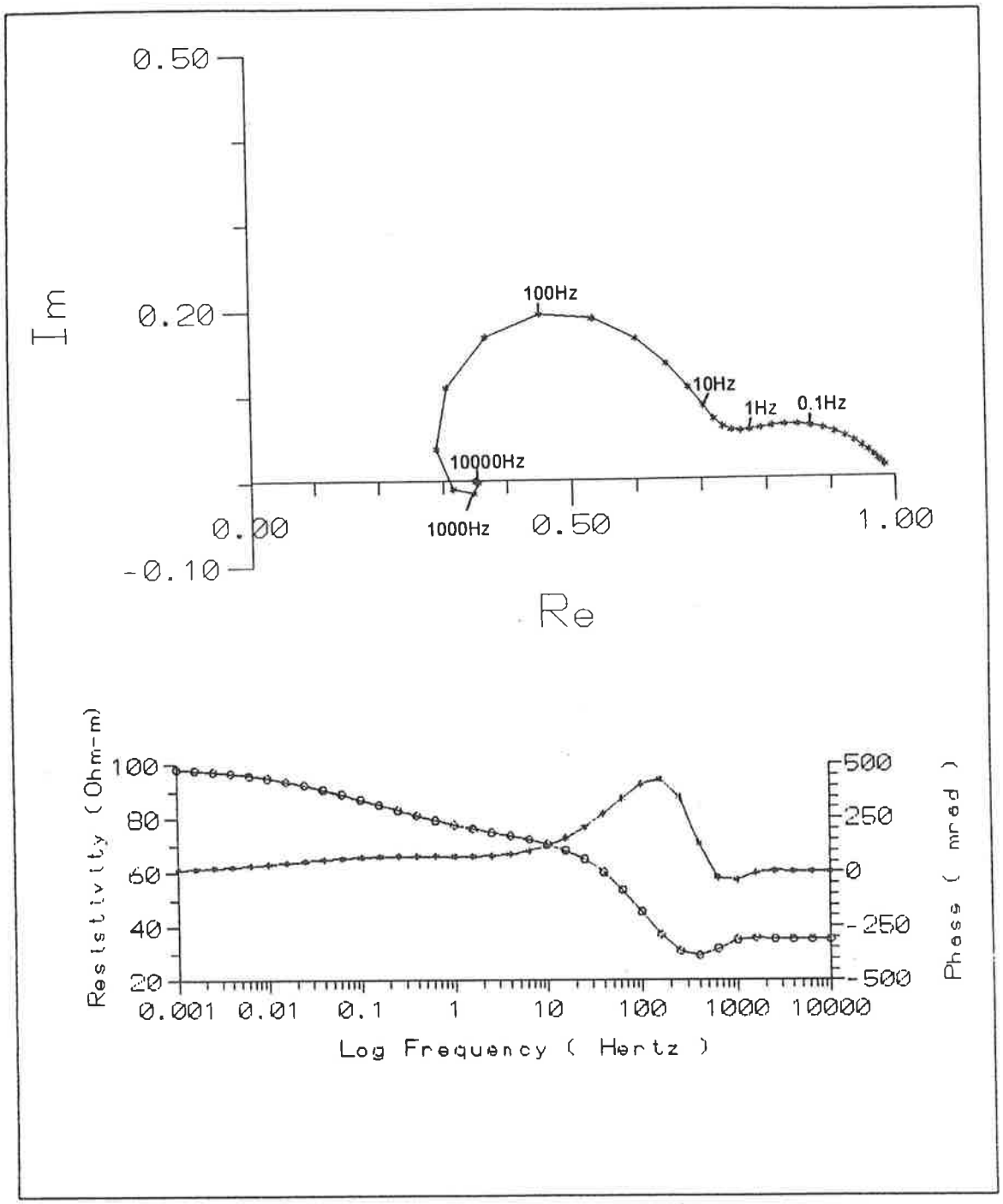

Fig. 3.5: The Complex Impedance curve and corresponding resistivity and phase angle data for an isotropic (K=1) half-space with Cole-Cole complex resistivities. The Cole-Cole dispersion has a mean dc resistivity (R_o) of 100 Ohm-m, chargeability (m) of 0.3, time constant (τ) of 1.0 and frequency dependence (c) of 0.5.

from the real resistivity case as it contains a low frequency peak corresponding to the IP effect and a high frequency peak corresponding to the EM coupling effect.

EM responses were calculated for the above Cole-Cole complex resistivity over anisotropic half-spaces with constants K of 5.0, 3.0, 0.5 and 0.2 (Fig 3.6). Again the responses are dominated by low and high frequency peaks. Components of the total response associated with EM coupling and IP effects are clearly separated and may be attributed to the choice of time constant. Comparing the responses to that for the isotropic case (Fig 3.5), the high frequency peak tends to change form dramatically while the low frequency peak is relatively unchanged. Thus, the influence of the frequency dependence parameter on the low frequency IP response is relatively unaffected by EM coupling. When the two responses are well separated, as is the case here, there is no dependence between the constant of anisotropy (K) and frequency dependence (c) parameters. However, when overprinting of the two responses occurs the effective contribution of the frequency dependence can be reduced by the presence of coupling.

To further investigate the effects of given parameters, the algorithm was run for an isotropic half-space (K=1) and various Cole-Cole parameter values (Figs 3.7 to 3.9).

The total response was calculated for values of chargeability (m) of 0.1, 0.5, 0.7 and 0.9 (Fig 3.7). A comparison of the results with figure 3.6 indicate that an increase in chargeability causes a flattening and elongation of the coupling curve along the real axis. As the chargeability is increased, magnitude decreases more rapidly with frequency and the maximum phase value is decreased in CR data.

The contribution of the IP component to the total EM response increases as the chargeability increases. From equation 3.2 it is apparent that an increase in the chargeability (m) will lead to an increase in the sensitivity of the complex resistivity to changes in the time constant (τ_o) and frequency dependence (c). Variations in chargeability affect the contributions of the imaginary as well as real components of the complex resistivity to the total EM spectral response.

The total response was calculated for values of time constant (τ_o) of 10^{-2}, 10^{-1}, 10^{1} and 10^{2} seconds (Fig 3.8). Comparing these results with figure 3.6 indicate that when the time constant is decreased the IP effect moves up in the frequency spectra, and overprinting by the EM coupling response occurs. For large values of the time constant τ_o, the IP response is small and is well separated from the EM coupling response with a sharp notch between the two. These results verify that separation of the EM coupling and IP responses is governed by the value of the time constant τ_o.

EM responses were calculated for values of frequency dependence (c) of 0.1, 0.25 0.4 and 0.65 (Fig 3.9). When compared to figure 3.6 it is apparent that the sharpness of the low frequency peak corresponding to the IP response is increased as the frequency dependence is increased. It also is apparent that the sharpness of the high frequency peak is also affected by changes in the frequency dependence. The sharpness of the high frequency peak tends to be governed by both the frequency dependence (c) and the anisotropic constant (K).

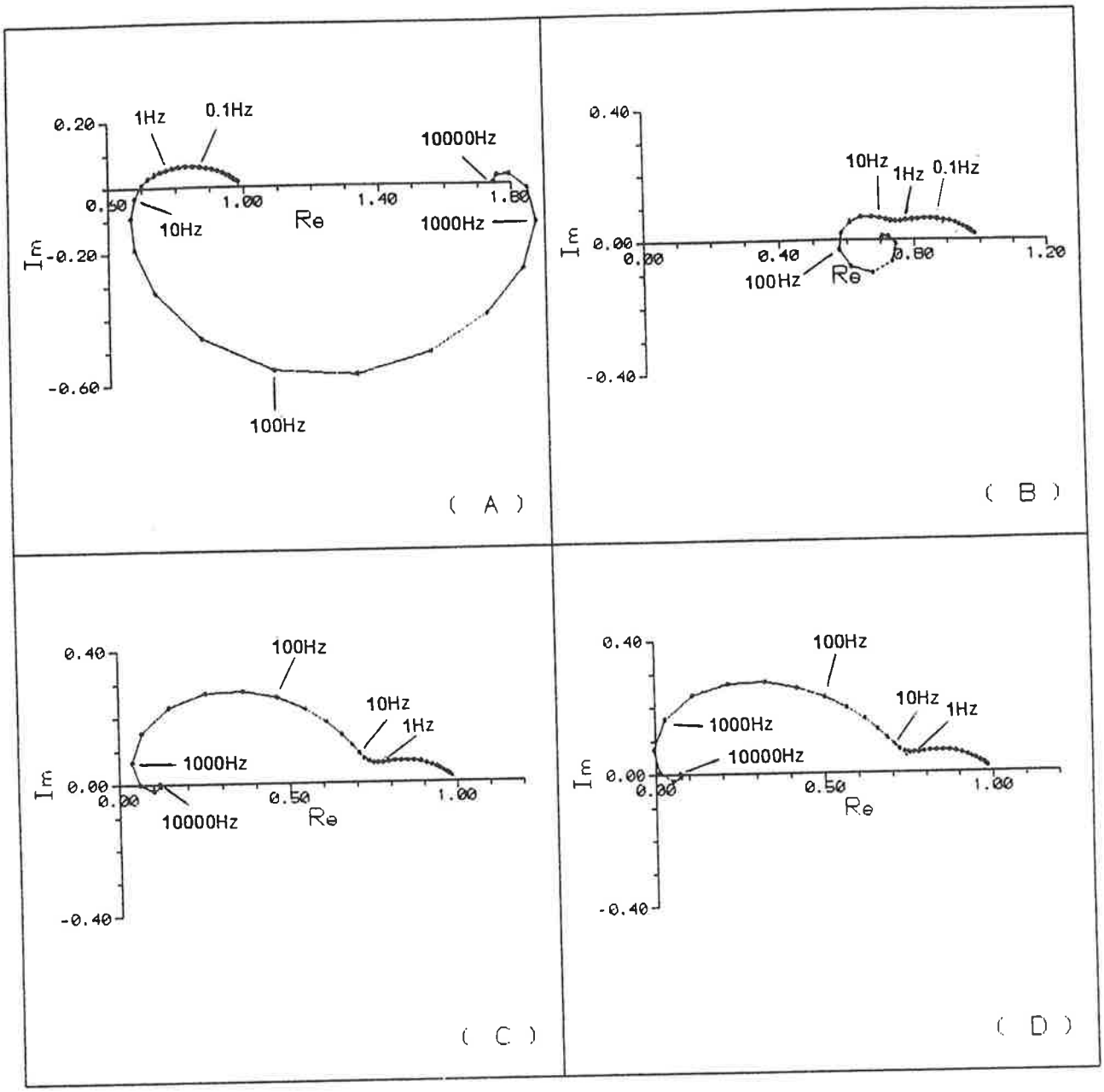

Fig. 3.6: Complex Impedance curves calculated for a 100 m dipole-dipole array over anisotropic half-spaces with a Cole-Cole dispersion. The Cole-Cole parameter values are R_0 = 100 Ohm-m, m = 0.3, τ = 1.0 sec and c = 0.5. With Anisotropic constants;
(a) K = 0.2 (b) K = 0.5 (c) K = 3.0 (d) K = 5.0

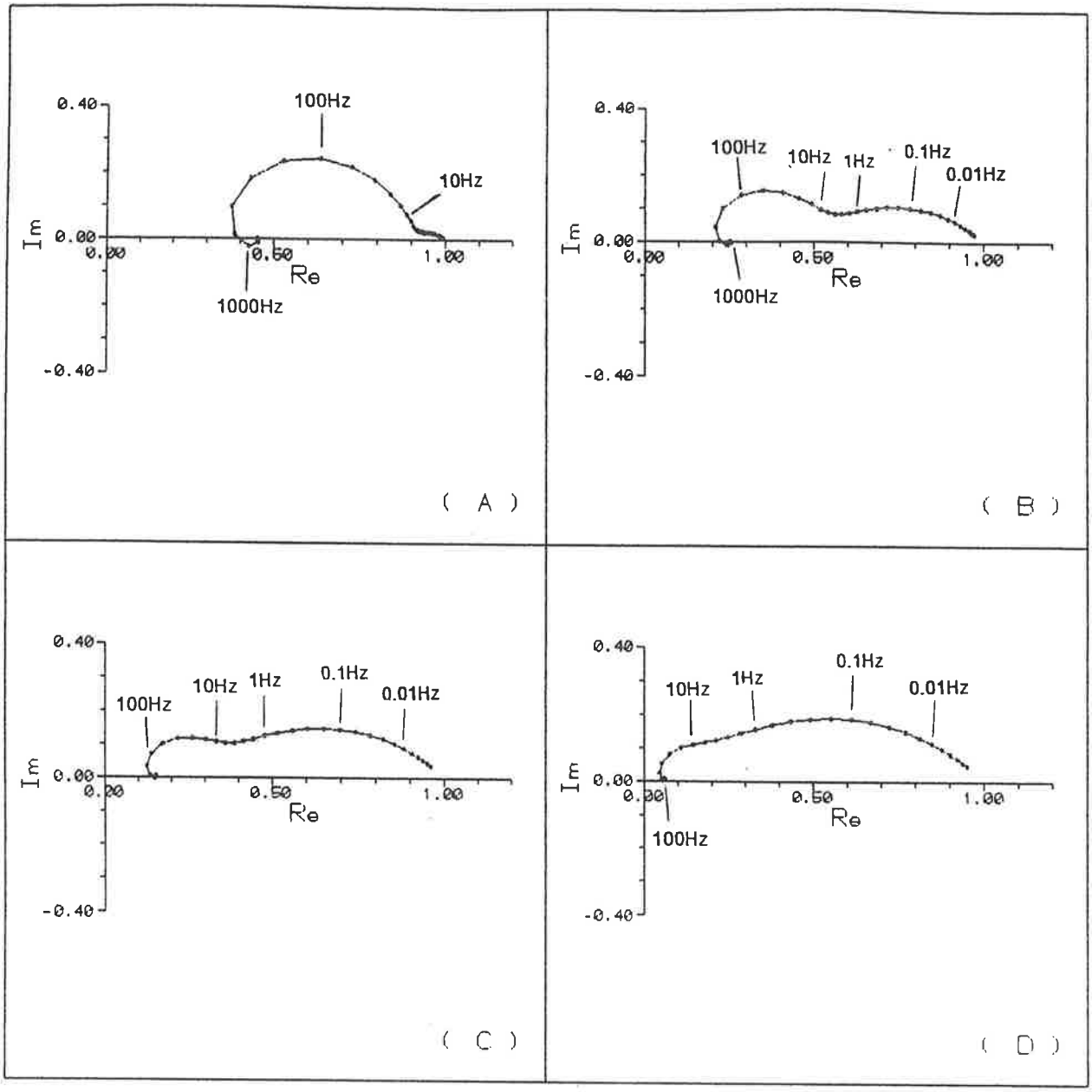

Fig. 3.7: Complex Impedance curves calculated for a 100 m dipole-dipole array over an isotropic (K=1) half-space with a Cole-Cole dispersion. Cole-Cole parameter values are R_0 = 100 Ohm-m, τ = 1.0 sec, c = 0.5 and chargeabilities of (a) m = 0.1 (b) m = 0.5 (c) m = 0.7 (d) m = 0.9

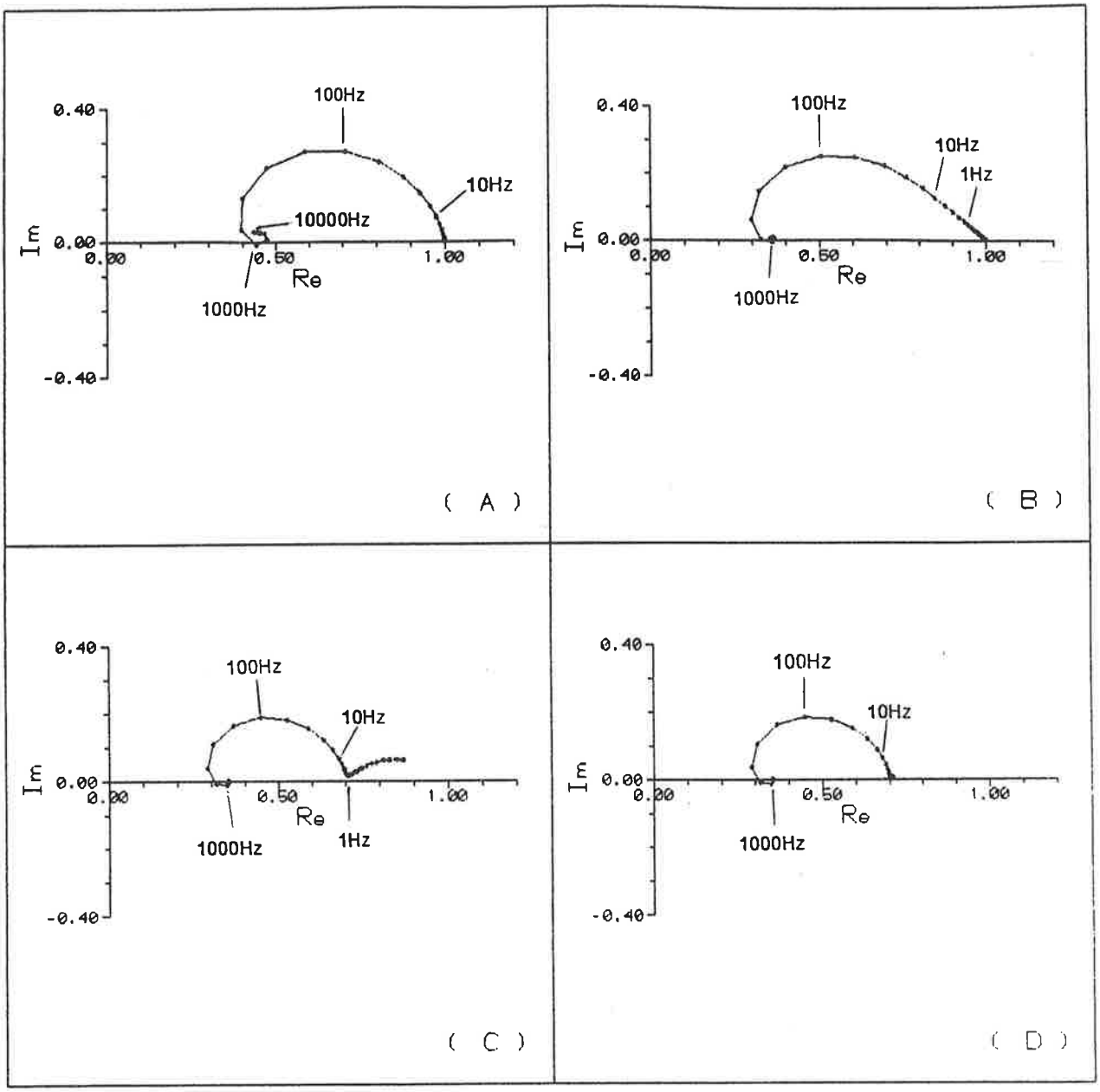

Fig. 3.8: Complex Impedance curves calculated for a 100 m dipole-dipole array over an isotropic (K=1) half-space with a Cole-Cole dispersion. Cole-Cole parameter values are R_0 = 100 Ohm-m, m = 0.3, c = 0.5 and time constants of (a) τ = 0.01 (b) τ = 0.1 (c) τ = 10.0 (d) τ = 100.0 sec

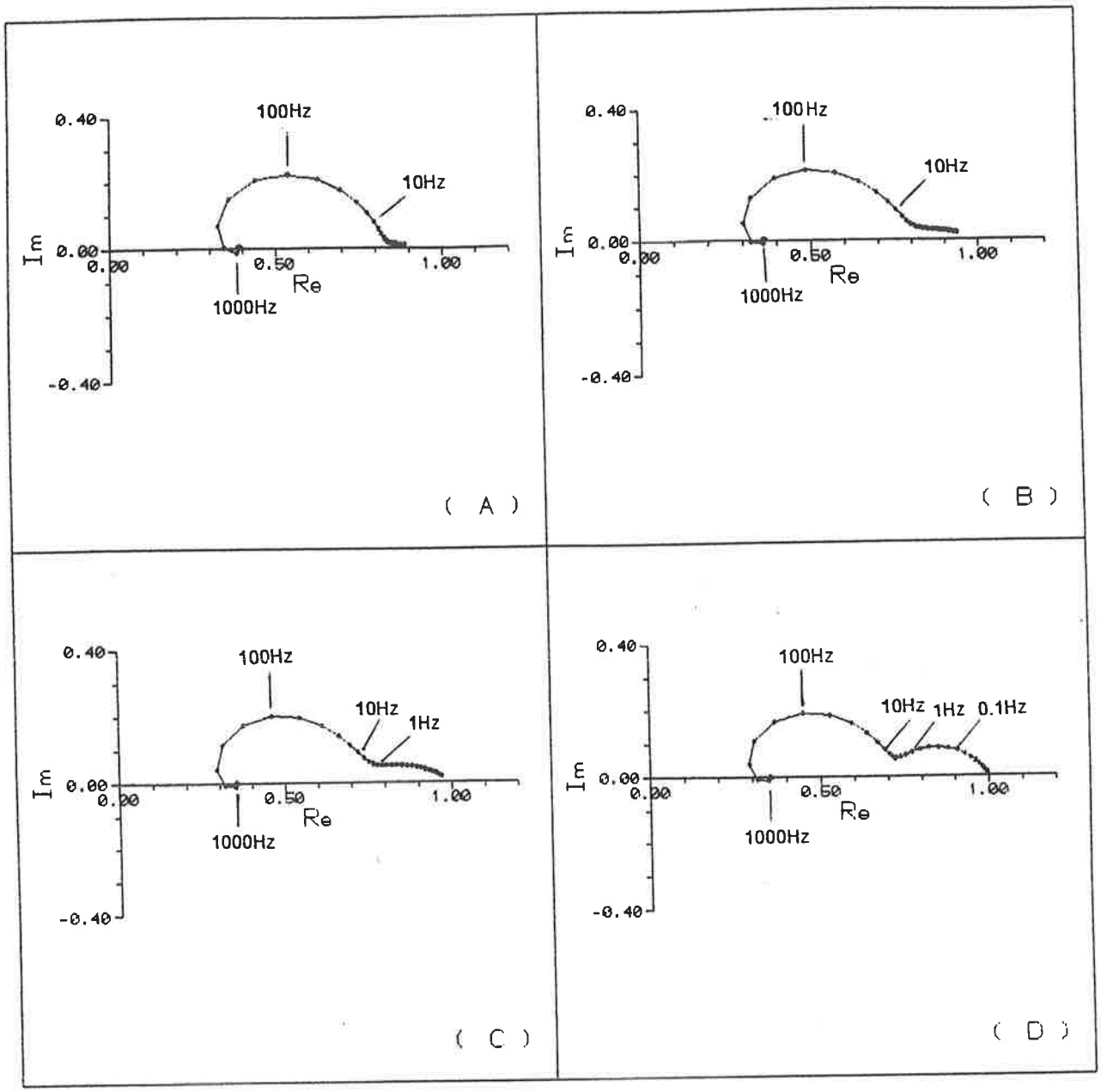

Fig. 3.9: Complex Impedance curves calculated for a 100 m dipole-dipole array over an isotropic (K=1) half-space with a Cole-Cole dispersion. Cole-Cole parameter values are R_0 = 100 Ohm-m, m = 0.3, τ = 1.0 sec and frequency dependence of (a) c = 0.1 (b) c = 0.25 (c) c = 0.4 (d) c = 0.65

(3.3) SUMMARY OF FORWARD MODELING

Forward models have been presented for a half-space varying from isotropic to anisotropic, with resistivities varying from real to complex. Increasing the anisotropic constant above one is equivalent to decreasing the horizontal dc resistivity of the half-space, causing an increase in lateral current flow and producing positive coupling curves. Decreasing the anisotropic constant below one is equivalent to decreasing the vertical dc resistivity of the half-space, causing an increase in vertical current flow and producing negative coupling curves.

The modeling of a polarizable anisotropic half-space was done using a constant IP phase shift complex resistivity. The effect on a positive coupling curve is to rotate it about the origin. Negative coupling curves tend to uncurl as the IP phase is increased.

The spectral response of an anisotropic half-space with Cole-Cole complex resistivities is characterized by a high frequency arc corresponding to EM coupling and a low frequency arc corresponding to the IP response.

Summarizing the effect of Cole-Cole parameter changes on CR survey data;

An increase in chargeability (m) leads to an increase in the IP component of the phase curve and a greater rate of decrease in the amplitude curve.

Increasing the frequency dependence (c) will affect the IP component by increasing the steepness of the phase peak and the slope of the amplitude. An increase in frequency dependence can also affect the high frequency peak associated with coupling when the EM coupling and IP responses overlap.

The Time constant (τ_o) shifts the IP component of the phase and magnitude curves along the frequency spectra. An increase in τ_o shifts the IP component towards lower frequencies and can cause overlapping of the high frequency EM coupling and low frequency IP responses.

dc resistivity will shift the amplitude vertically and has no effect on the phase curve.

SECTION II: UNIQUENESS OF THE INVERSE SOLUTION AND RESOLUTION OF MODEL PARAMETERS

(4.0) PREDICTION ERROR SURFACES AND THE INVERSE SOLUTION:

Choosing the appropriate iterative inversion technique to employ when decoupling CR-IP data requires a better understanding of the inversion problem. An anisotropic half-space with complex resistivities is proposed as the forward model to use in the iterative inversion. This forward model is non-linear in the sense that there is a complex non-additive relationship between the model parameters and the calculated data points. The calculated data is the complex impedance of the grounded wires of the array, which is related to the complex resistivity and anisotropy through the double integration (equation 2.4) of the complex inductive (equation 2.5) and resistive (equation 2.6) terms.

Uniqueness of the solution at convergence for a linear problem is easily determined. However, there is no simple means of determining the uniqueness of a solution for non-linear problems in the absence of prior information. To illustrate this, consider the simple non-linear model $d_i = m_1^2 + m_1 m_2 Z_i$ for data pairs (Z_i, d_i) and parameters m_1, m_2. This can be linearized by transformation to give parameters $m_1' = m_1^2$ and $m_2' = m_1 m_2$, which can be solved by the least squares method. The solutions of the primed parameters are unique; however, the unprimed parameters are non-unique, as the unprimed estimates m_1^{est} and $-m_1^{est}$ will produce identical solutions.

Investigating the question of uniqueness, when inverting for the total EM-IP response, requires an examination of the global properties of the fitting error. This is achieved using the error generated when fitting different pairs of model parameters to a given set of theoretical model parameters.

The measure of fit used is the Absolute Deviation error or L_1 Norm error and is given by

$$L_1 \text{ Norm} = \frac{1}{N-1} \sum_{i=1}^{N} \frac{|x_i - y_i|}{S_i^2} \qquad (4.0)$$

N is the number of data points

x_i is observed data (or data generated from a theoretical model)

y_i is calculated data (or data generated from a set of model parameters selected to fit to the observed or theoretical model data)

S_i is the observed variance of x_i

In an inversion the L1 Norm will be a measure of the fit between the calculated and observed complex impedance curve. CR-IP data is collected as apparent resistivity and phase angle, which are equivalent to the real and imaginary components of the complex impedance. The L1 Norm will be a measure of the difference between the observed and calculated resistivities and phase angles.

An error surface is produced by calculating the L_1 Norm inversion error using a grid search in parameter space over a given theoretical model. The grid search is performed by varying

a pair of model parameters, in discrete steps, over a range of parameter values. The prediction error is then calculated, at each point in the grid search, using the resistivity and phase angle data generated from the theoretical model parameters and that generated from a model containing the parameters being varied. A map of the prediction error, associated with a given theoretical model, is then produced with respect to this particular pair of parameters.

For a given theoretical model, an indication of the relationship between the prediction error and these parameters can be obtained as well as an idea of how sensitive the final inversion solution is to variations in these parameters.

This map of the error between a parameter guess and the true parameter values allows the uniqueness and resolution of the inversion solution to be determined. The geometry of the prediction error surface determines the convergence properties of the inversion, where the presence of multiple minima in the error surface indicate a non-unique solution. The amount of variation in the prediction error, caused by a change in a given parameter guess, is a representation of how sensitive the inversion will be to a given parameter. It follows that an indication of the ability of the inversion process to resolve a given parameter can be given.

An investigation of the effects of general survey geometry and dc resistivity of the earth on the resolution of the IP and anisotropic parameters is made. The effects of the anisotropic parameter and the Cole-Cole IP parameters on the prediction error are also examined. Interdependence of the of various model parameters should be apparent from the shape of the error surfaces.

(4.1) Effects of the General Survey Characteristics

Wait (1982) demonstrates the combined influence that survey geometry, frequency and dc resistivity have on the EM coupling response. Dey and Morrison (1973) give the resistive term Q (equation 2.6) of the complex impedance in terms of a quantity describing the combined influence of geometry, frequency and dc resistivity, where

$$Q(r) = \frac{I\ ds}{2\pi r^3 \sigma_n} \left\{ 1-(1-\delta)e^{(-\delta r)} \right\} \qquad (4.1)$$

δr is a combined quantity that determines the shape of the EM coupling curve and is given by,

$$\delta r = (iw\mu\sigma)^{\frac{1}{2}}\ r \qquad (4.2)$$

$\omega = 2\pi f$ is angular frequency
r is separation
$\sigma = \rho^{-1}$ is dc conductivity

It would be expected that EM coupling increases as frequency increases, dc resistivity decreases and the separation increases. This implies that frequency, separation and the dc resistivity will have an influence on the prediction error, as they will change the form of the complex impedance curve.

Error surfaces were produced for different separations (n-spacings), frequency ranges and dc resistivities (Figs 4.1 and 4.2) to investigate the effect that the combined parameter $\delta \cdot r$ has on the prediction error. The model used is that of an isotropic half-space with constant IP phase shift complex resistivities. The error surfaces are produced by doing a grid search for a range of anisotropic constant values and constant IP phases.

(4.1.1) Varying the Separation

Prediction errors were calculated by doing a grid search over an isotropic half-space with a constant IP phase shift effect of 25 mrad. The standard complex resistivity survey frequency range, the first five odd harmonics of 0.125, 1.0 and 8.0 hertz, was used when calculating the total EM response. DC resistivity was held constant at 100 Ohm-m and the basic survey geometry was of a 100 metre dipole-dipole array. The separation (n-spacing) between the transmitter and receiver arrays was varied and the error surface in anisotropic constant and constant IP phase parameter space was produced.

For an n-spacing of two (Fig 4.1a), separation is at 300 metres, the prediction error surface is dominated by the IP parameter. The presence of a minimum elongated over a range of anisotropic constant values indicates the amount of EM coupling present in the total EM response is minimal. At an n-spacing of four (Fig 4.1b), separation is at 500 metres, the error surface is dominated by two minima of similar intensity centered on the true IP phase parameter value but occurring at different values of anisotropic constant. The amount of EM coupling present in the

total response is increasing, which allows the anisotropy to be better resolved as its influence on the prediction error is greater. The prediction error for an n-spacing of six (Fig 4.1c), separation is at 700 metres, is dominated by a global minimum at the true parameter values and a local minimum situated at a higher value of anisotropy. Even though the anisotropic constant is better resolved at this n-spacing the inversion solution is still non-unique.

In general, the trend in prediction error would indicate that the anisotropic constant (K) is more readily resolved as the n-spacing (separation r) is increased. This can be related to an increase in the EM coupling component of the total EM response calculated over this frequency range.

(4.1.2) Survey Frequency Range

The prediction error was calculated using the same model for a 100 m dipole-dipole array with n-spacing held at six and the dc resistivity constant at 100 Ohm-m. The prediction error was calculated for a single frequency reading (Fig 4.1d), 0.125 Hz and its harmonics, and is dominated by the IP response. This frequency range is commonly used in the field for single frequency CR surveys, as it is possible to recover an IP response relatively free of coupling. The error map produced (Fig 4.1d) here is similar to that for an n-spacing of two (Fig 4.1a) using the spectral IP frequency range. The smaller frequency range, over low frequencies, contains minimal EM coupling information producing an error surface similar to that of figure 4.1a.

The prediction error was calculated using the same model for a 100 m dipole-dipole array with n-spacing held at six; however, the dc resistivity was set at 10 Ohm-m. Error surfaces were produced for single frequency (Fig 4.2a), spectral (Fig 4.2b) and an extended spectral CR-IP (Fig 4.2c) with 35 frequencies ranging from 0.1 to 10 000 Hertz. Inverting the total EM response to retrieve anisotropic information for a single frequency CR survey over conductive ground (Fig 4.2a) is a multi- minima problem. This situation is typical for field data collected in conductive areas. The reason for using so few frequencies is purely economic, as the field and data processing costs are greatly reduced using the single frequency CR method.

In general, as the frequency range goes to higher values it becomes easier to resolve the anisotropic constant. This is expected as EM coupling tends to dominate high frequency data.

(4.1.3) Varying the DC Resistivity

The error map produced for 10 ohm-m ground (Fig 4.2b) is dominated by an intense global minimum and a less intense local minimum, indicating that the use of the normal spectral CR frequency range is sufficient to retrieve anisotropic information. For the case of using a normal spectral CR frequency range over resistive ground (Fig 4.2d), where the dc resistivity was set at 1000 Ohm-m, the error map is dominated by the IP phase. This error surface is similar to those produced for a small n-spacing (Fig 4.1a) and small range over low frequencies (Fig 4.1d) and is indicative of a lack of an EM coupling component in the total EM response.

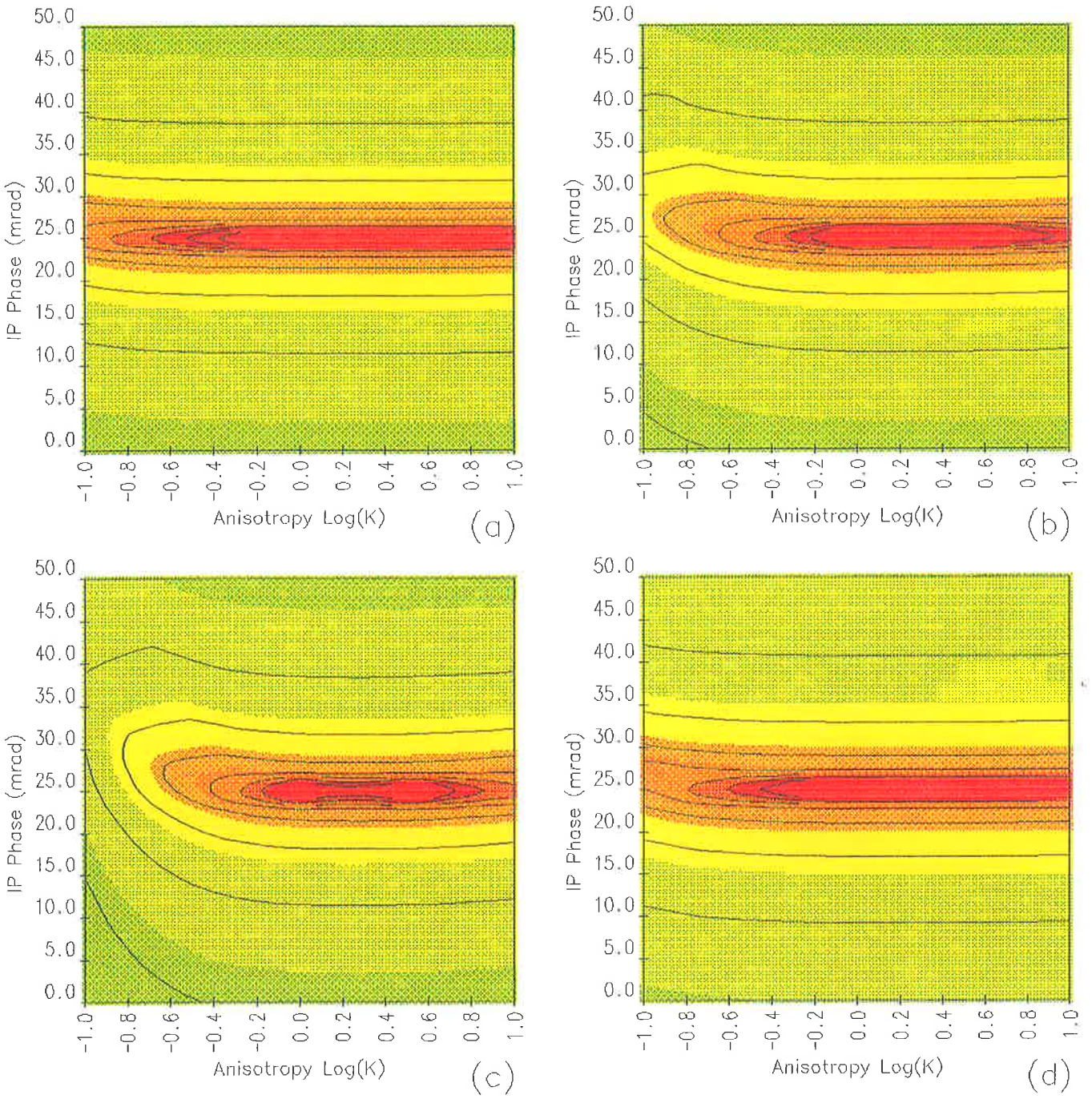

Fig. 4.1 : Inversion error generated by fitting Constant IP phase and log of Anisotropy (K) parameters to an isotropic (K=1) half-space with IP model parameters; DC Res. Ro = 100 Ohm-m and constant IP phase of 25.0 mrad with n-spacings of
(a) N = 2
(b) N = 4
(c) N = 6
(d) N = 6, 5 frequency CR (0.125 and harmonics).

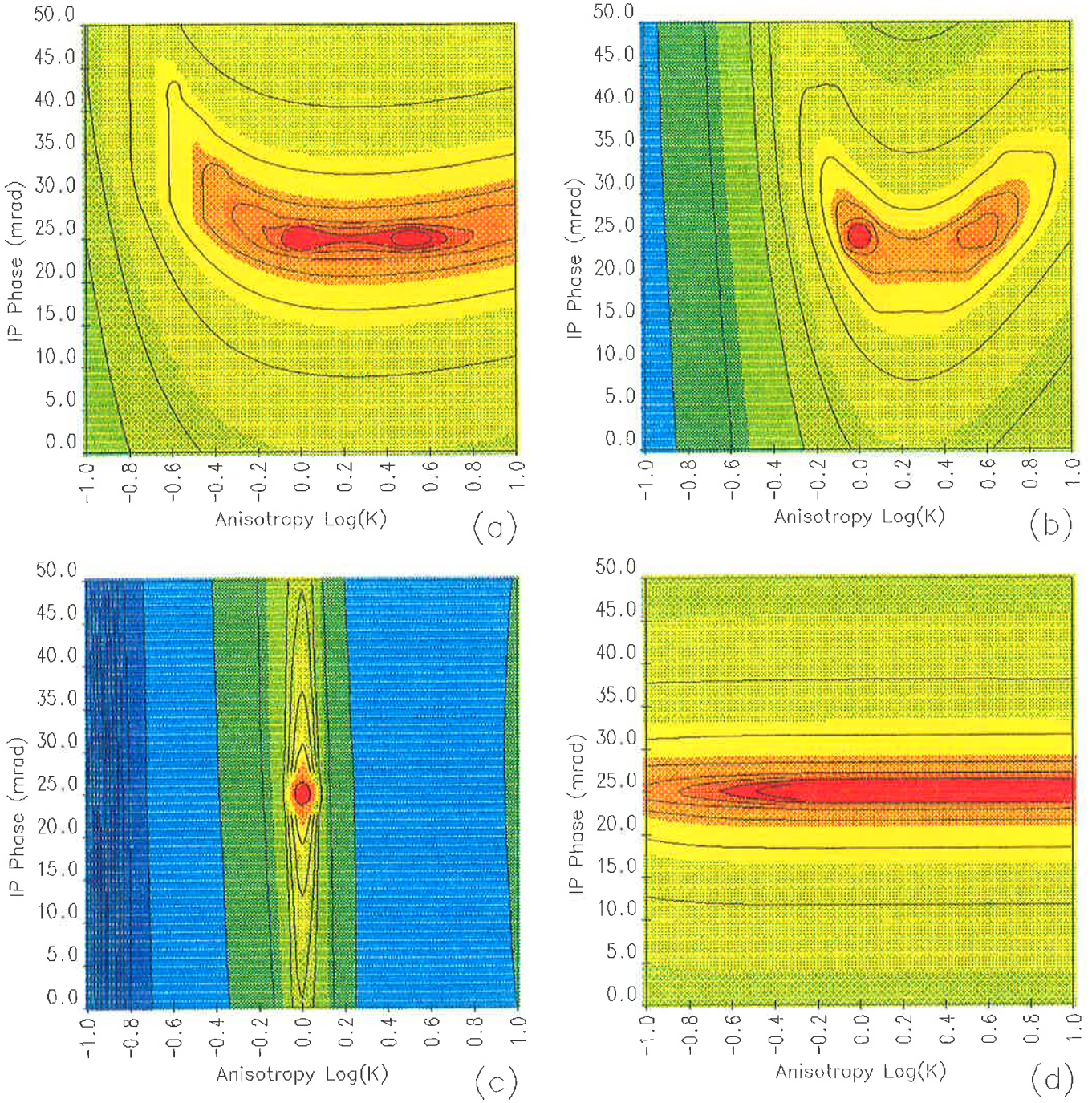

Fig. 4.2 : Inversion error generated by fitting Constant IP phase and log of Anisotropy (K) parameters to an isotropic (K=1) half-space with IP model parameters; Constant IP phase of 25.0 mrad with n-spacing of six and
(a) Ro = 10 Ohm-m, 5 frequency CR (1/8 Hz and Harmonics)
(b) Ro = 10 Ohm-m, 15 frequency CR (1/8, 1.0 and 8.0 Hz)
(c) Ro = 10 Ohm-m, 35 frequency CR
(d) Ro = 1000 Ohm-m, 15 frequency CR

On comparing the error surfaces for 10 Ohm-m (Fig 4.2b) and 1000 Ohm-m (Fig 4.2d) ground with the error surface for 100 Ohm-m ground (Fig 4.1c), it is apparent that the more conductive the ground the greater the influence of anisotropy on the total EM response. Also, the lower the resistivity the greater the influence of EM coupling at lower frequencies.

(4.2) Effect of Varying Anisotropy - K

The prediction error was calculated for a 100 m dipole-dipole array at an n-spacing of six using the standard spectral CR frequency range. Error surfaces were produced for a complex resistivity model consisting of 100 ohm-m earth with a constant IP phase shift of 25 mrad and anisotropic constants of 0.2, 0.5, 3.0 and 5.0 (Fig 4.3). Error was calculated with no background noise present.

For the case of an anisotropic constant (K) of 0.2, the horizontal to vertical resistivity ratio (K^2) is 0.04, the error surface (Fig 4.3a) is dominated by single intense minimum at the true parameter values. There is also a local minimum extending to large values of anisotropy. The shape of the error surface near the correct solution for anisotropy tends to suggest a relationship between the final inverse parameter solutions. If the final anisotropy chosen for a model is slightly less than the true value it is compensated by an increase in the IP phase parameter, as indicated by the minimum shifting along the IP phase parameter axis.

The prediction error surface for an anisotropic constant (K) of 0.5 (Fig 4.3b), with horizontal to vertical resistivity ratio of 0.25, is dominated by a global minimum at the true parameter solution and a shallower more elongate local minimum centered on an anisotropic constant value of 10. The local minimum has a relatively low base level and indicates a similarity between the shape of the spectral EM responses for K values of 0.5 and 10 over frequencies ranging from 0.125 to 72 Hertz. A ridge of high error, peaking at a K value of 1.8, occurs between the two minima.

When the anisotropic constant (K) is equal to 3.0, horizontal to vertical resistivity ratio is 9.0, the prediction error surface (Fig 4.3c) is almost identical to the error surface for the isotropic (K=1) case (Fig 4.1c). In both cases, the global minimum occurs at the true parameter solutions. When the K value is equal to 3.0 a local minimum occurs at a value of 1.0. When the K value is equal to 1.0 a local minimum occurs near a value of 3.0. This is a further indication of the similarity of the coupling curves for different values of anisotropic constant in 100 Ohm-m ground over frequencies ranging from 0.125 to 72 Hertz. In both cases a slight ridge of higher error peaks at a K value of 1.8 between the two minima.

The prediction error surface for an anisotropic constant (K) of 5.0 (Fig 4.3d) has a narrow low elongated over a range of K values punctuated by a global minimum at the true parameter values and a local minimum at a lower value of K. Again, an area of slightly higher error occurs at a K value of 1.8 between the two minima.

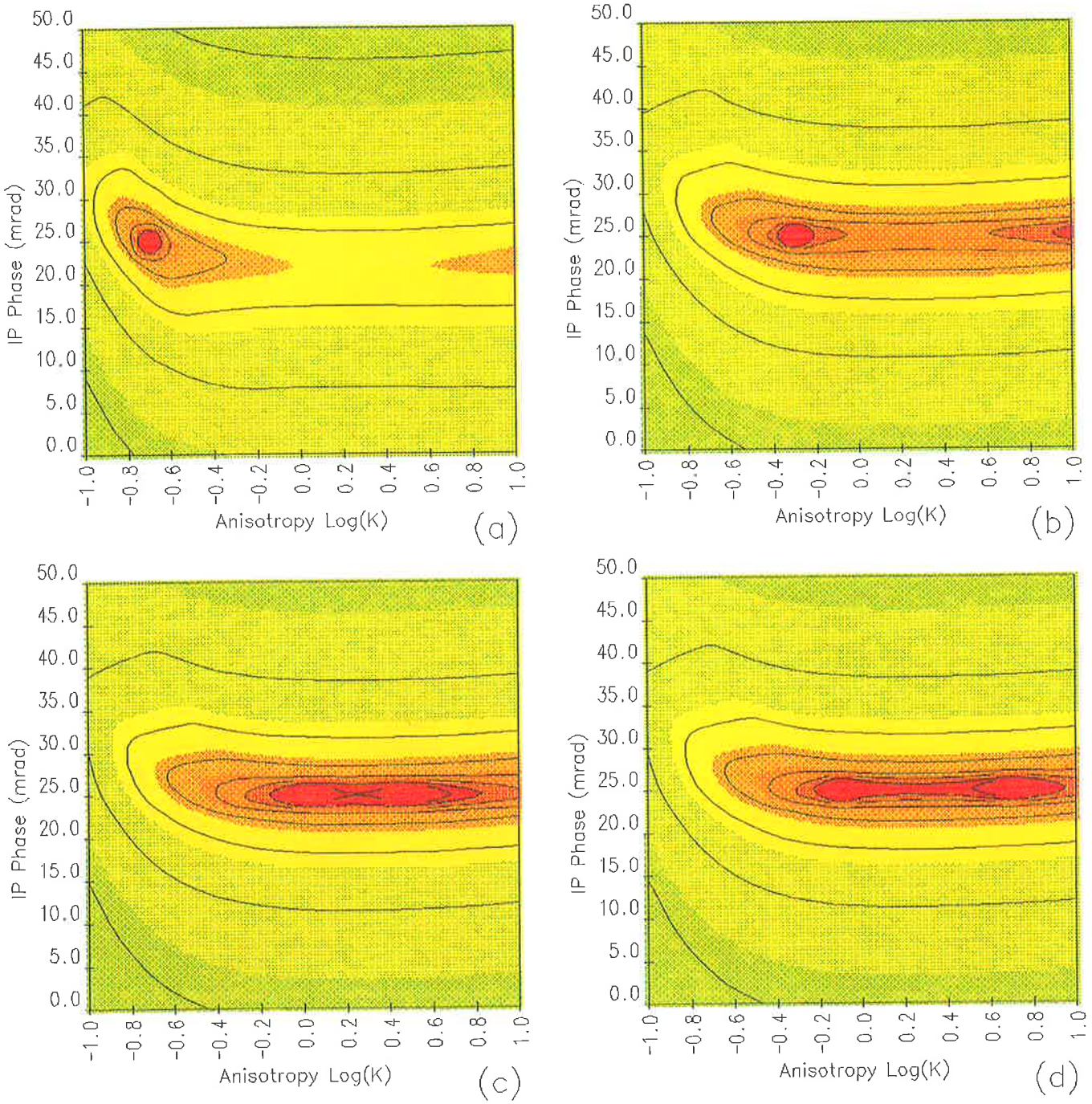

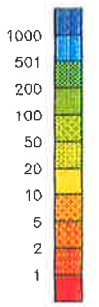

Fig. 4.3 : Inversion error generated by fitting Constant IP phase and log of Anisotropy (K) parameters to an anisotropic half-space with IP model parameters; Ro = 100 Ohm-m and constant IP phase of 25.0 mrad and anisotropic constants,
(a) K = 0.2
(b) K = 0.5
(c) K = 3.0
(d) K = 5.0

The general trend noticeable in the error surfaces is a mirror effect about an anisotropic constant (K) value of 1.8. If a global minimum is present to one side of the K value 1.8, then a shallower more elongate local minimum will occur on the opposing side. When the constant K is 1.8, the two minima become a single minimum. In all but this one case the inversion solution would have to be considered non-unique due to the presence of multi- minima. The presence of noise could make the global and local minima virtually indistinguishable for values of K near 1.8.

It is important to note that the range of anisotropic constant (K) values for which the inversion solution is unique or non-unique depends on the n-spacing and dc resistivity. From the previous chapter it is apparent that the behavior of the error surface for varying anisotropic constants will be dependent on the dc resistivity, the n-spacing as well as the frequency range over which spectral data is collected. The frequency range will almost always be set for a given CR survey, and the major difference from point to point will be the n-spacing and resistivity of the ground. It would be expected that as the ground becomes more conductive or the n-spacing is increased, the contrast between the global minimum and local minima would be greater. The final inversion solution for the anisotropic constant parameter would approach a unique solution.

(4.3) Effect of varying the Cole-Cole Parameters

The effects of different Cole-Cole parameters on the shape of the spectral EM response has been outlined in chapter 3.2. Equations 3.2.1 and 3.2.2 suggest a complex relationship exists between the different Cole-Cole parameters. From equation 3.2 it is apparent that an accurate choice of time constant (τ_o) and frequency dependence (c) is impossible when the chargeability (m) is equal or close to zero. Error surfaces have been produced to further investigate the effect that a given Cole-Cole parameter choice will have on the final inversion solution of the other Cole-Cole parameters as well as the relationship between the final inversion solution of anisotropy and the Cole-Cole IP parameters.

Prediction errors were calculated by doing a grid search in parameter space over an isotropic (K=1) half-space with Cole-Cole parameters chosen to model porphyry-copper type mineralization (O'Conner 1990) with a mean dc resistivity (R_o) of 100 Ohm-m, chargeability (m) of 0.3, time constant (τ_o) of 1.0 and frequency dependence (c) at 0.5. The EM response was calculated over the standard complex resistivity survey frequency range consisting of the first five odd harmonics of 0.125, 1.0 and 8.0 hertz for a 100 m dipole-dipole array at an n-spacing of six.

The error surfaces produced when fitting for the parameter pairs K versus m (Fig 4.4a), K versus τ_o (Fig 4.4b), K versus c (Fig 4.4c) as well as K versus R_o (Fig 4.4d) are all dominated by a low trough of error centered on the correct Cole-Cole parameter value but elongated over the anisotropic parameter axis. As is the case with a constant IP phase shift model, the elongated low is punctuated by a global minimum at the true anisotropic constant

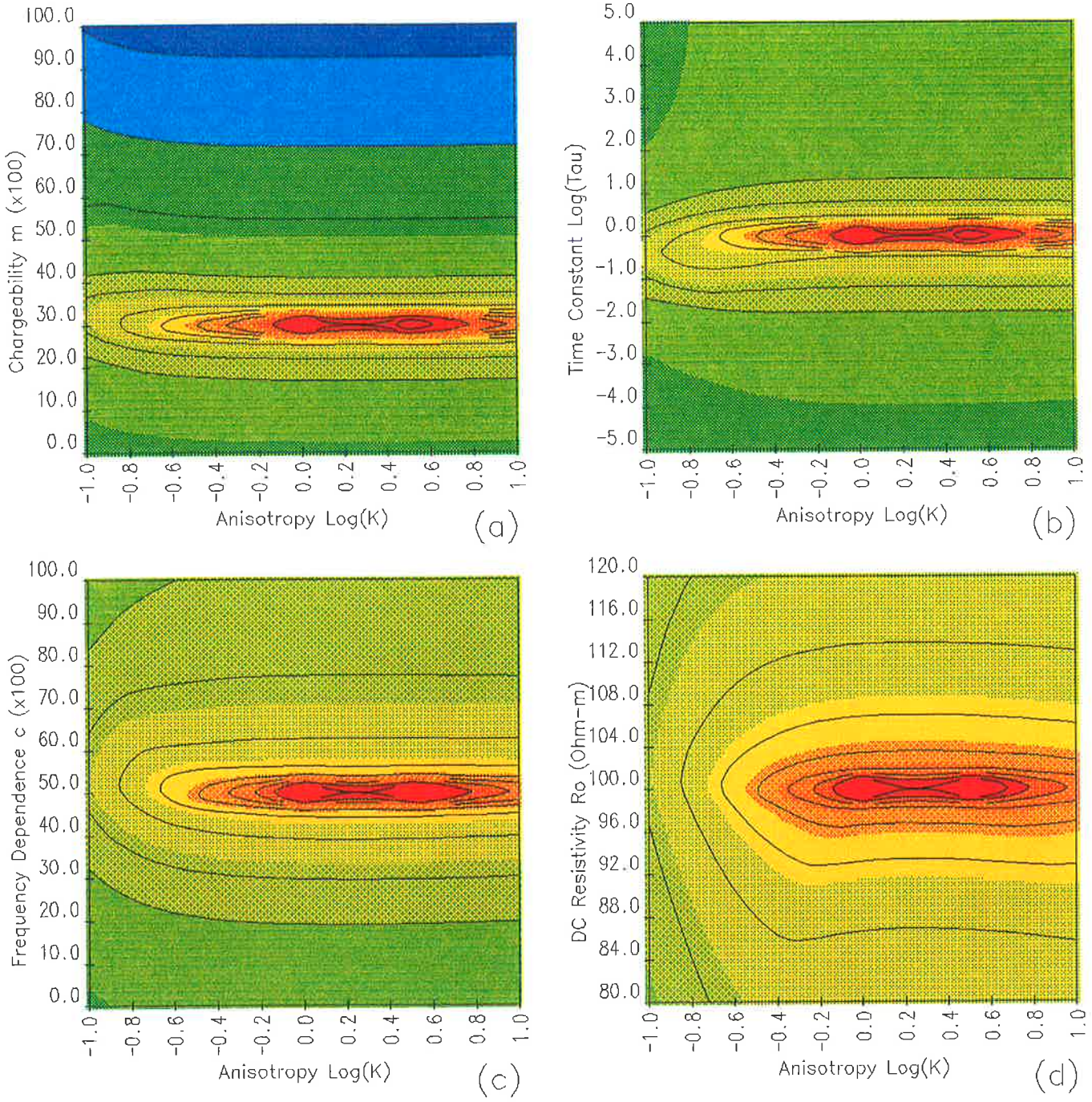

Fig. 4.4: Inversion error generated from an isotropic (K=1) half-space with Cole-Cole dispersion parameters; DC Res. Ro = 100 Ohm-m, Chargeability m = 0.3, Time constant Tau = 1.0 sec. and frequency dependence c = 0.5 when fitting parameter pairs,
(a) m Vs K
(b) Tau Vs K
(c) c Vs K
(d) Ro Vs K

value of one and a local minimum near a value of three. Again a ridge of high error occurs at about the K value of 1.8. The similarity to the error maps produced for a constant IP phase shift complex resistivity would suggest the final anisotropic constant inversion solution is relatively independent of the IP model used.

The error surface produced for chargeability (m) versus time constant (τ_o) (Fig 4.5a) is dominated by a parabolic shaped low extending over a wide range of m and is punctuated by the global minimum at the correct parameter values. This error surface is indicative of the complex relationship between final inversion solutions of the two Cole-Cole parameters. For frequency dependence (c) versus time constant (τ_o), the error surface (Fig 4.5b) has a low which is slightly elongated over the c parameter axis and punctuated by a global minimum at the correct parameter values. In the case of dc resistivity (R_o) versus time constant (τ_o) the error surface (Fig 4.5c) has a low centered on the correct value of τ_o and seems to be elongated over R_o. However, it should be pointed out that the low extends over twenty decades of τ_o values, from 10^{-1} to 10^{1}, while only extending over a single decade of R_o, implying that the final inversion solution for the time constant is poorly defined compared to that for the dc resistivity.

The error surfaces for chargeability (m) versus dc resistivity (R_o) (Fig 4.6a) and frequency dependence (c) versus dc resistivity (R_o) (Fig 4.6b) are both defined by a low extending over the R_o axis and punctuated by a central global minimum at the correct solution. The chargeability and frequency dependence in these cases have a well defined inverse solution. Fitting frequency dependence (c) and chargeability (m) to the

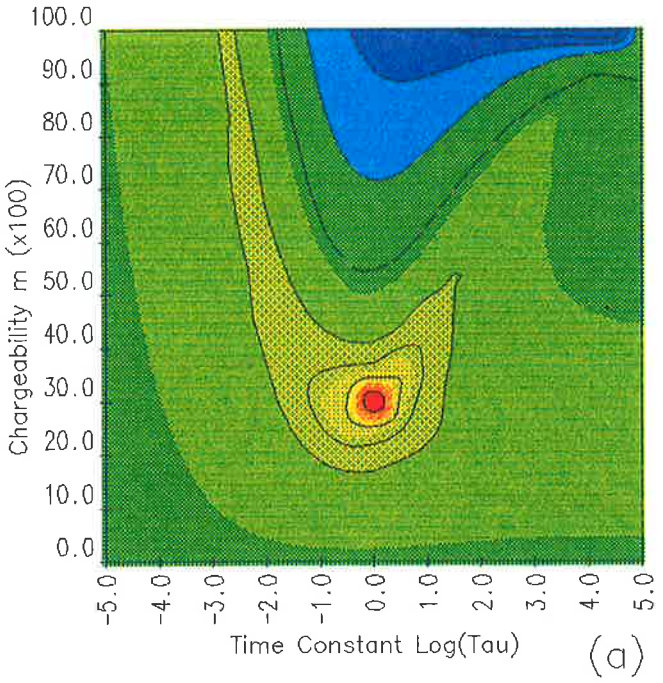

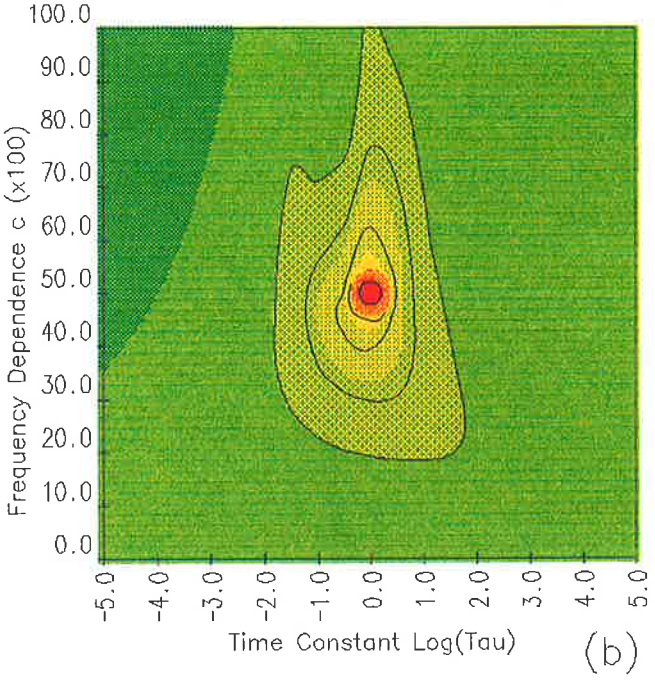

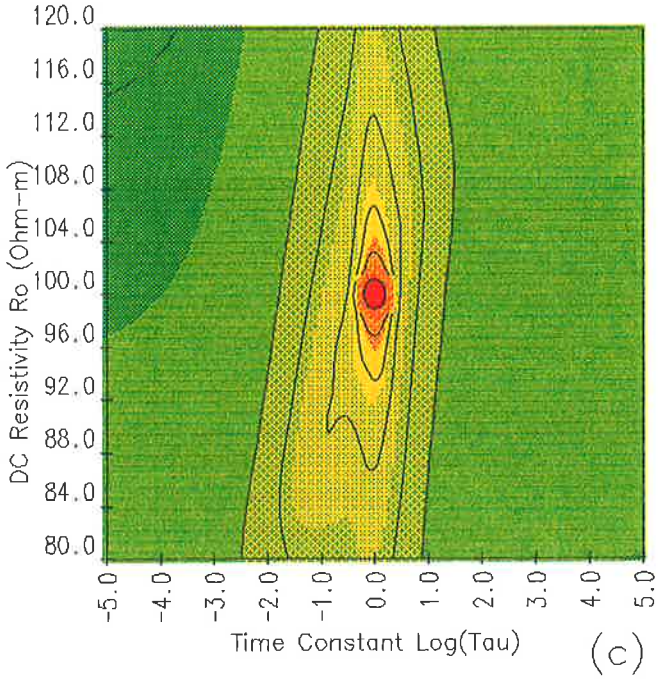

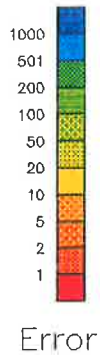

Fig. 4.5: Inversion error generated from an isotropic (K=1) half-space with Cole-Cole dispersion parameters; DC Res. Ro = 100 Ohm-m, Chargeability m = 0.3, Time constant Tau = 1.0 sec. and frequency dependence c = 0.5 when fitting parameter pairs,
(a) m Vs Tau
(b) c Vs Tau
(c) Ro Vs Tau

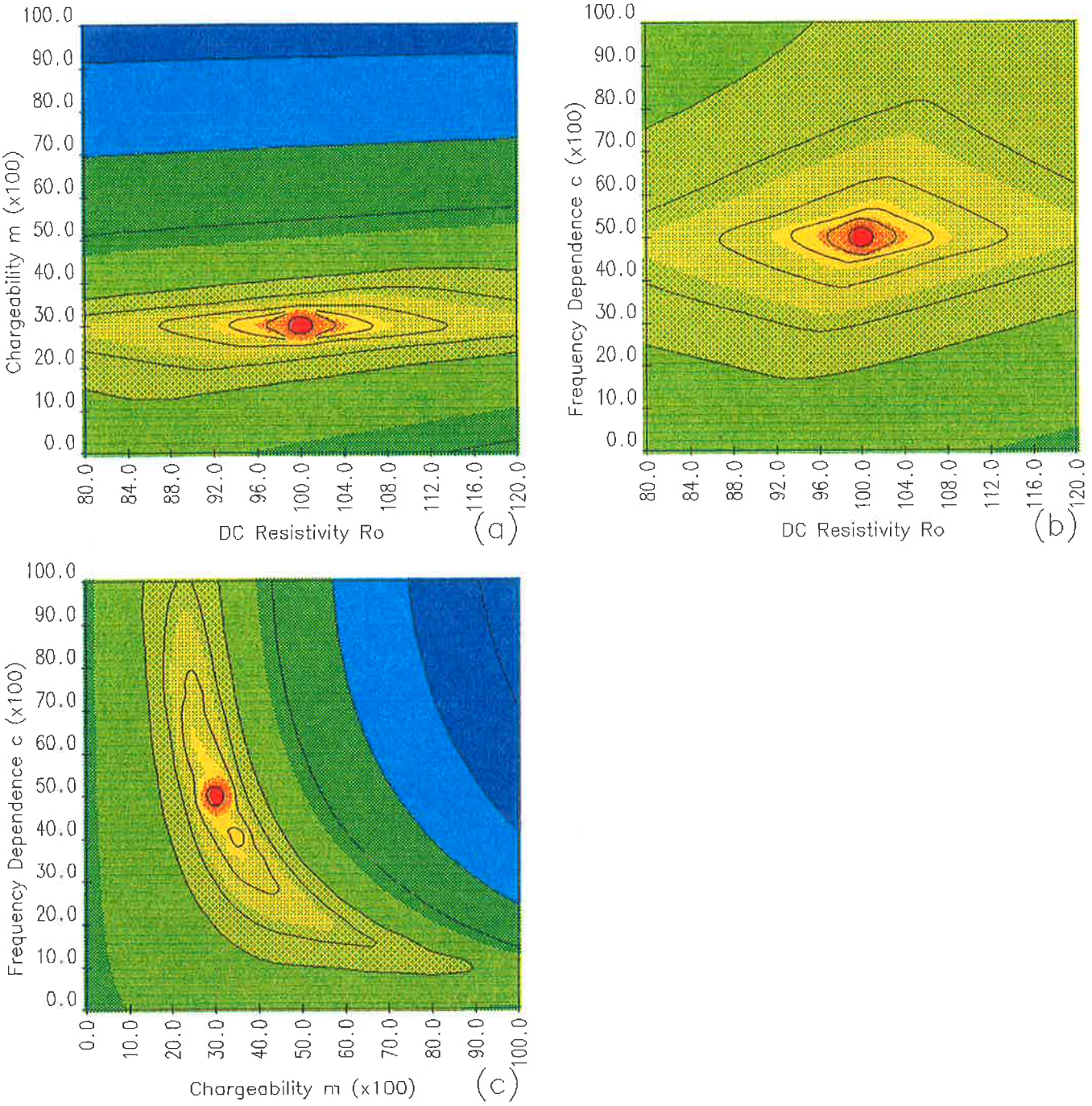

Fig. 4.6: Inversion error generated from an isotropic (K=1) half-space with Cole-Cole dispersion parameters; DC Res. Ro = 100 Ohm-m, Chargeability m = 0.3, Time constant Tau = 1.0 sec. and frequency dependence c = 0.5 when fitting parameter pairs,
(a) m Vs Ro
(b) c Vs Ro
(c) c Vs m

porphyry-copper mineralization Cole-Cole model produces an error surface (Fig 4.6c) dominated by a low elongated along the *c* parameter axis, punctuated by a global minimum at the correct solution and a small local minimum at a lower value of *c*. The shape of the error low is indicative of the relationship between the final inverse solutions of frequency dependence and chargeability.

(4.3.1) Chargeability (m)

The effect of an increase in chargeability (*m*) on the error surfaces of the different parameters is investigated by calculating error surfaces of chargeability versus the other parameters for the porphyry-copper Cole-Cole model with the chargeability set at 0.1 (Fig 4.7) and 0.7 (Fig 4.8).

When comparing the error surfaces for *m* versus *K* for a true chargeability set at 0.1 (Fig 4.7a) and 0.7 (Fig 4.8a) as well as 0.3 (Fig 4.4a), it is apparent that as the chargeability increases the final inverse solution for the *m* parameter is better defined. Also, the low elongated over the *K* parameter axis begins to become two distinct minima and the *K* parameter becomes slightly better defined.

Error surfaces are given for *m* versus τ_o with the true chargeability set at 0.1 (Fig 4.7b), 0.7 (Fig 4.8b) and 0.3 (Fig 4.5a). The general trend seems to be that as the true chargeability is decreased, the inverse solution for τ_o as well as *m* become more poorly defined. A similar trend is noticeable in the error surfaces of *c* versus *m* for varying chargeability (Figs 4.7c, 4.8c and 4.6c). The frequency dependence becomes very

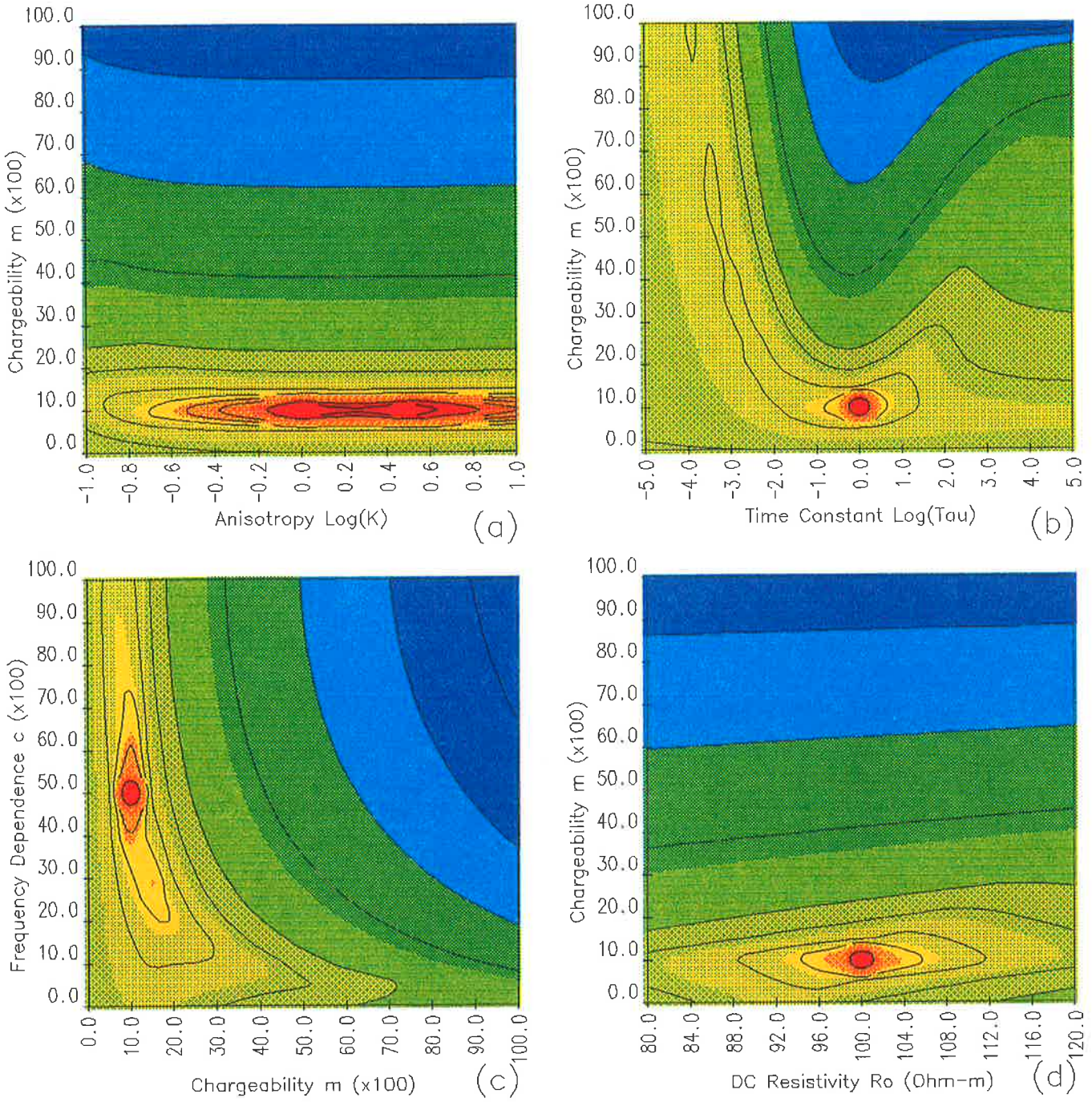

Fig. 4.7 : Inversion error generated from an isotropic (K=1) half-space with Cole-Cole dispersion parameters; DC Res. Ro = 100 Ohm-m, Chargeability m = 0.1, Time constant Tau = 1.0 sec. and frequency dependence c = 0.5 when fitting parameter pairs,
(a) m Vs K
(b) m Vs Tau
(c) c Vs m
(d) m Vs Ro

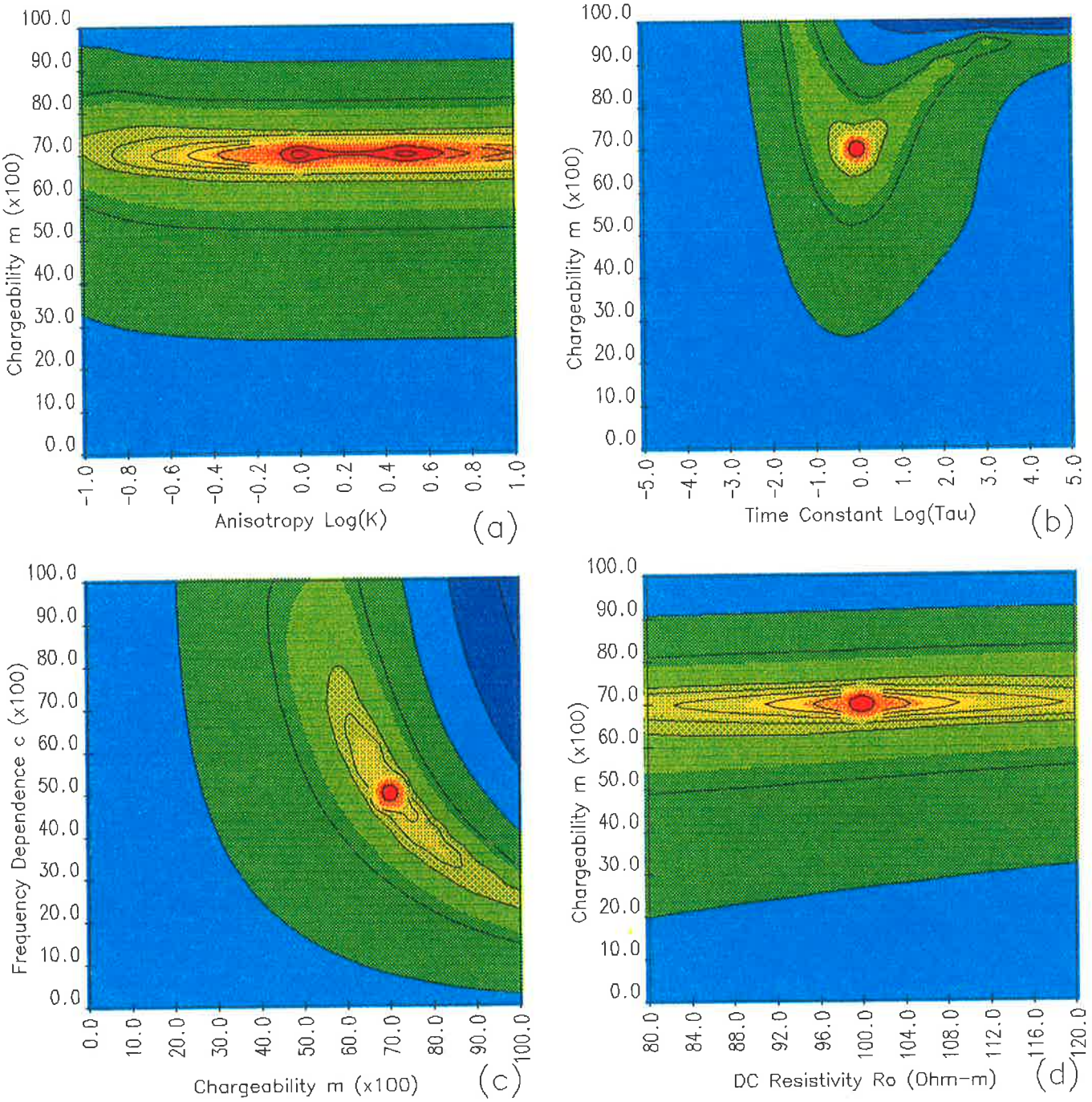

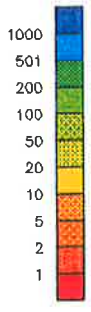

Fig. 4.8 : Inversion error generated from an isotropic (K=1) half-space with Cole-Cole dispersion parameters; DC Res. Ro = 100 Ohm-m, Chargeability m = 0.7, Time constant Tau = 1.0 sec. and frequency dependence c = 0.5 when fitting parameter pairs,
(a) m Vs K
(b) m Vs Tau
(c) c Vs m
(d) m Vs Ro

poorly resolved at low chargeability. These trends are not surprising when considering the form of the complex impedance (eq. 3.2), where the contributions of τ_o and c to the spectral response are governed by the m parameter.

Comparison of the error surfaces for m versus R_o when the true chargeability is set at 0.1 (Fig 4.7d), 0.7 (Fig 4.8d) and 0.3 (Fig 4.6a) indicate the trend in resolution of the inverse solution for R_o opposes that of the other Cole-Cole parameters. In this case, as the chargeability is increased the inverse solution for the R_o parameter tends to be more poorly resolved. When chargeability approaches zero the complex impedance (eq. 3.2) approaches R_o which leads to a domination of the R_o parameter in the error surfaces. As chargeability is increased the contributions from τ_o, c and m will increase and cause a slight reduction in the resolution of the final inverse solution of R_o.

(4.3.2) Time Constant (τ_o)

Error surfaces of time constant (τ_o) versus the other parameters were produced using the porphyry-copper Cole-Cole model with time constant set at 0.01 and 100 (Figs 4.9 and 4.10) to investigate the effects of varying the time constant.

Two areas of low error elongated over the anisotropic axis are present in the error surfaces for τ_o versus K at a true time constant value of 0.01 (Fig 4.9a) and 100 (Fig 4.10a). One area is centered on the correct value of τ_o and contains the global minimum and a local minimum at different K values. When τ_o is greater than one a broad depression in the error surface occurs

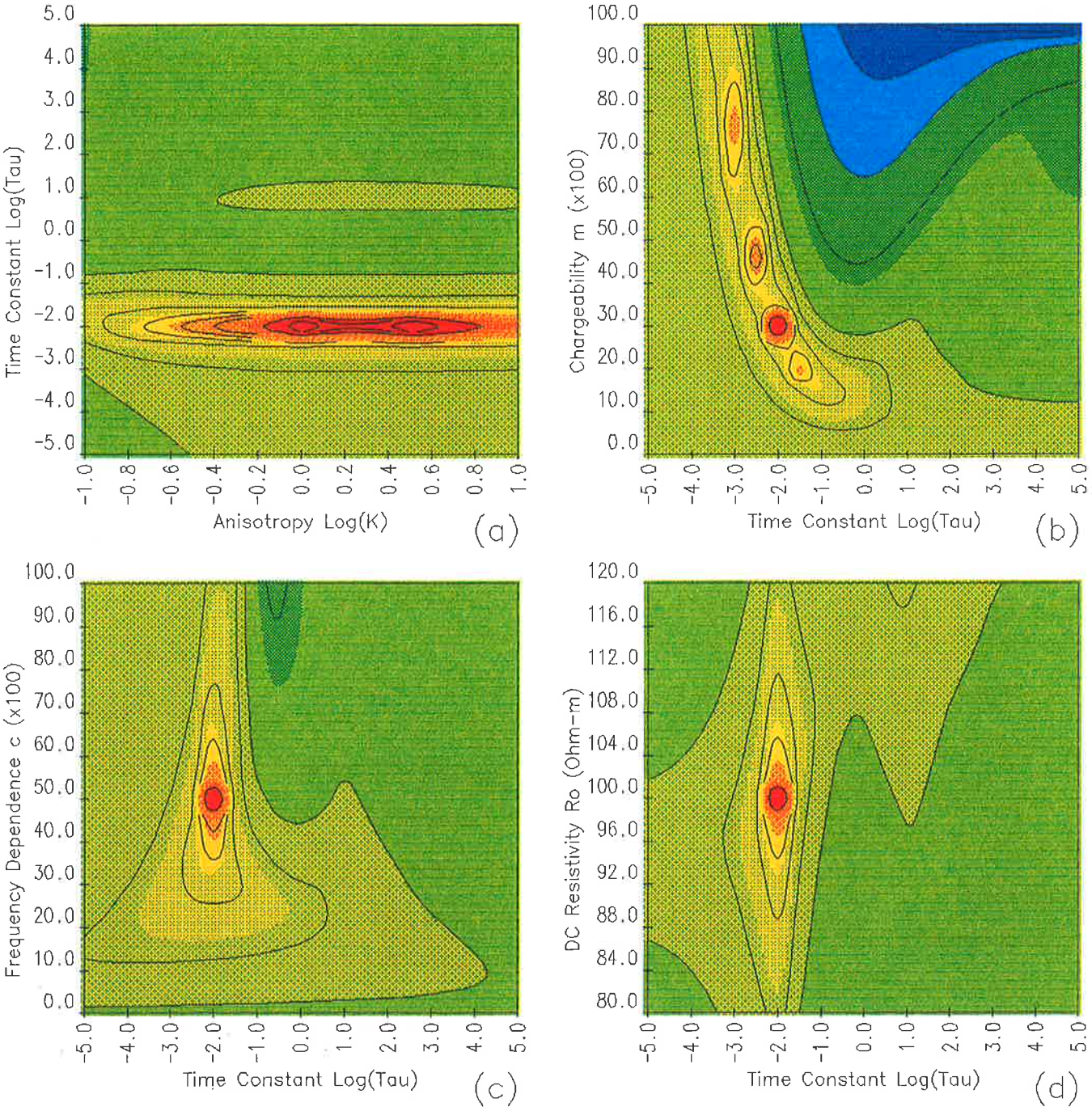

Fig. 4.9 : Inversion error generated from an isotropic (K=1) half-space with Cole-Cole dispersion parameters; DC Res. Ro = 100 Ohm-m, Chargeability m = 0.3, Time constant Tau = 0.01 sec. and frequency dependence c = 0.5 when fitting parameter pairs,
(a) Tau Vs K
(b) m Vs Tau
(c) c Vs Tau
(d) Ro Vs Tau

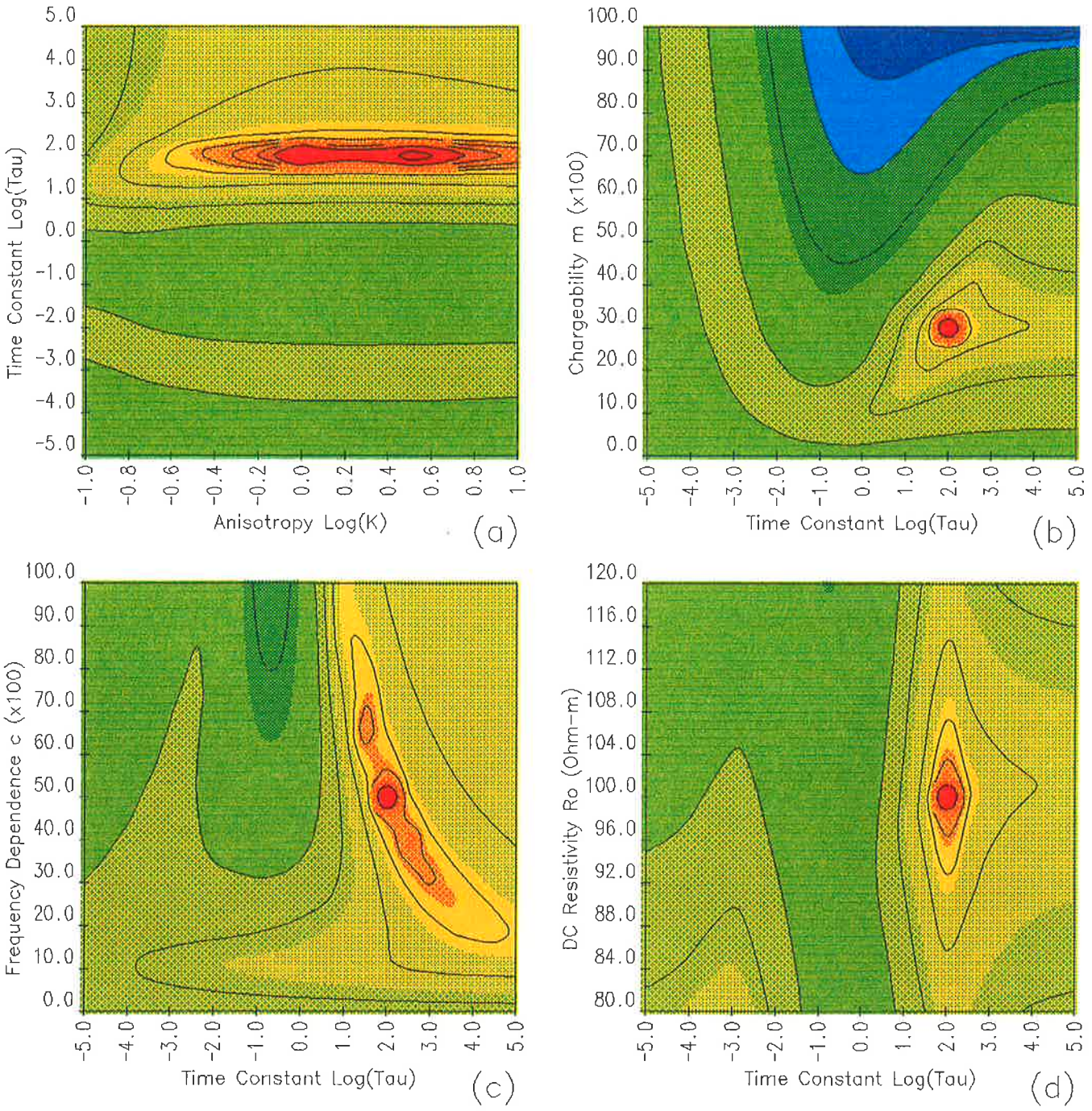

Fig. 4.10: Inversion error generated from an isotropic (K=1) half-space with Cole-Cole dispersion parameters; DC Res. Ro = 100 Ohm-m, Chargeability m = 0.3, Time constant Tau = 100 sec. and frequency dependence c = 0.5 when fitting parameter pairs,
(a) Tau Vs K
(b) m Vs Tau
(c) c Vs Tau
(d) Ro Vs Tau

at a value of τ_o less than one. When the true value of τ_o is less than one the broad depression occurs at a value greater than one. This suggests a slight mirror effect in the error surface about a value of τ_o equals one. The shape of these error surfaces indicate a partial dependence of τ_o on the value of K.

Error surfaces for m versus τ_o when the true time constant is less than one (Fig 4.9b) and when it is greater than one (Fig 4.10b) are considerably different. The error for τ_o equals 0.01 is marked by a low elongated along the m parameter axis and punctuated by the global minimum as well as a series of local minima occurring at different values of m. When τ_o equals 100 there is a single global minimum at the correct parameter values. As τ_o is decreased below one, multi-minima begin to appear in the error surface and the inverse solutions for m and τ_o become non-unique.

In the case of c versus τ_o, the trend seems to oppose that for m versus τ_o. When the true time constant equals 0.01 (Fig 4.9c) the error surface is marked by a single global minimum; however, when it equals 100 (Fig 4.10c) there are multi-minima present. As τ_o is increased above one multi-minima begin to develop in the error surface and the inverse solutions for c and τ_o become non-unique.

When the true time constant value is increased the trend in the error surface for R_o versus τ_o (Figs 4.9d and 4.10d) is toward a slight decrease in the resolution of both inverse parameter solutions. This is an indication of the diminishing dominance of R_o in the inverse solution as the imaginary component of the complex impedance is increased.

(4.3) Frequency Dependence (c)

Error surfaces for frequency dependence (c) versus the other parameters were produced using the porphyry-copper Cole-Cole model, outlined in chapter 3.2.1, with frequency dependence set at 0.1 (Fig 4.11) and 0.7 (Fig 4.12). Comparison of the error surfaces for c versus K for a true frequency dependence set at 0.1 (Fig 4.11a) and 0.7 (Fig 4.12a) as well as 0.3 (Fig 4.4c) indicates that as c increases its final inverse solution becomes slightly less defined.

Error surfaces for c versus τ_o with the true frequency dependence set at 0.1 (Fig 4.11b) and 0.7 (Fig 4.12b) indicate the general trend is for τ_o to become less defined as the true frequency dependence is decreased. This is consistent with the relationship between τ_o and c in the complex impedance (eq. 3.2), where the contribution of one parameter to the spectral response is dependent on the value of the other. When comparing these two error surfaces to that for a true c of 0.3 (Fig 4.5b), it is apparent that the resolution of τ_o is decreased rapidly as c approaches zero. It is interesting that c becomes slightly less resolvable when its value is increased.

The trend noticeable in the error surfaces of c versus m for varying true frequency dependence (Figs 4.11c and 4.12c) is that the c and m parameters become more resolved as the true frequency dependence is increased. Here c is better resolved when its value is increased.

The effect on the error surface for R_o versus c (Figs 4.11d and 4.12d) as the true c is increased is a slight reduction in the resolution of both parameters.

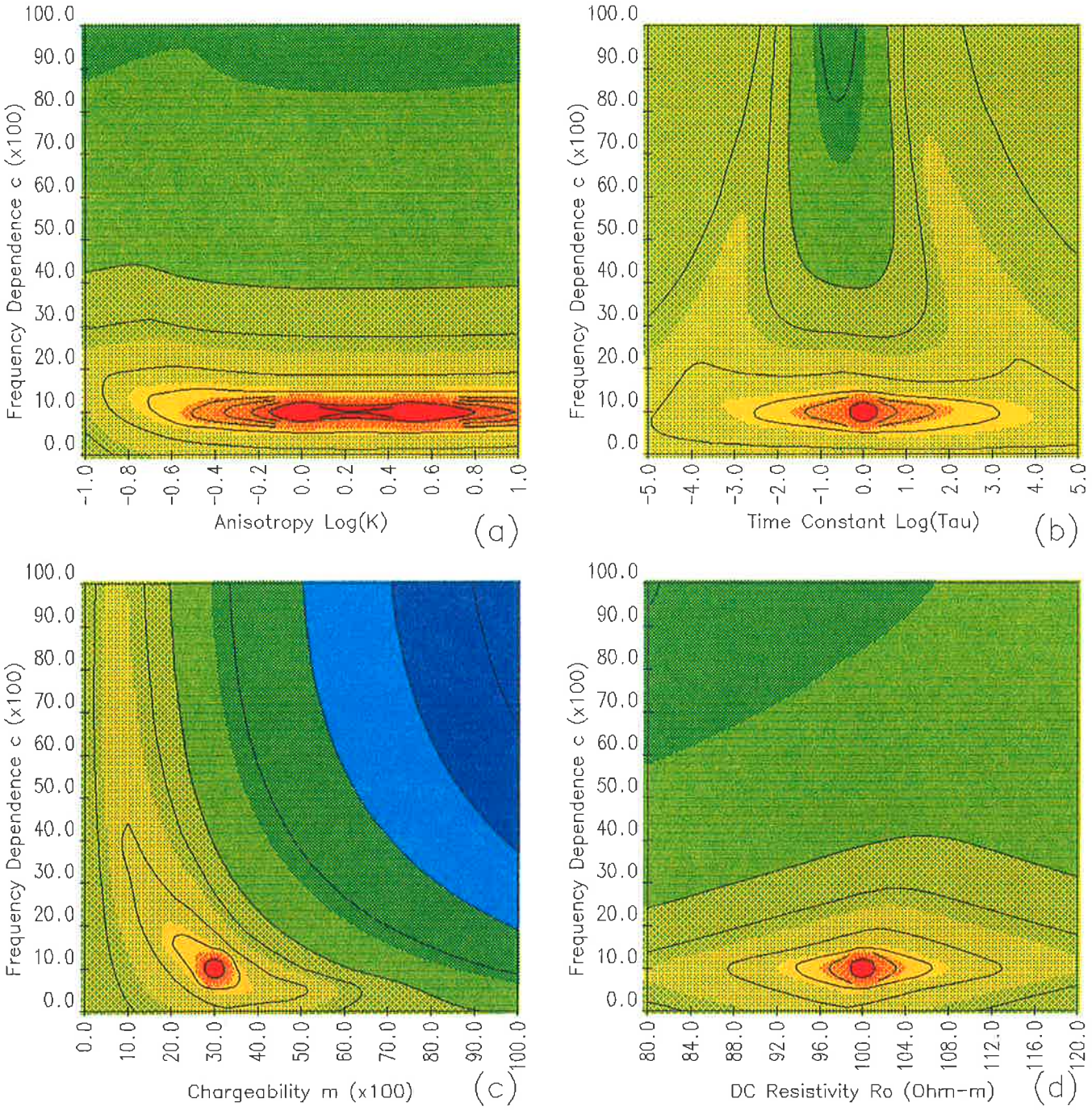

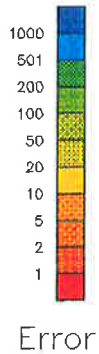

Fig. 4.11: Inversion error generated from an isotropic (K=1) half-space with Cole-Cole dispersion parameters; DC Res. Ro = 100 Ohm-m, Chargeability m = 0.3, Time constant Tau = 1.0 sec. and frequency dependence c = 0.1 when fitting parameter pairs,
(a) c Vs K
(b) c Vs Tau
(c) c Vs m
(d) c Vs Ro

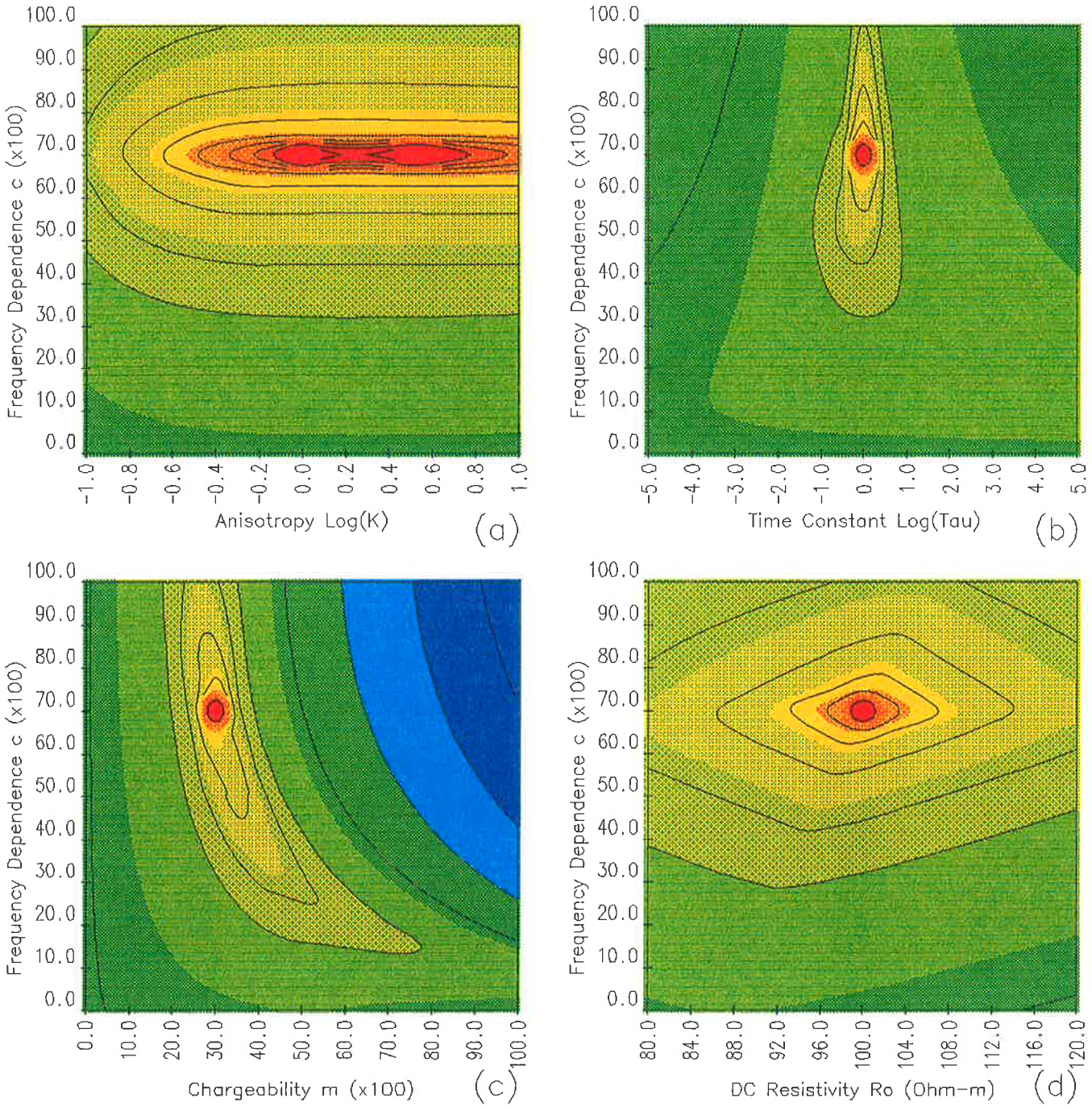

Fig. 4.12: Inversion error generated from an isotropic (K=1) half-space with Cole-Cole dispersion parameters; DC Res. Ro = 100 Ohm-m, Chargeability m = 0.3, Time constant Tau = 1.0 sec. and frequency dependence c = 0.7 when fitting parameter pairs,
(a) c Vs K
(b) c Vs Tau
(c) c Vs m
(d) c Vs Ro

(4.3.4) Interdependence of parameters

The main inference from the error surfaces has been the interdependence between the inverse solutions of the Cole-Cole parameters. It has also been shown that while the actual value of anisotropic constant is chosen independent of the IP model, the resolution of K can be enhanced by variations in the Cole-Cole parameters. To further investigate the interdependence of the various parameters it is useful to examine the effects, of varying a given parameter, on the error surfaces of parameter pairs which do not include the parameter being varied.

The effect of dc resistivity on the final inverse solution for an anisotropic half-space with a constant IP phase shift complex resistivity has been outlined previously (chapter 4.1.3). To investigate the effect of reducing the dc resistivity on the final inverse solution of the Cole-Cole parameters, error surfaces were produced for different parameter pairs with the dc resistivity (R_o) at 10 Ohm-m. Prediction errors were calculated by doing a grid search in parameter space over an isotropic (K=1) half-space with Cole-Cole parameters chosen to model porphyry-copper type mineralization. The EM response was calculated over the standard complex resistivity survey frequency range consisting of the first five odd harmonics of 0.125, 1.0 and 8.0 hertz for a 100 m dipole-dipole array at an n-spacing of six.

Error surfaces for the Cole-Cole parameters versus anisotropy (Fig 4.13) indicate that as the dc resistivity is reduced the anisotropic constant is easier to resolve. However, a significant reduction in the resolution of the Cole-Cole parameters is evidenced as a widening of the minima over the Cole-Cole parameter axis. The form of the error surfaces for τ_o

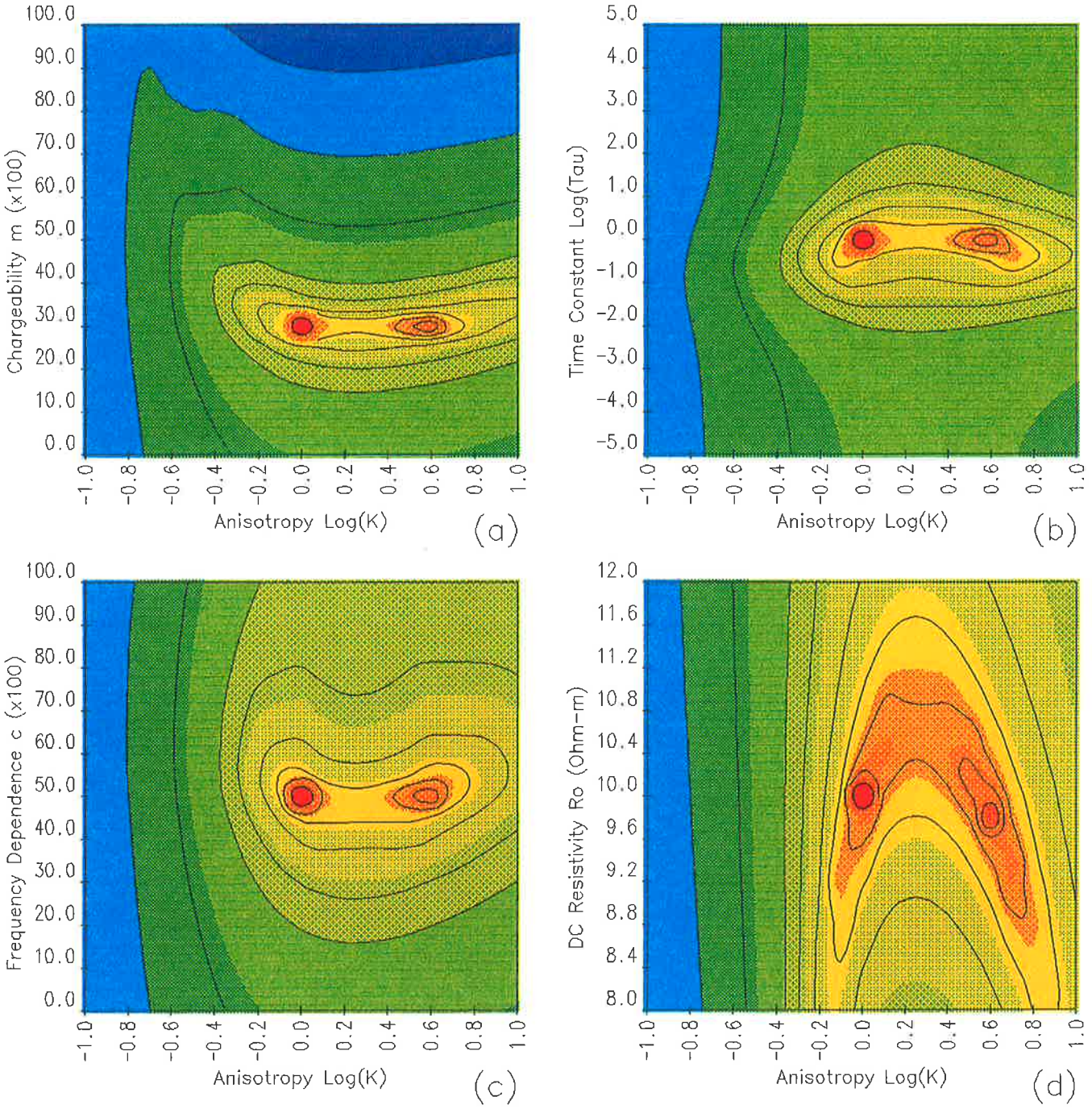

Fig. 4.13: Inversion error generated from an isotropic (K=1) half-space with Cole-Cole dispersion parameters; DC Res. Ro = 10.0 Ohm-m, Chargeability m = 0.3, Time constant Tau = 1.0 sec. and frequency dependence c = 0.5 when fitting parameter pairs,
(a) m Vs K
(b) Tau Vs K
(c) c Vs K
(d) Ro Vs K

versus K (Fig 4.13b) and c versus K (Fig 4.13c) are an indication of the dependence of the final inverse solutions for τ_o and c on the choice of K. It is apparent that as the dc resistivity is reduced, the EM coupling response dominates the spectral response, resulting in a reduction in the resolution of the Cole-Cole parameters. Also a mixing of the EM coupling and IP responses is represented by the increasing dependence between the Cole-Cole parameters and anisotropic constant.

The general trend in the error surfaces of the m versus τ_o, c versus τ_o and c versus m (Fig 4.14) further indicates a reduction in the resolution of the Cole-Cole parameters as the dc resistivity is reduced. Of particular interest is the development of multi-minima above and below a value of τ_o equal to one in the error surface of m versus τ_o (Fig 4.14a), indicating a decrease in the uniqueness of the final inverse solutions of τ_o and m as the dc resistivity is reduced. On comparing these error surfaces with those produced for a dc resistivity of 100 Ohm-m (Figs 4.5 and 4.6), it is apparent that variations in the mean dc resistivity of the ground will affect the ability of an inversion procedure to resolve the other model parameters.

Error surfaces for c versus m when τ_o is 0.01 (Fig 4.15a) and 100 (Fig 4.15b) show an increased dependence on the chargeability parameter as τ_o is varied from one. When τ_o is equal to 100 the final inversion parameter solutions are non-unique, as indicated by the presence of multi-minima. When the frequency dependence is set at 0.1 the error surface for m versus τ_o (Fig 4.15c) indicates the resolution of the m and τ_o parameters is poor, especially the inverse solution for τ_o which is very poorly defined. When the frequency dependence is increased to 0.7, the error surface (Fig 4.15d) indicates the final inverse solutions for m and τ_o are very well resolved.

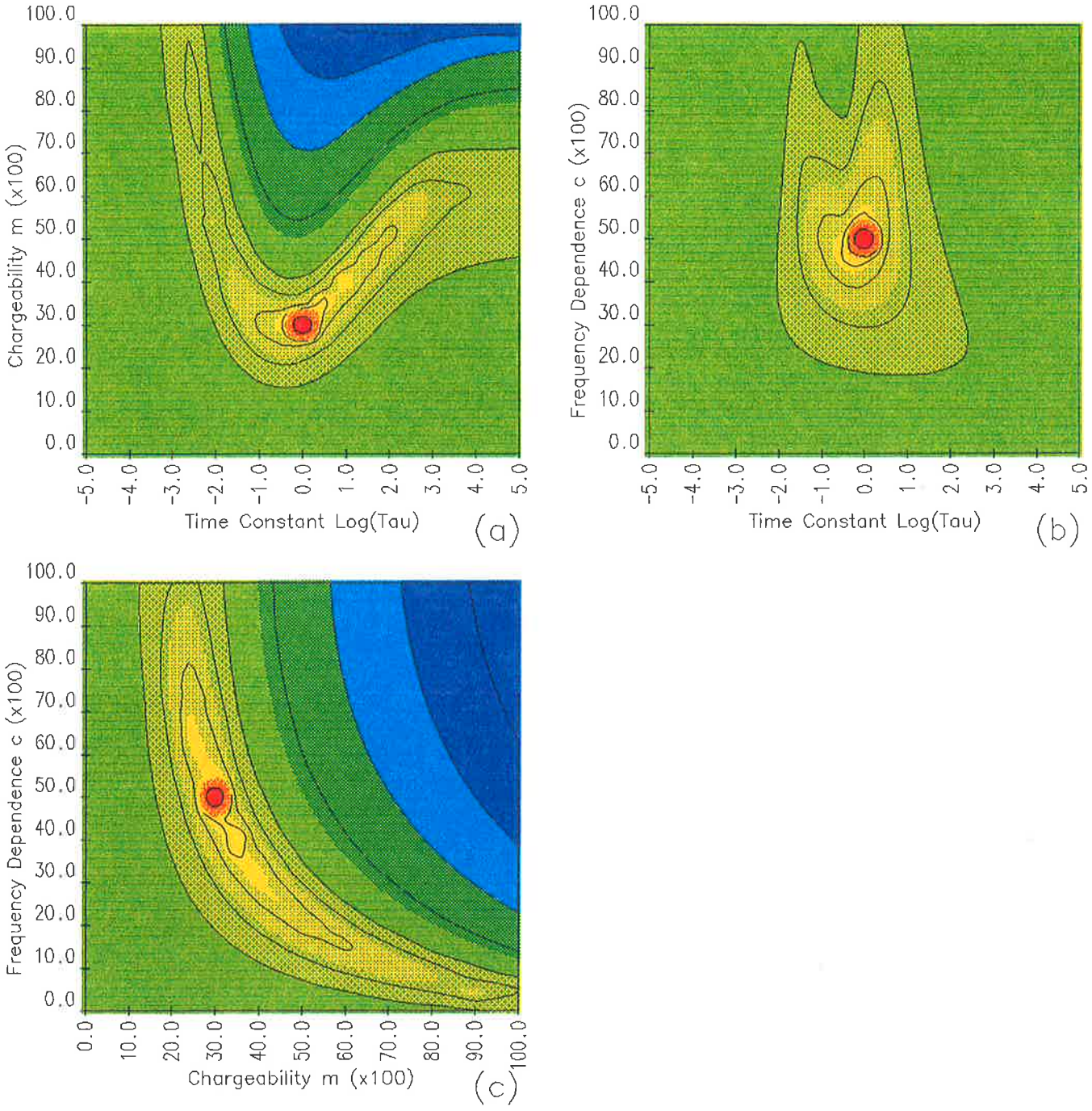

Fig. 4.14: Inversion error generated from an isotropic (K=1) half-space with Cole-Cole dispersion parameters; DC Res. Ro = 10.0 Ohm-m, Chargeability m = 0.3, Time constant Tau = 1.0 sec. and frequency dependence c = 0.5 when fitting parameter pairs,
(a) m Vs Tau
(b) c Vs Tau
(c) c Vs m

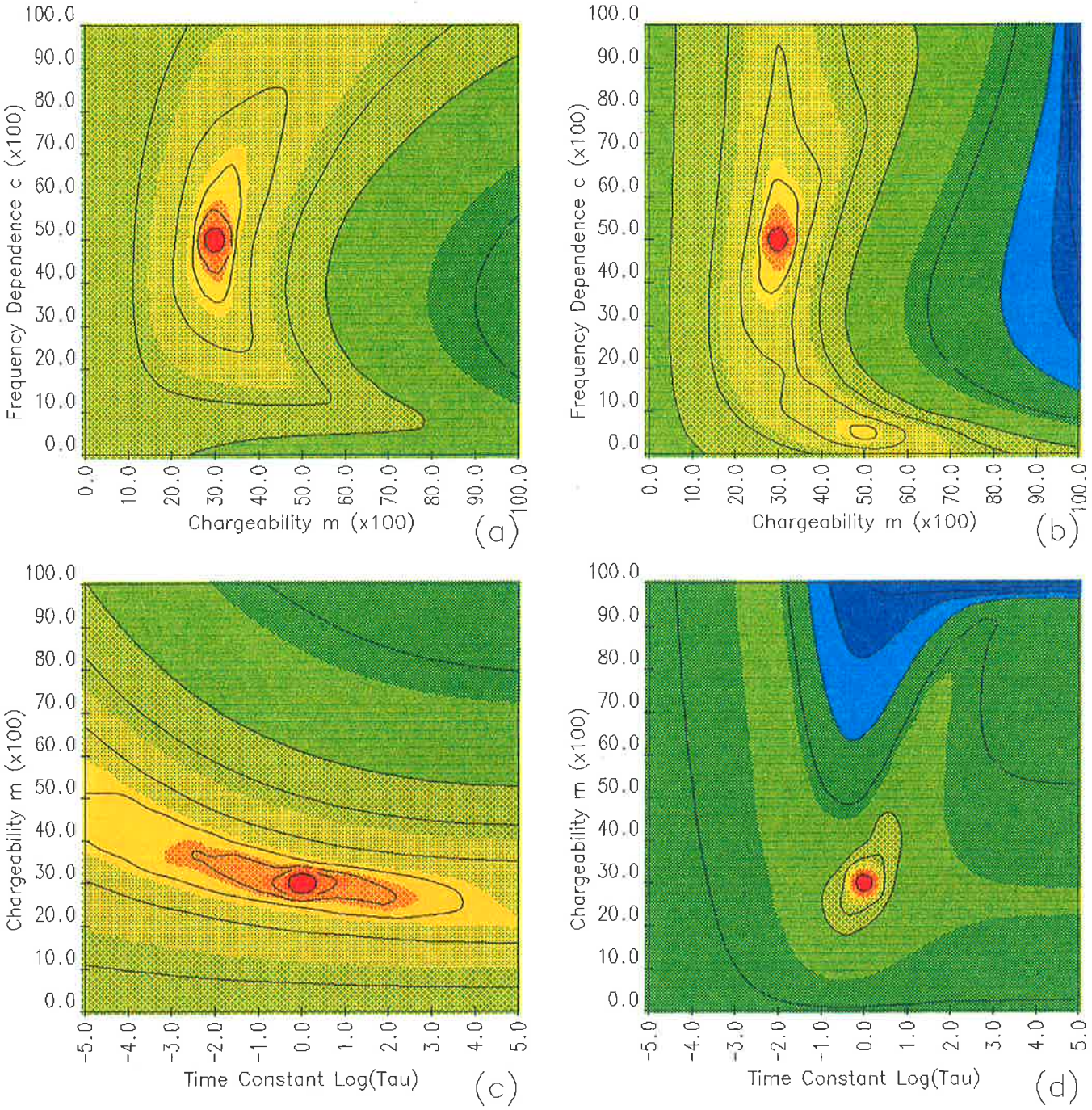

Fig. 4.15: Inversion error generated from an isotropic (K=1.0) half-space with Cole-Cole dispersion parameters; DC Res. Ro = 100 Ohm-m, Chargeability m = 0.3 when fitting parameter pairs
(a) c Vs m with Tau = 0.01
(b) c Vs m with Tau = 100.0
(c) m Vs Tau with c = 0.1
(d) m Vs Tau with c = 0.7

(4.4) SUMMARY

L_1-Norm inversion error surfaces were produced for differing n-spacing, frequency range and dc resistivity. Anisotropy is more easily resolved as n-spacing increases. A larger range of higher frequencies allows the anisotropy to be determined more readily. Also, the more conductive the ground the greater the contribution of anisotropy to the total EM response. The success of an inversion in retrieving anisotropic information will depend on the frequency range, n-spacing and dc resistivity.

Prediction error surfaces of models with varying anisotropy were produced and indicate that on the whole the inversion of CR data should be treated as a multi-minima problem. Even though there are specific values of anisotropy that produce single minimum error maps, it is impossible to know beforehand if the inversion is unique or non-unique due to the dependence of the outcome on dipole separation and dc resistivity.

The form of the prediction error is further complicated when the complex Cole-Cole dispersion is used to model the IP response. Final inverse solutions for the different Cole-Cole parameters will be interdependent when inverting CR data.

As the chargeability (m) approaches zero the final inverse solutions for the time constant (τ_o) and frequency dependence (c) become very poorly resolved.

The value of τ_o controls the presence of multi-minima in the prediction error and can cause the inversion to converge to an incorrect solution for the parameters m and c.

When dc resistivity is reduced the Cole-Cole parameters have a greater chance of inverting to the incorrect solution and will be poorly resolved. As the ground becomes more conductive the inverse solutions of parameters m and τ_o will become non-unique.

When dealing with non-unique inversion solutions, linear and standard non-linear iterative techniques can converge to an incorrect solution. Especially if the initial parameter guess is far from the global minimum and noise is present in the data. These types of techniques tend to follow the path of least resistance, that is they iteratively accept the choice of inversion parameters which most rapidly reduce the fitting error. Also, standard techniques fail to give an idea of how well resolved an inverse parameter solution is.

Global search procedures are more likely to recover the correct solution as they cover a wider area of parameter space and are not restricted to the path of least resistance towards the closest minima. The controlled random search technique is a global search procedure which returns a number of parameter solutions which have similar fitting errors. A range of parameter solutions are returned and give an idea of the uniqueness of the solution as well as the resolution of given parameters.

SECTION III: INVERSION OF THEORETICAL AND FIELD CR-IP DATA

(5.0) THE CONTROLLED RANDOM SEARCH ALGORITHM

Inversion error maps have been produced to investigate the convergence properties of the inversion process using the anisotropic half-space with complex resistivities. The presence of multi-minima in the error maps for several parameter combinations indicate the inversion has a non-unique solution. Also, the broadness of some of the global minimum indicate certain parameters will be poorly resolved.

Standard iterative techniques such as a Marquardt type inversion procedure (Marquardt 1963) have a strong dependence on the initial parameter guess. The majority of non-linear techniques require prior information as they tend to fail if the starting parameters are far from the global solution. Also, there is no general method for determining whether a solution obtained actually minimizes the error in the global sense.

The controlled random search (CRS) procedure (Price, 1967) covers a wide area of the parameter space, thereby reducing the reliance on prior information. Controlled random search procedures also attack the combined problem of multi-minima and parameter resolution by returning a large number of suitable parameter solutions. The reliability of the model parameters can be determined from the range of values generated for a given parameter. Best estimates of the model parameters are taken as the centroid of each parameter cloud. The basic structure of the controlled random search (CRS) procedure is outlined in the flow diagram of Figure 5.0.

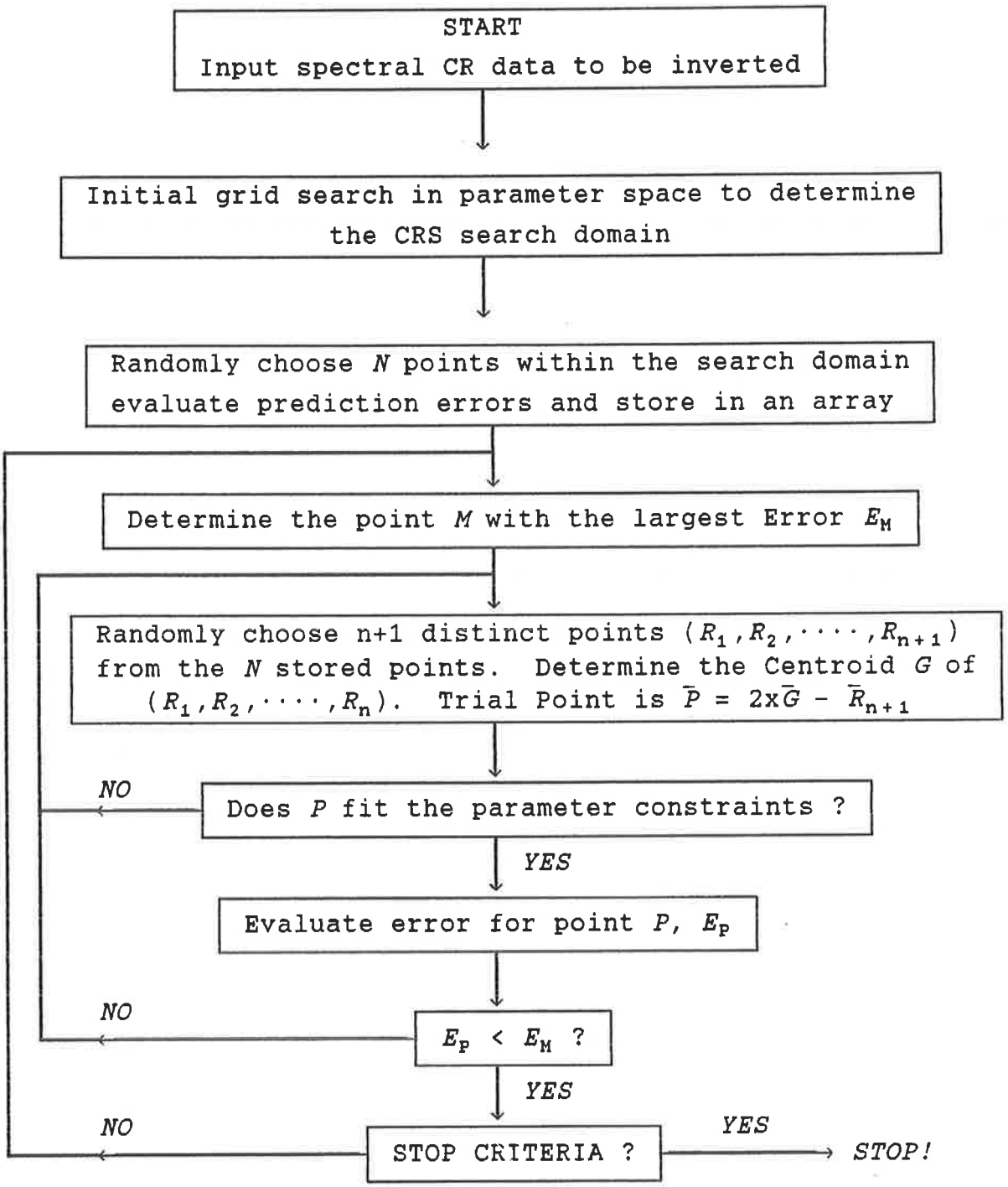

Figure 5.0: Flow diagram for the controlled random search (CRS) procedure.

The Controlled random search (CRS) algorithm begins by randomly choosing a number of trial points, N, within an initial search domain defined for the n parameters of the forward model. Initial values for the prediction error (eq. 4.0) are calculated and stored in an array. The point M in N with the largest error E_M is determined. As the algorithm begins each iteration a new trial point, P, is selected randomly from the set of N trial points using a simplex (Fig 5.1) of n+1 points in parameter space.

At each iteration n+1 different points $R_1, R_2, \cdots\cdots, R_{n+1}$ are chosen randomly from the N trials in the array, producing a simplex of points in n parameter space. The point R_{n+1} is arbitrarily taken as the pole of the simplex and the new trial point, P, is defined as the image point of R_{n+1} with respect to the centroid, G, of the remaining n points. This can be written in terms of the corresponding position vectors in n parameter space as

$$\overline{P} = 2 \times \overline{G} - \overline{R}_{n+1}$$

This method of choosing the trial point is what distinguishes the CRS procedure from other global search procedures. Figure 5.1 illustrates how a trial point is chosen in a two parameter system.

Once a trial point has been chosen that fits the parameter constraints, the prediction error for the trial point, E_p, is calculated and compared to the highest error, E_M, found for the previous N stored points. If the point P has an error, E_p, less than that of the point M, E_M, then P replaces M in the stored

array. If the trial point *P* fails to fit the parameter constraints or has an error higher than any found in the *N* stored points it is discarded and a fresh point chosen from the *N* stored points.

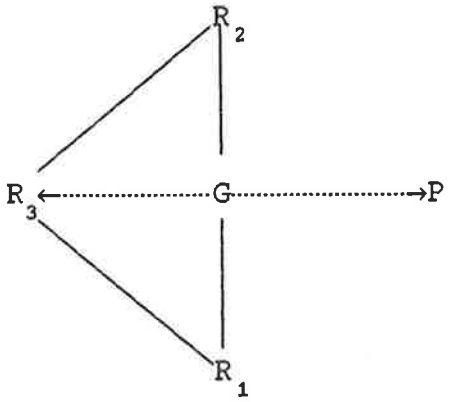

Figure 5.1: For the case where n equals two a trial point P is selected using a simplex of three points R_1, R_2, R_3 in parameter space. In this case P is the image of R_3 about the centroid G of R_1 and R_2.

As the algorithm proceeds the set of *N* stored points cluster around any minima which are lower than the error E_M. The convergence of the algorithm to the global minimum depends on the size of the set of trial points *N*, the complexity of the error surface and the constraints placed on the parameters. When convergence fails an idea of the reason can be obtained from the spread of the final set of *N* points returned.

(6.0) INVERTING THEORETICAL DATA

The effectiveness and efficiency of the controlled random search (CRS) algorithm was tested using theoretical data generated from an anisotropic half-space with constant IP phase shift complex resistivities.

Program CRS_CIP, written by the author,is used to invert the data to an anisotropic half-space with constant IP phase shift complex resistivities. The program begins by calculating the error distribution using a grid search over the anisotropic (K) and constant IP phase (ϕ_{ip}) parameters to determine a starting model. The initial search domain and cloud of initial parameters for the controlled random search procedure are generated from this starting model.

The controlled random search (CRS) procedure is employed to invert the data to find the parameter values for dc resistivity (R_o), constant IP phase shift (ϕ_{ip}) and the constant of anisotropy (K). Parameter constraints are a five percent variation in the resistivity (R_o) from the apparent resistivity, a constant IP phase shift (ϕ_{ip}) greater than zero as well as an anisotropic constant (K) between 0.001 and 1000. The maximum number of trials was set at 3000 with the number of stored parameter points being 50.

The centroid of the final set of the fifty stored parameter values returned is considered the best estimate of a given parameter.

The starting cloud of parameter points, for all inversions, does not include the minimum parameter point found in the grid search. This is to ensure the controlled random search algorithm has absolutely no prior knowledge of the model parameters.

Inversions, using the controlled random search (CRS) algorithm, are initially carried out on model data generated using varying anisotropic constants (K) and contaminated with varying amounts of noise. Noise is generated from a uniform random distribution.

In an attempt to increase the rate of convergence, an annealing condition is applied to the algorithm. Inversions, using the modified algorithm, are carried out on data, contaminated by noise, generated from models with varying anisotropy (K) and resistivity (R_o), to test the effectiveness of the annealing approach. Again, the data is contaminated by uniform random noise.

(6.1) Theoretical Data with Varying Amounts of Noise

Two model spectra were used to test the CRS algorithm and are representative of the positive as well as negative coupling cases. Both have a constant IP phase shift of 25 mrad and mean resistivity of 10 ohm. The first model is of an isotropic half-space, having an anisotropic constant (K) of one. The second model is of an anisotropic half-space, having an anisotropic constant of 0.5.

Error surfaces for constant IP phase shift (ϕ_{ip}) versus anisotropy (K) over the two models, with data contaminated by five and ten percent noise, are presented with the initial cloud of parameter points used superimposed (Fig 6.1). The initial cloud of parameters are well spread over parameter space.

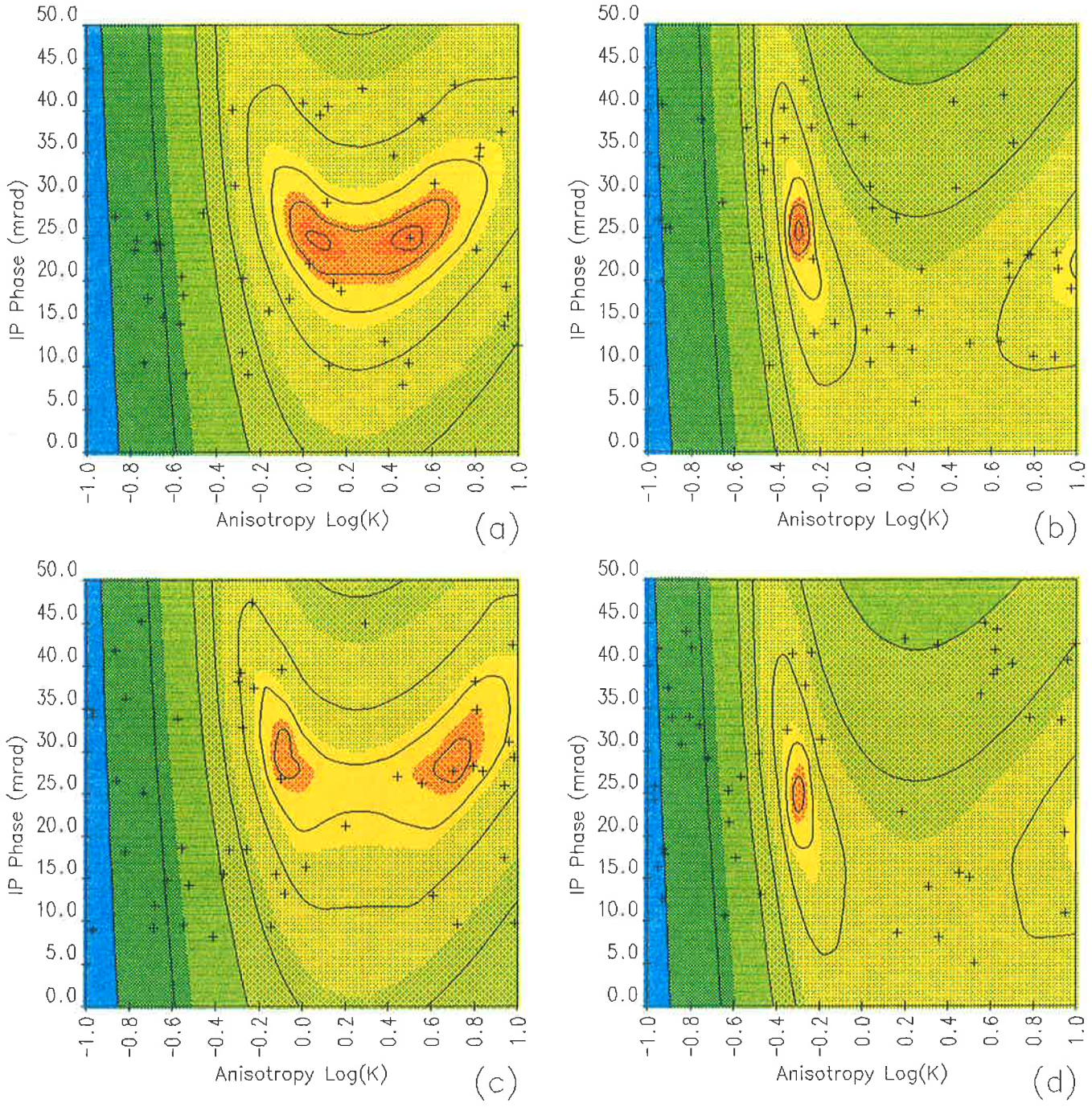

Fig. 6.1 : Initial parameter cloud superimposed on the inversion error surface for a model with Resistivity Ro = 10 Ohm-m, constant IP phase of 25 mrad and;
a) K = 1.0 and 5% random noise
b) K = 0.5 and 5% random noise
c) K = 1.0 and 10% random noise
d) K = 0.5 and 10% random noise

The error surfaces produced for the model data contaminated by ten percent noise (Figs 6.1c and 6.1d) have the global minimum slightly offset from the true, uncontaminated, parameter values. This is attributed to the noise contaminated model data being generated for fifteen frequencies only. The small sample is more readily affected by a bias in the data. The controlled random search (CRS) algorithm will be expected to converge to the global minimum, which is close to the uncontaminated parameter values.

It should be noted that the initial parameter clouds generated for these models, when the data is contaminated by five (Figs 6.1a and 6.1b) and ten (Fig 6.1c and 6.1d) percent noise, include parameter points located very close to or in a local minima. The application of a linear or standard non-linear inversion technique to this data, using those initial model parameters located near local minima, would converge towards the local minima and return an erroneous solution.

A stop criteria, based on the maximum and minimum error of the fifty stored parameter points, was employed as a test of convergence. The stop criteria is as follows;

$$Error_{min} - Error_{max} < 0.01$$

When the inversions were carried out this stop criteria was employed but in all cases was not satisfied after three thousand iterations and the algorithm was terminated.

The CRS_CIP program was run for three thousand iterations and the final best fifty estimates plotted onto the error surfaces (Fig 6.2). Results of the inversion indicate the CRS algorithm avoids converging to the local minima and has little trouble finding the global minimum.

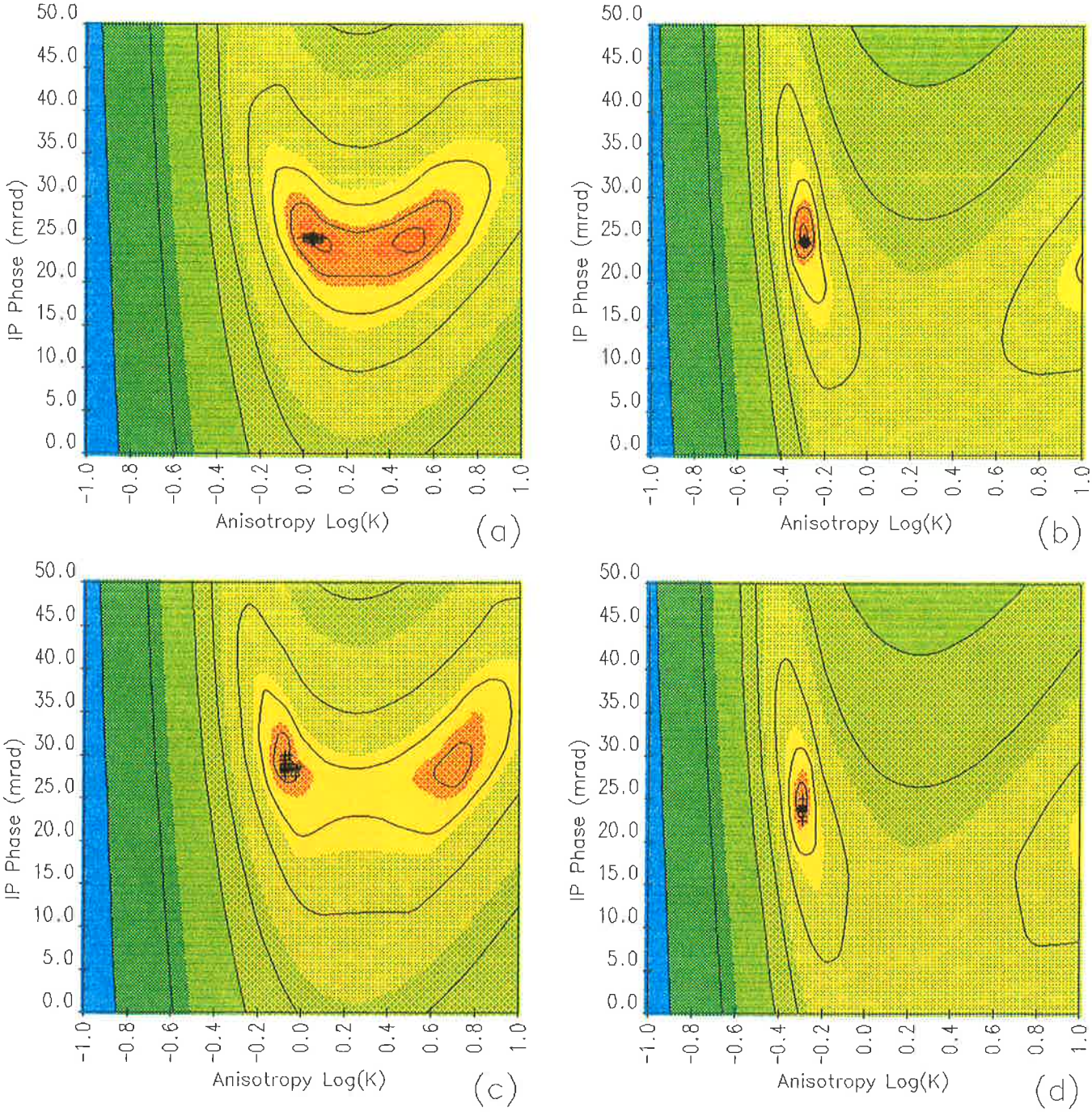

Fig. 6.2 : Final parameter cloud, superimposed on the inversion error surface, after running the CRS algorithm on a model with Resistivity Ro = 10 Ohm-m, constant IP phase of 25 mrad and;
a) K = 1.0 and 5% random noise
b) K = 0.5 and 5% random noise
c) K = 1.0 and 10% random noise
d) K = 0.5 and 10% random noise

When the data is contaminated with five percent noise the final parameter solutions form a cloud close to or at the correct solution (Figs 6.2a and 6.2b). When the data is contaminated with ten percent noise the final parameter solutions are centered on the global minimum (Figs 6.2c and 6.2d), which is close to the uncontaminated value (Table 1.0).

To verify the reliability of the CRS algorithm, the program was run another three times on the two models contaminated by ten percent noise, each time using a different set of random numbers to generate the initial cloud of parameters (Table 1.0). In all

Run	Range of K	Range of ϕ_{ip}	Final K	Final ϕ_{ip}	Error	Iter
1	0.73-0.96	26.89-30.31	0.831	28.29	4.959	3000
2	0.75-1.01	26.57-30.02	0.830	28.04	4.961	3000
3	0.77-1.08	26.74-30.15	0.834	28.53	4.960	3000
4	0.71-1.24	26.66-30.10	0.828	28.21	4.961	3000

A)

Run	Range of K	Range of ϕ_{ip}	Final K	Final ϕ_{ip}	Error	Iter
1	0.497-0.521	23.01-24.96	0.512	23.97	2.053	3000
2	0.504-0.527	23.41-25.74	0.515	24.06	2.061	3000
3	0.489-0.518	23.04-25.16	0.510	24.01	2.060	3000
4	0.487-0.515	23.02-24.97	0.512	23.91	2.053	3000

B)

TABLE 1.0: Results of inverting model data, contaminated by 10 percent random noise, using the CRS-CIP program.
A) Model: K = 1.0, ϕ_{ip} = 25 mrad, R_o = 10 ohm
Global: K = 0.83, ϕ_{ip} = 28.3 mrad, R_o = 10 ohm
B) Model: K = 0.5, ϕ_{ip} = 25 mrad, R_o = 10 ohm
Global: K = 0.512, ϕ_{ip} = 24 mrad, R_o = 10 ohm

cases, the best estimates are very similar to each other, and close to the global solution, even though the cloud of final parameter solutions differ between runs. The different ranges of final parameters returned between runs is indicative of the difference in the final cloud of parameter solutions.

The effect of noise on the resolution of the returned parameters can be seen when comparing the final cloud of parameters returned from data contaminated with five percent (Figs 6.2a and 6.2b) and ten percent (Figs 6.2c and 6.2d) random noise. As expected, the resolution of the constant IP phase (ϕ_{ip}) model parameter is dependent on the amount of noise present in the data. Of interest is the consistency in the resolution of the anisotropic constant (K) regardless of the noise present. These results indicate the resolution of the anisotropic parameter is influenced less by random noise in the data than that of the IP parameter.

The more noise present in the data the longer it will take for the algorithm to adequately resolve both parameters. The decrease in resolution of the IP parameter, compared to that of the anisotropic parameter, as the noise level is increased, is due to the different rate at which the two parameters are resolved by the algorithm. Essentially, the algorithm resolves the anisotropic constant early in the iteration process because the inversion error is more sensitive to changes in the anisotropy.

One solution would be to increase the number of iterations until the constant IP phase shift is adequately resolved. This is not desirable considering the time taken for 3000 iterations (approximately 4.5 minutes on a standard 486), which is excessive when a given pseudosection contains hundreds of points to be inverted. Another option would be to reduce the number of trial

points, effectively reducing the initial search domain of the algorithm, which would undermine the controlled random search process. A compromise would be to employ an annealing type of approach which effectively decreases the search domain of the algorithm as it progresses.

(6.2) Inverting Model Data of Varying Resistivities using an Annealing Condition

The accuracy of the final solution is dependent on the size of the cloud of final parameters returned. The larger the cloud the less influence outliers will have on the final solution. The rate at which the algorithm converges to a correct solution is dependent on the size of the solutions stored. The algorithm converges more quickly as the number of stored solutions is decreased.

In an attempt to find a balance between the rate of convergence and quality of the best estimate, an annealing condition was applied to the algorithm where the chance of selecting an extreme parameter value decreases as the number of iterations increases.

Rothman (1985) outlined similarities between the optimization of energy in the annealing process and the maximization of stack power in statics estimation in seismic processing. Rothman was able to draw an analogy between the two optimization problems and apply a modified metropolis algorithm to solve the statics estimation problem.

Rothman's method is essentially an iterative inversion technique that makes a random guess of a model parameter and then uses a decision process, the annealing function, to decide whether to accept or reject this parameter guess. A parameter guess that increases the objective function value is accepted

while those that decrease the objective function value have a certain probability of being accepted or rejected. The algorithm begins with many bad parameter guesses being accepted. As the algorithm continues the number of bad guesses accepted is reduced to a point where few or none are being selected.

The annealing condition used here is a simplified approximation of the classical annealing process employed by Rothman (1985). Here the annealing condition is applied by sorting the stored parameter points in order of error going from the minimum up to the maximum error. A random index used to select points from the stored points is derived by randomly choosing a number (X) between zero and one, then finding the nearest integer when putting this number to the power of an annealing condition and multiplying it by the number of stored points (Ncloud).

$$\mathrm{INDEX}(P) = 1 + \mathrm{NINT}\left\{ \left[\mathrm{RANDOM}(X)^{\mathrm{ANNEAL}}\right] \times N\mathrm{cloud} \right\}$$

Where INDEX(P) = 1 is the index of the parameter point with the lowest error.

The annealing condition at a given iteration (Iteration) for a number of stored parameter points (Ncloud) is:

$$ANNEAL = \frac{I\mathrm{teration}}{(\ N\mathrm{cloud} \times C\ )}$$

Where C is a control constant determining the rate of annealing.

As the program progresses the value of the annealing condition increases, causing the random selection of trial points to become more restricted to those near the lowest minima. This results in the cluster of stored parameter points contracting more rapidly about the lowest minima.

Four model spectra were used to test the modified CRS algorithm. All models have a constant IP phase shift of 25 mrad and are contaminated with ten percent noise. The first model is of an isotropic half-space, having an anisotropic constant (K) of 1.0, with a mean resistivity (R_o) of 1.0 ohm-m. The second model is of an anisotropic half-space, having an anisotropic constant (K) of 4.0, with a mean resistivity (R_o) of 10 ohm-m. Model three is isotropic with a mean resistivity (R_o) of 100 Ohm-m. While the fourth is anisotropic, having an anisotropic constant (K) of 4.0 and a mean resistivity (R_o) of 100 ohm-m.

Error surfaces for constant IP phase shift (ϕ_{ip}) versus anisotropy (K) over the four models, with ten percent noise present, are presented with the initial cloud of parameter points used superimposed (Fig 6.3). The initial cloud of parameters are spread over parameter space.

When the mean resistivity (R_o) is at 1.0 and 10 ohm-m the global minimum are well defined (Figs 6.3a and 6.3b). The error surfaces for the models with mean resistivities (R_o) of 100 ohm-m (Figs 6.3c and 6.3d) indicate that as the resistivity is increased, the error is flattened out, so that the location of the global minimum is not easily determined. The modified controlled random search (CRS) algorithm will be expected to converge to the global minimum, which should be close to the uncontaminated parameter values.

The modified CRS_CIP program, using the annealing condition, was run until errors from the stored parameter points were within an acceptable range. A stop criteria based on the maximum and minimum error of the fifty stored parameter points was employed as a test of convergence. The stop criteria is as follows;

$$Error_{min} - Error_{max} < 0.01$$

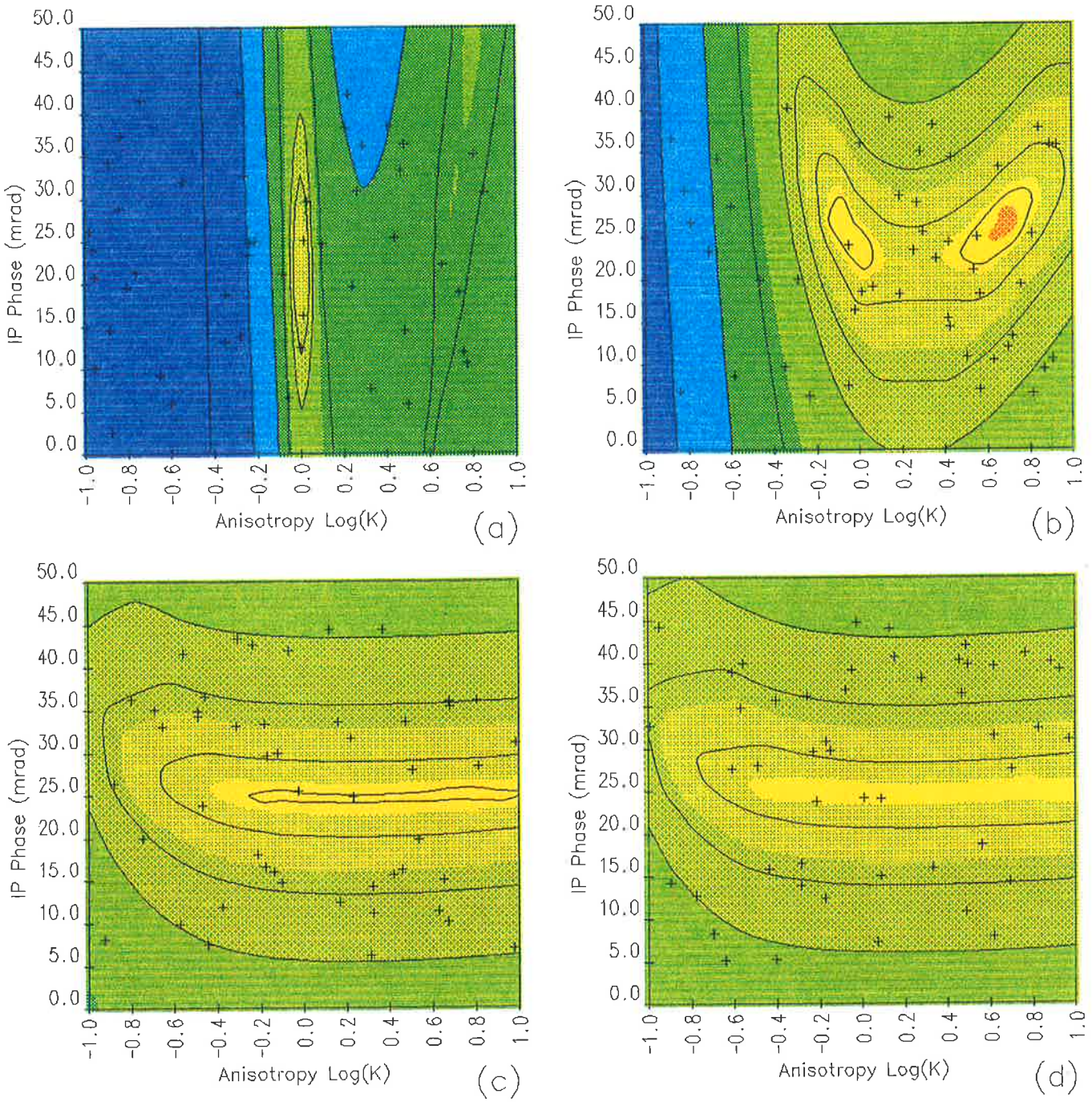

Fig. 6.3 : Initial parameter cloud superimposed on the inversion error surface for a model with a constant IP phase of 25 mrad and;
a) K = 1.0, Ro = 1.0 ohm-m and 10% random noise
b) K = 4.0, Ro = 10 ohm-m and 10% random noise
c) K = 1.0, Ro = 100 ohm-m and 10% random noise
d) K = 4.0, Ro = 100 ohm-m and 10% random noise

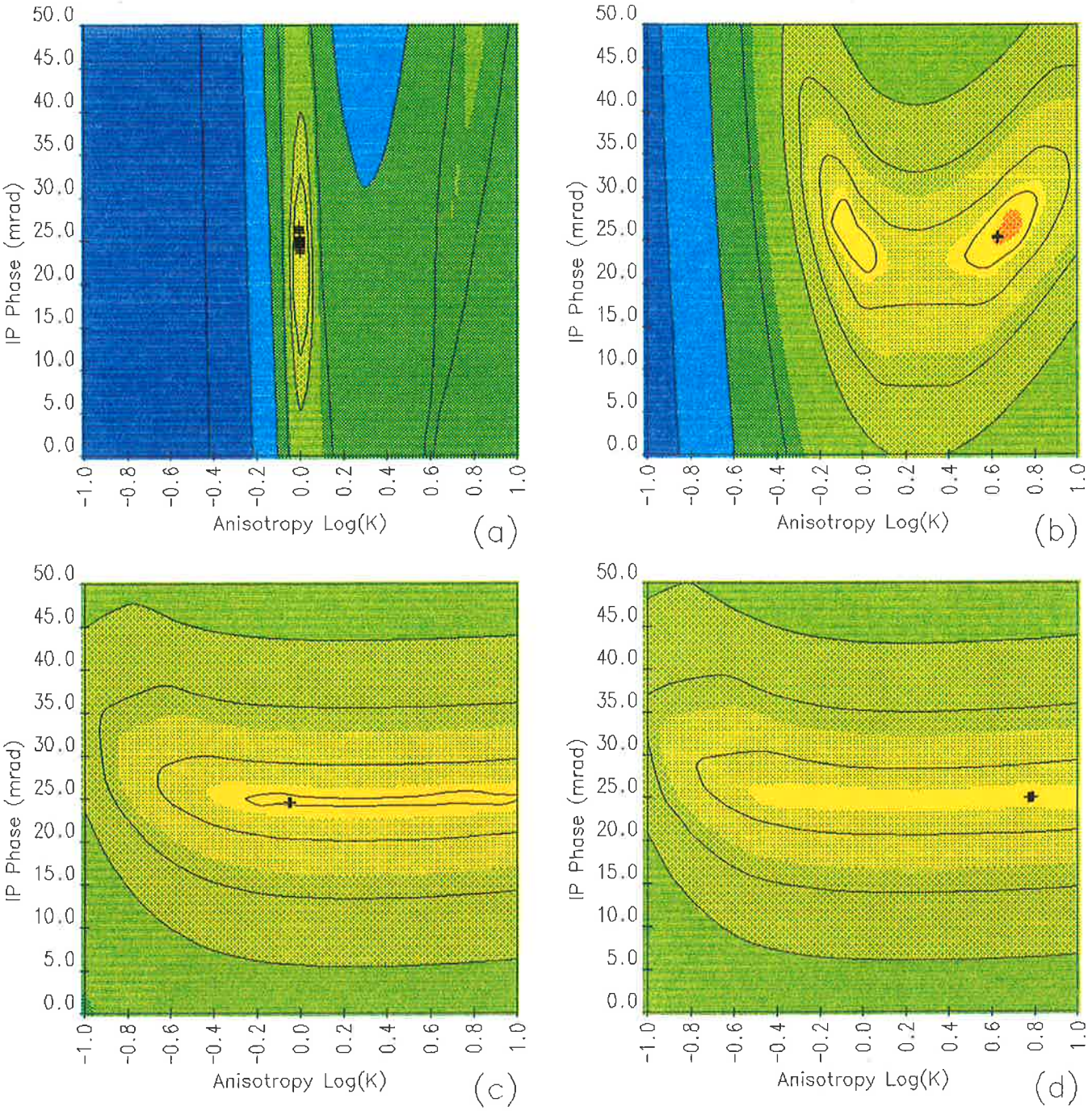

Fig. 6.4 : Final parameter cloud, superimposed on the inversion error surface, after running the CRS algorithm on a model with a constant IP phase of 25 mrad and;
a) K = 1.0, Ro = 1.0 ohm-m and 10% random noise
b) K = 4.0, Ro = 10 ohm-m and 10% random noise
c) K = 1.0, Ro = 100 ohm-m and 10% random noise
d) K = 4.0, Ro = 100 ohm-m and 10% random noise

MODEL	Range of K	Range of ϕ_{ip}	Final K	Final ϕ_{ip}	Error	Iter
A	0.988-0.998	23.91-26.18	0.993	24.99	15.42	1075
B	4.21-4.28	25.11-25.54	4.22	25.32	2.610	750
C	0.881-0.903	24.55-24.06	0.891	24.57	10.3	900
D	5.86-6.22	24.88-25.01	5.96	24.94	9.56	1050

TABLE 2.0: Results of inverting model data, contaminated by 10 percent random noise, using the modified CRS-CIP program.

A) Model: K = 1.0, ϕ_{ip} = 25 mrad, R_o = 1.0 ohm

B) Model: K = 4.0, ϕ_{ip} = 25 mrad, R_o = 10 ohm

C) Model: K = 1.0, ϕ_{ip} = 25 mrad, R_o = 100 ohm

D) Model: K = 4.0, ϕ_{ip} = 25 mrad, R_o = 100 ohm

The global minimum located for the model with a mean resistivity (R_o) of 100 ohm and anisotropy (K) of 4.0 (Fig 6.4d) indicates the anisotropy is substantially different from the uncontaminated parameter value (Table 2.0). This is attributed to a combination of the reduced contribution of the anisotropy to the total model response, due the increase in resistivity, and a bias in the random noise sample applied to the data. The implication, of this limited test, is that non random or skewed random noise samples have a greater effect on the anisotropic parameter returned as the mean resistivity increases.

(6.3) SUMMARY

Initial inversions indicate the controlled random search (CRS) algorithm is effective in locating the global minimum. Several inversions were carried out on the same data sets to test the repeatability of the algorithm and returned final parameter solutions close to each other and the global solution. The resolution of the final parameters, particularly the constant IP phase (ϕ_{ip}) parameter, and the inefficient nature of the controlled random search procedure, evident in the number of iterations used to invert the data, was of concern.

The application of an annealing condition in the controlled random search has proven to be beneficial to both the resolution of the final solution returned as well as to the rate at which the algorithm converges.

The results of inverting noise contaminated data, generated from models of varying mean resistivities (R_o), indicate that resistivity and elevated noise levels have a combined influence on the returned solution. When resistivity is low, the resolution of the returned IP parameter becomes more sensitive to noise. When resistivity is high, the resolution and final outcome of the anisotropic parameter become more sensitive to noise.

(7.0) DECOUPLING FIELD CR-IP SURVEY DATA

This chapter outlines the results of decoupling two lines of field dipole-dipole CR-IP survey data by inverting the individual spectra, at each pseudosection point, to an anisotropic half-space with complex resistivities. These two lines of data have been collected under differing conditions and over varying geological environments. The CR-IP data for both lines was recorded using a dipole size and a-spacing of 100 m in a seven spread receiver setup.

Complex resistivity measurements along both lines were recorded in the frequency domain by Zonge Engineering and Research Organization (ZERO) using the standard GGT 30 transmitter and GDP-16 receiver survey inventories.

Reciprocal readings are present in the data and are useful for data quality control, being an indication of possible problems with the data. Briefly, a reciprocal point is a point in the pseudosection at which the CR-IP data is taken twice, with the transmitter and receiver arrays swapping positions for the repeat reading. Even though the transmitter and receiver arrays have swapped positions the data is expected to repeat.

It is standard practice for Zonge Engineering and Research Organization (ZERO) to carry out a three point decoupling of phase data in the field. Pseudosection plots of the raw data consist of the apparent resistivity, raw phase angle at 0.125 Hz as well as the three point decoupled phase data.

Zonge Engineering's three point decoupled phase is produced by extrapolating the phase response of a primary frequency and its third and fifth harmonic, using a linear function to a approximate a zero frequency IP response. The three point decoupling function is;

$$\phi_{3pt} = 1.875\ \phi_1 - 1.25\ \phi_3 + 0.375\ \phi_5$$

ϕ_{3pt} is the three point decoupled phase
ϕ_1, ϕ_2, ϕ_3 are the primary frequency phase and its third and fifth harmonics

This technique of field decoupling data is derived from previous work (Hallof, 1974), based on the assumption that the EM coupling response is approximated by a linear or quadratic function at lower frequencies (below 0.5Hz). Hence, extrapolating to zero frequency, using low frequencies, will produce a DC phase value free of coupling effects. This method can fail where the IP response varies significantly over low frequencies or where the EM coupling response is not readily approximated by linear or quadratic functions.

The CR-IP data for each line is first decoupled using an anisotropic half-space with constant IP phase shift (ϕ_{ip}) to model the total EM-IP response. The decoupled IP response, generated from the constant IP phase shift model, is compared to the three point field decoupled phase. Decoupling of the data is then carried out using an anisotropic half-space with complex frequency dependent Cole-Cole dispersion to model the IP response. The decoupled IP response, generated from the Cole-Cole

dispersion, is compared to the three point decoupled phase. The decoupled IP phase response returned when using a Cole-Cole dispersion is then compared to that returned from Zonge Engineering's inhouse decoupling routine (GDPHM).

(7.1) Test Line 1

Test Line 1 is full spectral CR-IP data collected using the first five odd harmonics of the primary frequencies of 0.125, 1.0 and 8.0 Hz. This CR data was collected over a moderately polarizable non-economic source hosted within weakly polarizable shales and siltstones. It is characterized by a noise-free spectra containing a moderate amount of EM coupling contamination (Appendix I).

The raw CR-IP data (Plate 1.0) is characterized by apparent resistivities varying between 30 and 150 ohm-m. The resistive areas at the west end of the line, centered on 37000E and 37500E, have elevated values of three point phase, indicating they are polarizable. A large resistive area at the eastern end, occurring between 38200E and 38600E, tends to be weakly polarizable. Conductive regions along the line have three point phase values close to zero, indicating they tend to be non-polarizable.

The three point decoupled phase was calculated using the primary frequency of 0.125 Hz and its first two odd harmonics (at 0.375 and 0625 Hz). The minimal difference between the 0.125 Hz phase and three point phase plots indicate the low frequency response, at 0.125 Hz, is relatively free of coupling effects.

(7.1.1) Decoupled Using Program CRS_CIP

Inversion of the data was initially carried out using the program CRS_CIP (Version 2.1) which inverts the data to an anisotropic half-space with Constant IP phase shift complex resistivities.

The program begins by calculating the error distribution using a grid search over the anisotropic constant (K) and constant IP phase (ϕ_{ip}) parameters to determine a starting point for the controlled random search. Initially, the dc resistivity (R_o) is set at the measured apparent resistivity value. The maximum number of trials was set to 3000 with the number of stored parameter points being 50.

The parameter limits were set as follows;

DC Resistivity: $0.9 \; x \; R_{App} < R_o < 1.1 \; x \; R_{App}$ (ie. $\pm$ 10%)
Anisotropic Constant: $0.001 < K < 1000.0$
Constant IP Phase: $\phi_{ip} > 0.0$

Stop criteria: $$STOP = \frac{Error_{max} - Error_{min}}{Error_{max} + Error_{min}} < 0.05$$

Initial runs of the CRS_CIP algorithm on real data indicated the annealing condition should be allowed to reach unity faster. The annealing condition was employed and was reset with the control constant C as follows;

Annealing Condition: $$ANNEAL = \frac{Iteration}{(\; Ncloud \; x \; 10 \;)}$$

This annealing condition reaches unity after five hundred iterations and has the effect of speeding up the inversion while

still giving the algorithm plenty of opportunity to converge to a global solution.

The best parameter estimate is taken as the centroid of the returned fifty parameter points.

The CRS_CIP algorithm was applied to test line 1 and the resultant spectral responses of the IP, EM coupling and total EM-IP responses were plotted (Appendix II). The total EM-IP spectra are similar to the raw field spectra.

The dc resistivity (Plate 2.0) is well defined for all points and close to the apparent resistivity (Plate 1.0). There seems to be very little variation from the apparent resistivity values even at reciprocal points. Some reciprocals have a slight difference between the two values for apparent resistivity; which is reflected in the decoupled resistivity (Appendix II).

The constant IP phase shift (Plate 2.0) is well defined for most points in the pseudosection. In some cases the IP parameter is poorly resolved, with values widely spread about the minimum value. Reciprocals repeat well, with the poorest repeats being where the constant IP phase shift is poorly resolved.

On comparing the three point decoupled phase (Plate 1.0) and the decoupled constant IP phase response (Plate 2.0), it is apparent that the IP anomalies coincide at the western end of the line. Constant IP phase shift values are slightly higher than the three point decoupled phase. The major difference is the presence of point sources at depth, n = 7, in the constant IP phase shift pseudosection. The eastern end of the line differs significantly, where the decoupled constant IP phase indicates a more intense IP

anomaly than that indicated by the three point phase. The constant IP phase contains a phase anomaly at the eastern end with phase values significantly higher than the three point decoupled phase.

It should be noted that the inversion error returned in the resistive polarizable areas is considerably higher than those in the conductive non-polarizable areas. This is an indication of the failure of the constant IP phase shift model to adequately model the IP response in these areas. This may be due to a frequency varying IP response which is not able to be produced by the under parameterized constant IP phase shift complex resistivity model.

The anisotropic constant (Plate 2.0) is well defined for all points in the pseudosection, with the final cloud of parameters being tightly clustered about the minimum error solution.

Moderate values of the anisotropic constant ($K \cong 1.8$) are associated with the more resistive polarizable areas. The indication is that the resistive areas are fairly homogeneous geological units, with a gradual vertical variation in resistivity causing the current to have a predominantly horizontal path through the earth.

High values of anisotropic constant (K) tend to coincide with the conductive non-polarizable areas. The strongest response is seen in the conductive zone centered on 37250 E, at n = 2 to 4, which is surrounded by resistive ground. Current channeling effects, a good indication of anisotropy, would be expected to be greatest where a conductive zone resides in a resistive block. Comparing the resistivity (Plate 1.0) and anisotropy (Plate 2.0), would suggest that there is a direct relationship between the two. The anisotropy tends to be at a maximum when the resistivity is at its lowest.

(7.1.2) Decoupled Using Program CRS_CC

Inversion of the data was carried out using the program CRS_CC (Version 3.0), which inverts the data to an anisotropic half-space with Cole-Cole complex resistivities. The program begins by calculating the error distribution using a grid search over the anisotropic constant (K) and the Cole-Cole time constant (τ_o), chargeability (m) and frequency dependence (c) parameters to determine a starting model as well as an initial search domain for the controlled random search procedure. Initially, the dc resistivity (R_o) is set at the measured apparent resistivity value. The maximum number of trials was set to 5000 with the number of stored parameter points being 100.

The parameter limits were set as follows;

DC Resistivity: $0.9 \; x \; R_{App} < R_o < 1.1 \; x \; R_{App}$ (ie. $\pm$ 10%)
Anisotropic Constant: $0.001 < K < 1000.0$
Chargeability: $0.0 < m < 1.0$
Time Constant: $10^{-4} < \tau_o < 10^{+4}$
Frequency Dependence: $0.0 < c < 0.75$

Stop criteria: $$STOP = \frac{Error_{max} - Error_{min}}{Error_{max} + Error_{min}} < 0.01$$

Again initial runs of the CRS_CC algorithm on real data indicated the annealing condition should be allowed to reach unity faster.The annealing condition was employed and was set as follows;

Annealing Condition: $$ANNEAL = \frac{Iteration}{(\; Ncloud \; x \; 10 \;)}$$

The best parameter estimate is taken as the centroid of the returned one hundred parameter points.

Several initial runs of the CRS_CC program were made on test line 1 to fine-tune the procedure. From these runs it became apparent that the anisotropic constant (K) and dc resistivity (R_o) parameters were rapidly resolved early in the inversion. The error is less sensitive to changes in the Cole-Cole IP parameters. In the initial stages of the controlled random search bad choices of chargeability (m) and frequency dependence (c) are accepted into the cloud of parameter values because a certain value of anisotropic constant (K) or dc resistivity (R_o) is close to the correct value. This can lead to a cloud of parameters loaded with bad choices of chargeability (m) and frequency dependence (c), making it difficult to converge to reasonable values for these parameters.

To combat the problem constraints are initially placed on the Cole-Cole parameters, frequency dependence (c) and chargeability (m), restricting them to values near the starting values. After the anisotropic (K) and dc resistivity (R_o) parameters are settled, the constraints are removed and a full search is begun on the Cole-Cole parameters. Application of these constraints improves the repeatability and resolution of the final Cole-Cole parameter values returned after each run, although there are still problems with certain points. These are discussed later.

A modified CRS algorithm, CRS_CC (version 5.2) which initially constrains the frequency dependence (c) and chargeability (m), was applied to test line 1. The resultant spectral responses of the IP, EM coupling and total EM-IP

responses were plotted (Appendix II). The total EM-IP spectra compare well with the raw field spectra. Even points which have poorly resolved and varying Cole-Cole model parameter values produce spectral responses which compare well with the raw spectra over this range of frequencies.

Again, the dc resistivity (Plate 3.0) is well defined for all points and close to the apparent resistivity (Plate 1.0). There is a little more variation from the apparent resistivity value than that seen with the dc resistivity returned using a constant IP phase shift complex resistivity model.

Plots of the decoupled IP phase response at the primary frequencies of 0.125, 1.0 and 8.0 Hz (Plate 3.0) are characterized by a dramatic increase in the IP phase response, as the frequency increases, over the resistive polarizable areas. The IP phase response remains constant or at zero, as the frequency increases, over the conductive areas.

On comparing the three point decoupled phase (Plate 1.0) and the Cole-Cole decoupled phase responses (Plate 3.0), it is apparent that the IP anomalies coincide at the western end of the line. At low frequencies the orientation of the main anomaly, at the western end, follows that of the three point phase anomaly. At high frequencies the orientation of the phase anomaly follows that of the resistive feature. Again, the eastern end of the line differs in that the Cole-Cole decoupled IP phase indicates a more intense IP anomaly than that indicated by the three point phase.

When comparing the Cole-Cole phase response and the three point decoupled phase it is important to realize that the three point phase is calculated assuming the IP response is independent

of frequency, over a limited low frequency range, while the Cole-Cole dispersion IP model is frequency dependent.

It should be noted that the low frequency phase response for the Cole-Cole response is less than that indicated by the three point decoupled phase. The largest values do coincide with the anomaly apparent at the western end of the line in the three point decoupled data. However, a large amount of the total phase response at low frequencies has been accounted for by the EM coupling response calculated over the anisotropic half-space. The indication is that a larger amount of coupling is present at the lower frequencies than that indicated by the three point decoupled phase.

The IP response at the eastern end of the line seems better enhanced by a Cole-Cole dispersion than by the three point extrapolation to a zero frequency response. This may be an indication of the presence of a higher frequency IP response which is not enhanced by the three point extrapolation of low frequency phases. Alternatively, it may be an indication of the presence of residual high frequency EM coupling effects not accounted for by the anisotropic half-space forward model.

The chargeability (m) (Plate 4.0) is fairly well defined at most points in the pseudosection. High chargeabilities in the pseudosection (Plate 4.0) are associated with the resistive polarizable areas. The eastern end of the line is dominated by a very intense chargeability anomaly. This anomaly is more intense than the western chargeability anomaly that is associated with the main response apparent in the three point phase.

Frequency dependence (c) is fairly well defined for majority of points in the pseudosection (Plate 4.0). For points at which

chargeability is below $2x10^{-3}$, the frequency dependence is poorly defined and marked with TN (for too noisy). The frequency dependence (c) has low values which are loosely associated with the non-polarizable conductive areas. High values of frequency dependence are associated with the polarizable resistive areas.

The highest values of frequency dependence are associated with the anomaly at the eastern end of the line. This points to either a high frequency dependent IP response or the failure of the anisotropic half-space forward model to adequately model the EM coupling response. The presence of a residual EM coupling response would be accounted for by an increase in the frequency dependence of the Cole-Cole model.

Time constant (τ_o) is well resolved for most points in the pseudosection (Plate 4.0). For the points at which chargeability is below $2x10^{-3}$ or is poorly resolved, the time constant is deemed to have no significant contribution to the total response and marked with TN. Resistive polarized areas in the pseudosection are associated with values less than 0.001, while conductive non-polarizable areas are dominated by values greater than 1.0.

The anisotropic constant (K) is well defined in all cases (Plate 4.0). The values returned compare well to those obtained when decoupling is done using constant IP phase shift complex resistivities to model the IP response (Plate 2.0). Only a small number of points show a slight difference in the anisotropic constant (K) when different IP models are used. The results of modeling the EM coupling response for this particular set of CR-IP data, using an anisotropic half-space with complex resistivities, is relatively independent of the IP model used.

(7.2) Test Line 2

Test Line 2 is full spectral CR-IP data collected using the first five odd harmonics of the primary frequencies of 0.125, 1.0 and 8.0 Hz. This CR-IP data was collected over a moderate to strongly polarizable economic source associated with a steeply dipping structure, hosted in weakly polarizable shales and siltstones. This line also contains highly resistive non-polarizable limestones overlying a relatively conductive and moderately polarizable unit. The CR-IP data is characterized by noise affected spectra containing moderate amounts of EM coupling contamination (Appendix III).

The raw CR-IP data (Plate 5.0) is characterized by apparent resistivities widely varied from 30 to 1800 ohm-m. The conductive south end of the line has relatively high values of three point decoupled phase, indicating it is highly polarizable. A large resistive unit at the northern end, occurring between 27300N and 27800N, tends to be weakly to non-polarizable. This unit overlies a moderately polarizable conductive region.

The three point decoupled phase was calculated using the primary frequency of 0.125 Hz and its first two odd harmonics. The three point decoupled phase differs from the 0.125 Hz phase, indicating the low frequency response has some EM coupling effects present.

(7.2.1) Decoupled Using Program CRS_CIP

The data was inverted using the program CRS_CIP (Version 2.1) which inverts the data to an anisotropic half-space with Constant IP phase complex resistivities. The initial anisotropic

constant (K) and constant IP parameters are determined by calculating the error using a grid search in parameter space. Initially, the dc resistivity (R_o) is set at the measured apparent resistivity value. The maximum number of trials was set to 3000 with the number of stored parameter points being 50.

The parameter limits were set as follows;

DC Resistivity: $0.9 \times R_{App} < R_o < 1.1 \times R_{App}$ (ie. $\pm$ 10%)
Anisotropic Constant: $0.001 < K < 1000.0$
Constant IP Phase: $\phi_{ip} > 0.0$

Again, a stop criteria and the annealing condition were employed and are those used for decoupling Test line 1.

The best parameter estimate is taken as the centroid of the returned fifty parameter points.

The spectral responses of the IP, EM coupling and total EM-IP responses were plotted (Appendix IV). The total EM-IP spectra are similar to the raw field spectra (Appendix III).

The dc resistivity (Plate 6.0) is well defined for all points and close to the apparent resistivity (Plate 5.0). The greatest variation from the apparent resistivity is seen in the resistive unit at the northern end of the line.

The constant IP phase (Plate 6.0) is well defined at all points in the pseudosection and compares well with the three point phase (Plate 5.0) at most points. The general trend is for

the constant IP phase shift to be slightly higher than the three point phase. There is good correlation between the IP anomalies at the southern end of the line. The constant IP phase shift gives an approximation of the zero frequency IP phase response, which is similar to the three point decoupled phase. The northern end of the line differs in that the decoupled constant IP phase shift contains a point source at 27750, n of 7, which is attributed to the noisy nature of the spectra at this point (Appendix IV).

The anisotropic constant (Plate 6.0) is well defined for all points in the pseudosection. Values of anisotropic constant (K) less than one are associated with the high over low resistivity contrast at the northern end of the line. This is consistent with the downward vertical channeling of current due to a high over low coupling environment (chapt. 2.2). Moderate values of the anisotropic constant ($K \cong 1.8$) are associated with the less resistive polarizable areas. High values of the anisotropic constant ($1.8 < K < 20$) tend to be associated with the non-polarizable conductive areas.

Of interest are the extreme and wildly varying values of anisotropy ($K > 20$) which are associated with the contact between the resistive and conductive units as well as the conductive unit underlying the resistive feature. The extreme anisotropic constant (K) values associated with the conductive unit underlying the resistive feature, are indicative of very strong horizontal current channeling. Extreme and wildly varying values occurring as point sources, associated with the contact, are more likely an indication of the failure of the anisotropic half-space to give a good approximation of the complex nature of the resistivity structure at these points.

(7.2.2) Decoupled Using Program CRS_CC

Inversion of the data was carried out using the program CRS_CC (Version 5.2), which inverts the data to an anisotropic half-space with Cole-Cole complex resistivities. The program calculates the error distribution and determines initial values of the anisotropic constant (K) and the Cole-Cole time constant (τ_o), chargeability (m) and frequency dependence (c) parameters. Initially, the dc resistivity (R_o) is set at the measured apparent resistivity value. The maximum number of trials was set to 5000 with the number of stored parameter points being 100.

The parameter limits were set as follows;

DC Resistivity: $0.9 \times R_{App} < R_o < 1.1 \times R_{App}$ (ie. $\pm$ 10%)
Anisotropic Constant: $0.001 < K < 1000.0$
Chargeability: $0.0 < m < 1.0$
Time Constant: $10^{-4} < \tau_o < 10^{+4}$
Frequency Dependence: $0.0 < c < 0.75$

Again, a stop criteria and the annealing condition were employed and are those used for decoupling Test line 1.

The best parameter estimate is taken as the centroid of the returned one hundred parameter points.

Plots of the total EM-IP spectra (Appendix IV) compare well with the raw field spectra (Appendix III). Only points badly affected by noise differ markedly. There are also marked differences in the spectra of some of the reciprocal points near the sharp resistivity contrast evident at the northern end of the line.

Again, the dc resistivity (Plate 7.0) is well defined for all points and close to the apparent resistivity (Plate 5.0). The variation from the apparent resistivity values is greater for the dc resistivity returned using a Cole-Cole complex resistivity than that using a constant IP phase shift complex resistivity model.

Plots of the decoupled IP phase response at the primary frequencies of 0.125, 1.0 and 8.0 Hz (Plate 7.0) are characterized by a moderate increase in the IP phase response, as the frequency increases, over the polarizable areas. The IP phase response remains constant or at zero, as the frequency increases, over the non-polarizable areas.

The low frequency phase response for the Cole-Cole response over the lobe anomalies to the south of the line are less than that indicated by the three point decoupled phase. The phase response at low frequencies has been partially accounted for by the EM coupling response returned from the anisotropic half-space.

There is good correlation between the IP anomalies from the Cole-Cole dispersion and that evident in the three point phase, at the southern end of the line. The northern end of the line differs in that the decoupled IP phase contains a lobe of moderate phase values associated with the boundary between the resistive and conductive units.

The chargeability (m) (Plate 8.0) is fairly well defined in most areas with high chargeabilities being associated with the polarizable areas at the southern end of the line. The northern end of the line is dominated by moderate to low chargeabilities. The intense point source is attributed to noise contamination in the observed data.

The frequency dependence (c) is well resolved at most points in the pseudosection where the chargeability is high enough, above $2x10^{-3}$, for the frequency dependence (c) to have a significant effect on the IP response (Plate 8.0). Moderate to high values of frequency dependence are loosely associated with the polarizable areas. The highest values of frequency dependence are associated with the anomaly at the very southern end of the line. This indicates either a high frequency dependent IP response or the failure of the anisotropic half-space forward model to adequately model the high frequency EM coupling response.

Time constant (τ_o) is well resolved at most points in the pseudosection where the chargeability (m) is high enough, above $2x10^{-3}$, for the time constant (τ_o) to have a significant contribution to the total response (Plate 8.0). The polarizable areas at the southern end of the line are associated with values around 0.001. Moderately polarizable areas are dominated by values between 0.01 and 1.0. The weakly and non-polarizable areas have values for the time constant (τ_o) greater than one.

The anisotropic constant (K) has a varying degree of resolution along the line (Plate 8.0). The values returned for the southern section of the line, up to about 27200N, are well resolved and are comparable to those obtained when decoupling using constant IP phase shift complex resistivities to model the IP response (Plate 6.0). However, the northern section of the line is riddled with a number of points which are poorly resolved and are significantly different from those obtained using a constant IP phase shift complex resistivity. In this case, the results of modeling the EM coupling response with an anisotropic half-space is dependent of the IP model used.

The inversion error generated by CRS_CC over the northern end of the line is similar and in some cases greater than that generated using a constant IP phase shift IP model. This further indicates a Cole-Cole dispersion offers no benefits when used to decouple CR-IP data taken over the non-polarizable resistive unit.

(7.3) Discussion of Problem Points and Algorithm Failure

During the inversion of the CR-IP field data, lines one and two, certain points were found to return inconsistent and poorly resolved parameter values.

Decoupling using an anisotropic half-space with Cole-Cole complex resistivities produced the worst results. The Cole-Cole dispersion IP model tended to return poorly resolved and poorly repeating Cole-Cole parameters at certain points in the pseudosections. These "bad" points might be explained in terms of the interdependence of the Cole-Cole parameters and influence of other parameters on the inversion error, with respect to the Cole-Cole parameters.

Problems were also experienced with the anisotropic constant (K) parameter returned at certain points on line two. Inversion of some reciprocal points returned extremely different reciprocal values for the anisotropic constant (K). It was also found that at some points the values of anisotropy returned using a constant IP phase shift were different from those returned using a Cole-Cole complex resistivity. The modeled EM coupling response, for these problem points, appears to be affected by the IP model use.

When inverting theoretical model data contaminated by noise, it was found that the combined influence of high resistivity and noise distorted the inversion error surface relative to the anisotropic parameter (chapt 6.0). The result was the inversion error no longer had the correct solution of anisotropy at its minimum. Perhaps examination of inversion error surfaces generated over selected bad points in the CR-IP field data will give an insight into the failure of the anisotropic half-space model at these points.

(7.3.1) Ambiguities in the Cole-Cole Dispersion Parameters

When decoupling line one with CRS_CC, some points have failed to give repeatable results for the chargeability (m) and frequency dependence (c) parameters from one inversion run to the next. Also, some reciprocal points present in the line data appear to have values for chargeability (m) which are significantly different from each other (Appendix II). These results are surprising considering that line one is relatively noise-free and only moderately contaminated by EM coupling.

The worst points tended to be where the mean resistivity of the ground was low and the IP response was not significantly contributing to the total response.

Previously (chapt 4.3), the inversion error was calculated using Cole-Cole parameter pairs to produce error surfaces and indicated a dependence between the different Cole-Cole parameters under certain conditions. This dependence indicated that as the mean resistivity decreased the Cole-Cole parameters would have a greater chance of inverting to an incorrect solution.

The controlled random search (CRS) algorithm fails to overcome the multi-minima problem apparent for the Cole-Cole parameters when the ground is conductive and there is no significant IP contribution to the total response.

It is interesting that the relationship between frequency dependence (c) and chargeability (m) appears as an inverse relationship in the resolution of the two parameters. That is, one is well resolved when the other is poorly resolved. This apparent relationship between frequency dependence (c) and chargeability (m) is actually dependent on the value of the time constant (τ_o). Error surfaces produced in chapter 4.3 suggested that the resolution and final parameter value returned for the frequency dependence (c) and chargeability (m) can be highly sensitive to the value of the time constant (τ_o).

The chargeability is most badly affected at points in the pseudosection with small values of time constant (τ_o). The error surfaces produced (chapt 4.3.1) over a response generated from a Cole-Cole dispersion model with the time constant (τ_o) set at 0.01, for chargeability (m) versus time constant (τ_o), is dominated by a series of local minima of near equal intensity to the global minimum (Fig 4.9b). At low values of time constant the frequency dependence (c) is well defined (Fig 4.9c).

Minima occur at different chargeabilities (m) but remain near the correct value for time constant (τ_o). Noise in the field data causes the algorithm to fail in overcoming the multi-minima problem, returning different values of chargeability after each run.

The frequency dependence (c) is most badly affected at points in the pseudosection with large values of time constant (τ_o). The error surface produced (chapt 4.3.2) over a model with the time constant (τ_o) set at 100, for frequency dependence (c) versus time constant (τ_o), is dominated by a series of local minima of near equal intensity to the global minimum(Fig 4.10c). At high values of time constant the chargeability (m) is well defined (Fig 4.10b).

(7.3.2) Problems with the Anisotropic Half-Space Model

When decoupling line two, with CRS_CC and CRS_CIP, some data points returned poorly resolved and questionable values for the anisotropic constant (K). Also, some reciprocal points in the data have values for anisotropic constant significantly different from each other (Appendix IV).

The worst points tended to be where the mean resistivity of the ground was high or near the boundary between resistive and conductive units, where the CR-IP data is noisy.

Plots of the anisotropic constant(K) for line 2 (plates 6.0 and 8.0) contain a number of points which are poorly resolved and have reciprocals which are significantly different from each other (Appendix IV).

Inversion of the reciprocal points at 27300N, n = 4, to an anisotropic half-space with either constant IP phase shift or Cole-Cole complex resistivities, produces extremely different reciprocal values for anisotropy (Appendix IV).

Error surfaces of the reciprocals at point 27300N, n = 4, were produced for anisotropy (K) versus constant IP phase (ϕ_{ip}) with the dc resistivity (R_o) set at the final decoupled value returned by CRS_CIP (Figs 7.1a and 7.1b). The error surfaces are similar to each other and are both dominated by two minima of similar error centered on different values of anisotropic constant.

In this case the presence of noise in the data has obscured the absolute minimum. The algorithm has failed to overcome the multi-minima problem. This is an example of relatively high resistivities combined with noise obscuring the global minimum causing the algorithm to fail.

Unfortunately, there is no definite way of determining which value is due to a local minimum in the error. However, the surrounding values of anisotropy would indicate the global minimum has an anisotropic constant (K) less than one. The reciprocal value with an anisotropic constant (K) of 0.3 seems to fit the general trend.

Inversion of the reciprocal points at 27250N, n = 3, to an anisotropic half-space with either constant IP phase shift or Cole-Cole complex resistivities produces different reciprocal values for anisotropy (Appendix IV).

Error surfaces of the reciprocals at point 27250N, n = 3, were produced for anisotropy (K) versus constant IP phase (ϕ_{ip}) with the dc resistivity (R_o) set at the final decoupled value returned by CRS_CIP (Figs 7.1c and 7.1d) and differ considerably.

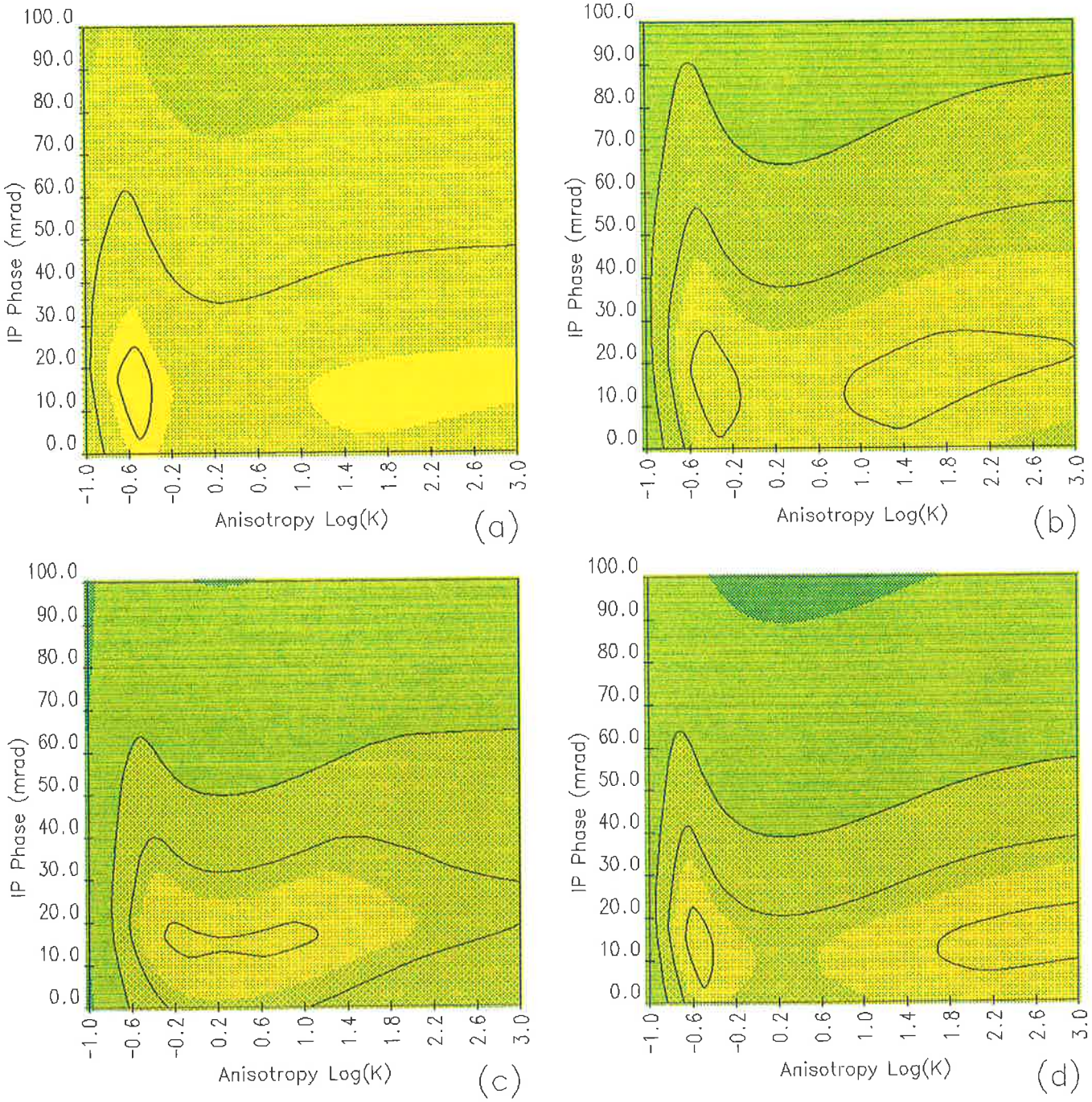

Fig. 7.1 : Inversion Error Surfaces for Constant IP Phase Vs. Anisotropy of problem data in Test Line 2; Reciprocal points with different final inversion parameter values for anisotropy
a) Station = 27300N, n = 4, Res. = 124.6 ohm-m
b) Station = 27300N, n = 4, Res. = 132.6 ohm-m
c) Station = 27250N, n = 3, Res. = 149.3 ohm-m
d) Station = 27250N, n = 3, Res. = 145.4 ohm-m

The form of the inversion error is different for the two reciprocal points. Regardless of the inversion process or the IP model used, the final solutions for anisotropy would always differ for this set of reciprocal measurements. This can be considered an example of the combination of a reduced contribution of EM coupling to the total response, due the increase in resistivity, and non-random noise causing different values of anisotropy to be returned.

When inverting to an anisotropic half-space with Constant IP phase shift complex resistivities the anisotropy at points 27500N, n = 4, and 27600N, n = 4, have similar reciprocal values. When the more complex Cole-Cole dispersion IP model is used the reciprocal values, at these points, differ considerably (Appendix IV).

Error surfaces of the reciprocals at points 27600N, n = 4, and 27500N, n = 4, were produced for anisotropy (K) versus constant IP phase (ϕ_{ip}) with the dc resistivity (R_o) set at the final decoupled value returned by CRS_CIP (Fig 7.2). The error surfaces at each point for the reciprocals differ from each other in form. However, they do contain global minimum centered on similar values of anisotropic constant.

Error surfaces for the same reciprocals were produced for anisotropy (K) versus chargeability (m) with the frequency dependence (c), time constant (τ_o) and dc resistivity (R_o) set at the final decoupled values returned by CRS_CC (Fig 7.3). The error surfaces for the reciprocals at each point are now more complex. The relationship between the anisotropy and the inversion error has been changed due to an increase in the complexity of the IP model.

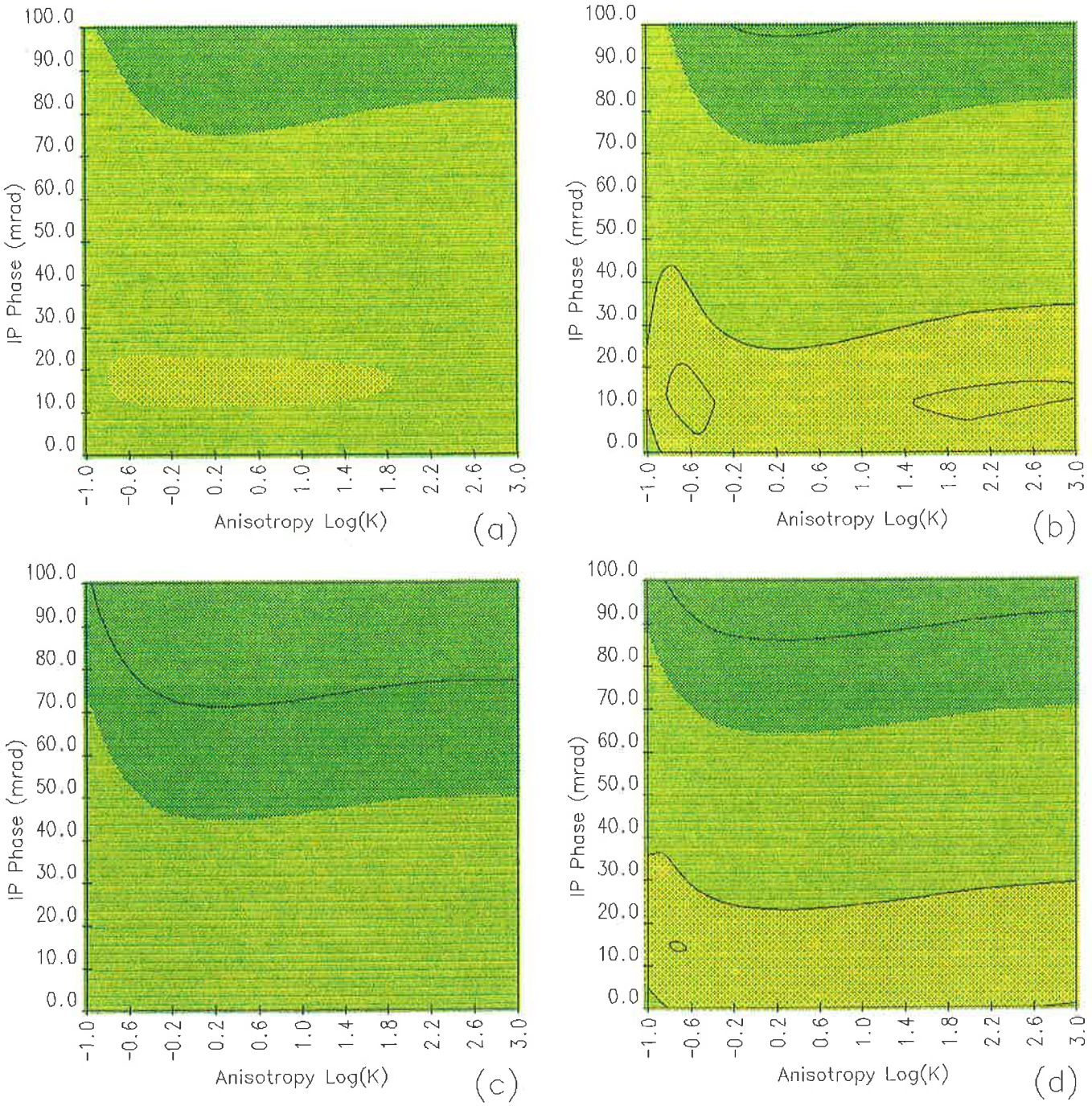

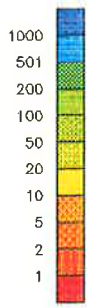

Fig. 7.2 : Inversion Error Surfaces for Costant IP Phase Vs. Anisotropy of problem data in Test Line 2; Reciprocal points with different final inversion parameter values for anisotropy
a) Station = 27600N, n = 4, Res. = 548.0 ohm-m
b) Station = 27600N, n = 4, Res. = 438.3 ohm-m
c) Station = 27500N, n = 4, Res. = 874.7 ohm-m
d) Station = 27500N, n = 4, Res. = 875.7 ohm-m

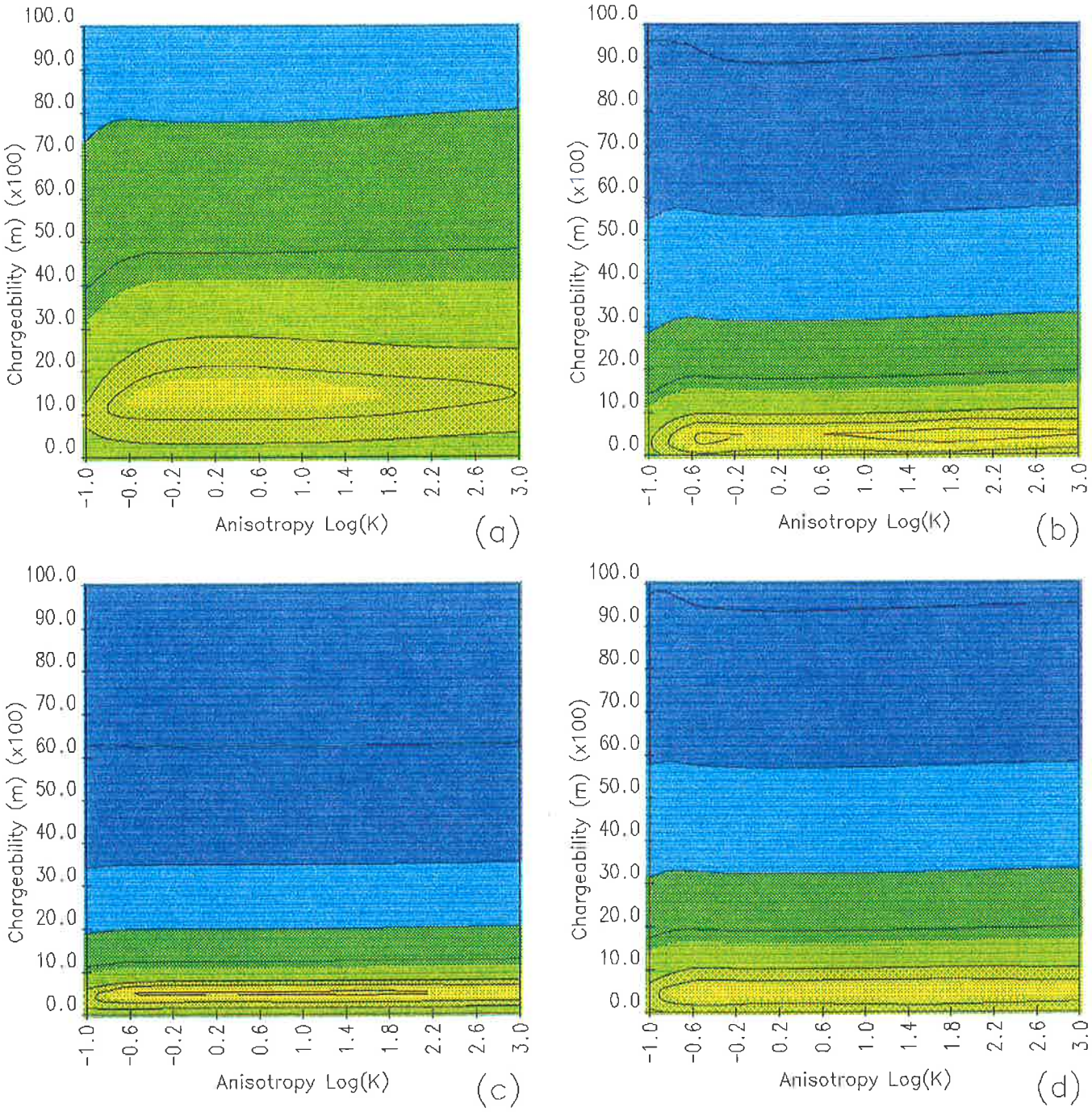

Fig. 7.3 : Inversion Error Surfaces for Chargeability (m) Vs Anisotropy (K) of problem data in Test Line 2; Reciprocal points with different final inversion parameter values for anisotropy

a) Station = 27600N, n = 4, Tau = 10E-4, c = 0.196
b) Station = 27600N, n = 4, Tau = 10E-0.7, c = 0.436
c) Station = 27500N, n = 4, Tau = 10E-0.8, c = 0.49.9
d) Station = 27500N, n = 4, Tau = 10E-0.2, c = 0.29.1

Of particular interest are the error surfaces of the reciprocal at point 27500N, n = 4, (Figs 7.3c and 7.3d), which have changed considerably with respect to the anisotropy, from those produced using the constant IP phase shift (Figs 7.2c and 7.2d). The result is that both reciprocals are now fitted by model data generated from a constant of anisotropy greater than one when using a Cole-Cole complex resistivity.

When the mean resistivity of the ground is increased the modeling of the EM coupling response is being influenced more by the type of IP model used. When the mean resistivity of the ground is high, the contribution of EM coupling to the total response is greatly reduced. A constant IP phase shift model is independent of frequency and cannot account for the frequency varying EM coupling response. The Cole-Cole dispersion IP model is frequency dependent and is more successful at accounting for the EM coupling response. Since the contribution of EM coupling to the total response is reduced, the inversion solution for the anisotropic constant (K) parameter is more sensitive to variations in the Cole-Cole parameters.

(7.4) The GDPHM Decoupling Routine

EM coupling responses are calculated by solving Sunde's (1949) equations for the mutual impedance of grounded wires over a given model of the earth. Methods for calculating the mutual impedance over isotropic homogeneous half-spaces and layered earth models have been outlined (Dey and Morrison, 1973; Hohmann, 1973; Wynn and Zonge, 1977). This work has led to the development of iterative decoupling routines which attempt to model the combined IP and EM coupling responses.

The program GDPHM was developed by Zonge Engineering and Research Organization (ZERO) in the early 1980's to decouple field CR-IP data by iteratively fitting total EM-IP responses calculated from a given EM model and an empirically derived IP model.

In GDPHM the EM coupling response is calculated using either an isotropic homogeneous half-space or a given layered earth model. The choice of the model to use is made by the operator or is automatically selected by the program. Selecting the initial model and inversion parameters is achieved by normalizing the field data by a standard coupling curve generated at n=6. Differences between the field data and standard coupling curve are used to determine the coupling environment. The most common coupling environments found are high over low resistivity (HIGH/LOW) or low over high resistivity (LOW/HIGH). GDPHM will normally select one or the other, as an initial model, automatically. More complex combinations usually have to be set as the initial model by the operator.

GDPHM generates IP curves based on the three point phase, or the 0.125 Hz phase if selected, and different type of phase response slopes. The Hilbert transform relationships between the magnitude and phase components of the spectral response are used as a guide for the decoupling routine. Magnitude is calculated from phase parameters determined assuming a phase response that varies either linearly with frequency or as the log of frequency. Limits are applied to the slope of the phase response, dependent on whether a linear or log relationship to frequency has been specified. These limits have been experimentally determined from a large sample of spectra taken from varying geological environments.

The following is a comparison of the results of decoupling the two test lines using CRS_CC (version 5.2) and the inhouse decoupling routine GDPHM developed by Zonge Engineering and Research Organization (ZERO).

When decoupling with GDPHM the initial model was set for a multiple layered coupling environment, which is standard when the resistivity structure of earth is not known. The environment type was set to the response expected for a typical hard rock environment, which is for low to moderate coupling.

(7.4.1) Line 1: Comparison of Decoupling Results Returned From the CRS algorithms and GDPHM

GDPHM was used to decouple line one and the resulting decoupled IP spectra were plotted (Appendix V). Comparing these spectra with those returned as the IP response from CRS_CC (Appendix II), it is apparent the GDPHM routine returns a much flatter IP response over the polarizable areas. There is less frequency dependence evident in the spectra returned from the GDPHM routine.

Plots of the decoupled IP phase response at the primary frequencies of 0.125, 1.0 and 8.0 Hz (Plate 9.0) indicate the decoupled IP phase response is relatively constant as the frequency increases, over the resistive polarizable areas to the west. There is, however, a slight increase in the phase as the frequency increases, over the polarizable area at the eastern end of the line. The IP phase response remains constant or near zero as the frequency increases, over the conductive areas.

On comparing the three point decoupled phase (Plate 1.0) and the GDPHM decoupled phase responses (Plate 9.0), it is apparent the GDPHM phase response remains at a value near the three point phase as the frequency increases.

The final phase response slope, after decoupling, was close to zero. That is the phase response remains fairly constant as the frequency increases. It would seem the GDPHM routine has generated an IP response by using the three point phase as an initial starting point and then placed constraints so as to prevent any significant variation from this starting point.

The Constant IP phase response (Plate 2.0) is comparable with the GDPHM decoupled phase responses at the primary frequencies of 0.125, 1.0 and 8.0 Hz. The indication is that the IP phase curves fitted to this data, by GDPHM, are similar to those generated by a constant IP phase shift complex resistivity model.

It is not surprising that on comparing the Cole-Cole phase response (Plate 3.0) and the GDPHM decoupled phase responses, at the primary frequencies of 0.125, 1.0 and 8.0 Hz (Plate 9.0), significant differences are apparent between the IP responses returned by the two algorithms. The phase response at 0.125 Hz, over the polarizable areas, is consistently lower than that returned by GDPHM, while the phase response at 8.0 Hz, over the polarizable areas, is considerably higher. The response at 1.0 Hz is comparable with that returned by GDPHM.

This may be an indication that the limits set by GDPHM, on the phase response slope are too restrictive. The IP model produced by GDPHM is unable to account for a frequency dependent IP response. The layered earth model, generated by GDPHM, is

forced to account for the frequency dependent IP response as well as the EM coupling response. Effectively, the frequency dependent IP response would be treated by the routine as a result of EM coupling. The result is an over decoupling of the CR-IP data, removing the frequency dependent IP response present.

Alternatively, it may indicate the failure of the anisotropic homogeneous half-space to adequately fit the EM coupling response of the underlying earth, especially that found at the eastern end of the line, although there is a slight increase in the phase response for the IP model returned from GDPHM in this area. The values of frequency dependence (c) returned from CRS_CC are very high, approaching the upper limit set before inversion.

High values of frequency dependence (c) (approaching one) are thought to indicate the presence of coupling. This tends to indicate the failure of the Anisotropic Half-space to adequately model the EM coupling response in this area. This leaves a residual response which the Cole-Cole IP model attempts to fit through the frequency dependence (c) parameter. Under parameterization of the EM coupling model causes a distortion of the IP parameters.

For this line, the results of decoupling using a CRS_CIP seem to agree with the results returned from CRS_CC, especially in indicating a more intense IP anomaly at the eastern end of the line. The results of decoupling using GDPHM tend to follow the three point field decoupled phase. Areas showing an increased frequency dependence in the IP phase response coincide for the responses returned from a Cole-Cole model and the GDPHM program.

(7.4.2) Line 2: Comparison of Decoupling Results Returned From CRS_CC and GDPHM

GDPHM was used to decouple line two and the decoupled IP spectra plotted (APPENDIX IV). These spectra are less frequency dependent than the IP response spectra returned from CRS_CC (APPENDIX III). GDPHM returns flatter IP responses over the polarizable areas.

Plots of the decoupled IP phase response at the primary frequencies of 0.125, 1.0 and 8.0 Hz (Plates 10.0) indicate the decoupled IP phase response increases very slightly with increasing frequency over the polarizable areas to the south. The polarizable area to the north shows a significant increase in the phase as the frequency increases. The IP phase response remains constant or near zero as the frequency increases, over the conductive areas.

On comparing the three point decoupled phase (Plate 5.0) and the GDPHM decoupled phase responses (Plate 10.0), it is apparent the GDPHM phase response remains at a value near the three point phase as the frequency increases. The IP model returned by GDPHM is similar to that expected using a constant IP phase shift complex resistivity which has the constant IP phase shift set at the three point phase value.

The Constant IP phase response (Plate 6.0) is very similar to the GDPHM decoupled phase responses at the primary frequencies of 0.125, 1.0 and 8.0 Hz. It would indicate that the EM coupling response generated by CRS_CIP is similar to that generated by GDPHM.

The Cole-Cole phase response (Plate 7.0) generated at the primary frequencies of 0.125, 1.0 and 8.0 Hz demonstrate a significant increase in the phase response with an increase in frequency, compared to the phase response returned from GDPHM (Plate 10.0).

In this case the results of decoupling using a constant IP phase shift model agree with the results returned from GDPHM. The results of decoupling using a Cole-Cole dispersion, to model the IP response, indicate a more frequency dependent IP phase response. However those areas showing more frequency dependence in the IP phase response, returned from a Cole-Cole model and GDPHM, coincide.

The IP phase response returned from GDPHM over the resistive unit to the north is smoother than that returned from CRS_CC. The anisotropic half-space with Cole-Cole complex resistivities has been shown to have produced spurious results over the resistive unit. The cleaner IP phase response returned from GDPHM and CRS_CIP is a further indication of the failure of anisotropic half-space with Cole-Cole complex resistivities to adequately model the total response in this area.

(8.0) CONCLUSION

The main purpose of this study has been an investigation of employing an automated decoupling routine which inverts field CR-IP data to a homogeneous anisotropic half-space with complex resistivities.

The convergent properties of a homogeneous anisotropic half-space with complex resistivities was investigated through the use of L_1-Norm inversion error surfaces. It was apparent that the basic survey characteristics and mean ground resistivity affect the resolution of model parameters and final values returned for model parameters. L1-norm inversion error surfaces of models with varying anisotropy and IP parameters indicate the inversion of CR_IP data to an anisotropic half-space with complex resistivities must be treated as a multi-minima problem. The interdependence of the inverse solutions for the Cole-Cole parameters was demonstrated.

A controlled random search (CRS) procedure was thought to be the appropriate inversion technique to use as it is able to overcome the multi-minima problem, it covers a wider area of parameter space and is not restricted to the path of least resistance towards the nearest minimum. The controlled random search procedure will return a range of parameter solutions giving an indication of the uniqueness of the inverse parameter solution as well as how well resolved the parameters are.

Initial inversions of theoretical model data contaminated by noise indicated the controlled random search (CRS) algorithm was effective in locating the global solution. The algorithm was found to be inefficient as it converges slowly in the vicinity of

the global minimum. The application of an annealing condition was found to increase the rate at which the algorithm converges as well as improve the resolution of the final parameter solutions.

Decoupling of field CR-IP data using an anisotropic half-space with constant IP phase shift complex resistivities returns repeatable and well resolved parameters for all points on the pseudosections. Inverting using this simple model tends to produce the largest error over the polarizable areas implying the constant IP phase shift model is under parameterized and fails to adequately model the IP response. This is further demonstrated by the vast improvement in the inversion error, associated with the polarizable areas, seen when inverting test line one to an anisotropic half-space with Cole-Cole complex resistivities.

The constant IP phase response returned for both lines is comparable to the three point phase at most points in the pseudosections, implying the constant IP phase shift is a good approximation of the zero frequency phase response. In the polarizable areas the constant IP phase response contributes more to the total EM-IP response at low frequencies than the response generated from the Cole-Cole complex resistivity IP model.

The high frequency dependence of the Cole-Cole model returned for the polarizable source on test line one implies the presence of a high frequency IP response. However, high values of frequency dependence can also be indicative of the presence of EM coupling effects (Major and Silic, 1981; Wong and Strangeway, 1981). An anisotropic half-space may be inadequate to model the EM response of these more resistive polarizable areas leaving a high frequency residual EM response which is accounted for by an increased frequency dependence of the Cole-Cole dispersion.

Inverting test line two to an anisotropic half-space with Cole-Cole and constant IP phase shift complex resistivities returns unlikely values of anisotropy near the strong resistivity contrasts at the northern end of the line. The anisotropic half-space model is failing to model the complex EM coupling response generated along this contact. The two dimensional representation for anisotropy is under parameterized and inadequate at these points as it assumes the horizontal components parallel and perpendicular to the survey line are equal. It may be more appropriate to use a three component representation for the anisotropy, which would account for current channeling effects perpendicular to the survey line.

There are points in both pseudosections at which the controlled random search (CRS) algorithms (CRS_CIP and CRS_CC) fail to overcome the multi-minima problem. Questionable values for anisotropy were returned when inverting line two with the worst points being near the boundary between resistive and conductive units or where the mean resistivity of the ground was high. Investigations of the data at these points, using inversion error surfaces, has indicated noise in the data coupled with high resistivities have caused the decoupling algorithm to fail.

Modeling of the EM coupling response is influenced more by the type of IP model used as the mean resistivity of the ground is increased. Interaction between the anisotropic and Cole-Cole dispersion parameters and a reduction in the EM coupling contribution to the total response, due to high apparent resistivities, have caused the anisotropy to be poorly defined.

On comparing the results of decoupling CR-IP data using the controlled random search algorithm CRS_CC with those returned from GDPHM it is apparent that GDPHM returns a less frequency dependent IP response over the polarizable areas. The limits set by GDPHM on the phase response slope may be to restrictive causing the layered earth model to account for the frequency dependent IP response as well as the EM coupling response. However, it is probably a further indication of the failure of the anisotropic homogeneous half-space to adequately fit the EM coupling response. This is especially so for areas where the frequency dependence (c) approaches the upper limit set in CRS_CC before inversion.

The under parameterization of the EM coupling model, homogeneous anisotropic half-space, is causing a distortion of the Cole-Cole dispersion parameters when it fails to account for the total EM coupling response. The more complicated layered earth model is able to account for the EM coupling response but may be removing a frequency dependent IP effect in some areas. Where the frequency dependence (c) is moderate to low for the moderately polarizable areas this is particularly noticeable.

References

Carlson, N.R., Hughes, L.J. and Zonge, K.L., 1981, Hydrocarbon exploration using induced polarization, apparent resistivity and electromagnetic scattering: 51st Annual International S.E.G. Meeting Technical Papers, v3, p1339-1358.

Brown, R.J., 1985, EM coupling in multi-frequency IP and a generalization of the Cole-Cole impedance model, Geophysical Prospecting, v33, p282-302.

Bodmer, R., Ward, S.H. and Morrison, H.F., 1968, On induced electrical polarization and groundwater: Geophysics, v33, p805-821

Dey, A. and Morrison, H.F., 1973, Electromagnetic coupling in frequency and time domain induced polarization surveys over a multilayered earth, v38, p380

Frischknecht, F.C., 1966, Application of electromagnetic surveying to geological mapping in North Maine. Mining Geophysics, v1, (case histories), p10-17

Hallof, P.G., 1974, The IP phase measurement and inductive coupling, Geophysics, v39, p650-665

Hallof, P.G. and Pelton, W.H., 1980, The removal of inductive coupling effects from spectral IP data; Paper presented at the 50th Annual International SEG Meeting, Houston, Nov. 16-20; abs. Geophysics, v46, p464

Hohmann, G.W., 1973, Electromagnetic coupling between grounded wires on the surface of a two layer earth, Geophysics, v38, p854-863.

Hughes, L.J., 1983, Case histories of an electromagnetic method for petroleum exploration: Tucson, Zonge Engineering and Research Organization, Inc.

Jagger, S.R. and Fell, P.A., 1988, Forward and inverse Cole-Cole modeling in the analysis of frequency domain electrical impedance data: Exploration Geophysics, v19, p463-470

Kauahikauna, J., 1984, Updated programs EMCUPL and SCHCPL, computation of electromagnetic coupling on a layered half-space with complex conductivities: Addenda to USGS OFR 79-1430.

Kauahikauna, J. and Anderson, W.L., 1979, Programs EMCUPL and SCHCPL, computation of electromagnetic coupling on a layered half-space with complex conductivities: USGS OFR 79-1430, 92p.

Keller, G.V. and Frischknecht, F.C., 1966, Electrical methods in geophysical prospecting: New York, Pergamon Press.

Major, J. and Silic, J., 1981, Restrictions on the use of Cole-Cole dispersion models in complex resistivity interpretation, Geophysics, v46, p916-931.

Marshall, D.J. and Madden, T.R., 1959, Induced polarization, a study of its causes, Geophysics, v34, p790-816.

Millet, F.B., 1967, Electromagnetic coupling of collinear dipoles on a uniform half-space, in Mining Geophysics, v2: SEG press, Tulsa, p401-419.

Marquardt, D.W., 1963, Journal of the Society for Industrial and applied mathematics, v11, p431-441.

O'Conner, L.J., 1990, Electromagnetic coupling of grounded wires on an anisotropic, polarizable, layered earth, M.S. thesis, University of Arizona.

Pelton, W.H., Ward,S.H., Hallof,P.G., Sill,W.R., and Nelson,P.H. 1978, Mineral discrimination and removal of inductive coupling with multi-frequency IP, Geophysics, v43, p588-609.

Price, W.L. 1976, A controlled random search procedure for global optimization. The Computer Journal v20 No4 p367-370

Rothman, D.H. 1985, Non-linear inversion, statistical mechanics and residual statics estimation, Geophysics, v50, No12, p2784-2796

Rothman, D.H. 1986, Automatic estimation of large residual statics estimation, Geophysics, v51, No2, p332-346

Song, L., 1984, A new decoupling scheme, Exploration Geophysics, v15, p99-112

Sunde, E.D., 1949, Earth conduction effects in transmission systems: New York, Van Nostrand.

Tripp, A.C., Klein,J.D., Halverson, M.O., Kingman, J., Grant, T.W., 1990, Induced-polarization spectral interpretation including electromagnetic coupling data - a field example, Induced Polarizations, Applications and Case Histories, SEG

Vacquier, V., Holmes, C.R., Kintzinger, P.R. and Lavergne, M., 1957, Prospecting for ground water by induced electrical polarization: Geophysics, v22, p660-687.

Wait, J.R., 1959, The variable frequency method, in Wait,J.R. (ed), Overvoltage research and Geophysical applications: New York, Pergamon Press Inc.

Wait, J.R., 1966, Fields of a horizontal dipole over an anisotropic half-space, Can. Jour. Physics, v44, p2387-2401.

Wait, J.R., 1982, GeoElectromagnetism: New York, Academic Press.

Wait, J.R. and Gruszka, T.P. 1986, On electromagnetic coupling "removal" from induced polarization surveys, Geoexploration, v24, p21-27.

Wong, J. and Strangeway, D.W., 1981, Induced polarization in disseminated sulphide ores containing elongated mineralization, Geophysics, v46, p1258-1265.

Wynn, J.C., 1974, Electromagnetic coupling in induced polarization, Ph.D. dissertation, University of Arizona.

Wynn, J.C., and Zonge, K.L, 1975, EM coupling, its intrinsic value, its removal and the cultural coupling problem, Geophysical Prospecting, v23, p831-850.

Wynn, J.C., and Zonge, K.L, 1977, Electromagnetic coupling, Geophysical Prospecting, v25, p29-51.

Zonge, K.L., 1972, Electrical properties of rocks as applied to geophysical prospecting, Ph.D. dissertation, University of Arizona.

Zonge, K.L. and Wynn J.C., 1975, Recent advances and applications in complex resistivity measurements, Geophysics, v40, p851-864

APPENDIX I

TEST LINE 1

Pseudosections of
Apparent Resistivity
0.125 Hz Raw Phase Angle
3 pt. Decoupled Phase
Spectral Plots

Line Field DC
RAW CR-IP DATA
for
TEST LINE 1

ZONGE ZPLOT 7.12 Duplicates Not Used
Plotted 01 Mar 97

CR-IP SURVEY DATA
Apparent RESISTIVITY

values in ohm-meters
0.125 Hz

SURVEY LINE DATA
Line Orient= East
A - Spacing= 100 m

Survey Date= FEB.97

[Plot limits] and LOGARITHMIC CONTOURS
(Interval: 0.20)
[20.7]
25.1
39.8
63.1
100.
158.
[195.]

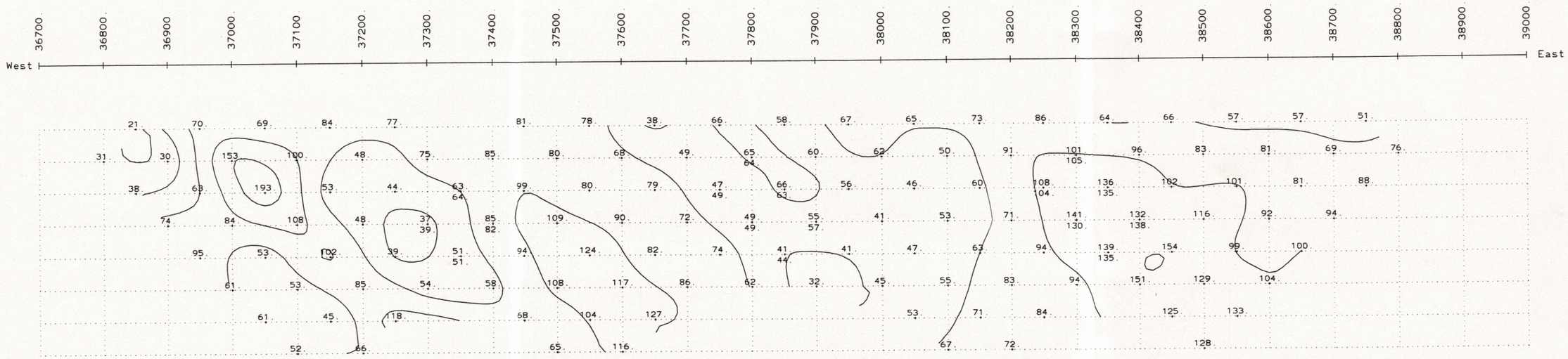

Line Field DC
RAW CR-IP DATA
for
TEST LINE 1

ZONGE ZPLOT 7.12 Duplicates Not Used
Plotted 01 Mar 97

CR-IP SURVEY DATA
Raw PHASE Angle

values in milliRadians
0.125 Hz

SURVEY LINE DATA
Line Orient= East
A - Spacing= 100 m

Survey Date= FEB.97

[Plot limits] and ARITHMETIC CONTOURS
(Interval: 5.00)
[1.22]
5.00
10.0
[14.9]

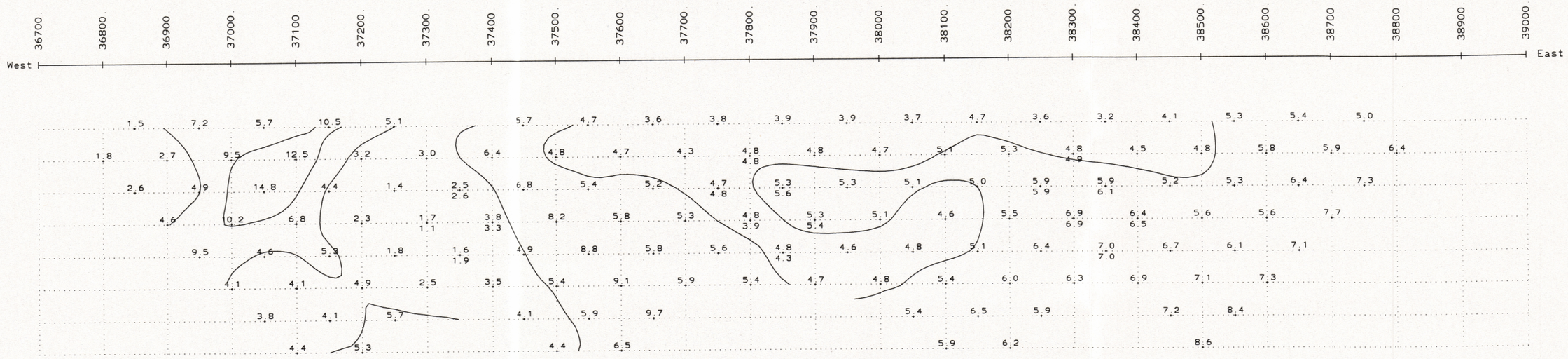

Line Field DC
RAW CR-IP DATA
for
TEST LINE 1

ZONGE ZPLOT 7.12 Duplicates Not Used
Plotted 01 Mar 97

CR-IP SURVEY DATA
3-PT DC PHASE

values in milliRadians
.125, .375, .625 Hz

SURVEY LINE DATA
Line Orient= East
A - Spacing= 100 m

Survey Date= FEB.97

[Plot limits] and ARITHMETIC CONTOURS
(Interval: 5.00)
[13.5m]
5.00
10.0
15.0
[15.3]

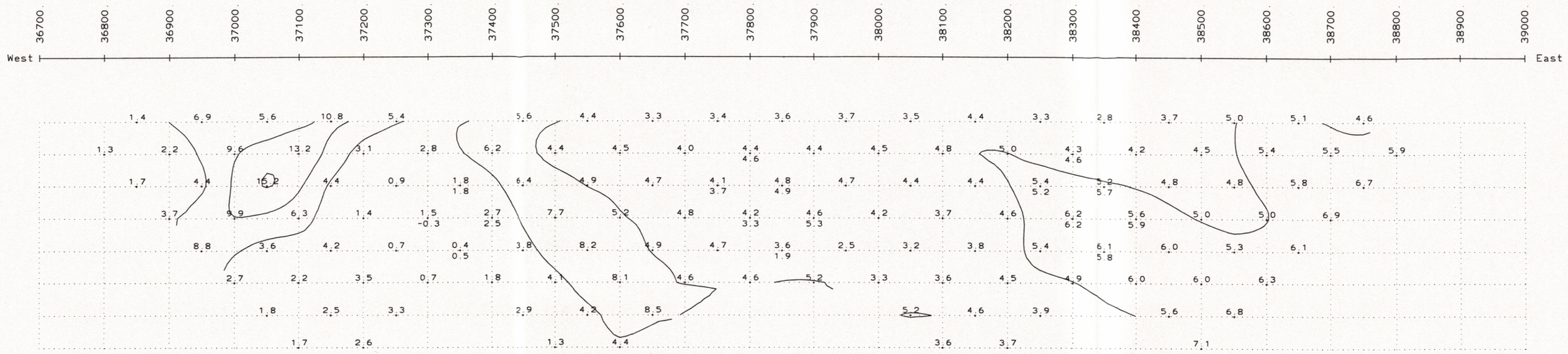

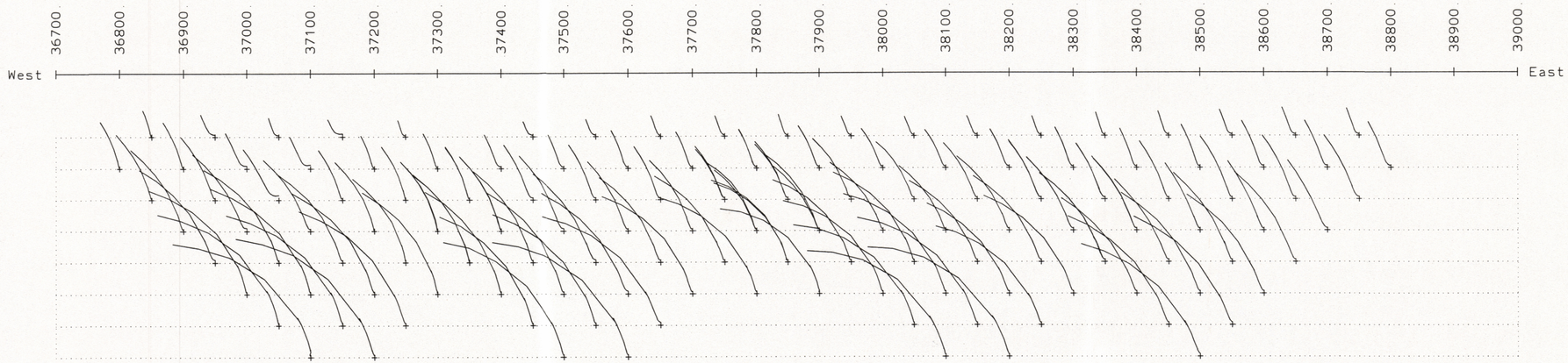

Project: RAW CR-IP DATA
For : TEST LINE 1

Line : Field DC Asp: 100.m
Date : FEB.97
Line Orientation : East

SPECTRAL PSEUDOSECTION
Plot of: RAW DATA
Scale: 5.000 Asp per Spectral unit
Scale: 10.0 cm per Spectral unit

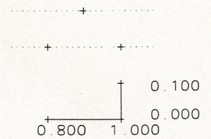

ZONGE PPLOT 7.00
Plotted 24 Feb 97

APPENDIX II

TEST LINE 1

Pseudosections of CRS Decoupled Data

Constant IP Parameters: DC Resistivity
Anisotropic Constant (K)
Constant IP Phase (ϕ_{ip})
L_1 Norm Error

Cole-Cole IP Response: 0.125 Hz IP phase
1.0 Hz IP phase
8.0 Hz IP phase

Cole-Cole Dispersion Parameters: DC Resistivity
Anisotropic Constant (K)
Chargeability (m)
Time Constant (τ_o)
Frequency Dependence (c)
L_1 Norm Error

Line DECOUPLED
CONSTANT IP PHASE
for
TEST LINE 1

ZONGE ZPLOT 7.12 Duplicates Not Used
Plotted 31 Oct 95

Constant IP Parameters
DC Resistivity
(Ohm-m)

SURVEY LINE DATA
Line Orient= East

Survey Date= OCT.95

[Plot limits] and LOGARITHMIC CONTOURS
(Interval: 0.20)
[20.7]
25.1
39.8
63.1
100.
158.
[190.]

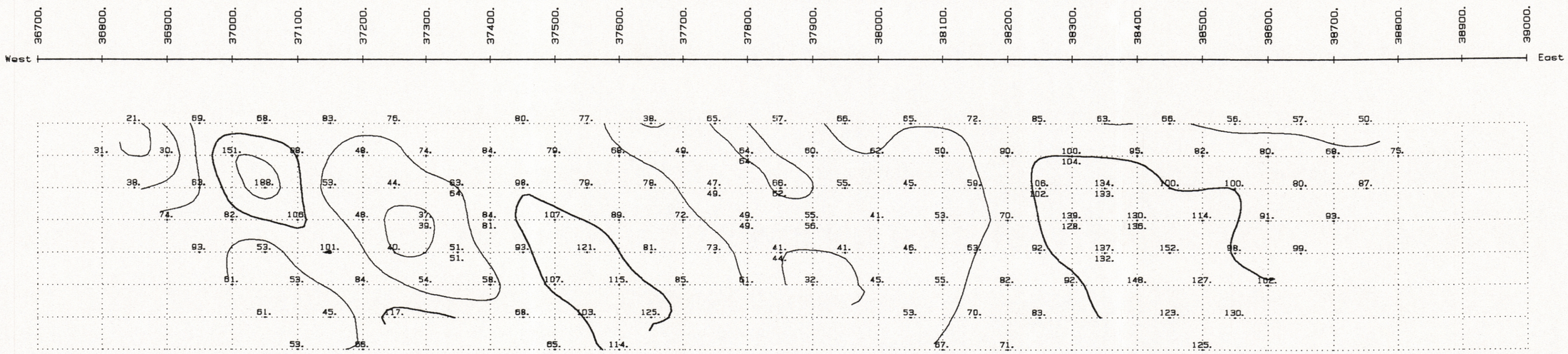

Line DECOUPLED
CONSTANT IP PHASE
for
TEST LINE 1

ZONGE ZPLOT 7.12 Duplicates Not Used
Plotted 31 Oct 95

Constant IP Parameters
Anisotropic Constant K
(unitless)

SURVEY LINE DATA
Line Orient= East

Survey Date= OCT.95

[Plot limits] and ARITHMETIC CONTOURS
(Interval: 5.00)
[-95.0m]
0.00
5.00
10.0
15.0
20.0
[20.1]

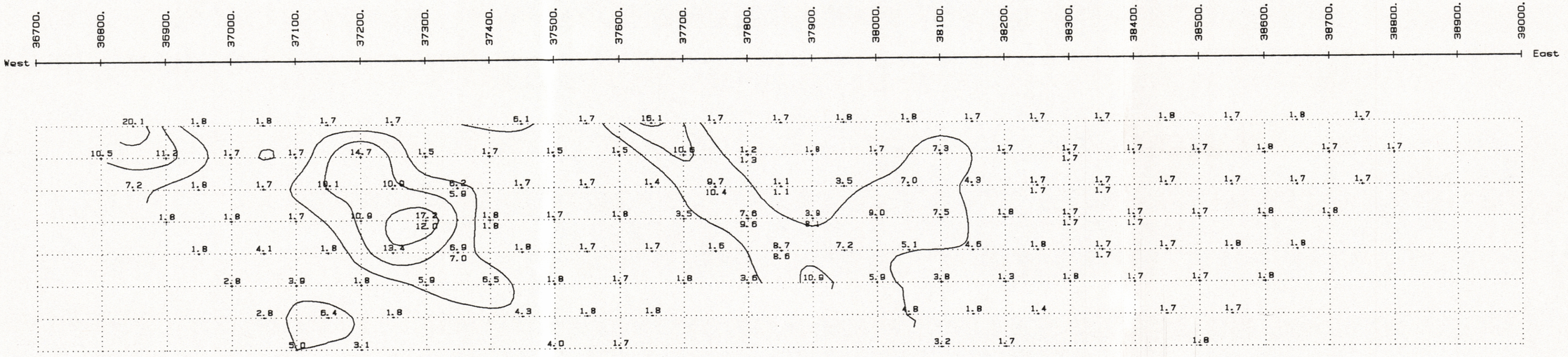

Line DECOUPLED
CONSTANT IP PHASE
for
TEST LINE 1

ZONGE ZPLOT 7.12 Duplicates Not Used
Plotted 31 Oct 95

CP

Constant IP Parameters
L1 Norm Error
(unitless)

SURVEY LINE DATA
Line Orient= East

Survey Date= OCT 95

[Plot limits] and ARITHMETIC CONTOURS
(Interval: 5.00)
[-.446] [41.3]
0.00
5.00
10.0
15.0
20.0
25.0
30.0
35.0
40.0

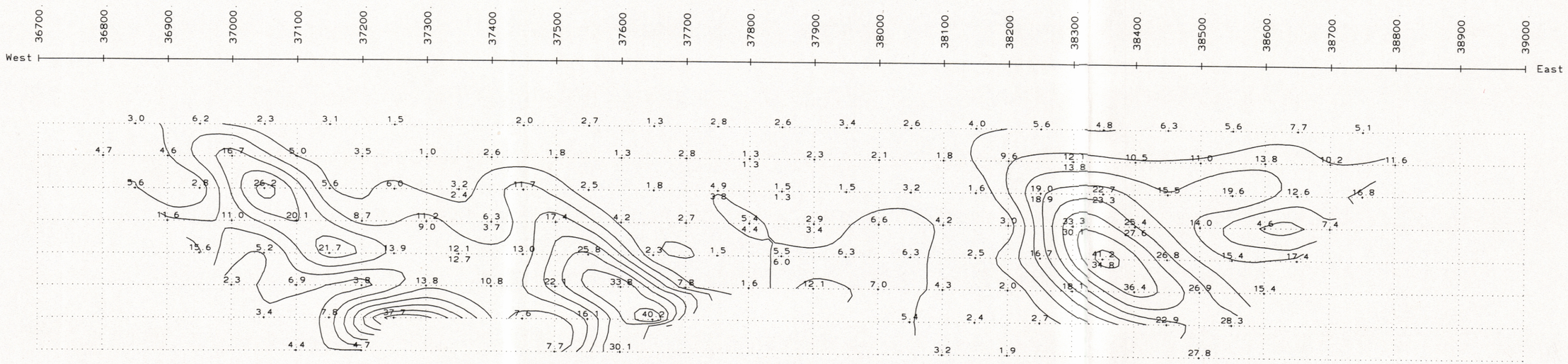

Line DECOUPLED
CONSTANT IP PHASE
for
TEST LINE 1

ZONGE ZPLOT 7.12 Duplicates Not Used
Plotted 31 Oct 95

Constant IP Parameters
Constant IP Phase
(mrad)

SURVEY LINE DATA
Line Orient= East

Survey Date= OCT.95

[Plot limits] and ARITHMETIC CONTOURS
(Interval: 5.00)
[-3.46]
0.00
5.00
10.0
15.0
20.0
25.0
[25.5]

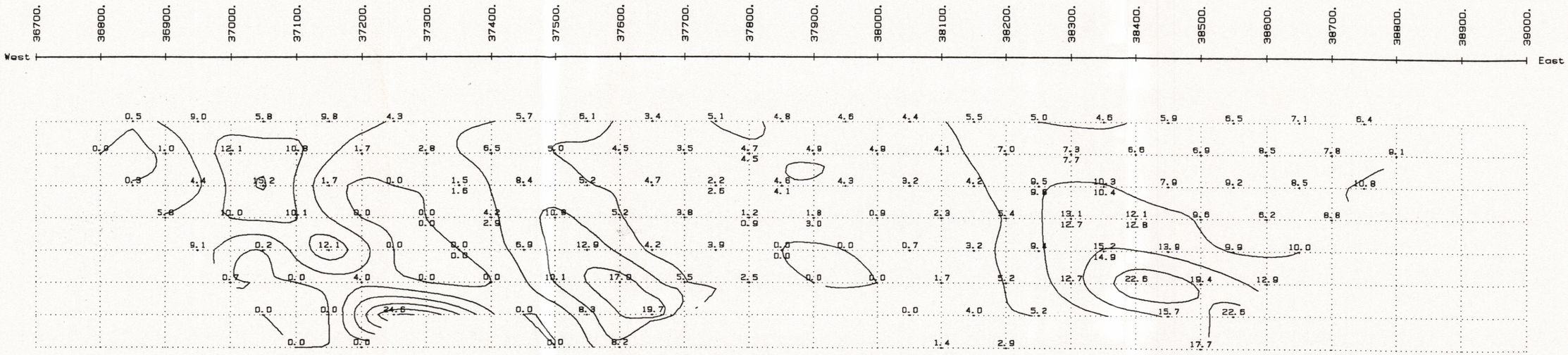

Line DECOUPLED
Cole-Cole Dispersion
for
TEST LINE 1

ZONGE ZPLOT 7.12 Duplicates Not Used
Plotted 24 Feb 97

cp

Cole-Cole Parameters
0.125 Hz DC Phase
(mrad)

SURVEY LINE DATA
Line Orient= East

Survey Date= FEB.97

[Plot limits] and ARITHMETIC CONTOURS
(Interval: 5.00)
[-.853]
0.00
5.00
[8.81]

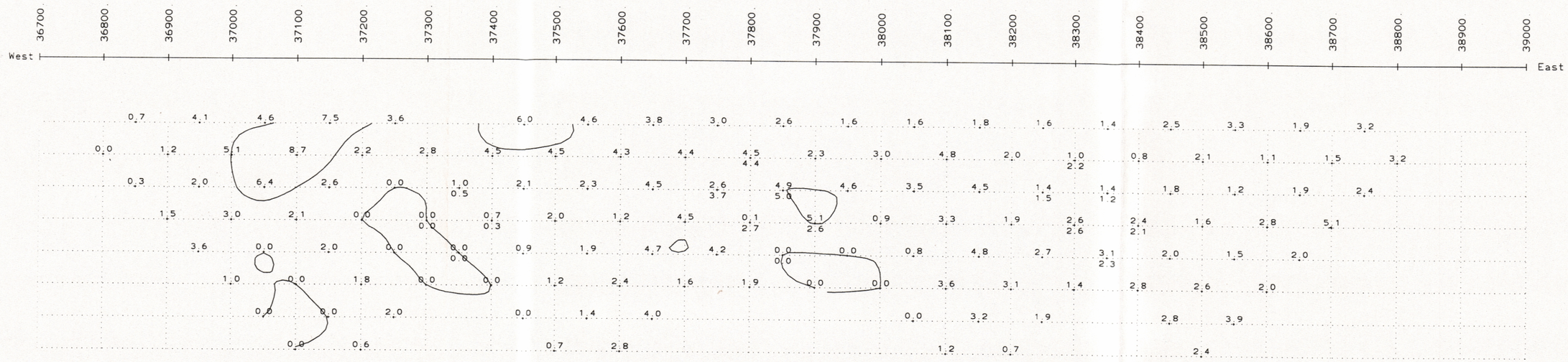

Line DECOUPLED
Cole-Cole Dispersion
for
TEST LINE 1

ZONGE ZPLOT 7.12 Duplicates Not Used
Plotted 24 Feb 97

Cole-Cole Parameters
1.0 Hz DC Phase
(mrad)

SURVEY LINE DATA
Line Orient= East

Survey Date= FEB.97

[Plot limits] and ARITHMETIC CONTOURS
(Interval: 5.00)
[-1.08]
0.00
5.00
10.0
[14.6]

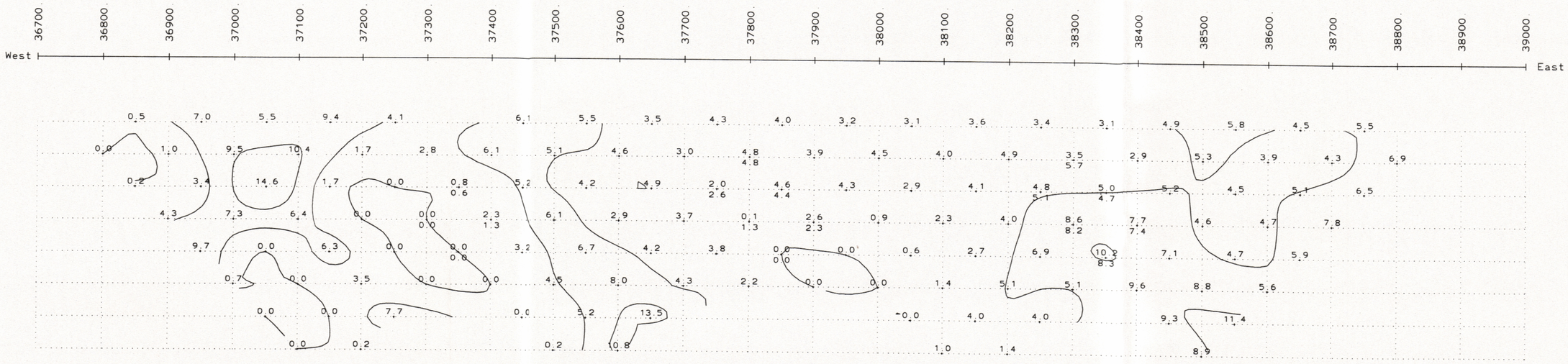

Line DECOUPLED
Cole-Cole Dispersion
for
TEST LINE 1

ZONGE ZPLOT 7.12 Duplicates Not Used
Plotted 24 Feb 97

cp

Cole-Cole Parameters
8.0 Hz DC Phase
(mrad)

SURVEY LINE DATA
Line Orient= East

Survey Date= FEB.97

[Plot limits] and ARITHMETIC CONTOURS
(Interval: 5.00)
[-4.12] [44.4]
0.00
5.00
10.0
15.0
20.0
25.0
30.0
35.0
40.0

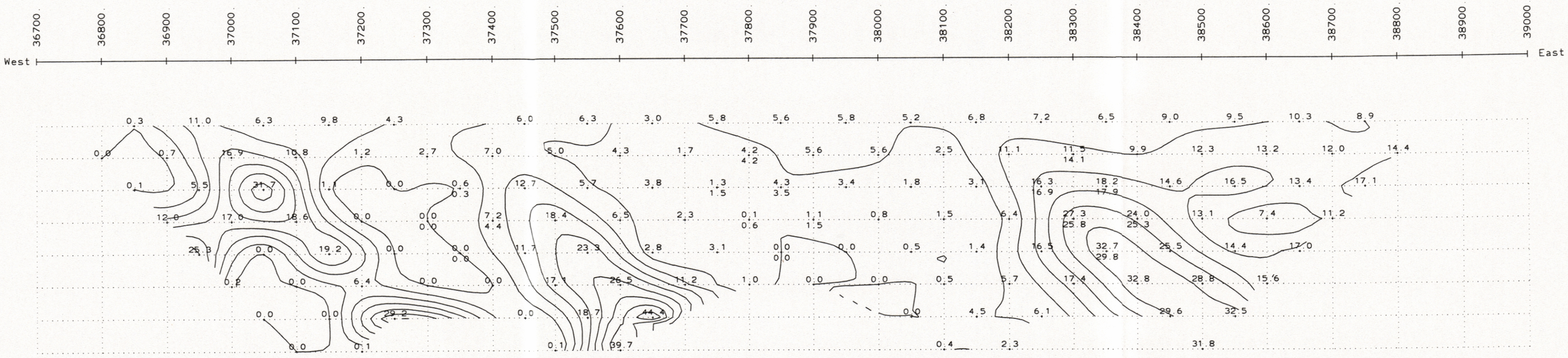

Line DECOUPLED
Cole-Cole Dispersion
for
TEST LINE 1

ZONGE ZPLOT 7.12 Duplicates Not Used
Plotted 24 Feb 97

CD

Cole-Cole Parameters
DC Resistivity
(Ohm-m)

SURVEY LINE DATA
Line Orient= East

Survey Date= FEB.97

[Plot limits] and LOGARITHMIC CONTOURS
(Interval: 0.20)
[20.9]
25.1
39.8
63.1
100.
158.
[197.]

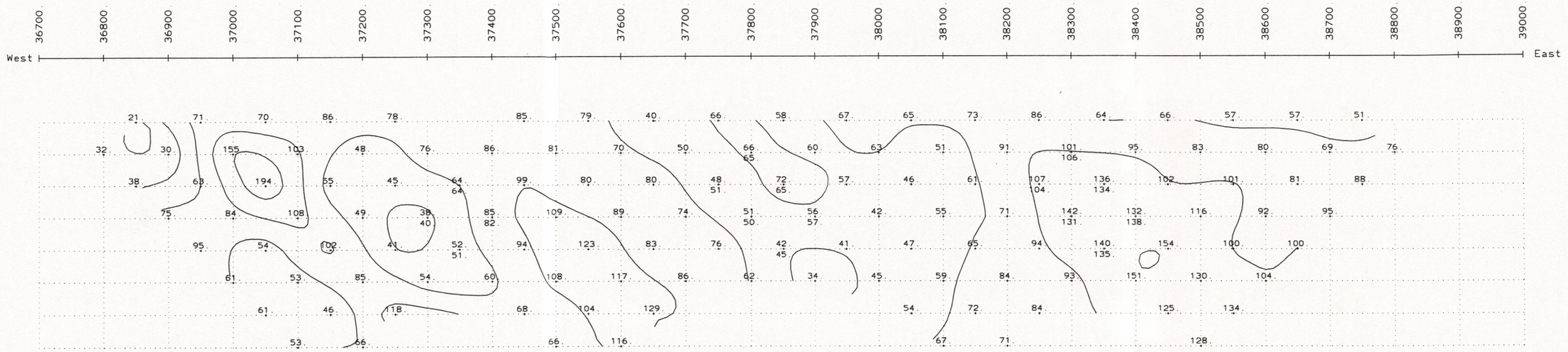

Line DECOUPLED
Cole-Cole Dispersion
for
TEST LINE 1

ZONGE ZPLOT 7.12 Duplicates Not Used
Plotted 24 Feb 97

Cole-Cole Parameters
Anisotropic Constant K
(unitless)

SURVEY LINE DATA
Line Orient= East

Survey Date= FEB.97

[Plot limits] and ARITHMETIC CONTOURS
(Interval: 5.00)
[12.9m]
5.00
10.0
15.0
[19.9]

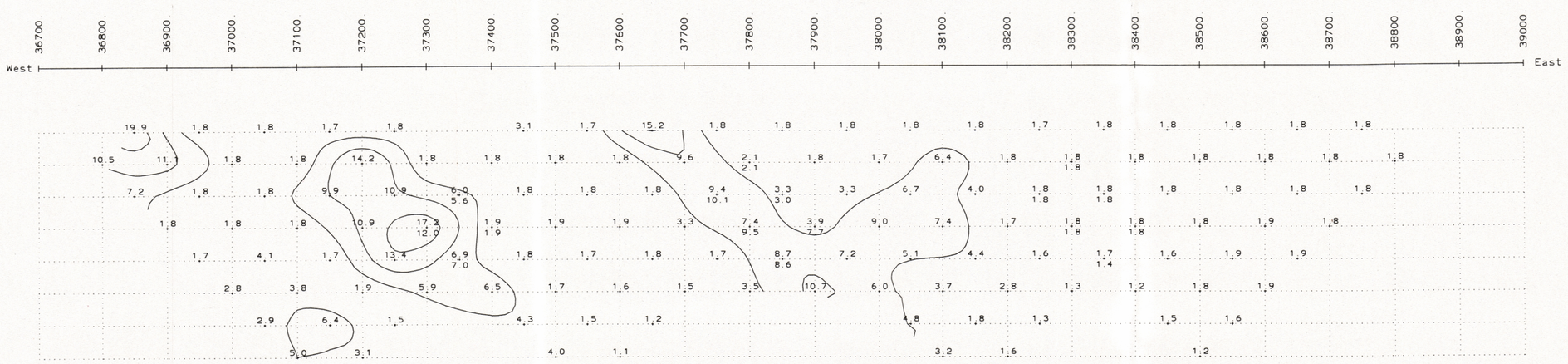

Line DECOUPLED
Cole-Cole Dispersion
for
TEST LINE 1

ZONGE ZPLOT 7.12 Duplicates Not Used
Plotted 24 Feb 97

CO

Cole-Cole Parameters
Chargeability Rm
(X 100)

SURVEY LINE DATA
Line Orient= East

Survey Date= FEB.97

[Plot limits] and ARITHMETIC CONTOURS
(Interval: 10.00)
[-11.4] 80.0
-10.0 [84.8]
0.00
10.0
20.0
30.0
40.0
50.0
60.0
70.0

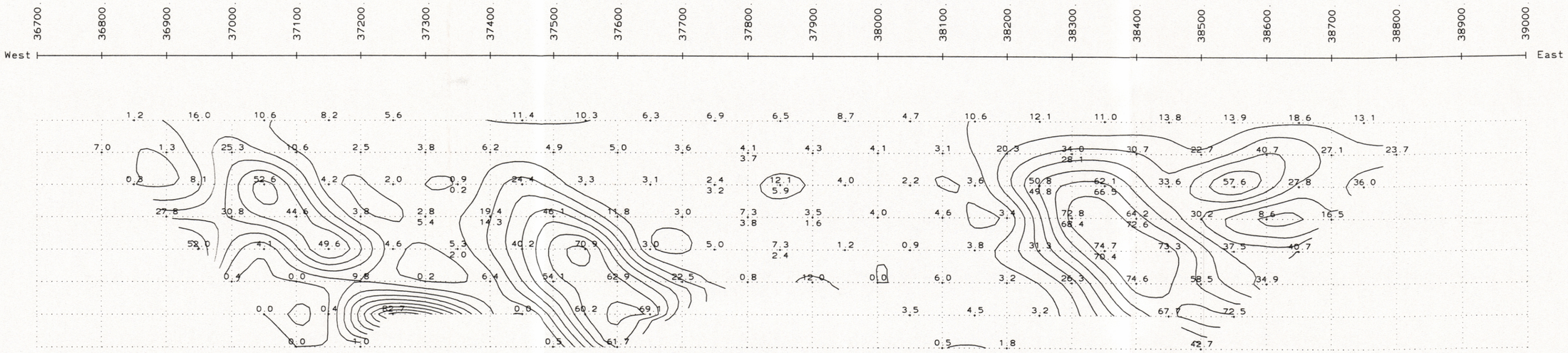

Line DECOUPLED
Cole-Cole Dispersion
for
TEST LINE 1

ZONGE ZPLOT 7.12 Duplicates Not Used
Plotted 24 Feb 97

Cole-Cole Parameters
Time Constant
Log(TAU) (Sec)

SURVEY LINE DATA
Line Orient= East

Survey Date= FEB.97

[Plot limits] and ARITHMETIC CONTOURS
(Interval: 5.00)
[-4.81]
0.00
[4.01]

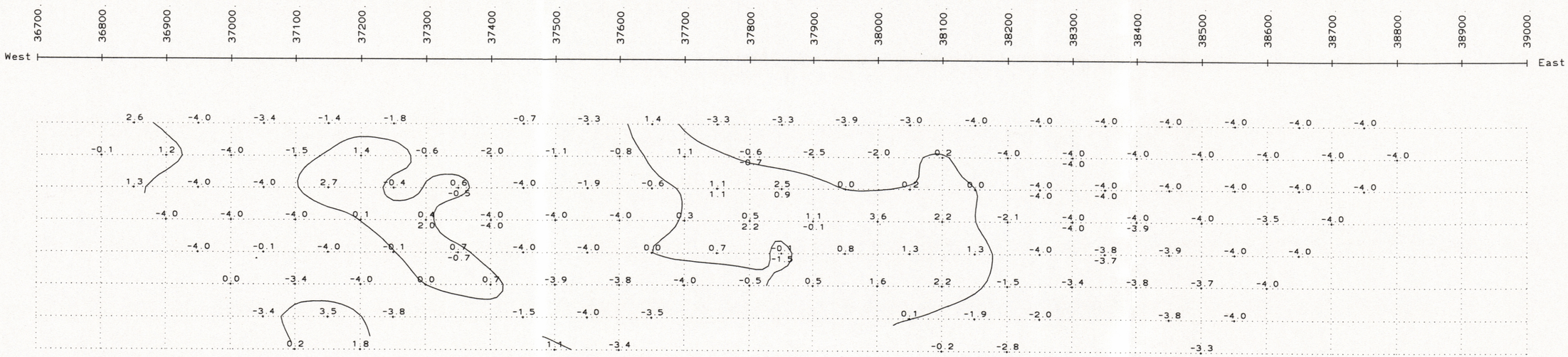

Line DECOUPLED
Cole-Cole Dispersion
for
TEST LINE 1

ZONGE ZPLOT 7.12 Duplicates Not Used
Plotted 24 Feb 97

Cole-Cole Parameters
Frequency Dep. C
(X 100)

SURVEY LINE DATA
Line Orient= East

Survey Date= FEB.97

[Plot limits] and ARITHMETIC CONTOURS
(Interval: 10.00)
[-8.21]
0.00
10.0
20.0
30.0
40.0
50.0
60.0
[65.2]

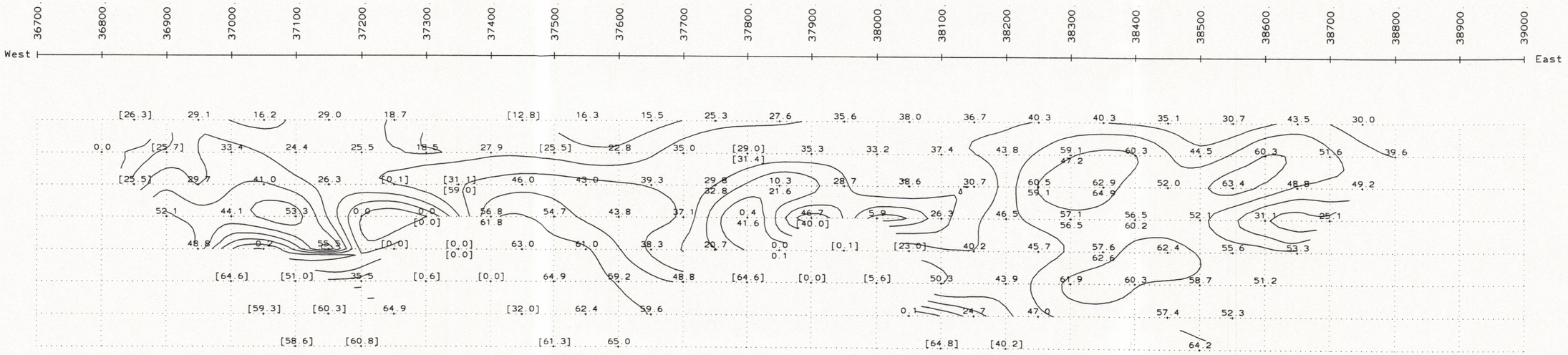

Line DECOUPLED
Cole-Cole Dispersion
for
TEST LINE 1

ZONGE ZPLOT 7.12 Duplicates Not Used
Plotted 24 Feb 97

Cole-Cole Parameters
L1 Norm Error
(unitless)

SURVEY LINE DATA
Line Orient= East

Survey Date= FEB.97

[Plot limits] and ARITHMETIC CONTOURS
(Interval: 5.00)
[-.269]
0.00
5.00
10.0
[15.0]

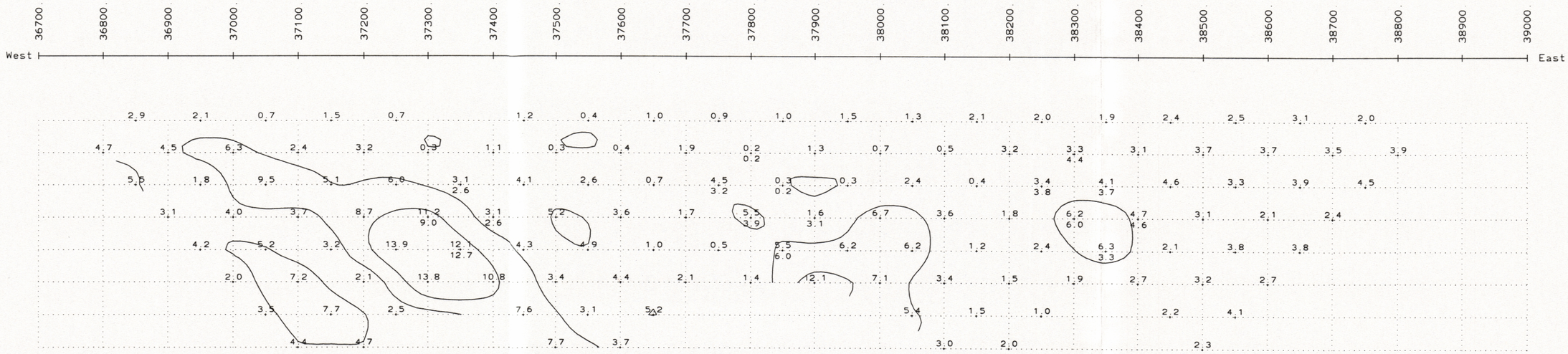

APPENDIX III

TEST LINE 2

Pseudosections of
Apparent Resistivity
0.125 Hz Raw Phase Angle
3 pt. Decoupled Phase
Spectral Plots

Line DECOUPLED
RAW CR-IP DATA
for
TEST LINE 2

ZONGE ZPLOT 7.12 Duplicates Not Used
Plotted 01 Nov 95

CR-IP SURVEY DATA
Apparent RESISTIVITY

values in ohm-meters
0.125 Hz

SURVEY LINE DATA
Line Orient= North
A - Spacing= 100 m

Survey Date= OCT. 95

[Plot limits] and LOGARITHMIC CONTOURS
(Interval: 0.20)
[28.1] [1910]
39.8
63.1
100.
158.
251.
398.
631.
1000
1585

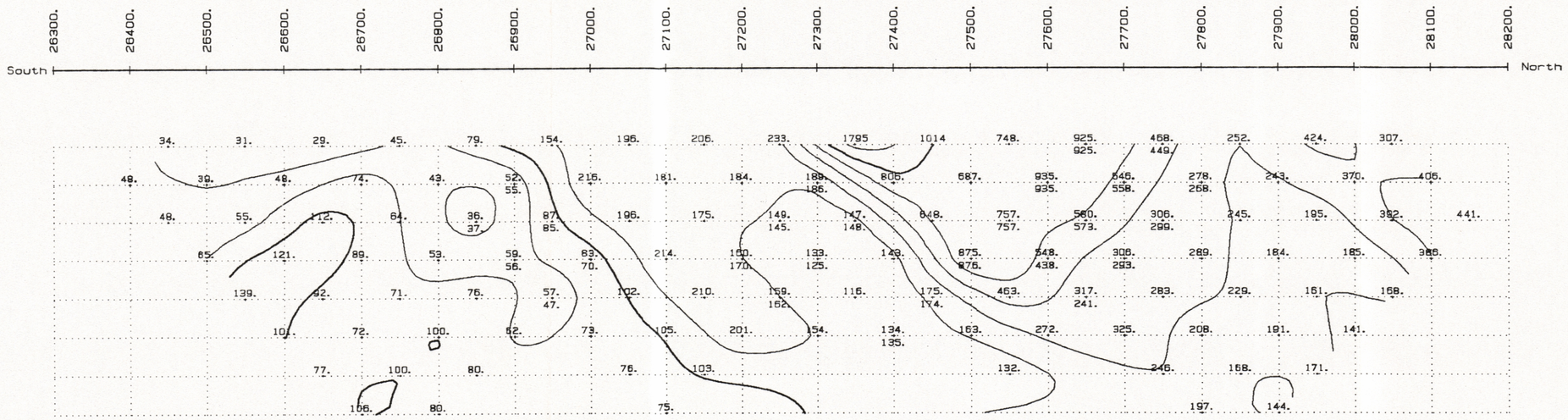

Line DECOUPLED
RAW CR-IP DATA
for
TEST LINE 2

ZONGE ZPLOT 7.12 Duplicates Not Used
Plotted 01 Nov 95

CR-IP SURVEY DATA
Raw PHASE Angle

values in milliRadians
0.125 Hz

SURVEY LINE DATA
Line Orient= North
A - Spacing= 100 m

Survey Date= OCT. 95

[Plot limits] and ARITHMETIC CONTOURS
(Interval: 5.00)
[-.680]
0.00
5.00
10.0
15.0
20.0
25.0
[25.8]

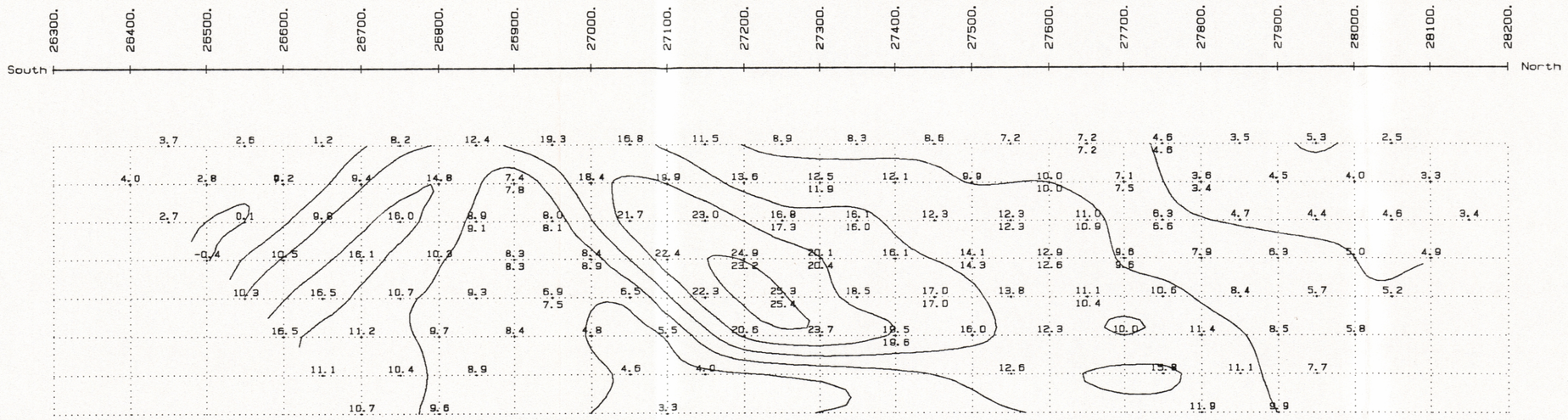

Line DECOUPLED
RAW CR-IP DATA
for
TEST LINE 2

ZONGE ZPLOT 7.12 Duplicates Not Used
Plotted 01 Nov 95

CR-IP SURVEY DATA
3-PT DC PHASE

values in milliRadians
.125..375..625 Hz

SURVEY LINE DATA
Line Orient= North
A - Spacing= 100 m

Survey Date= OCT. 95

[Plot limits] and ARITHMETIC CONTOURS
(Interval: 5.00)
[-1.83]
0.00
5.00
10.0
15.0
20.0
25.0
[25.6]

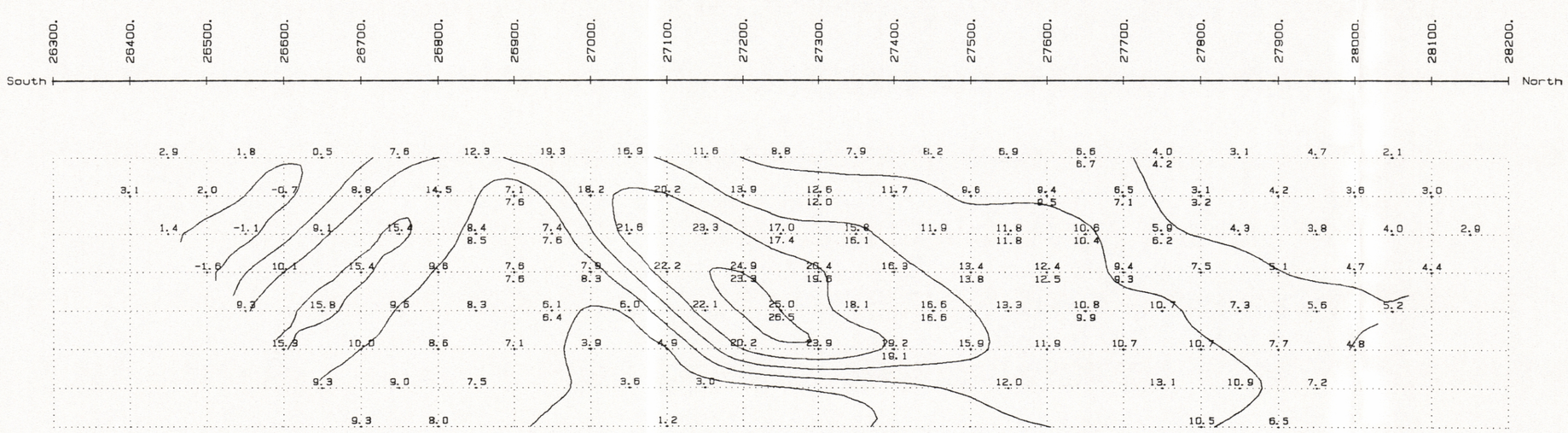

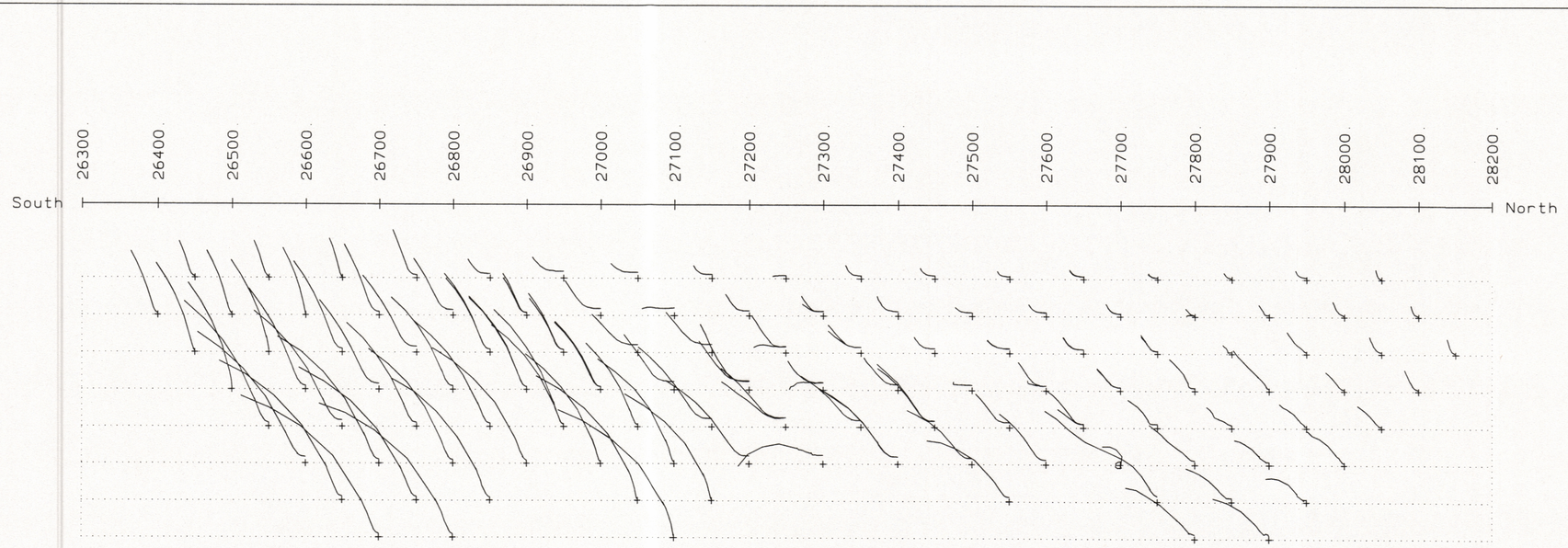

Project: RAW CR-IP DATA
For : TEST LINE 2

Line : Field DC Asp: 100.m
Date : FEB.97
Line Orientation : North

SPECTRAL PSEUDOSECTION
Plot of: RAW DATA
Scale: 5.000 Asp per Spectral unit
Scale: 10.0 cm per Spectral unit

Scale:

0.100
0.000
0.800 1.000

ZONGE PPLOT 7.00
Plotted 24 Feb 97

APPENDIX IV

TEST LINE 2

Pseudosections of CRS Decoupled Data

Constant IP Parameters: DC Resistivity
Anisotropic Constant (K)
Constant IP Phase (ϕ_{ip})
L_1 Norm Error

Cole-Cole IP Response: 0.125 Hz IP phase
1.0 Hz IP phase
8.0 Hz IP phase

Cole-Cole Dispersion Parameters: DC Resistivity
Anisotropic Constant (K)
Chargeability (m)
Time Constant (τ_o)
Frequency Dependence (c)
L_1 Norm Error

Line DECOUPLED
CONSTANT IP PHASE
for
TEST LINE 2

ZONGE ZPLOT 7.12 Duplicates Not Used
Plotted 31 Oct 95

Constant IP Parameters
DC Resistivity
(Ohm-m)

SURVEY LINE DATA
Line Orient= North

Survey Date= OCT.95

[Plot limits] and LOGARITHMIC CONTOURS
(Interval: 0.20)
[28.1] [1878]
39.8
63.1
100.
158.
251.
398.
631.
1000
1585

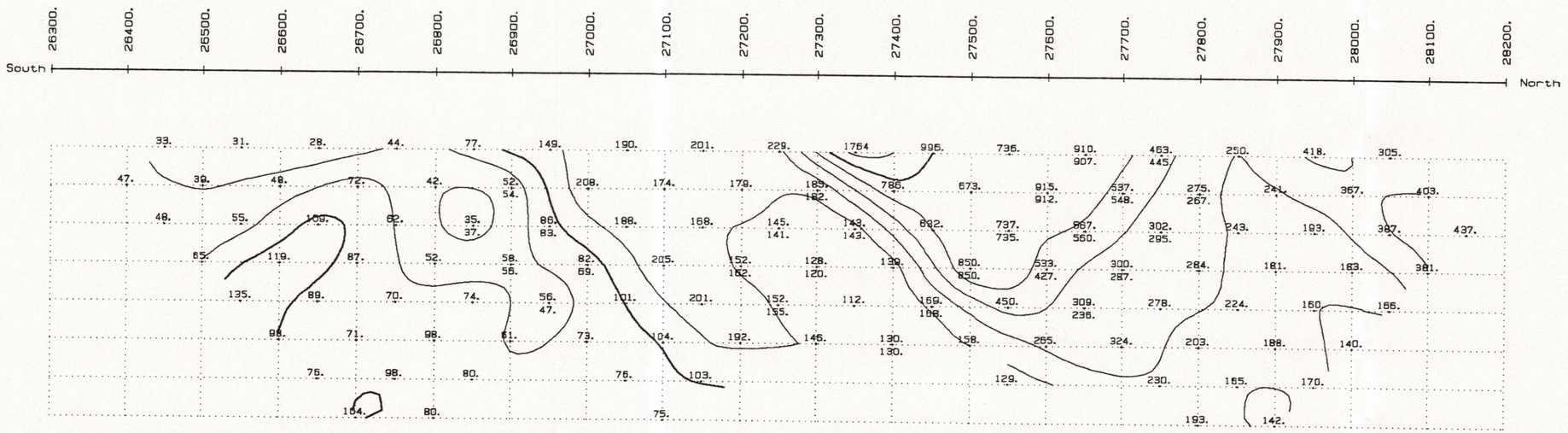

Line DECOUPLED
CONSTANT IP PHASE
for
TEST LINE 2

ZONGE ZPLOT 7.12 Duplicates Not Used
Plotted 31 Oct 95

Constant IP Parameters
Anisotropic Constant K
(unitless)

SURVEY LINE DATA
Line Orient= North

Survey Date= OCT.95

[Plot limits] and ARITHMETIC CONTOURS
(Interval= 5.00)

[-10.2]	35.0	85.0
-10.0	40.0	90.0
-5.00	45.0	95.0
0.00	50.0	[99.3]
5.00	55.0	
10.0	60.0	
15.0	65.0	
20.0	70.0	
25.0	75.0	
30.0	80.0	

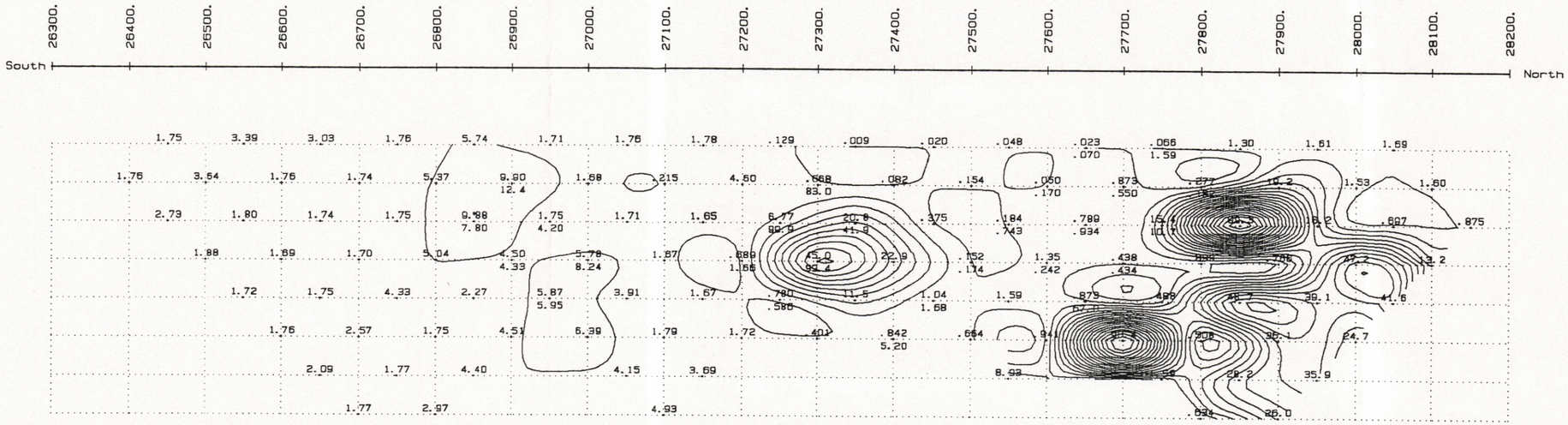

Line DECOUPLED
CONSTANT IP PHASE
for
TEST LINE 2

ZONGE ZPLOT 7.12 Duplicates Not Used
Plotted 31 Oct 95

Constant IP Parameters
Constant IP Phase
(mrad)

SURVEY LINE DATA
Line Orient= North

Survey Date= OCT.95

[Plot limits] and ARITHMETIC CONTOURS
(Interval: 5.00)

[-1.81]	45.0
0.00	50.0
5.00	55.0
10.0	60.0
15.0	[62.3]
20.0	
25.0	
30.0	
35.0	
40.0	

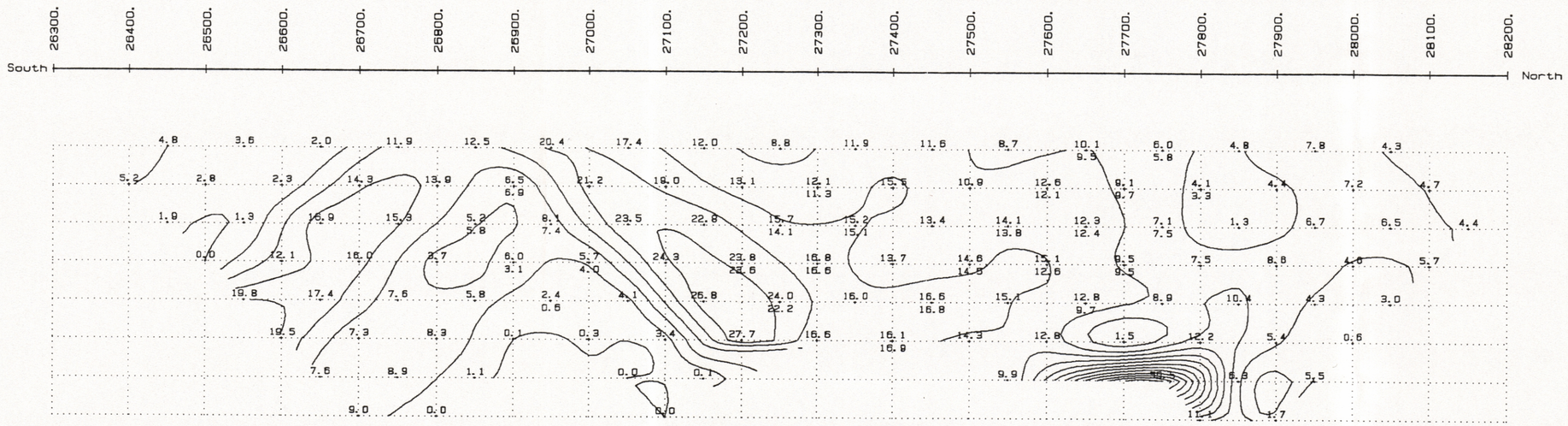

Line DECOUPLED
CONSTANT IP PHASE
for
TEST LINE 2

ZONGE ZPLOT 7.12 Duplicates Not Used
Plotted 31 Oct 95

CP

Constant IP Parameters
L1 Norm Error
(unitless)

SURVEY LINE DATA
Line Orient= North

Survey Date= OCT.95

[Plot limits] and ARITHMETIC CONTOURS
(Interval: 5.00)

[-4.09]	45.0
0.00	50.0
5.00	55.0
10.0	60.0
15.0	[61.5]
20.0	
25.0	
30.0	
35.0	
40.0	

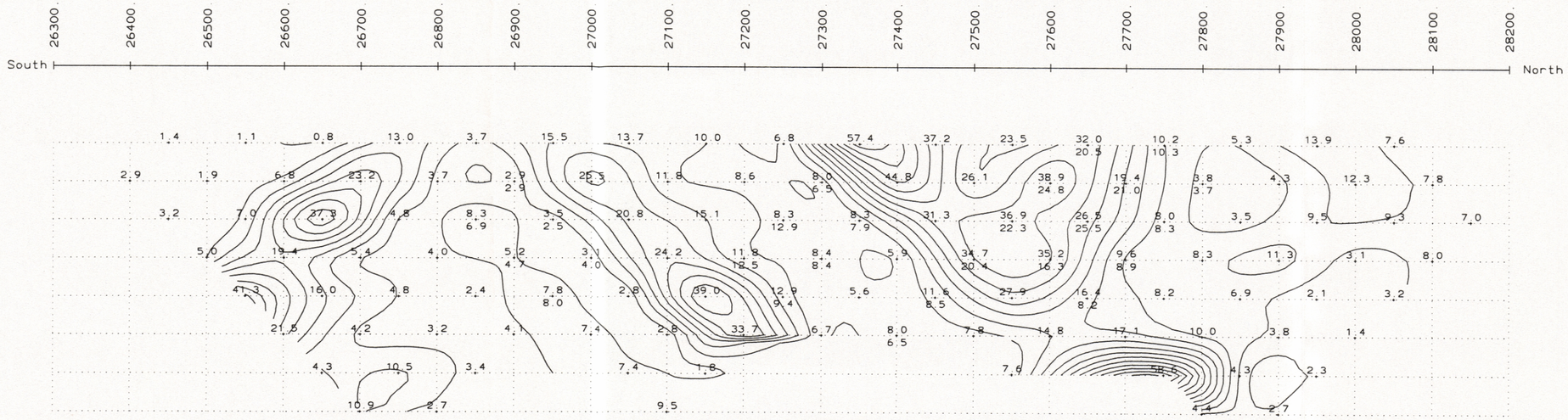

Line DECOUPLED
Cole-Cole Dispersion
for
TEST LINE 2

ZONGE ZPLOT 7.12 Duplicates Not Used
Plotted 02 Nov 95

Cole-Cole Parameters
0.125 Hz DC Phase
(mrad)

SURVEY LINE DATA
Line Orient= North

Survey Date= OCT.95

[Plot limits] and ARITHMETIC CONTOURS
(Interval: 5.00)
[-.523]
0.00
5.00
10.0
15.0
[19.6]

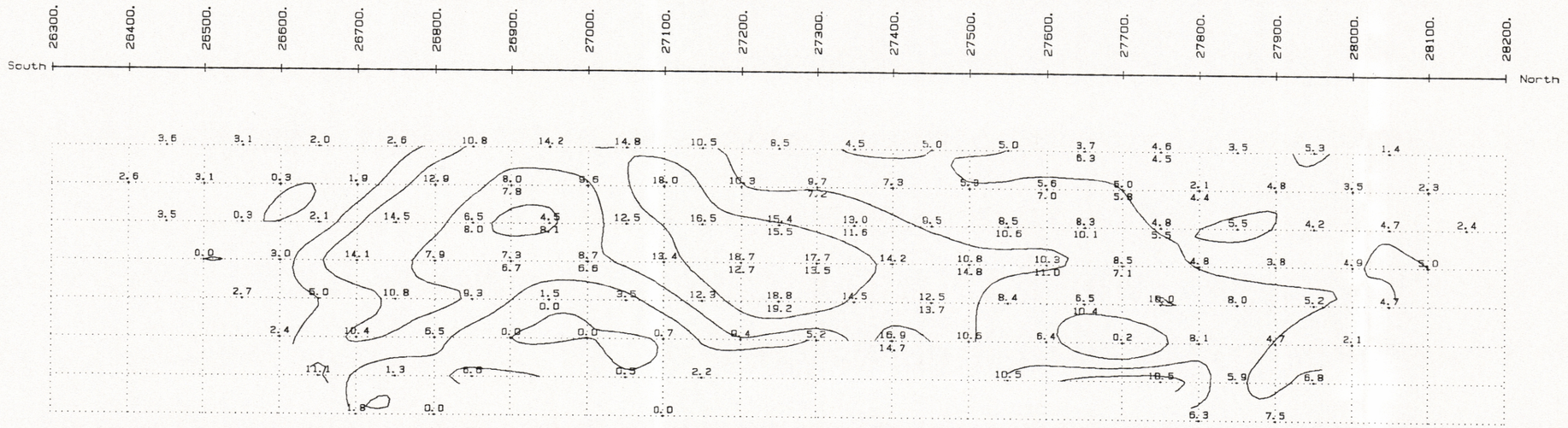

Line DECOUPLED
Cole-Cole Dispersion
for
TEST LINE 2

ZONGE ZPLOT 7.12 Duplicates Not Used
Plotted 02 Nov 95

Cole-Cole Parameters
1.0 Hz DC Phase
(mrad)

SURVEY LINE DATA
Line Orient= North

Survey Date= OCT.95

[Plot limits] and ARITHMETIC CONTOURS
(Interval: 5.00)
[-.691] [42.2]
0.00
5.00
10.0
15.0
20.0
25.0
30.0
35.0
40.0

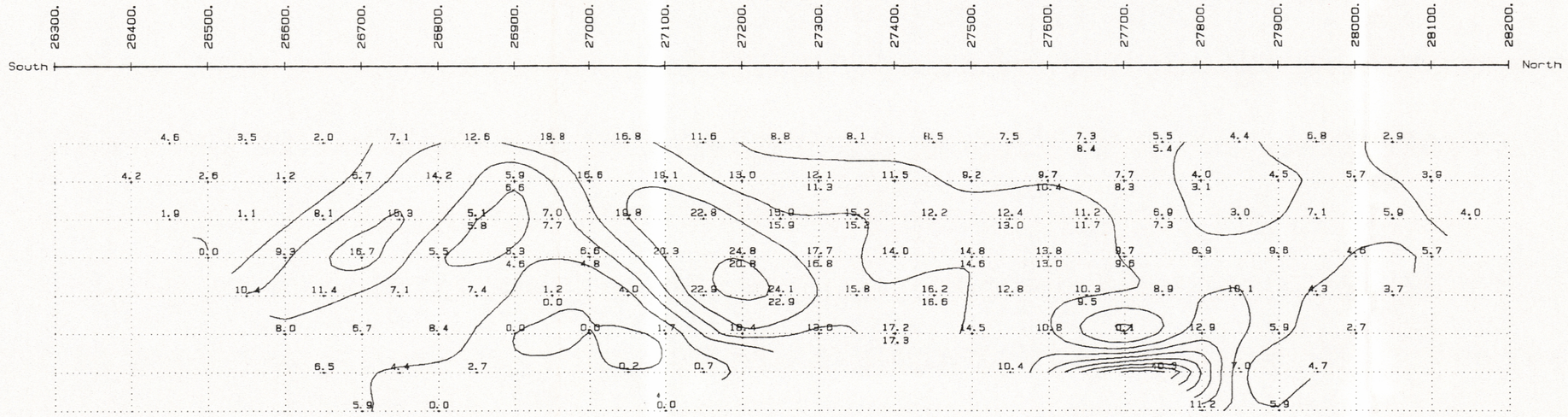

Line DECOUPLED
Cole-Cole Dispersion
for
TEST LINE 2

ZONGE ZPLOT 7.12 Duplicates Not Used
Plotted 02 Nov 95

Cole-Cole Parameters
8.0 Hz DC Phase
(mrad)

SURVEY LINE DATA
Line Orient= North

Survey Date= OCT.95

[Plot limits] and ARITHMETIC CONTOURS
(Interval: 5.00)

[-7.47]	40.0	[87.8]
-5.00	45.0	
0.00	50.0	
5.00	55.0	
10.0	60.0	
15.0	65.0	
20.0	70.0	
25.0	75.0	
30.0	80.0	
35.0	85.0	

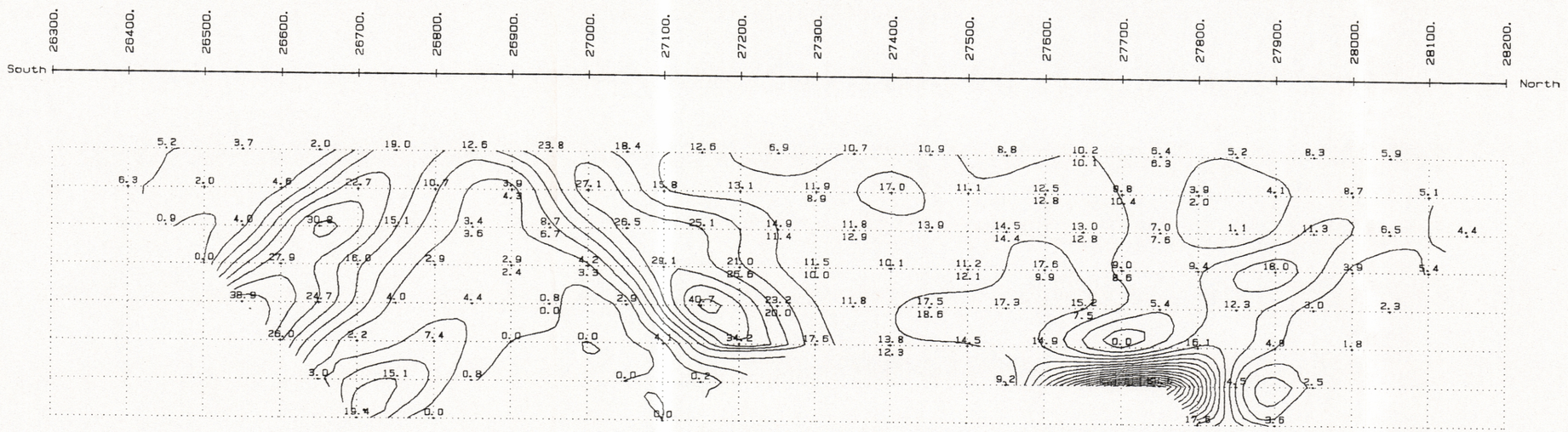

Line DECOUPLED
Cole-Cole Dispersion
for
TEST LINE 2

ZONGE ZPLOT 7.12 Duplicates Not Used
Plotted 02 Nov 95

Cole-Cole Parameters
DC Resistivity
(Ohm-m)

SURVEY LINE DATA
Line Orient= North

Survey Date= OCT.95

[Plot limits] and LOGARITHMIC CONTOURS
(Interval: 0.20)
[29.1] [1915]
39.8
63.1
100.
158.
251.
398.
631.
1000
1585

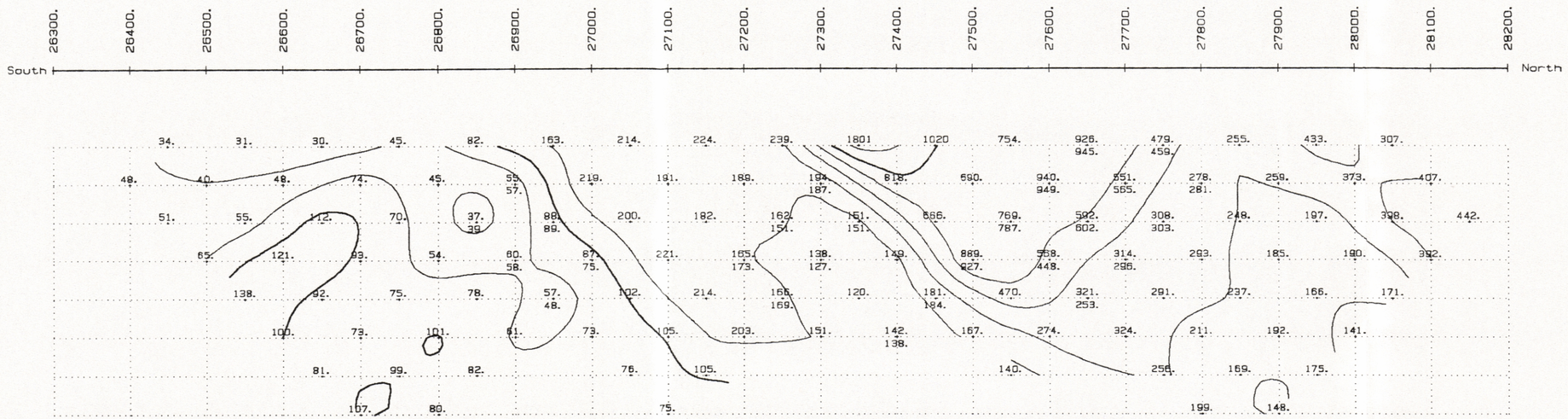

Line DECOUPLED
Cole-Cole Dispersion
for
TEST LINE 2

ZONGE ZPLOT 7.12 Duplicates Not Used
Plotted 02 Nov 95

Cole-Cole Parameters
Anisotropic Constant K
(unitless)

SURVEY LINE DATA
Line Orient= North

Survey Date= OCT.95

[Plot limits] and ARITHMETIC CONTOURS
(Interval: 5.00)
[-4.90] 45.0
0.00 50.0
5.00 55.0
10.0 [55.6]
15.0
20.0
25.0
30.0
35.0
40.0

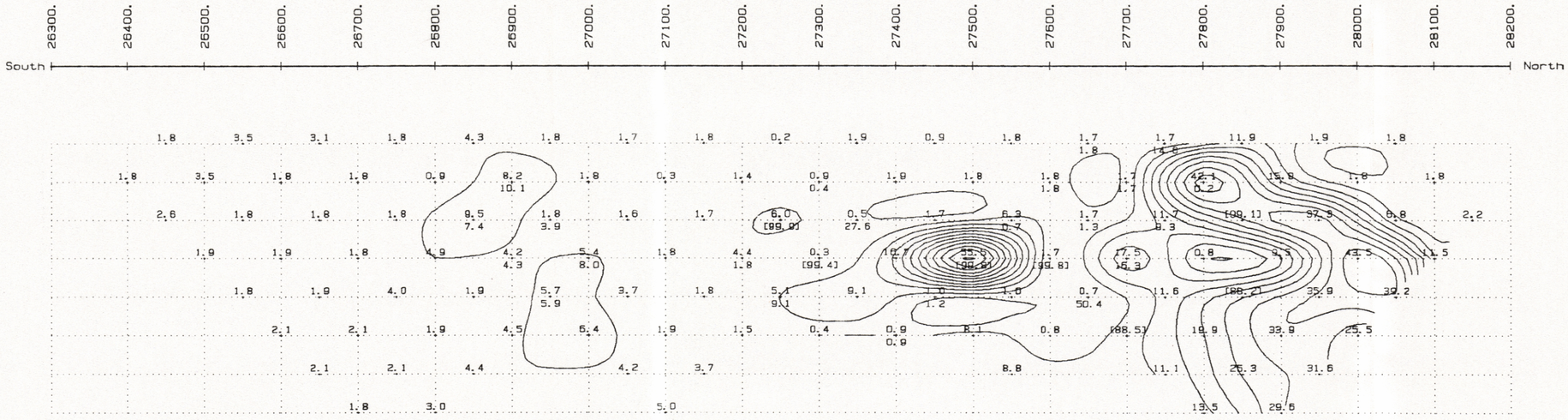

Line DECOUPLED
Cole-Cole Dispersion
for
TEST LINE 2

ZONGE ZPLOT 7.12 Duplicates Not Used
Plotted 02 Nov 95

Cole-Cole Parameters
Chargeability (m)
(X 100)

SURVEY LINE DATA
Line Orient= North

Survey Date= OCT.95

[Plot limits] and ARITHMETIC CONTOURS
(Interval: 10.00)
[-9.11] 90.0
0.00 [96.1]
10.0
20.0
30.0
40.0
50.0
60.0
70.0
80.0

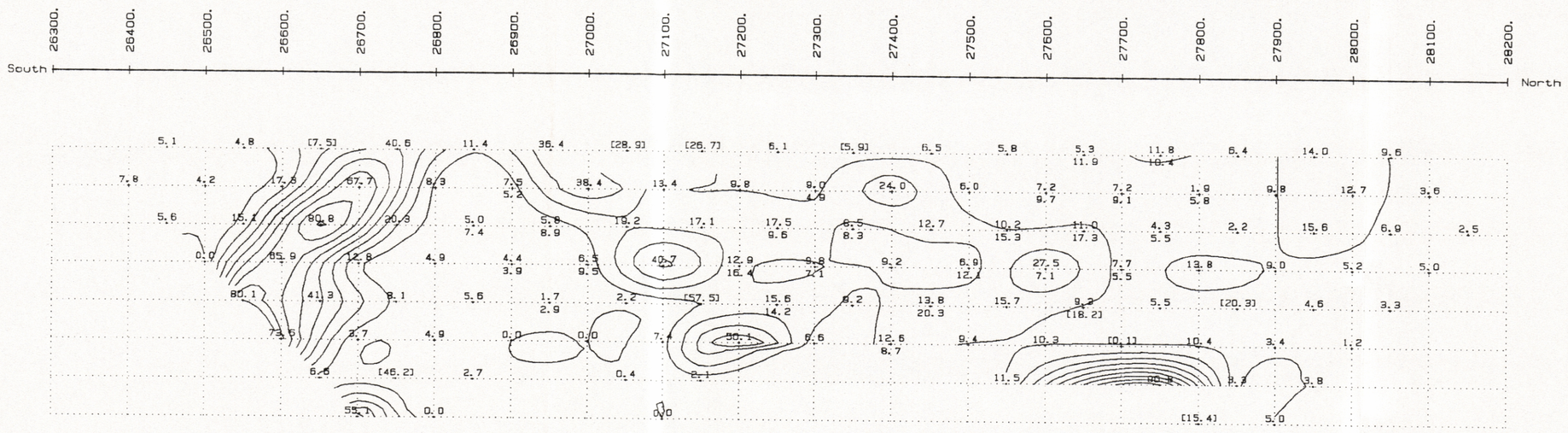

Line DECOUPLED
Cole-Cole Dispersion
for
TEST LINE 2

ZONGE ZPLOT 7.12 Duplicates Not Used
Plotted 02 Nov 95

Cole-Cole Parameters
Time Constant

Log(TAU) (Sec)

SURVEY LINE DATA
Line Orient= North

Survey Date= OCT.95

[Plot limits] and ARITHMETIC CONTOURS
(Interval: 5.00)
[-4.83]
0.00
[2.68]

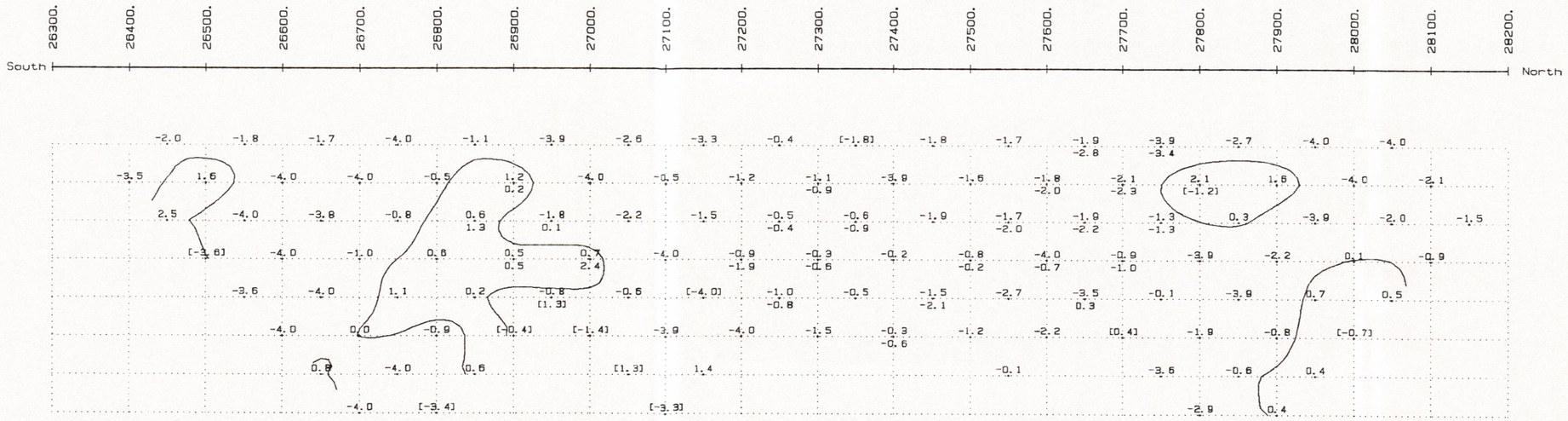

Line DECOUPLED
Cole-Cole Dispersion
for
TEST LINE 2

ZONGE ZPLOT 7.12 Duplicates Not Used
Plotted 02 Nov 95

Cole-Cole Parameters
Frequency Dep. (c)
(X 100)

SURVEY LINE DATA
Line Orient= North

Survey Date= OCT.95

[Plot limits] and ARITHMETIC CONTOURS
(Interval: 10.00)
[.266]
10.0
20.0
30.0
40.0
50.0
60.0
70.0
[73.4]

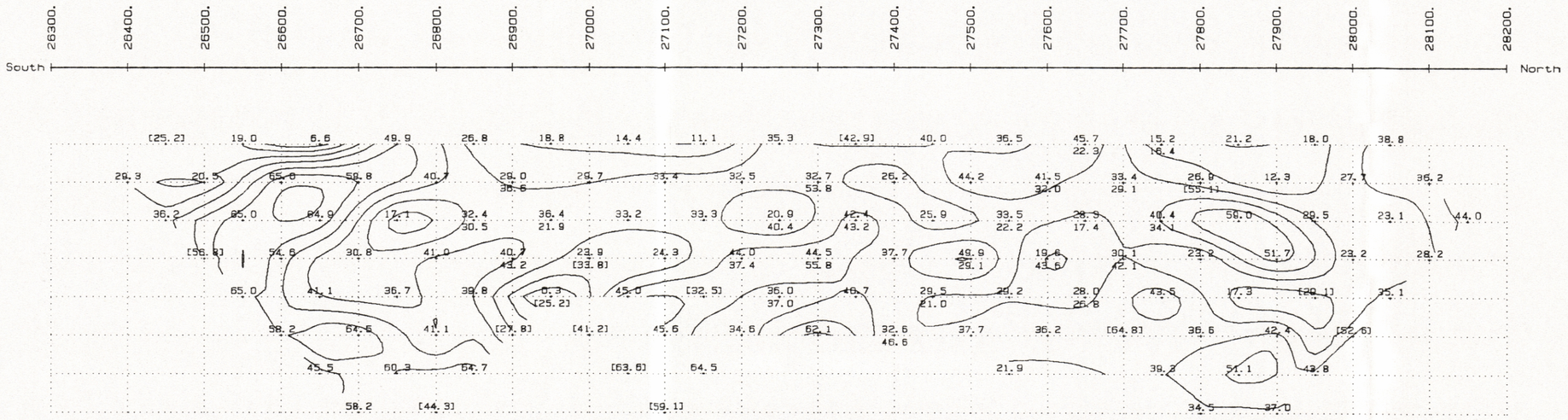

Line DECOUPLED
Cole-Cole Dispersion
for
TEST LINE 2

ZONGE ZPLOT 7.12 Duplicates Not Used
Plotted 22 Nov 95

CD

Cole-Cole Parameters
L1 Norm Error
(unitless)

SURVEY LINE DATA
Line Orient= North

[Plot limits] and ARITHMETIC CONTOURS
(Interval: 5.00)
[-.988]
0.00
5.00
10.0
15.0
[17.1]

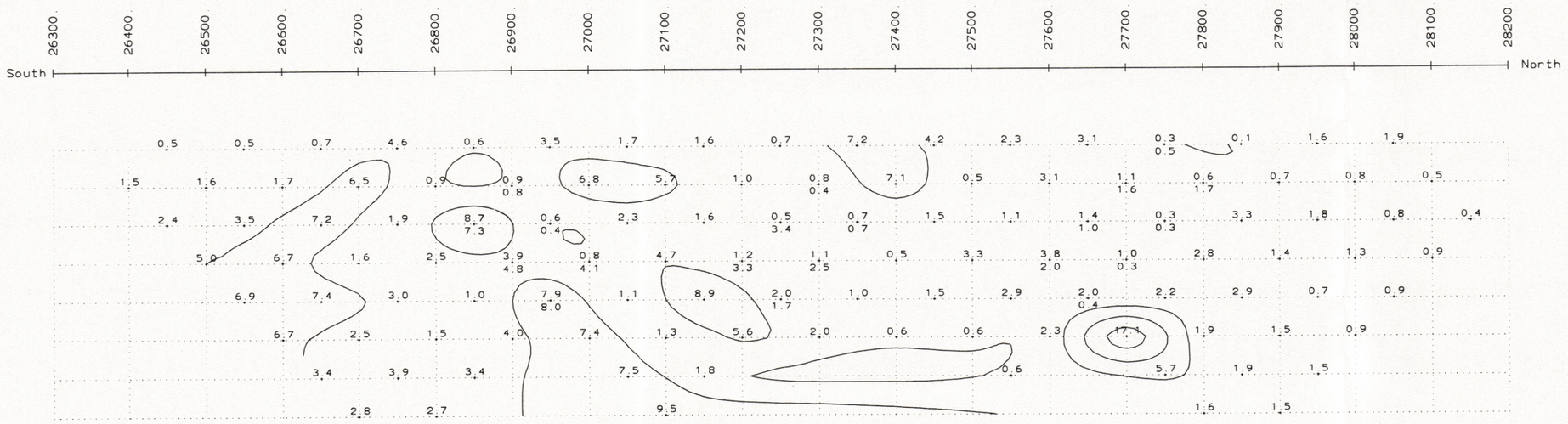

APPENDIX V

TEST LINE 1 and 2

Pseudosections of GDPHM Decoupled Data

GDPHM IP Response: 0.125 Hz IP phase
1.0 Hz IP phase
8.0 Hz IP phase

Line DECOUPLED
GDPHM: Decoupled Response
for
TEST LINE 1

ZONGE ZPLOT 7.12 Duplicates Not Used
Plotted 01 Nov 95

REM SURVEY DATA
IP RESPONSE

PHASE ANGLE (0.125 Hz)
(using DECOUPLED PHASE)

SURVEY LINE DATA
Line Orient= East
A - Spacing= 100 m

Survey Date= OCT.95

[Plot limits] and ARITHMETIC CONTOURS
(Interval: 5.00)
[.220]
5.00
10.0
[14.5]

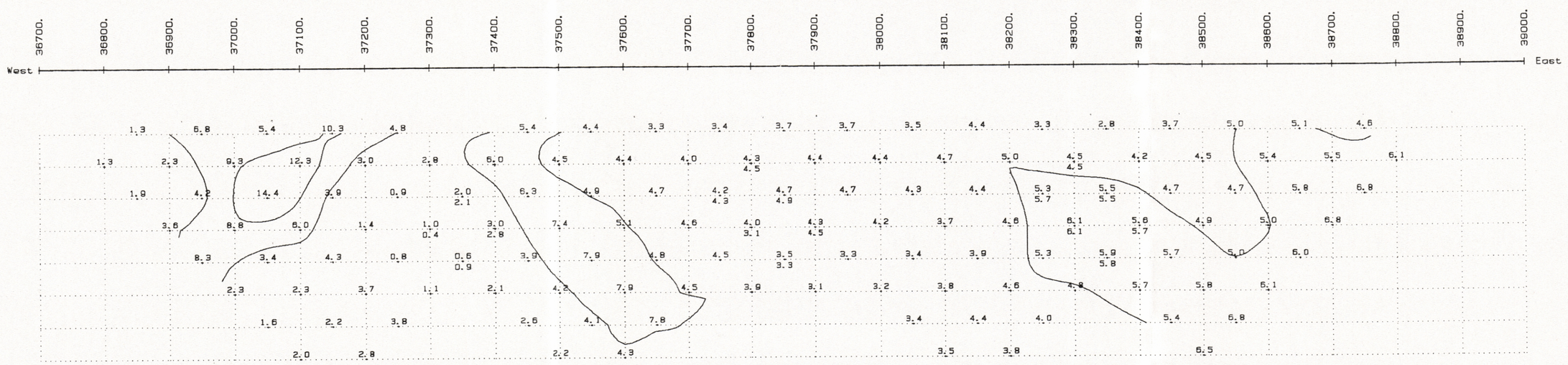

Line DECOUPLED

GDP-M: Decoupled Response

for

TEST LINE 1

ZONGE ZPLOT 7.12 Duplicates Not Used
Plotted 01 Nov 95

REM SURVEY DATA
IP RESPONSE

PHASE ANGLE (1 Hz)
(Using DECOUPLED PHASE)

SURVEY LINE DATA
Line Orient= East
A - Spacing= 100 m

Survey Date= OCT.95

[Plot limits] and ARITHMETIC CONTOURS
(Interval: 5.00)
[.931]
5.00
10.0
[13.2]

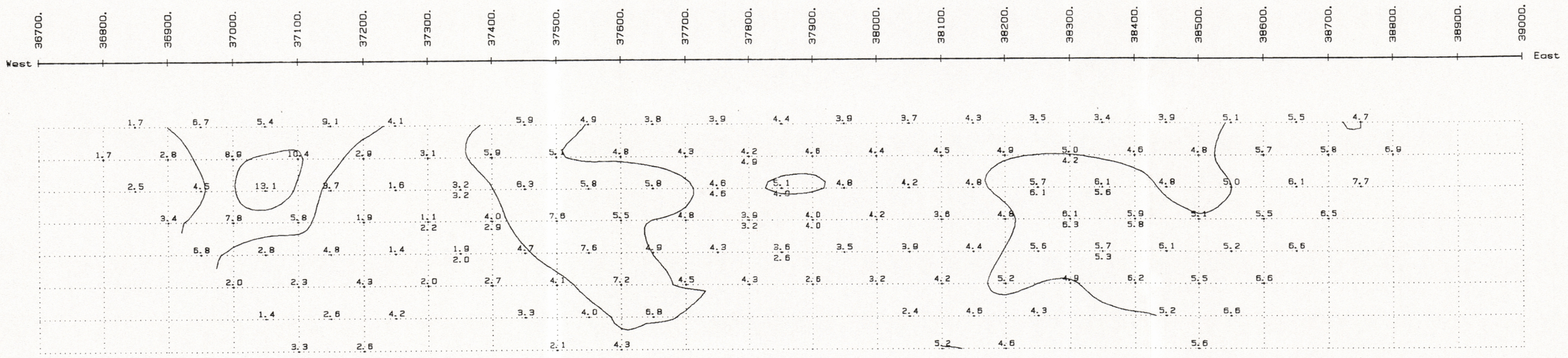

Line DECOUPLED
GDPHM: Decoupled Response
for
TEST LINE 1

ZONGE ZPLOT 7.12 Duplicates Not Used
Plotted 01 Nov 95

REM SURVEY DATA
IP RESPONSE

PHASE ANGLE (8 Hz)
(using DECOUPLED PHASE)

SURVEY LINE DATA
Line Orient= East
A - Spacing= 100 m

Survey Date= OCT.95

[Plot limits] and ARITHMETIC CONTOURS
(Interval: 5.00)
[-.602]
0.00
5.00
10.0
[13.3]

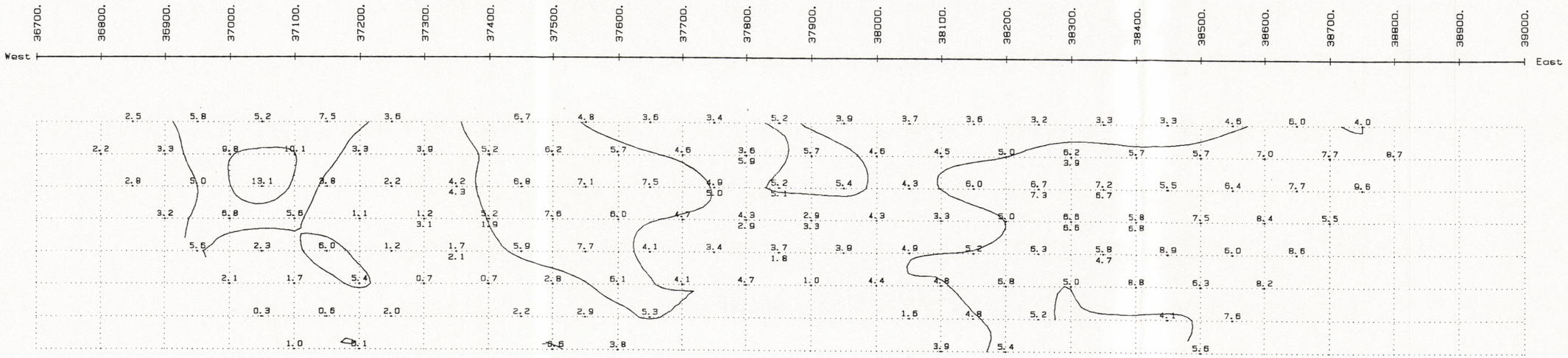

Line DECOUPLED
GDPHM: Decoupled Response
for
TEST LINE 2

ZONGE ZPLOT 7.12 Duplicates Not Used
Plotted 31 Oct 95

REM SURVEY DATA
IP RESPONSE

PHASE ANGLE (0.125 Hz)
(using DECOUPLED PHASE)

SURVEY LINE DATA
Line Orient= North
A - Spacing= 100 m

Survey Date= OCT.95

[Plot limits] and ARITHMETIC CONTOURS
(Interval: 5.00)
[-1.53]
0.00
5.00
10.0
15.0
20.0
25.0
[25.1]

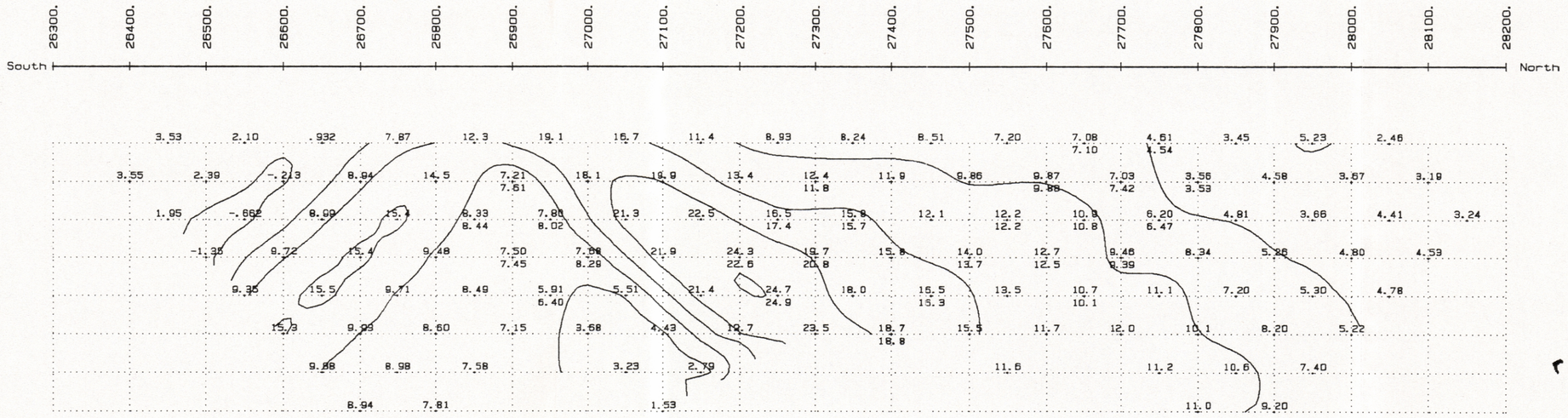

Line DECOUPLED
GDPHM: Decoupled Response
for
TEST LINE 2

ZONGE ZPLOT 7.12 Duplicates Not Used
Plotted 31 Oct 95

REM SURVEY DATA
IP RESPONSE

PHASE ANGLE (1 Hz)
(using DECOUPLED PHASE)

SURVEY LINE DATA
Line Orient= North
A - Spacing= 100 m

Survey Date= OCT.95

[Plot limits] and ARITHMETIC CONTOURS
(Interval: 5.00)
[-9.08m]
0.00
5.00
10.0
15.0
20.0
25.0
[26.8]

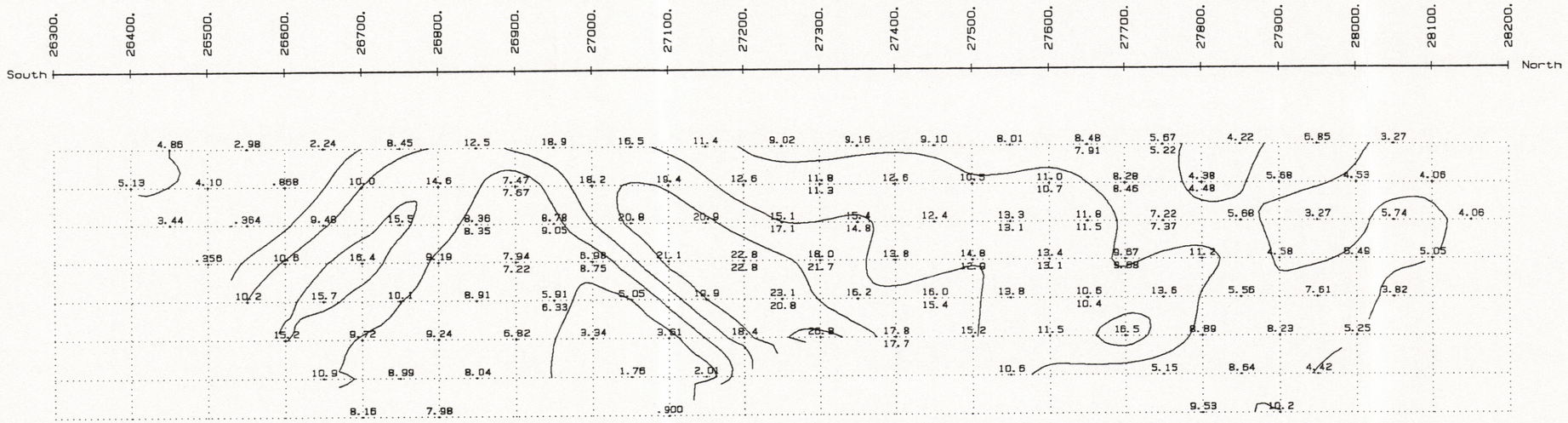

Line DECOUPLED
GDPHM: Decoupled Response
for
TEST LINE 2

ZONGE ZPLOT 7.12 Duplicates Not Used
Plotted 31 Oct 95

REM SURVEY DATA
IP RESPONSE

PHASE ANGLE (8 Hz)
(using DECOUPLED PHASE)

SURVEY LINE DATA
Line Orient= North
A - Spacing= 100 m

Survey Date= OCT.95

[Plot limits] and ARITHMETIC CONTOURS
(Interval: 5.00)
[.148]
5.00
10.0
15.0
20.0
25.0
[26.5]

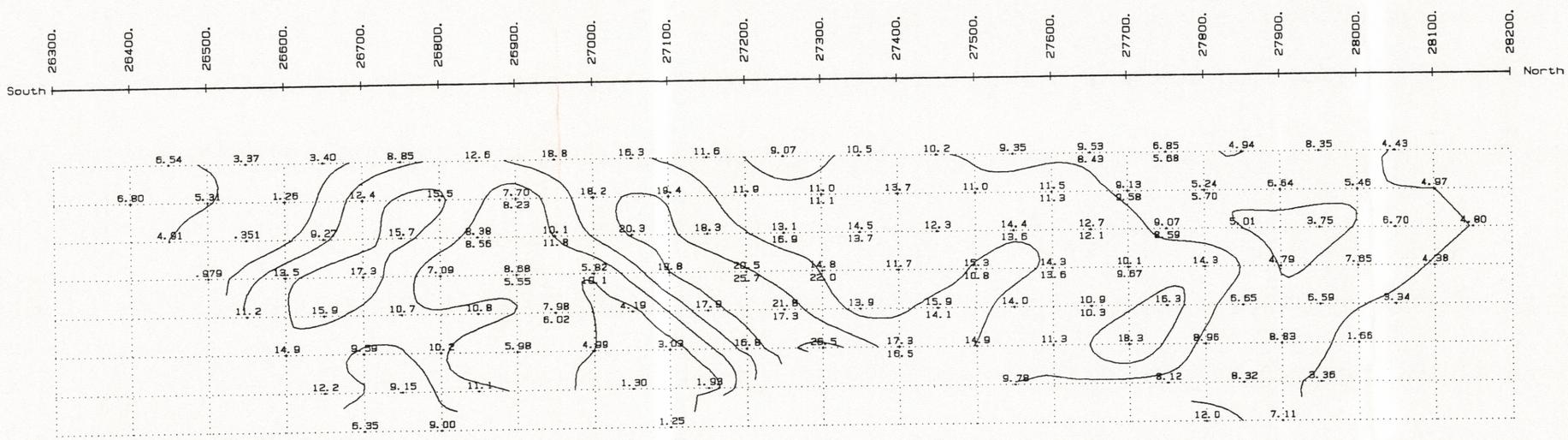

APPENDIX VI: Brief description of decoupling programs CRS_CC and CRS_CIP

Inversion programs CRS_CC (v5.2) and CRS_CIP (v2.1) have been written in LAHEY Fortran 77 on an IBM PC compatible computer running MS-DOS, version 6.0.

Program CRS_CIP decouples dipole-dipole CR-IP data by inverting the total response to an anisotropic half-space with constant IP phase shift complex resistivities. Program CRS_CC decouples dipole-dipole CR-IP data by inverting the total response to an anisotropic half-space using a Cole-Cole dispersion to model the IP response.

The programs read in a Zonge tabular format *.AVG file (see file formats in this appendix) containing data averaged from multiple stacks by Zonge's inhouse program CRAVG. The programs read in nine columns of data; transmitter location, receiver location, pseudosection station location, n-spacing, frequency, apparent resistivity, phase, percent error of the resistivity and error of the phase. The n-spacing, transmitter and receiver locations are used to determine the a-spacing of the array. The errors from the *.AVG file are used to apply weights to the measurements taken at each frequency. The programs will only invert data which consists of resistivity and phase measurements made at no more than twenty frequencies for a given pseudosection point.

Both programs are fully automated, requiring only that data be in the correct format. The programs are run by typing the program name followed by the filename, no extension is required;

i.e. for a file TEST.AVG

TYPE >> CRS_CC TEST (the program assumes the .AVG extension)

The rate of annealing and constraints placed on the Cole-Cole parameters have been predetermined and are included as part of the code in the main program.

Both programs output Zonge tabular format *.Z and *.P files (see file formats in this appendix). The *.Z file contains plotting data for the apparent resistivity, final parameter values as well as the 0.125, 1.0 and 8.0 Hz IP phase response. Zonge's inhouse program ZPLOT uses the *.Z file to produce HPGL vector plotting files. The *.P file contains spectral data which is converted into HPGL vector plotting files by Zonge's inhouse program PPLOT.

The author can be contacted to obtain further information on these programs or a current version of the source code. The main program for CRS_CIP is included in this appendix as an example of the code.

File Formats:

***.AVG - averaged field CR-IP survey data in a tabular format.**
From CRAVG

```
\ CRAVG 7.20: "GERARD01.FLD", Dated 95-12-04, Processed 10 Sep 95
$ ASPACE= 100.0m
\ 0.Hz Mag= RhoA @  0.125 Hz, Phz= 3-Pt Phz @ .125,.375,.625 Hz
```

skp	Tx	Rx	PltPt	NSp	Freq	Cmp	Amps	Resistivity	Phase	Real	Imag	%Rho	sPhz
2	36900.00	36700.00	36850.00	1.0	0.000	Ex	0.	2.0713e+1	1.4	1.0000e+0	0.0000e+0	0.0	0.2
2	36900.00	36700.00	36850.00	1.0	.1250	Ex	9.95	1.3991e-2	1.5	1.0000e+0	1.5000e-3	0.0	0.0
2	36900.00	36700.00	36850.00	1.0	.3750	Ex	9.95	1.3976e-2	1.9	9.9896e-1	1.8980e-3	0.0	0.1
2	36900.00	36700.00	36850.00	1.0	.6250	Ex	9.95	1.3971e-2	2.5	9.9856e-1	2.4964e-3	0.0	0.1
2	36900.00	36700.00	36850.00	1.0	.8750	Ex	9.95	1.3964e-2	3.0	9.9809e-1	2.9444e-3	0.0	0.1
2	36900.00	36700.00	36850.00	1.0	1.125	Ex	9.95	1.3962e-2	3.3	9.9791e-1	3.2931e-3	0.0	0.0
2	36900.00	36700.00	36850.00	1.0	1.000	Ex	9.95	1.3954e-2	3.1	9.9800e-1	3.1188e-3	0.0	0.0
2	36900.00	36700.00	36850.00	1.0	3.000	Ex	9.95	1.3936e-2	6.1	9.9670e-1	6.1049e-3	0.0	0.0
2	36900.00	36700.00	36850.00	1.0	5.000	Ex	9.95	1.3925e-2	9.1	9.9585e-1	9.0376e-3	0.0	0.1
2	36900.00	36700.00	36850.00	1.0	7.000	Ex	9.95	1.3918e-2	11.6	9.9535e-1	1.1621e-2	0.0	0.1
2	36900.00	36700.00	36850.00	1.0	9.000	Ex	9.95	1.3907e-2	14.6	9.9456e-1	1.4547e-2	0.0	0.1
2	36900.00	36700.00	36850.00	1.0	8.000	Ex	9.95	1.3911e-2	12.9	9.9496e-1	1.3084e-2	0.0	0.0
2	36900.00	36700.00	36850.00	1.0	24.00	Ex	9.95	1.3847e-2	33.3	9.8996e-1	3.3276e-2	0.0	0.1
2	36900.00	36700.00	36850.00	1.0	40.00	Ex	9.95	1.3780e-2	52.0	9.8432e-1	5.1430e-2	0.0	0.0
2	36900.00	36700.00	36850.00	1.0	56.00	Ex	9.95	1.3708e-2	69.6	9.7813e-1	6.8486e-2	0.0	0.1
2	36900.00	36700.00	36850.00	1.0	72.00	Ex	9.95	1.3632e-2	85.9	9.7152e-1	8.3908e-2	0.0	0.0

File Formats:

*.Z - Zonge format plotting file contains up to eleven plots.
Used by ZPLOT

```
 CRS_V1, V12.0
CRS Cole-Cole Z-File
Cl Cn Ce Ns Nd Yl  Plot file  6
 0  2  1  3  1  0
Cole-Cole Parameters
 L1 Norm Error
  (unitless)
IIxxxxxxxxYYYYYYYYzzzzzzzzzzzz
236850.00     1.00     2.910E+0
236800.00     2.00     4.676E+0
236950.00     1.00     2.124E+0
236900.00     2.00     4.485E+0
236850.00     3.00     5.530E+0
237050.00     1.00     7.400E-1
237000.00     2.00     6.334E+0
236950.00     3.00     1.808E+0
236900.00     4.00     3.130E+0
237150.00     1.00     1.510E+0
237100.00     2.00     2.383E+0
237050.00     3.00     9.538E+0
237000.00     4.00     4.011E+0
236950.00     5.00     4.222E+0
237250.00     1.00     7.215E-1
```

File Formats:

*.P - Zonge format plotting file for producing spectral plots.
Used by PPLOT

```
\* 09/21/95
$ ASPACE= 100.0
"GERARD01.P", from CRS_V1 12.0
 modelled spectra
 EM Coupling Response
 Rx:36700. Tx:36900. NSp: 1.0
 1 0 0 15        0.0    0.0    0.0
    0.0    0.0    0.0    0.0    0.0
    0.0    0.0    0.0    0.0    0.0
  0.125  1.000E+00  3.542E-04
  0.375  9.999E-01  1.027E-03
  0.625  9.998E-01  1.672E-03
  0.875  9.998E-01  2.296E-03
  1.125  9.996E-01  2.902E-03
  1.000  9.997E-01  2.601E-03
  3.000  9.986E-01  7.054E-03
  5.000  9.974E-01  1.095E-02
  7.000  9.960E-01  1.446E-02
  9.000  9.945E-01  1.768E-02
  8.000  9.953E-01  1.611E-02
 24.000  9.835E-01  3.617E-02
 40.000  9.727E-01  5.003E-02
 56.000  9.631E-01  6.083E-02
 72.000  9.545E-01  6.983E-02
```

```
C                    PROGRAM CRS_CIP v2.1 Decoupling routine
C SEPTEMBER 1995
C-----------------------------------------------------------------------
C-----------------------------------------------------------------------
C VERSION 2.1
C Reads and decouples IP data from .AVG-files.
C Inverts the dipole-dipole IP/EM response to an anisotropic half-space.
C Uses a Constant IP phase to model the IP response.
C Uses a controlled random search proceedure for global optimisation.
C Outputs Zonge format .Z files for parameter plots
C Outputs Zonge format .P files for spectral plots
C Outputs 0.125, 1.0 and 8.0 Hz DC phase data into the .Z file
C
C Variables:
C AVGFILE - character, name of CR .AVG file.
C NP      - integer, total number of points.
C STN     - real array, list of station numbers.
C FRQ     - real array, list of frequencies (hertz).
C ANSP    - real array, list of n-spacings.
C ARES    - real array, apparent resistivities (ohm-m).
C RERR    - real array, apparent resistivity error (percent).
C APHZ    - real array, apparent IP phase (mrad).
C IERR    - integer, 0 if no input error.
C-----------------------------------------------------------------------
      CHARACTER  VERSN*5,        UPDATE*10
      PARAMETER( VERSN='2.1',    UPDATE='20/09/95' )

      INTEGER    MF,     MN,    MS,      MSN,         MP
      PARAMETER( MF=16, MN=8, MS=150, MSN=MS*MN, MP=MF*MN*MS/4 )
      INTEGER   NTTY,    NIN,     NOUT,     NDK1,     NDK2,     NDK3
      PARAMETER(NTTY=6, NIN=15, NOUT=16, NDK1=17, NDK2=18, NDK3=19)

      REAL       PI
      PARAMETER( PI=3.141593 )


      INTEGER I, II, J, JJ, K, K1, L, N, NP, P, K2, NS, NF,
     &        IERR, JSORT(MP), NUM, NNTR, NSTOP, IMAX, IMIN,
     &        INSP(MSN), ITERMAX, NCLOUD, IA(10)

      REAL    Tx(MP),Rx(MP),STN(MP),FRQ(MP),ANSP(MP),ARES(MP),RERR(MP),
     &        APHZ(MP),PERR(MP),DMOD(2*MF),K0,IP0,SEED,IPRAN(MP),
     &        ASP,ADSMIN,REZOT,R0,DOBS(2*MF),DERR(2*MF),SUM,
     &        PRT(10),KRT,CP(10),KR(MS),IPR(MS),IP(MS),
     &        REZO(MS),ERROR(MS),ERRMIN,ERRMAX,ERRANG,
     &        FNCLOUD,ERRT,PR(10,MS),IPMIN,KMIN,ANNEAL,
     &        KRC(MSN),IPC(MSN),REZOC(MSN),PRC(10),
     &        ADSF,FMODERR,IPT,ERRC(MSN)

      COMPLEX    QARES,QAREP(MP),QAPHZ,QC,QV,QRES,QIPHALF

      CHARACTER AVGFILE*32,CDATE*8,CTIME*8,FSTEM*28,ZFILE*32,
     &          HEADER(8)*80, HEADp(6)*80, PFILE*32

C-----------------------------------------------------------------------
C-----------------------------------------------------------------------
      WRITE(NTTY,'(/4A/A/A/2A/A/)')
     &' CRS_CIP v',VERSN,', ',UPDATE,
     &' Decouples Frequeny Domain Spectral IP data',
     &' Using an Anisotropic Half-space with Cole-Cole Dispersion',
     &' MS-DOS version implemented ',UPDATE,
     &' by Gerard M. McNeill.'
```

```
C-----Open input file and read data.
      CALL GetFile( AVGFILE, '.AVG' )
      CALL UPCASE( AVGFILE )
      IF( INDEX( AVGFILE, '.AVG' ) .EQ. 0) THEN
        PRINT*,'ERROR: Input file must be an *.AVG format file.'
        STOP
      ENDIF

      I = INDEX(AVGFILE,'.AVG') - 1
      IF( I .LT. 0 ) I = 28
      FSTEM = AVGFILE(1:I)

C.....Get data from *.AVG file:
       CALL READAVG(AVGFILE,HEADER,NS,NP,Tx,Rx,STN,FRQ,ANSP,ARES,
     &              RERR,APHZ,PERR,IERR)

          ASP  = ABS(Tx(1)-Rx(1))/(ANSP(1)+1.0)

      PRINT '(A,f8.2)',' ASP =', ASP

C-------------------------------------------------------------------------
C       Set inversion control parameters
C-------------------------------------------------------------------------
      NF = 3
      NCLOUD = 60
      ITERMAX = 5000

      SEED = RRAND()

C-------------------------------------------------------------------------
C START DOING INVERSION => Grid Search + Controlled Search
C-------------------------------------------------------------------------

C-------------------------------------------------------------------------
C SET UP COUNTERS TO ENSURE ONLY 0.125 TO 72 Hz FRQUENCY RANGE IS USED
C IN INVERSION => 0 Hz HAS 3PT PHASE - ONLY WANT TO USE THE DC RESIST.
C-------------------------------------------------------------------------

      NSTOP=0
      P=0
      N = 1
      K1=2

  230 K=N

      N=N+1

      IF (STN(K).LE.0.0)  GOTO 990
      IF ((STN(K).NE.STN(N)).OR.(ANSP(K).NE.ANSP(N)))  GOTO 240

      GOTO 230

  240 CONTINUE

      P=P+1
      NSTOP = N-1

      PRINT '(A,I5)',' Grid searching on point ' , P

          ADSMIN=1000.0

          K2 = K1-1
          RO = ARES(K2)
```

```
                    INSP(P) = NINT(ANSP(K))

      QC=CMPLX(PI*ASP*FLOAT(INSP(P)*(INSP(P)+1)*(INSP(P)+2)),0.0)

C-----------------------------------------------------------------------
C GRID SEARCH OVER ANISOTROPY (K) AND TAU
C-----------------------------------------------------------------------

          Do J=0,4

              KO = 10.0**(float(J-2))

              Do I=0,50

                  IPO = FLOAT(2*I)/1000.0

         QRES=RO/(CMPLX(COS(IPO),SIN(IPO)))

C-----------------------------------------------------------------------
C            CALCULATE FREQUENCY RESPONSE
C-----------------------------------------------------------------------

          NUM=0

          DO L = K1,NSTOP
          NUM=NUM+1
             QV = QC*QIPHALF( ASP, INSP(P), KO, QRES, FRQ(L) )
             QARES = CONJG(QV)
             QAPHZ = CLOG(QV)

             DOBS(2*NUM-1) = ARES(L)
             DOBS(2*NUM) = APHZ(L)

             DMOD(2*NUM-1) = REAL(QARES)
             DMOD(2*NUM) = -1000.0*AIMAG(QAPHZ)

             DERR(2*NUM-1) = RERR(L)
             DERR(2*NUM) = PERR(L)

             ENDDO

             ADSF = FMODERR(2*NUM,DOBS,DMOD,DERR)

             IF (ADSF.LT.ADSMIN) THEN
                ADSMIN = ADSF
                KMIN = KO
                IPMIN = IPO
             ENDIF

           ENDDO
            ENDDO
C-----------------------------------------------------------------------
C DETERMINE INITIAL SEARCH DOMAIN
C-----------------------------------------------------------------------

      PRINT '(A,F8.2)',' ADSMIN =', ADSMIN
      PRINT '(A,F8.2)',' KMIN =', KMIN
      PRINT '(A,F8.2)',' IPMIN =',1000.0*IPMIN
      PRINT '(A,F8.2)',' RESISTIVITY =', RO

      PRINT '(/A)',' Determining the initial search domain '

      CP(1) = 4.0
      CP(2) = 40.0/1000.0
      CP(3) = 0.05
```

```
      DO I=1,NCLOUD

      IF (I.EQ.1) THEN
      KR(I) = KMIN
      IPR(I) = IPMIN
      REZO(I)  = RO

      DO J=1,NF
      PR(J,1)=0.0
      ENDDO
      GOTO 2000
      ENDIF

1995      CONTINUE

      PR(1,I) = (RND()-0.5)*CP(1)
      PR(2,I) = (RND()-0.5)*CP(2)
      PR(3,I) = (RND()-0.5)*CP(3)

            KR(I) = KMIN*(10**(PR(1,I)))
              IF (KR(I).GT.100.0) GOTO 1995
              IF (KR(I).LT.0.001) GOTO 1995
             IPR(I) = IPMIN+PR(2,I)
              IF (IPR(I).LT.0.0) GOTO 1995
           REZO(I) = RO*(1.0+PR(3,I))

2000  CONTINUE

       QRES=REZO(I)/(CMPLX(COS(IPR(I)),SIN(IPR(I))))

C-------------------------------------------------------------------------------
C            CALCULATE FREQUENCY RESPONSE
C-------------------------------------------------------------------------------

       NUM=0

       DO L = K1,NSTOP
       NUM=NUM+1
          QV = QC*QIPHALF( ASP, INSP(P), KR(I), QRES, FRQ(L) )
          QARES = CONJG(QV)
          QAPHZ = CLOG(QV)

          DMOD(2*NUM-1) = REAL(QARES)
          DMOD(2*NUM) = -1000.0*AIMAG(QAPHZ)

          ENDDO

          ERROR(I) = FMODERR(2*NUM,DOBS,DMOD,DERR)

      ENDDO

      CALL ERRSORT(NCLOUD,ERROR,JSORT)
        IMIN = JSORT(1)
        IMAX = JSORT(NCLOUD)
        ERRMIN = ERROR(IMIN)
        ERRMAX = ERROR(IMAX)

C-------------------------------------------------------------------------------
C BEGIN THE CONTROLLED RANDOM SEARCH
C-------------------------------------------------------------------------------

      FNCLOUD = FLOAT(NCLOUD) - 1.0E-4

      PRINT *,(A,I5)"
```

```
     &     ' Beginning Controlled Random Search on point ' , P

           NNTR   = 0

           PRINT '(A/)',' L1 Data Residuals '
           PRINT '(A/)',' Trial     Minimum       Median       Maximum '

           DO II=1,ITERMAX

           NNTR = NNTR + 1

            ANNEAL = 1.0 + FLOAT(II)/(FNCLOUD*7.5)

 1020       DO J=1,NF+1
 1025       IA(J)=JSORT(1+INT((RND()**ANNEAL)*FNCLOUD))
              DO JJ = 1,J-1
                IF(IA(JJ) .EQ. IA(J)) GOTO 1025
              ENDDO
           ENDDO

           DO J = 1,NF
              SUM=0.0
            DO JJ = 1,NF
               SUM = SUM + PR(J,IA(JJ))
             ENDDO
              PRT(J) = 2.0*SUM/FLOAT(NF) - PR(J,IA(NF+1))
               IF(ABS(PRT(J)).GT.2.0*CP(J)) GOTO 1020
           ENDDO

                   KRT = KMIN*(10**(PRT(1)))
                   IF (KRT.LT.0.001) GOTO 1020
                   IF (KRT.GT.100.0) GOTO 1020
                   IPT = IPMIN+PRT(2)
                   IF (IPT.LT.0.0) GOTO 1020
                  REZOT = R0*(1.0+PRT(3))

            QRES=REZOT/(CMPLX(COS(IPT),SIN(IPT)))

C-----------------------------------------------------------------------
C              CALCULATE FREQUENCY RESPONSE
C-----------------------------------------------------------------------

            NUM=0

            DO L = K1,NSTOP
            NUM=NUM+1
               QV = QC*QIPHALF( ASP, INSP(P), KRT, QRES, FRQ(L) )
               QARES = CONJG(QV)
               QAPHZ = CLOG(QV)

               DMOD(2*NUM-1) = REAL(QARES)
               DMOD(2*NUM) = -1000.0*AIMAG(QAPHZ)

               ENDDO

               ERRT = FMODERR(2*NUM,DOBS,DMOD,DERR)

              IF(ERRT.LT.ERRMAX) THEN
                   ERROR(IMAX) = ERRT
              DO J=1,NF
                    PR(J,IMAX) = PRT(J)
              ENDDO
                ENDIF

C  FIND MINIMUM AND MAXIMUM ERRORS
```

```
      CALL ERRSORT(NCLOUD,ERROR,JSORT)
        IMIN = JSORT(1)
        IMAX = JSORT(NCLOUD)
        ERRMIN = ERROR(IMIN)
        ERRMAX = ERROR(IMAX)

      ERRANG = ERRMIN*(ERRMAX - ERRMIN)/(ERRMAX+ERRMIN)

      IF ((ERRANG.LT.0.005).AND.(ERRMIN.LT.20.0)) GOTO 5000

      IF(NNTR.EQ.150) THEN
       PRINT '(1X,I5,2X,3(F10.2,2X))', II, ERROR(IMIN),
     &                    ERROR(JSORT(NCLOUD/2)),ERROR(IMAX)
         NNTR = 0
        ENDIF

      ENDDO

        GOTO 5002

 5000     PRINT "(A/)"," Parameter Solutions have converged "

          GOTO 5006

 5002     PRINT "(A/)"," Parameter Solutions have FAILED to converge "

 5006  CONTINUE
C-------------------------------------------------------------------------
C DETERMINE THE FINAL PARAMETER VALUE
C-------------------------------------------------------------------------

      DO J = 1,NF
         SUM=0.0
       DO JJ = 1,NCLOUD
          SUM = SUM + PR(J,JJ)
         IP(JJ) = IPMIN+PR(2,JJ)
        ENDDO
      PRC(J) = SUM/FLOAT(NCLOUD)
      ENDDO

            KRC(P) = KMIN*(10**(PRC(1)))
            IPC(P) = IPMIN+PRC(2)
          REZOC(P) = RO*(1.0+PRC(3))

      QRES=REZOC(P)/(CMPLX(COS(IPC(P)),SIN(IPC(P))))

C-------------------------------------------------------------------------
C DETERMINE THE ERROR ASSOCIATED WITH THE FINAL PARAMETER VALUES
C-------------------------------------------------------------------------

        NUM=0

        DO L = K1,NSTOP
        NUM=NUM+1
           QV = QC*QIPHALF( ASP, INSP(P), KRC(P), QRES, FRQ(L) )
           QARES = CONJG(QV)
           QAPHZ = CLOG(QV)

           DMOD(2*NUM-1) = REAL(QARES)
           DMOD(2*NUM) = -1000.0*AIMAG(QAPHZ)

           QAREP(L) = QARES/REZOC(P)
```

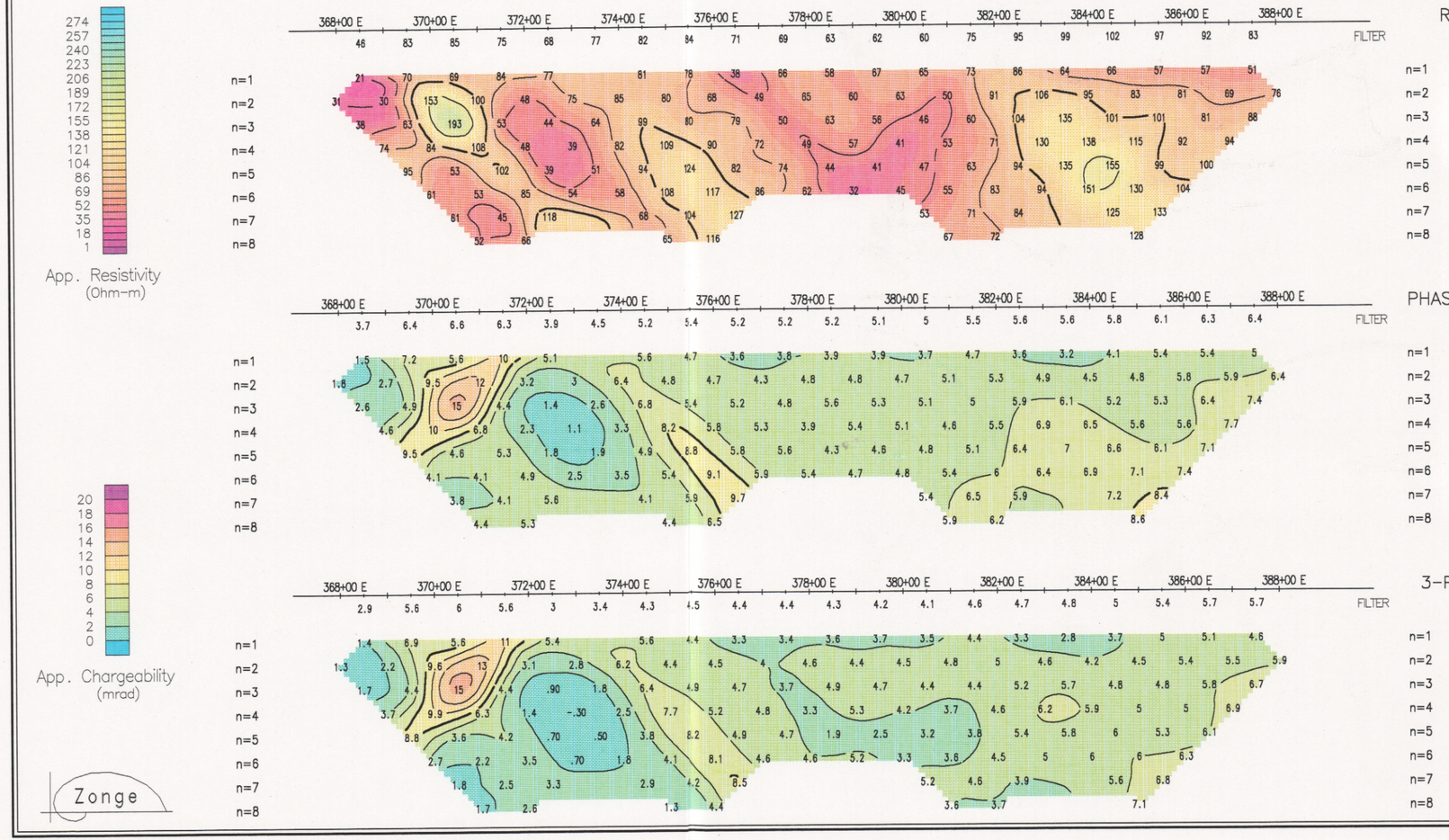

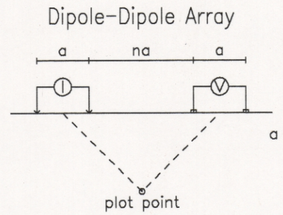

Logarithmic Contours 1, 1.5, 2, 3, 5, 7.5 10,..

Linear Contours 0.0, 2.0, 4.0, 6.0, 8.0,..

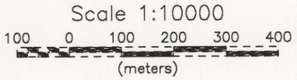

PLATE 1.0

TEST LINE 1

RAW DATA

3pt Field Decoupled Phase

CR-IP Survey Data

AUTHOR	DRAWN	DATE	SCALE	REPORT
Zonge	Zonge	16/01/96	1:10000	
REF. Masters Thesis		FILE	PLAN No.	

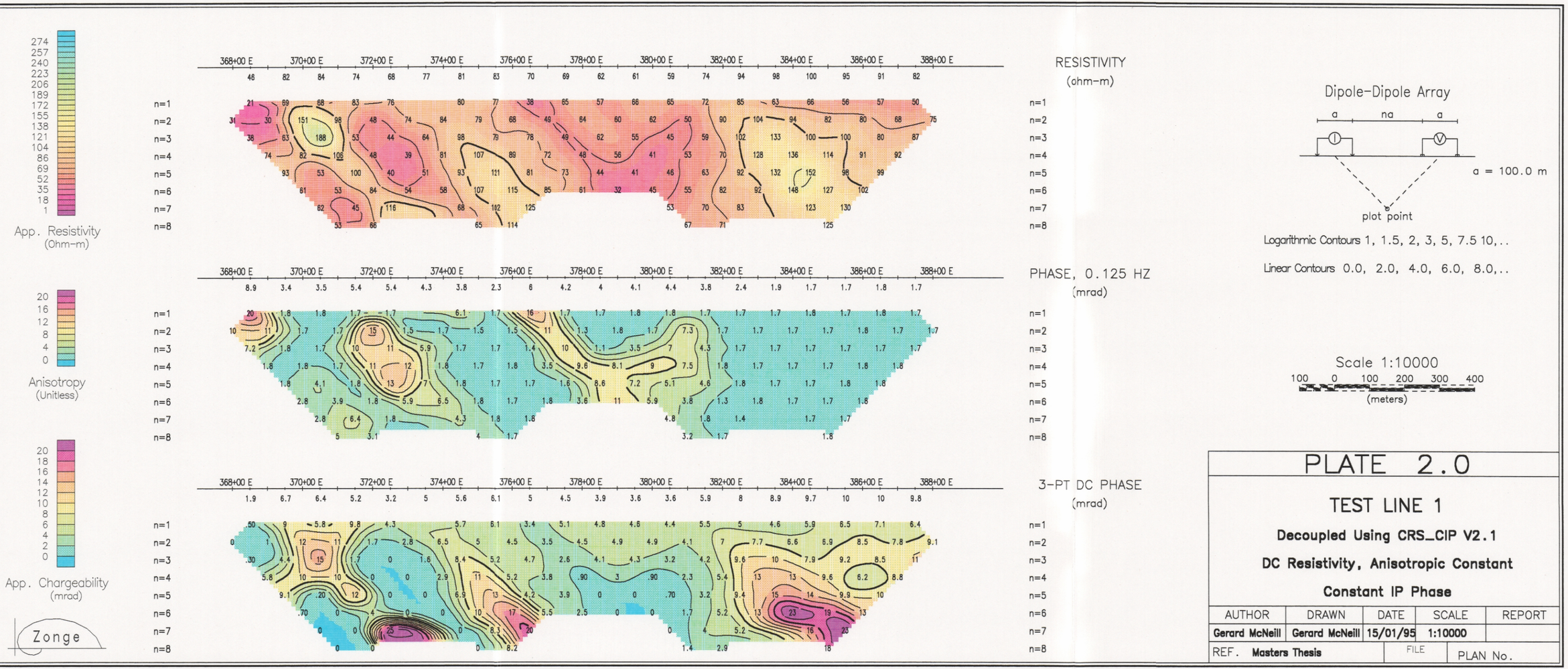

PLATE 2.0

TEST LINE 1

Decoupled Using CRS_CIP V2.1

DC Resistivity, Anisotropic Constant

Constant IP Phase

AUTHOR	DRAWN	DATE	SCALE	REPORT
Gerard McNeill	Gerard McNeill	15/01/95	1:10000	
REF. Masters Thesis		FILE	PLAN No.	

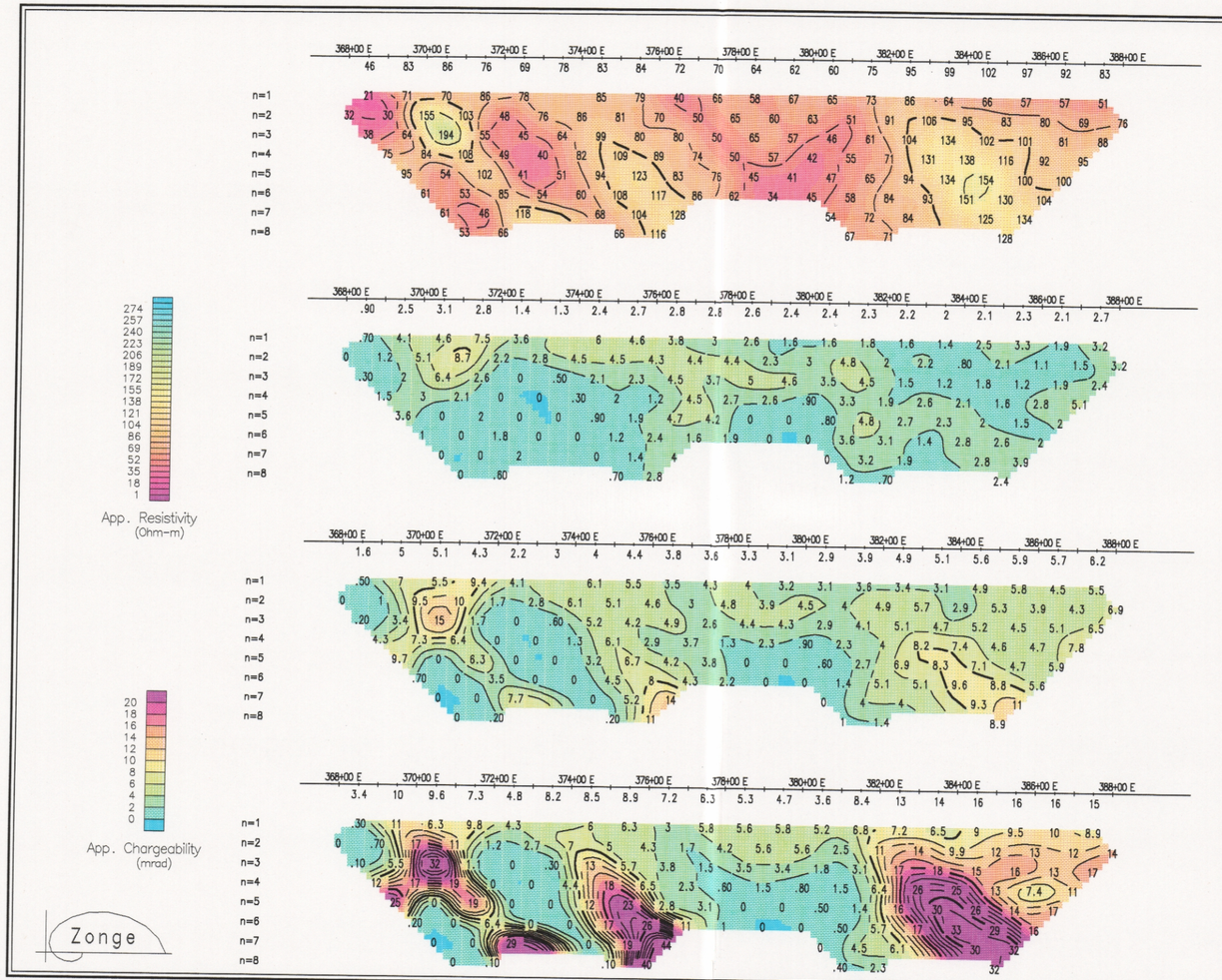

DC Resistivity
(ohm-m)

0.125 Hz DC PHASE
(mrad)

1.0 Hz DC PHASE
(mrad)

8.0 Hz DC PHASE
(mrad)

Dipole-Dipole Array

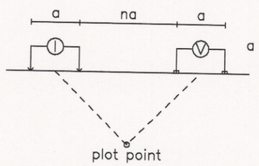

a = 100.0 m

Logarithmic Contours 1, 1.5, 2, 3, 5, 7.5 10,..

Linear Contours 0.0, 2.0, 4.0, 6.0, 8.0,..

Scale 1:10000

100 0 100 200 300 400
(meters)

PLATE 3.0

TEST LINE 1

Decoupled using CRS_CC V5.2

DC Resistivity

DC Phase at 0.125, 1.0 and 8.0 Hz

AUTHOR	DRAWN	DATE	SCALE	REPORT
Gerard McNeill	Gerard McNeill	16/01/96	1:12500	
REF. Master's Thesis		FILE	PLAN No.	

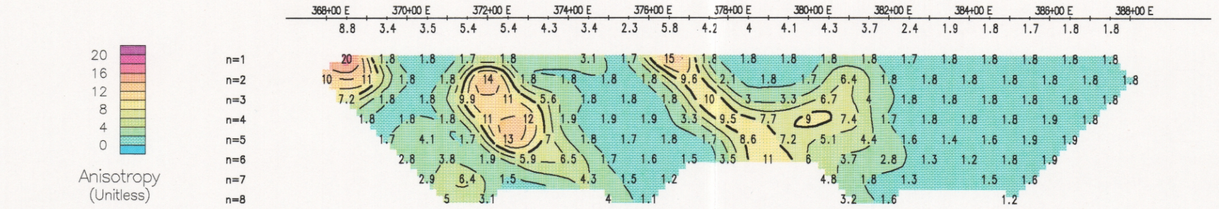

App. Anisotropy
(Unitless)

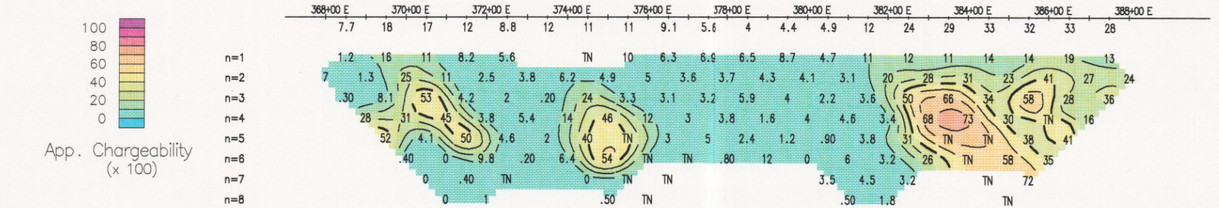

App. CHARGEABILITY
(x 100)

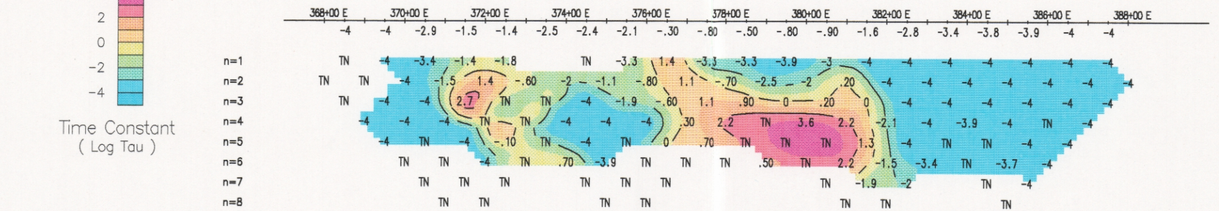

Log {Tau}
(SEC)

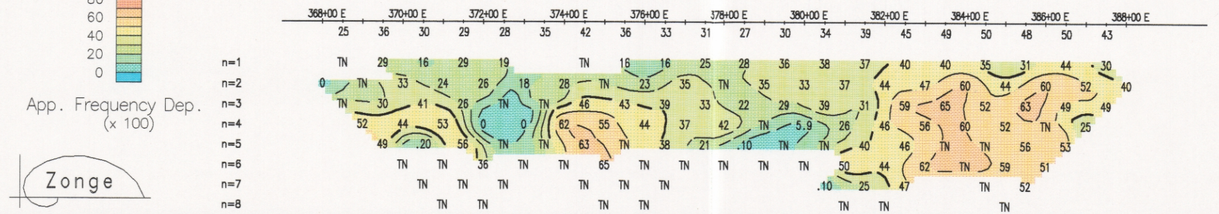

App. FREQUENCY DEP.
(x 100)

Anisotropy
(Unitless)

App. Chargeability
(x 100)

Time Constant
(Log Tau)

App. Frequency Dep.
(x 100)

Zonge

Dipole-Dipole Array

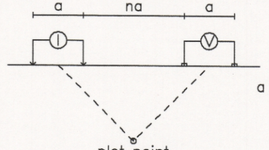

a = 100.0 m

Logarithmic Contours 1, 1.5, 2, 3, 5, 7.5 10,..

Linear Contours 0.0, 10.0, 20.0, 30.0, 40.0,..

Scale 1:10000

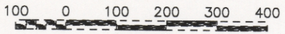

PLATE 4.0

TEST LINE 1

Forward Model returned from CRS_CC V5.2

Anisotropic Constant

Cole-Cole Dispersion Parameters

AUTHOR	DRAWN	DATE	SCALE	REPORT
Gerard McNeill	Gerard McNeill	16/01/96	1:12500	
REF. Master's Thesis		FILE	PLAN No.	

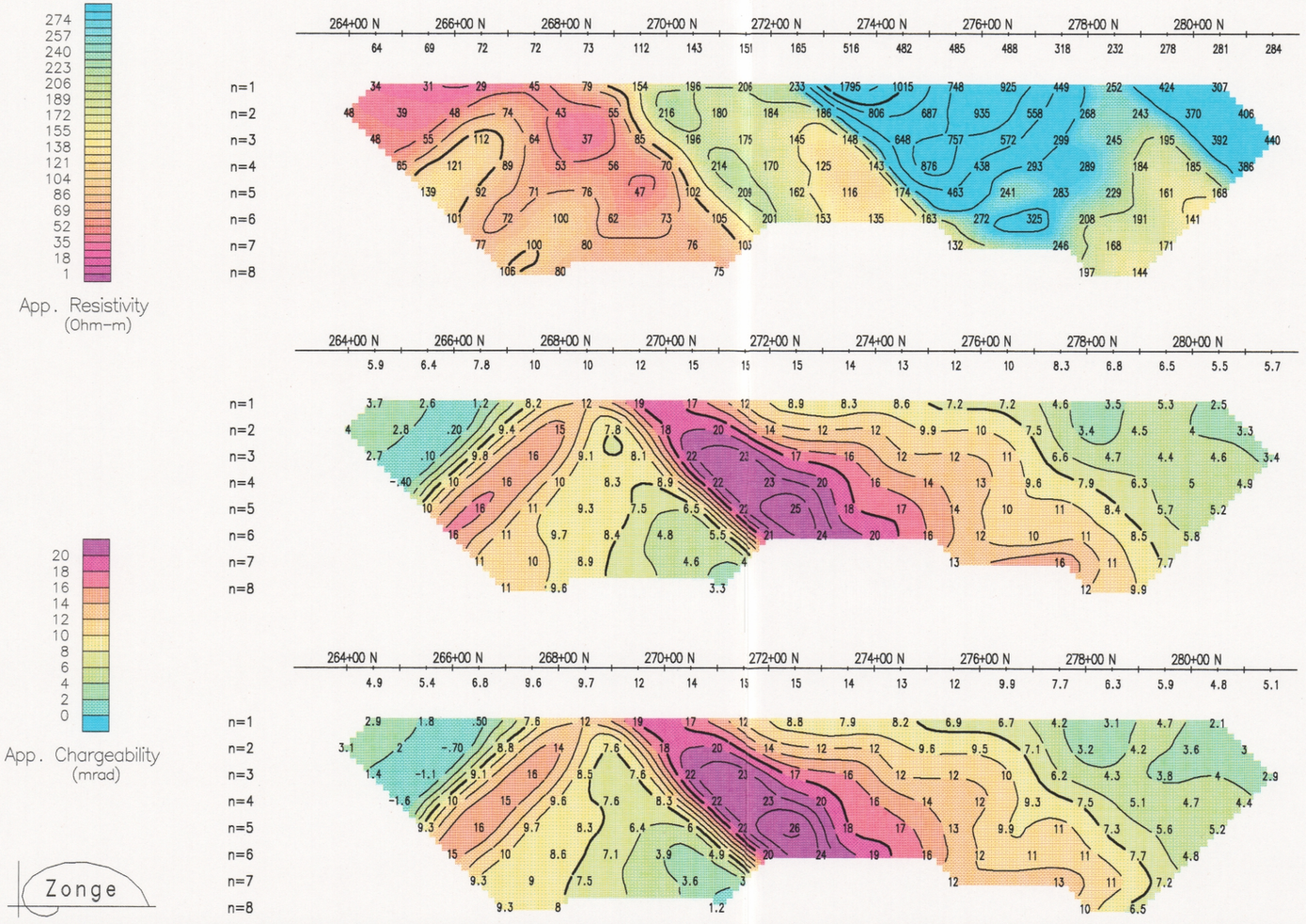

Dipole-Dipole Array

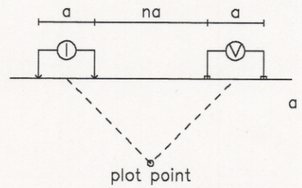

Logarithmic Contours 1, 1.5, 2, 3, 5, 7.5 10,..

Linear Contours 0.0, 2.0, 4.0, 6.0, 8.0,..

Scale 1:10000

100 0 100 200 300 400

(meters)

PLATE 5.0

TEST LINE 2

RAW DATA

3pt Field Decoupled Phase

CR-IP Survey Data

AUTHOR	DRAWN	DATE	SCALE	REPORT
Gerard McNeill	Gerard McNeill	16/01/96	1:10000	
REF. Masters Thesis		FILE	PLAN No.	

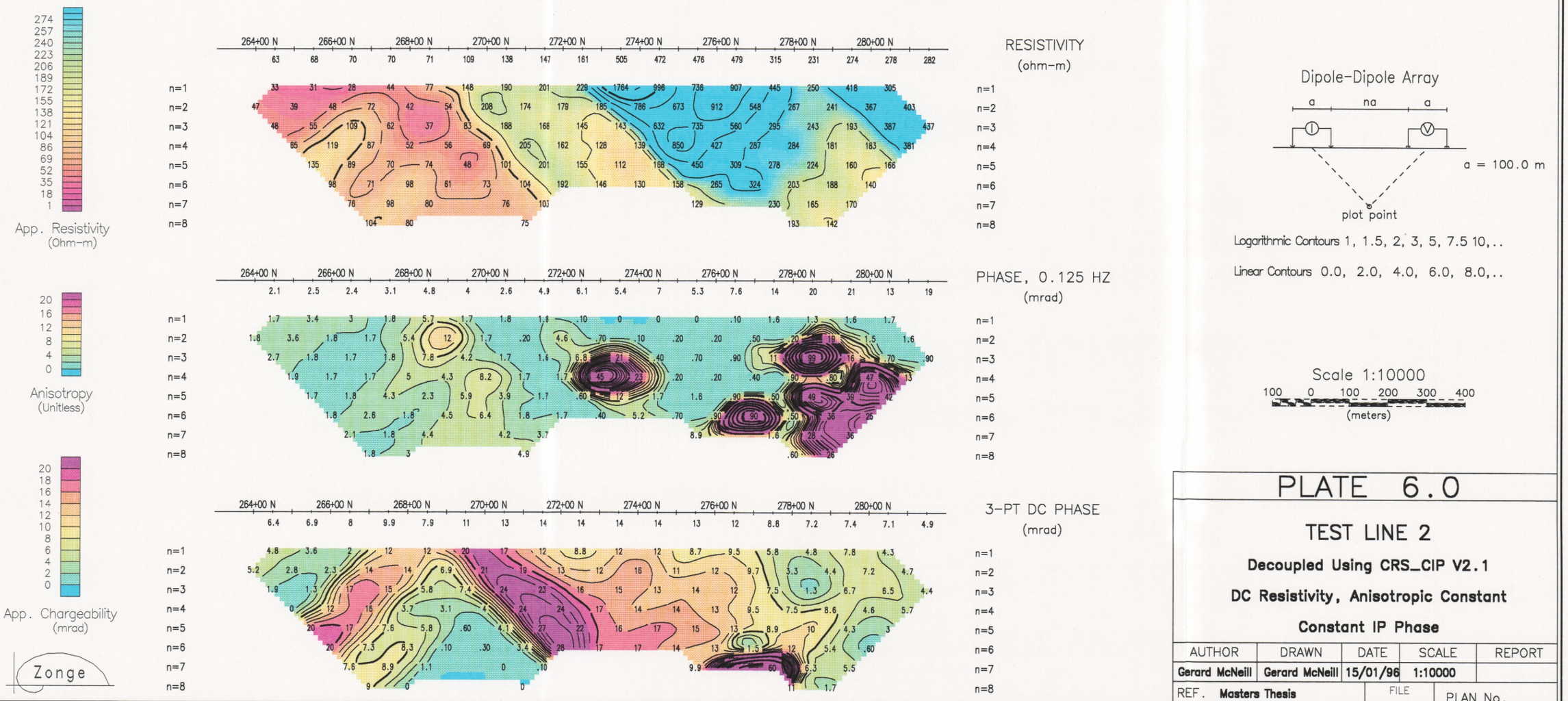

PLATE 6.0

TEST LINE 2

Decoupled Using CRS_CIP V2.1

DC Resistivity, Anisotropic Constant

Constant IP Phase

AUTHOR	DRAWN	DATE	SCALE	REPORT
Gerard McNeill	Gerard McNeill	15/01/96	1:10000	
REF. Masters Thesis		FILE	PLAN No.	

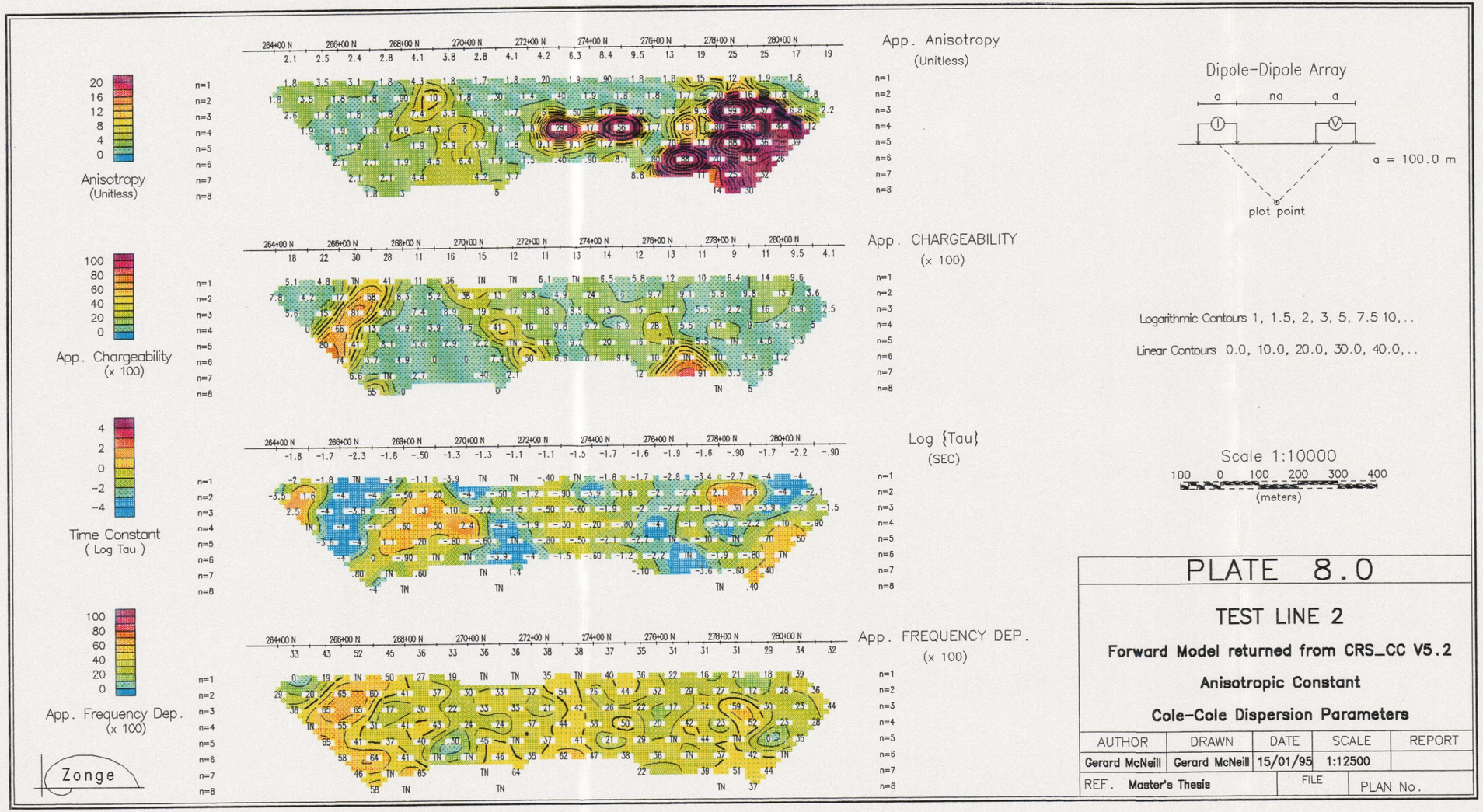

PLATE 8.0

TEST LINE 2

Forward Model returned from CRS_CC V5.2

Anisotropic Constant

Cole-Cole Dispersion Parameters

AUTHOR	DRAWN	DATE	SCALE	REPORT
Gerard McNeill	Gerard McNeill	15/01/95	1:12500	
REF. Master's Thesis		FILE	PLAN No.	

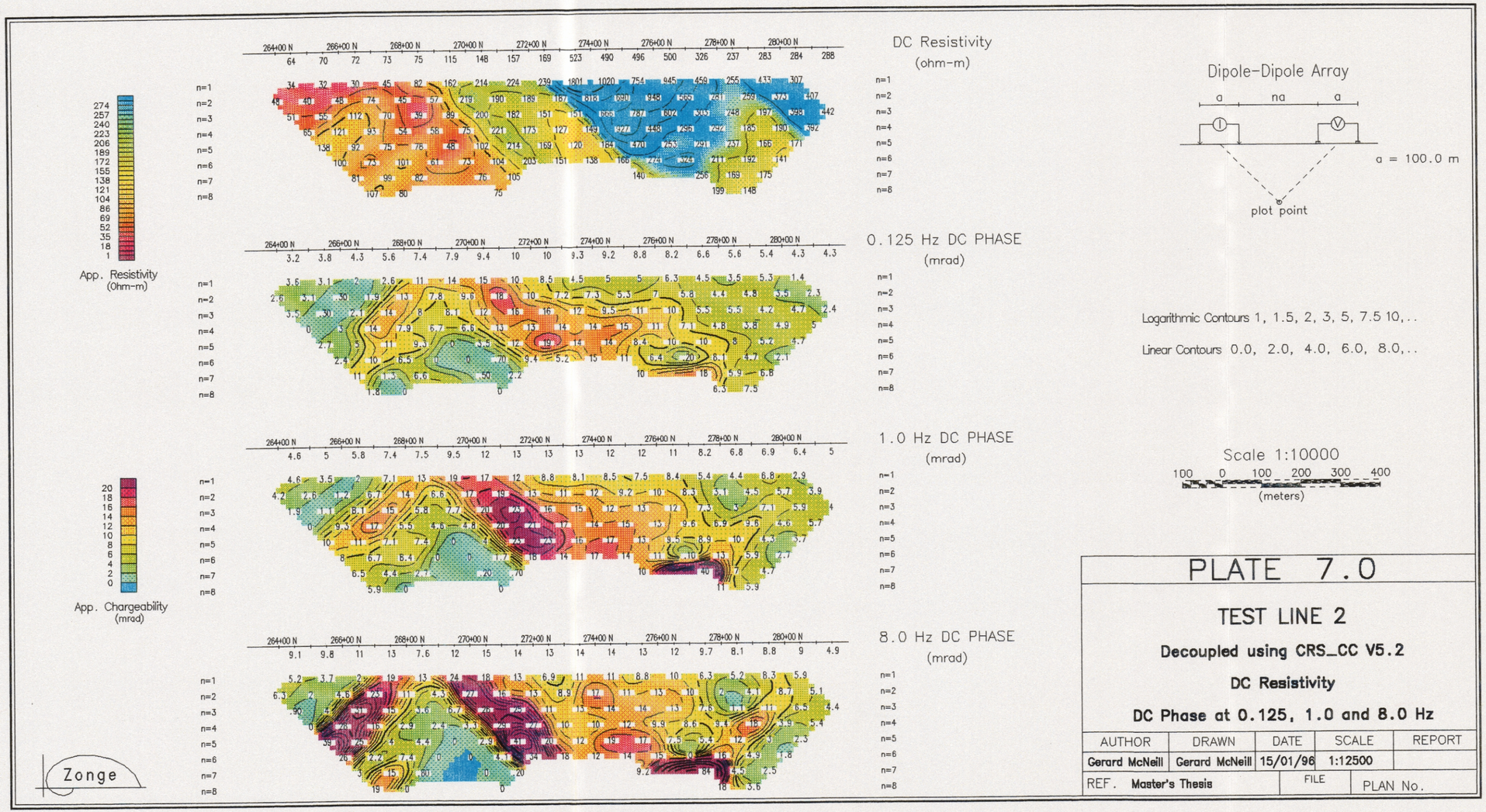

Dipole-Dipole Array

Logarithmic Contours 1, 1.5, 2, 3, 5, 7.5 10,..

Linear Contours 0.0, 2.0, 4.0, 6.0, 8.0,..

Scale 1:10000

100 0 100 200 300 400

(meters)

PLATE 7.0

TEST LINE 2

Decoupled using CRS_CC V5.2

DC Resistivity

DC Phase at 0.125, 1.0 and 8.0 Hz

AUTHOR	DRAWN	DATE	SCALE	REPORT
Gerard McNeill	Gerard McNeill	15/01/96	1:12500	
REF. Master's Thesis		FILE	PLAN No.	

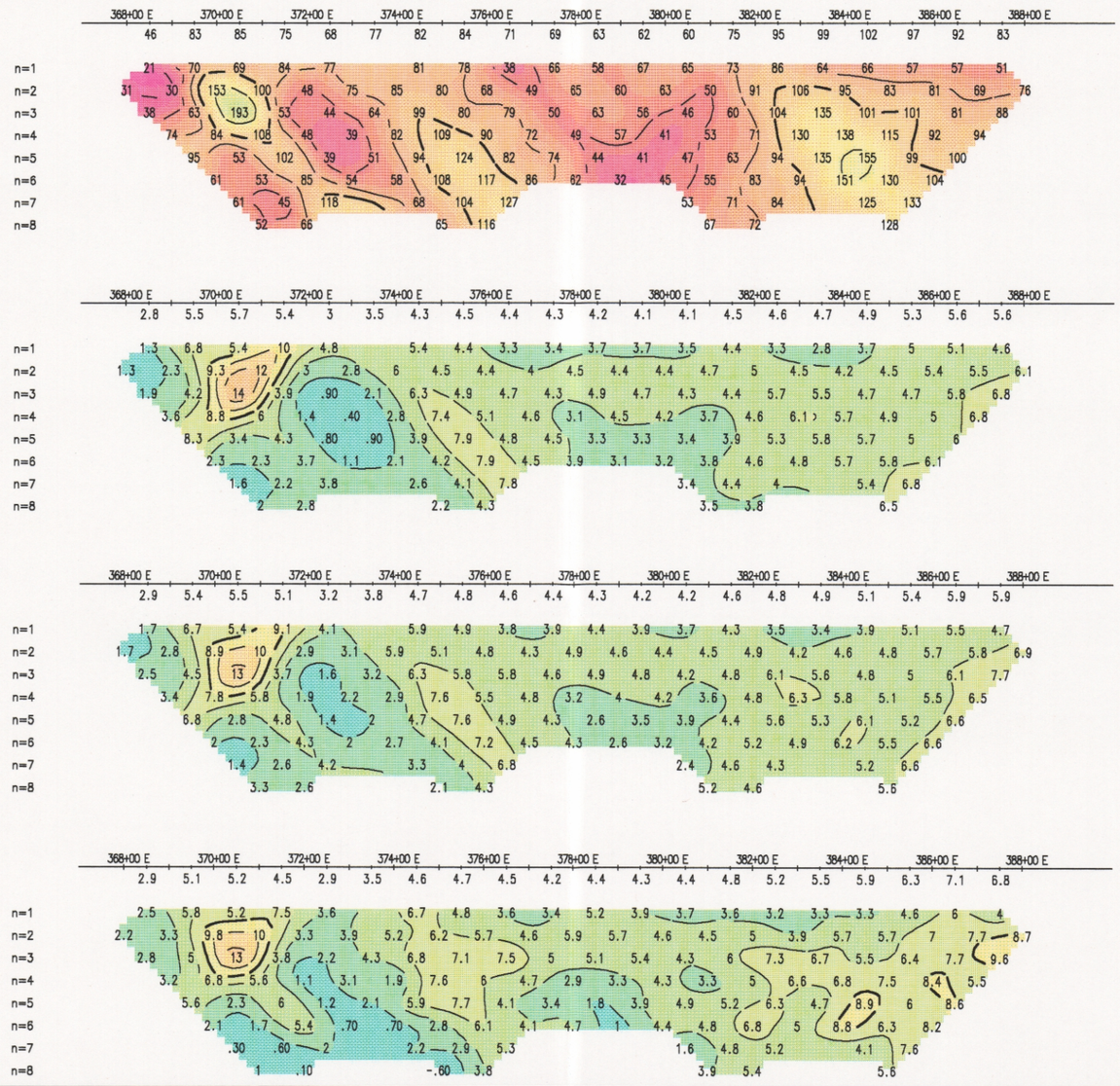

App. Resistivity
(ohm-m)

274 257 240 223 206 189 172 155 138 121 104 86 69 52 35 18 1

App. Resistivity
(Ohm-m)

0.125 Hz DC PHASE
(mrad)

1.0 Hz DC PHASE
(mrad)

8.0 Hz DC PHASE
(mrad)

20 18 16 14 12 10 8 6 4 2 0

App. Chargeability
(mrad)

Zonge

Dipole-Dipole Array

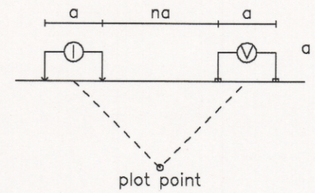

Logarithmic Contours 1, 1.5, 2, 3, 5, 7.5 10,..

Linear Contours 0.0, 2.0, 4.0, 6.0, 8.0,..

Scale 1:10000

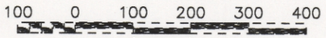

PLATE 9.0

TEST LINE 1

Decoupled using GDPHM

App. Resistivity

DC Phase at 0.125, 1.0 and 8.0 Hz

AUTHOR	DRAWN	DATE	SCALE	REPORT
Gerard McNeill	Gerard McNeill	16/01/96	1:10000	
REF. Master's Thesis		FILE	PLAN No.	

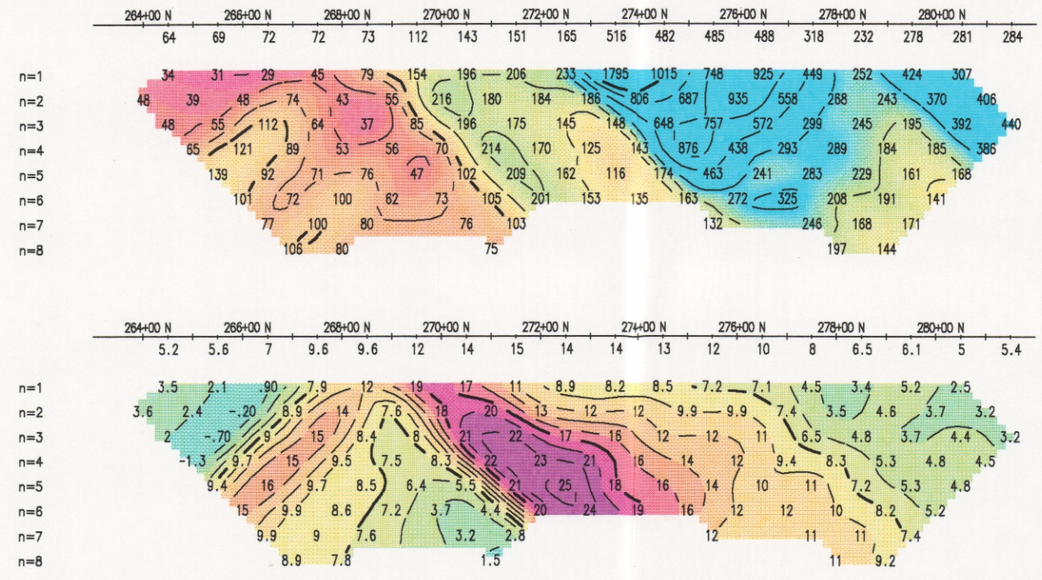

DC Resistivity
(ohm-m)

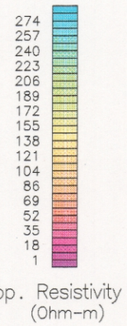

0.125 Hz DC PHASE
(mrad)

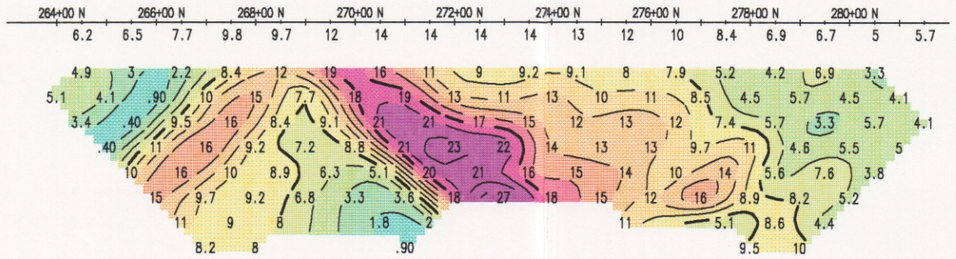

1.0 Hz DC PHASE
(mrad)

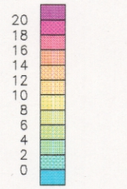

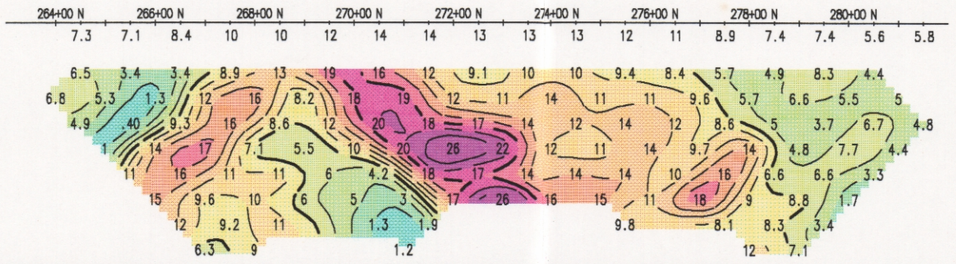

8.0 Hz DC PHASE
(mrad)

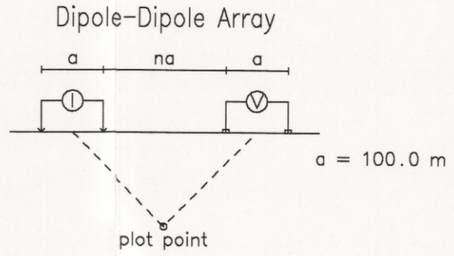

Logarithmic Contours 1, 1.5, 2, 3, 5, 7.5 10,..

Linear Contours 0.0, 2.0, 4.0, 6.0, 8.0,..

Scale 1:10000

100 0 100 200 300 400

(meters)

PLATE 10.0

TEST LINE 2

Decoupled using GDPHM

App. Resistivity

DC Phase at 0.125, 1.0 and 8.0 Hz

AUTHOR	DRAWN	DATE	SCALE	REPORT
Gerard McNeill	**Gerard McNeill**	**16/01/96**	**1:10000**	
REF. **Master's Thesis**		FILE	PLAN No.	

Zonge